WOOD RESEARCH doi.org/10.37763/wr.1336-4561/66.4.517527
e-ISSN 2729-8906
66(4): 2021 517-527 pp.

STUDY ON PROPAGATION LAW OF ACOUSTIC EMISSION SIGNALS ON ANISOTROPIC WOOD SURFACE

TINGTING DENG, SHUANG JU, MINGHUA WANG, MING LI
SOUTHWEST FORESTRY UNIVERSITY
CHINA

(RECEIVED OCTOBER 2020)

ABSTRACT

In order to explore the influence of wood's anisotropic characteristics on Acoustic Emission (AE) signals' propagation, the law of AE signals' propagation velocity along different directions was studied. First, The center of the specimen's surface was took as the AE source, then 24 directions were chose one by one every 15º around the center, and 2 AE sensors were arranged in each direction to collect the original AE signals. Second, the wavelet analysis was used to denoise the original AE signals, then the AE signals were reconstructed by Empirical Mode Decomposition (EMD). Finally, time difference location method was utilized to calculate AE signals' propagation velocity. The results demonstrate that AE signals' propagation velocity has obvious feature of quadratic function. In the range of 90º, as the angle of propagation direction increases, the propagation velocity of the AE signals presents a downward trend.

KEYWORDS: Wood, acoustic emission, propagation velocity, empirical mode decomposition.

INTRODUCTION

Acoustic Emission Technology (AET) is an initiative non-destructive testing method, which has been widely used in damage detection of concrete structures and rocks. Noorsuhada (2016) and Noorsuhada et al. (2014) applied AET to evaluate the fatigue damage of reinforced concrete structures. Muhamad et al. (2006) calculated the propagation velocity of AE signals on the surface of concrete beams utilizing the time difference method. The experiments results demonstrate that as the distance between the source and sensor increases, the wave velocity decreases. Based on this, Noorsuhada et al. (2013) studied the AE signals' propagation velocity inside reinforced concrete beams making use of waveform analysis. In addition, Yin and Tang (2005) applied AET to study the change law of the AE fractal features and fractal values with time in the rock failure process, and established the fractal model of AE intensity. Antonaci et al. (2011) took masonry as specimens and used AET to evaluate the damage evolution and mechanical properties of masonry.

In recent years, AET has been gradually utilized in nondestructive testing of wood and composites (Niemz et al. 2009, Krauss and Kudela 2011). Diakhate et al. (2017) explored the internal crack propagation of wood with the help of AET. Yoon et al. (2015) adopted AET to investigate the AE signals' features of layered fracture of carbon fiber reinforced polymer. Wu et al. (2014) and Zhuoping (2009) took flawless and defective timber as the specimens, and summarized the specimens' microstructure evolution under bending failure through recording the AE signals' characteristics. What's more, several types of damage were identified according to different feature parameters. Li et al. (2018) found that wavelet analysis can accurately locate the AE signals' source. Nasir et al. (2019) applied AE sensors to collect stress wave data and created a neural network model to classify thermal modified materials.

AET has been extensively put into use in wood nondestructive testing, but the research on the anisotropic propagation features of AE signals was rare. Heo et al. (2004) detected the propagation velocity of AE signals in anisotropic rocks under triaxial compression. Zhang et al. (2018) extracted the fractal characteristics of anisotropic shale in Brazil with AE principle. Nozawa et al. (2014) utilized wavelet analysis to classify the features of AE signals during the crack propagation of anisotropic composite materials SiC. The tests results demonstrate that wavelet analysis is effective for AE signal classification. Ciampa and Meo (2010a,b) adopted continuous wavelet transform to analysis the time domain and frequency domain of the AE signals from the surface of carbon fiber composites. The conclusion proves that this method can reduce the location error result full and realize AE source location. Ju et al. (2018, 2019) explored the propagation law of AE signals from the surface of *Pinus massoniana* plywood by wavelet analysis. An artificial AE source was produced by snapping 2H pencil lead in the experiment. Although there are few studies with respect to the effects of wood anisotropy on AE signal propagation law, the above researches are enlightening .

This paper took rubber wood (*Hevea brasiliensis* Muell. Arg) as the specimen to study the frequency features and propagation law of the AE signals spreading along different directions, while the AE signals came from the same AE source. First, the direction of bonding gap on the specimen surface was set as the standard. The AE signals was produced by snapping the pencil lead at the location of the AE source, and the raw AE signals were collected counterclockwise and clockwise respectively. Then, AE signals were extracted from the original signals containing noises through wavelet analysis. After that the AE signals were decomposed into several Intrinsic Mode Function (IMF) components by EMD algorithm. The correlation between each IMF components and its original AE signal was analyzed, at the same time, the correlation coefficient was calculated. In addition, the frequency analysis was carried out on the component with the largest correlation coefficient. Thus the characteristic frequency of the signals can be confirmed. Finally, the propagation velocity was calculated according to the time difference location method. The function between the propagation velocity of AE signals on specimen's surface and the angles of propagation directions was constructed through polynomial fitting method.

MATERIALS AND METHODS

Materials

The specimen is laminated finger-joint board made by rubber wood. The size of the specimen is 2000 × 1000 × 10 mm (length × width × thickness) and the moisture content is 8-12%. In order to ensure the quality of AE signals, a 4-channel AE signal acquisition system was built by the data acquisition card (NI USB-6366) and LabVIEW software. What's more, single-ended resonant AE sensors (SR150) with an acquisition frequency range of 20-220 kHz were connected to preamplifiers (PAI, gain set at 40 dB). According to Shannon Sampling Theorem, the sampling frequency of each channel was set to 500 kHz, and the acquisition voltage range of each channel was from -5V to +5V.

Methods

Firstly, a circular area with a radius of 350 mm on the surface of the specimen was selected, and according to the American Society for Testing Materials standards (ASTM E976-99), AE signals were generated by snapping 0.3 mm-diameter 2H pencil leads at point A which was in the center of the circle. The angle between the pencil leads and the surface of the specimen were 30º and the length of each snap of pencil lead was 2.5 mm. Secondly, the direction of the bonding gap of the specimen was set to 0º and the AE signals were and clockwise collected every 15º starting from 0º as shown in Fig. 1. In addition, 10 measurements were realized at each direction. After the AE signals were processed by the designed algorithms, the AE signals' propagation velocity in each direction was obtained. Therefore, the law of AE signals' propagation velocity in different directions was studied.

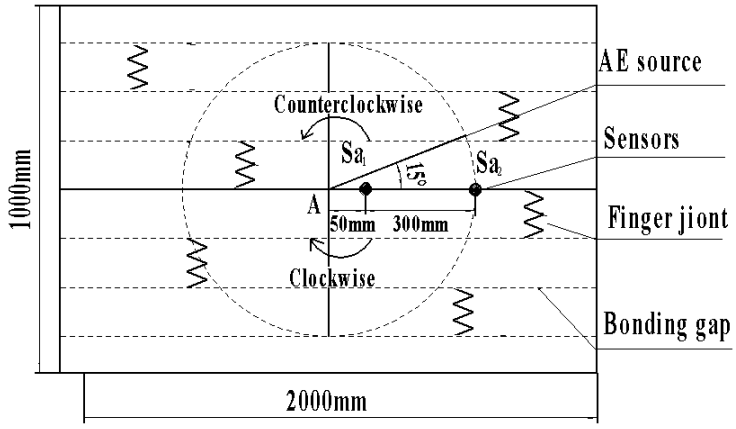

Fig. 1: Sketch of the experiment scheme.

Due to the influence of the propagation paths, measurement system and environmental noises of AE signals, the output electric signals of the AE sensors are a kind of typical nonlinear and non-stationary random signal (Jiang and Xu 2017). Therefore the wavelet analysis method was used to denoise the original AE signals. After that the AE signals were reconstructed by EMD algorithm (Huang 2000). The process of EMD decomposition was as follows:

Firstly, local maximum points and minimum points of the AE signals $x(t)$ were chosen, and the upper envelope curve $y_0(t)$ formed by the maximum points and the lower envelope curve $z_0(t)$ formed by the minimum points were fitted by cubic spline interpolation. Then the average value

$m_1(t)$ of the upper and lower envelope curves was calculated:

$$m_1(t) = \frac{y_0(t) + z_0(t)}{2} \quad (1)$$

After the instantaneous average $m_1(t)$ was subtracted from the original AE signals $x(t)$, a new sequence $v_1(t)$ was got:

$$v_1(t) = x(t) - m_1(t) \quad (2)$$

Secondly, the judgment conditions of IMF include two parts. One condition is that the number of extreme points and zero-crossing points must be equal or differ by at most 1. The other one is that the average value of the upper and lower envelope curves should be zero. If the conditions were satisfied, then $v_1(t)$ was the first IMF component of $x(t)$ named $imf_1(t)$ and that meant $imf_1(t) = v_1(t)$. The original signals minus the component equaled that $h_1(t) = x(t) - imf_1(t)$. If the conditions were not satisfied, took $v_1(t)$ as a new data to repeat the above steps. IMF components were presented in turn, $imf_2(t)$, $imf_3(t)$, … $imf_n(t)$; $h_2(t) = h_1(t) - imf_2(t)$, …, $h_n(t) = h_{n-1}(t) - imf_n(t)$. When $h_n(t)$ was a single sequence which no longer contained any modal information; it was the residual term of the original AE signals. After decomposition the original AE signals could be expressed as:

$$x(t) = \sum_{i=1}^{n} imf_i(t) + h_n(t) \quad (3)$$

Finally, the IMF component which had the largest correlation coefficient with the raw signals was adopted as the final AE signal and the principal component which was analyzed to identify the characteristic frequency of AE signal.

RESULTS AND DISCUSSION

Features of AE signals on the specimen's surface

There were too many AE signals collected in different directions to list all of them. Actually they were generated by the same AE source and their features of time and frequency domain were similar. Therefore, the signals collected by the sensor Sa_1, which were parallel to the bonding gap and closest to point A were taken as an example. Fig. 2a was a graph of the original signals' time domain. It can be seen from the graph of the original signals' frequency domain as shown in Fig. 2b that the frequency of main component signals Sa_1 was 2 kHz, which was very low. For AE source was generated instantaneously through snapping pencil lead, its energy was weak and the original signals contained a lot of noise signals. So the raw signals needed to be denoised by wavelet analysis.

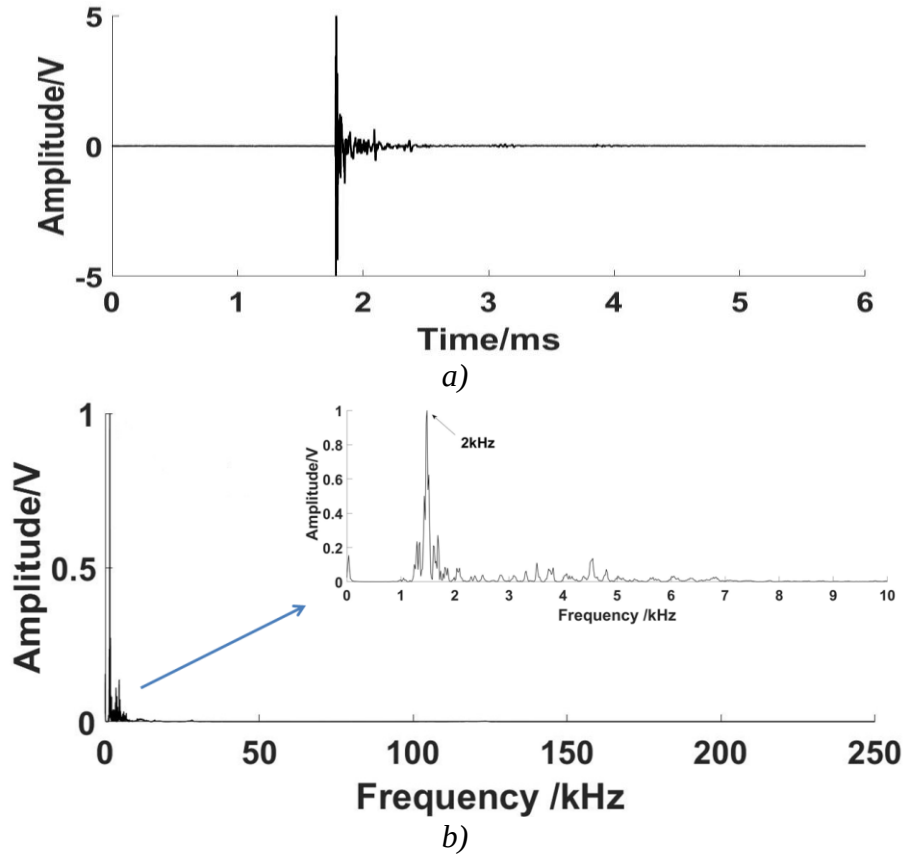

a)

b)

Fig. 2: The original AE signals: a) the signal of time domain. b) the signal of frequency domain.

After noises reduction, the AE signals were decomposed by EMD. Then 15 IMF components and 1 residual term were obtained as shown in Fig. 3. In order to identify the principal component, each component was made correlated analysis with the original signals. The IMF6 component's correlation coefficient was 0.1146 and the components after it had smaller correlation coefficient. So only the first 6 components were listed in Tab. 1. As shown in Tab. 1, the IMF3 component had the largest correlation coefficient; therefore it was the principal component. Then, the IMF3 component was analyzed in the frequency domain and its spectrum is showed in Fig. 4. In order to highlight the signals' proportion, the signals were normalized during analysis. Fig. 4 indicates that the AE signals' energy concentrates on the frequency of 35 kHz.

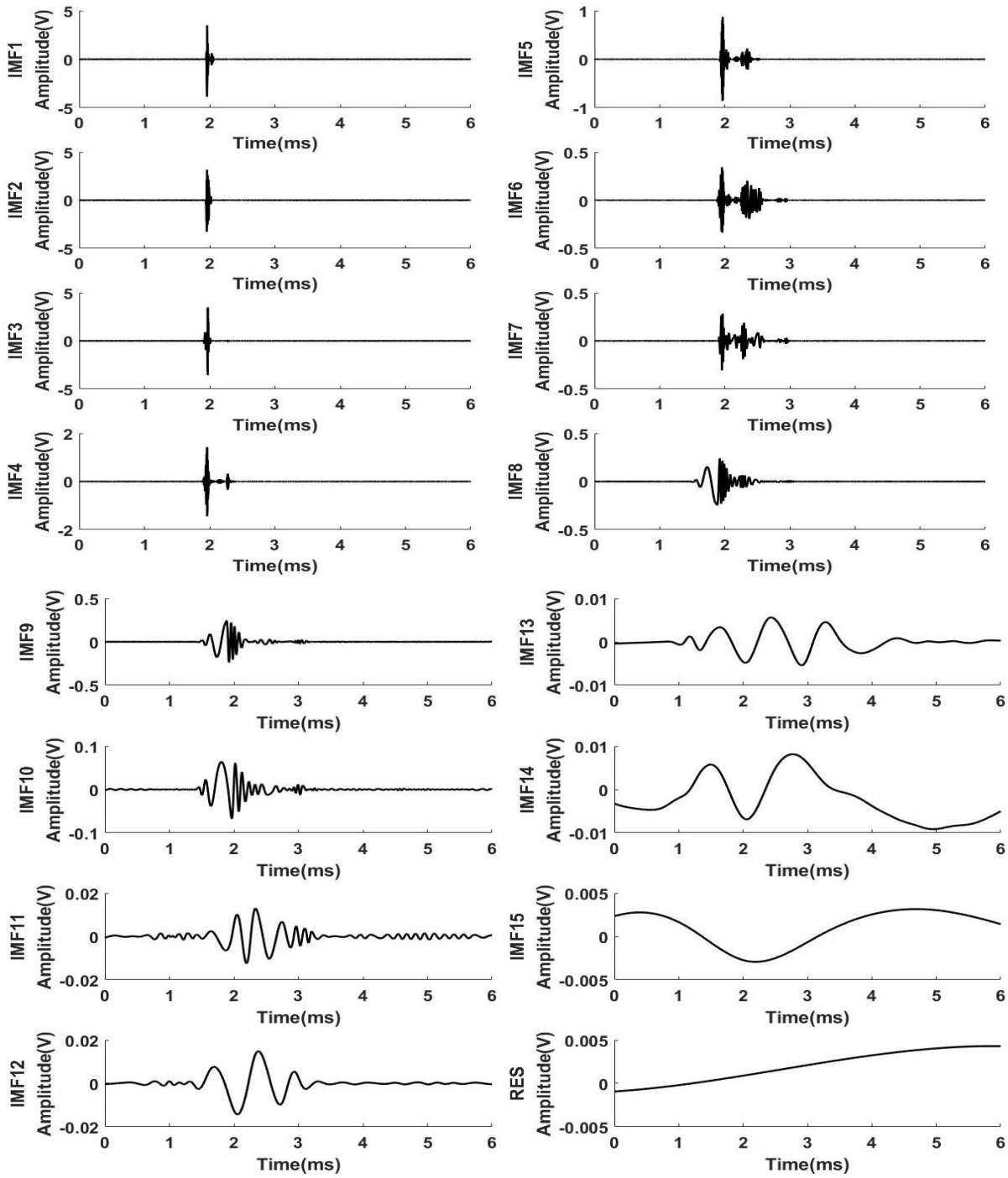

Fig. 3: The IMF components and residual term decomposed by EMD.

Tab. 1: The correlation coefficients of IMF with the original signals.

Intrinsic Mode Function	IMF1	IMF2	IMF3	IMF4	IMF5	IMF6
Correlation Coefficient	0.4952	0.5748	**0.8951**	0.3573	0.2657	0.1146

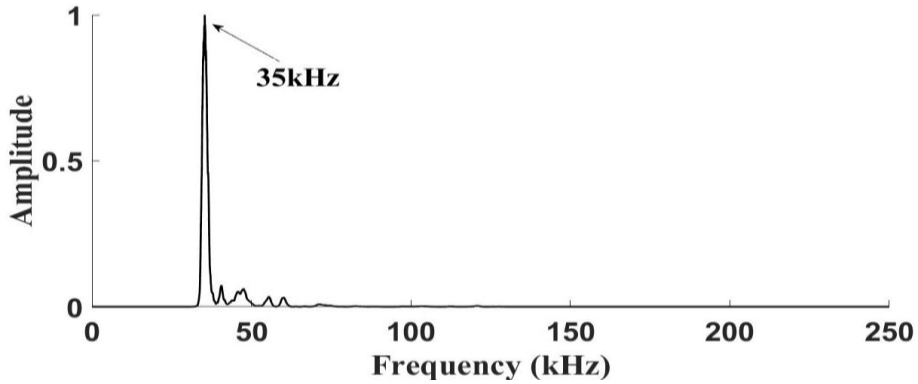

Fig. 4: The AE signals' reconstruction spectrum.

Propagation law of AE signals in different directions

The time difference location method and cross-correlation analysis method were used to calculate the propagation velocity of AE signals. Firstly, the sensors were arranged at points which were 50 mm away from point A. The relative distances between the 2 AE sensors were all set as Δs = 300 mm as shown in Fig. 1. Then the AE signals cost different time to reach the 2 AE sensors and the time differences named Δt were calculated by cross-correlation analysis method. The cross-correlation function mainly describes the degree of similarity between 2 signals (Asari et al. 2014, Mao et al. 2002). The cross-correlation function of the signals $j(t)$ and $k(t)$ were defined as:

$$R_{jk}(\tau) = \lim \frac{1}{T} \int_0^T j(t)k(t+\tau)\,\mathrm{d}\,t \quad (4)$$

According to the definition of cross-correlation function, if when $\tau = \tau_0$, the absolute value $|R_{jk}(\tau_0)|$ of the cross-correlation function equals the maximum value. The signal $k(t)$ is most similar to signal $j(t)$ after it is translated τ_0 units along the time axis. Therefore, the time difference Δt can be figured out indirectly by cross-correlation function. The propagation velocity of AE signals was calculated as: $v = \Delta s/\Delta t$. In order to minimize the impact of the random affection of the test, 10 independent tests were made in each direction. The calculation results were showed in Tab. 2 and Tab. 3. As can be seen, when the angle between AE signals' propagation direction and the direction of bonding gap was 90^o, the minimum propagation velocity was about 810 $m{\cdot}s^{-1}$, and when the angle was 180^o, the maximum propagation velocity was about 1410 $m{\cdot}s^{-1}$. The angle was taken as a variable and the AE signals' average velocity function of Tab. 2 and Tab. 3 was fitted by a quadratic polynomial method. The results were as follows:

$$v_1(\alpha_1) = 0.063\alpha_1^2 - 11.22\alpha_1 + 1388.1 \quad (5)$$

$$v_2(\alpha_2) = 0.068\alpha_2^2 - 11.90\alpha_2 + 1400.7 \quad (6)$$

where: v_1 and v_2 are the AE signals' average velocity ($m{\cdot}s^{-1}$); α_1 and α_2 are angles (0^o-180^o).

Tab. 2: The average velocity from 0° to 180° counterclockwise.

Angles (°)	Velocity ($m \cdot s^{-1}$)										Average velocity ($m \cdot s^{-1}$)	Standard deviation
0	1451.4	1462.5	1451.4	1478.9	1462.5	1351.4	1430.6	1562.5	1351.4	1451.4	1445.4	57.8
15	1120.4	1181.1	1102.9	1111.1	1250.0	1271.9	1227.4	1230.0	1171.9	1207.4	1187.4	57.1
30	1056.3	980.4	1041.7	1049.0	986.8	1141.7	1056.3	1041.7	1056.3	1041.7	1035.2	41.6
45	986.8	986.8	986.8	1094.9	986.8	986.8	986.8	986.8	1102.9	1094.9	1020.0	50.8
60	937.5	1041.7	1034.5	1027.4	1041.7	937.5	1027.4	937.5	937.5	937.5	986.0	48.7
75	881.3	850.0	850.0	993.4	902.9	902.9	885.0	986.8	993.4	986.8	923.3	57.2
90	750.0	806.0	753.8	810.8	897.2	810.8	852.3	721.2	897.2	852.3	815.2	57.6
105	990.2	892.9	897.2	955.2	801.3	902.9	895.2	932.9	897.2	885.2	905.0	47.0
120	910.8	939.3	990.5	1010.0	953.8	915.2	1039.3	1090.5	915.2	910.8	967.5	59.6
135	1171.9	1041.7	1043.4	1139.9	1037.5	1171.9	1041.7	1043.4	1139.9	1037.5	1086.9	57.3
150	1136.4	1045.0	1153.8	1153.8	1145.0	1041.7	1145.0	1153.8	1103.8	1145.0	1122.3	41.9
165	1071.9	1192.8	1239.3	1227.4	1194.9	1182.8	1171.9	1162.8	1227.4	1192.8	1186.4	44.9
180	1415.8	1415.1	1462.5	1404.3	1304.3	1401.9	1393.1	1428.6	1339.7	1415.1	1398.0	42.7

Tab 3: The average velocity from 0° to 180° clockwise.

Angles (°)	Velocity ($m \cdot s^{-1}$)										Average velocity ($m \cdot s^{-1}$)	Standard deviation
0	1455.4	1462.5	1351.4	1478.9	1562.5	1451.4	1530.6	1562.5	1562.5	1451.4	1486.9	64.5
15	1050.0	1086.8	1060.5	1093.4	1150.0	1150.0	1160.5	1086.8	1260.5	1193.4	1149.2	62.5
30	1171.9	1102.9	1011.1	1031.7	1000.0	1020.0	1102.9	1011.1	1031.7	931.7	1041.5	63.9
45	954.0	924.0	1049.0	1162.8	1049.0	954.0	924.0	1029.0	1019.0	1032.8	1021.8	69.6
60	943.4	937.5	1102.9	1111.1	937.5	931.7	1020.4	943.4	937.5	931.7	979.7	68.3
75	924.0	986.8	881.3	950.0	1049.0	962.8	949.0	962.8	881.3	850.0	939.7	55.3
90	742.6	781.3	781.3	867.1	777.2	785.3	819.7	862.1	867.1	777.2	806.1	42.6
105	923.6	887.5	936.4	1039.7	973.8	893.8	887.8	883.8	895.2	921.3	924.3	46.9
120	1111.1	980.4	937.5	937.5	986.8	924.0	980.4	1111.1	980.4	986.8	993.6	62.7
135	943.4	994.9	992.9	903.6	1020.4	1094.9	1020.4	1094.9	943.4	1094.9	1010.4	65.2
150°	1102.9	1102.9	1250.0	1250.0	1239.7	1102.9	1111.1	1111.1	1102.9	1239.7	1161.3	68.3
165°	1381.1	1330.6	1330.6	1371.9	1190.5	1234.5	1330.6	1330.6	1271.9	1190.5	1296.3	66.6
180°	1405.8	1415.1	1402.5	1392.5	1504.3	1501.9	1415.1	1428.6	1385.8	1405.1	1425.7	40.3

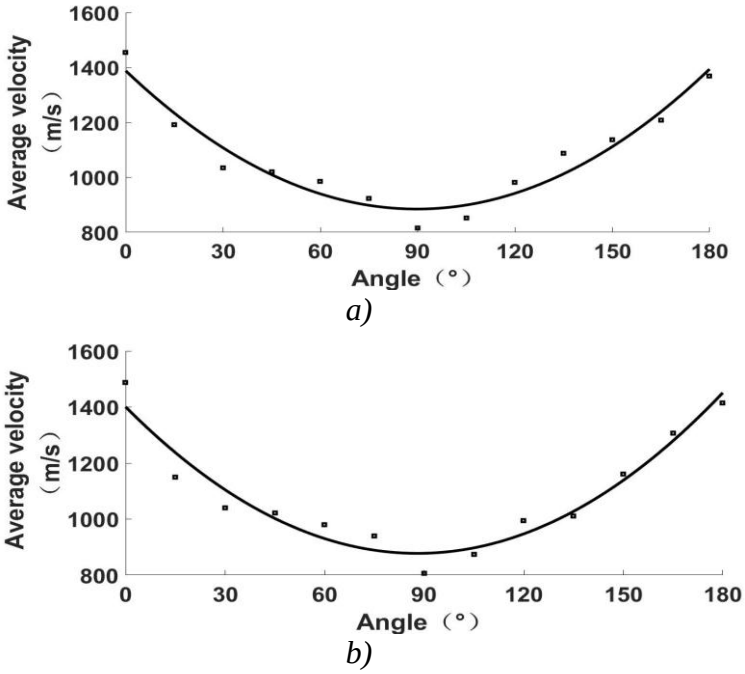

Fig. 5: The fitting curves of average velocity and angles: a) angles from 0° to 180° counterclockwise, b) angles from 0° to 180° clockwise.

As shown in Fig. 5, the propagation velocity of AE signal varies in different directions due to the influence of propagation paths and adhesive. The AE signals' propagation velocity both decreases first and then increases when the angles change clockwise and counterclockwise from 0^o to 180^o. But comparing Fig. 5a with Fig. 5b, it can be seen that the propagation velocity of the same AE source was almost the same in two opposite directions of the same line.

CONCLUSIONS

This paper is a preliminary exploration of the propagation law of AE signals within anisotropy wood. The AE source was produced on the anisotropy wood specimen's surface by snapping pencil lead and the AE signals' features and propagation velocity in different direction was studied through wavelet analysis and EMD. The results show that the AE signals' feature frequencies mainly concentrate around 35 kHz and the AE signals' propagation velocity both decreases first and then increases when the angle of propagation direction increases clockwise and counterclockwise from 0^o to 180^o. The propagation velocity along the bonding gap is the maximum and the minimum velocity appears in the orientation perpendicular to the bonding gap. Thus, it provides data for the research of the AE source's localization on the wood's surface and it has reference value for the AE source's localization of other anisotropic materials.

ACKNOWLEDGEMENTS

The authors are grateful for the support of the China Natural Science Foundation (NO: 31760182, 31100424) and Department of Education of Yunnan Provincial (NO: 2020Y0376 NO: 2021J0158).

REFERENCES

1. Antonaci, P., Bocca, P.G., Masera, D., 2011: Fatigue crack propagation monitoring by acoustic emission signal analysis. Key Engineering Materials 465: 370-373.
2. Asari, D., Hasegawa, H., Kanai, H., 2014: Improvement of myocardial displacement estimation using subkernels for cross correlation between ultrasonic RF echoes. Japanese Journal of Applied Physics 53(7S): 07-21.
3. Ciampa, F., Meo, M., 2010a: Acoustic emission source localization and velocity determination of the fundamental mode A0 using wavelet analysis and Newton-based optimization technique. Smart Materials and Structures 19(4): 27-45.
4. Ciampa, F., Meo, M., 2010b: A new algorithm for acoustic emission localization and flexural group velocity determination in anisotropic structures. Composites Part A: Applied Science and Manufacturing 41(12): 1777-1786.
5. Diakhate, M., Bastidas-Arteaga, E., Moutou, P.R., 2017: Cluster analysis of acoustic emission activity within wood material: Towards a real-time monitoring of crack tip propagation. Engineering Fracture Mechanics 180: 254-267.
6. Heo, J.S., Lee, C.I., Jeon S.K, 2004: Measurement of acoustic emission and source location considering anisotropy of rock under triaxial compression. Key Engineering Materials 270-273:1574-1579.
7. Jiang, Y., Xu, F., 2017: A novel acoustic emission source location method in the crane based on EEMD-fast ICA. Journal of Mechanics Engineering and Automation (7): 17-25.
8. Huang, N.E., 2000: New method for nonlinear and nonstationary time series analysis: empirical mode decomposition and Hilbert spectral analysis. Proceedings of SPIE - The International Society for Optical Engineering 4056: 197-209.
9. Ju, S., Li, X.C., Luo, T.F., 2018: Characteristics of acoustic emission signals on the surface of Masson Pine glulam with wavelet analysis method. Journal of Northeast Forestry University 46(08): 86-92.
10. Ju, S., Li, X.C., Luo, T.F., 2019: Study on the anisotropic propagation of acoustic emission signal on *Pinus massoniana* plywood surface. Journal of Forestry Engineering 4(02): 48-53.
11. Krauss, A., Kudela, J., 2011: Ulrasonic wave propagation and Young's modulus of elasticity along the grain of Scots pine wood (*Pinus sylvestris* L.) varying with distance from the pith. Wood Research 56(4): 479-488.
12. Li, Y., Yu, S.S., Dai, L., 2018: Acoustic emission signal source localization on plywood surface with cross-correlation method. Journal of Wood Science 64(2): 78-84.
13. Mao, J.D., Hundal, L.S., Thompson, M.L., Schmidt-Rohr, k., 2002: Correlation of poly(methylene) -rich amorphous aliphatic domains in humic substances with sorption of a nonpolar organic contaminant, phenanthrene. Environmental Science & Technology 36(5): 929-936.
14. Muhamad, B.N., Pullin, R., Holford, K.M., Lark, R., 2006: A practical investigation into acoustic wave propagation in concrete structures. Advanced Materials Research 13-14: 205-212.

15. Nasir, V., Nourian, S., Avramidis, S., 2019: Stress wave evaluation by accelerometer and acoustic emission sensor for thermally modified wood classification using three types of neural networks. European Journal of Wood and Wood Products 77(1): 45-55.
16. Niemz, P., Brunner, A.J., Walter, O., 2009: Investigation of the mechanism of failure behaviour of wood based materials using acoustic emission analysis and image processing. Wood Research 54(2): 49-62.
17. Noorsuhada, M.N., 2016: An overview on fatigue damage assessment of reinforced concrete structures with the aid of acoustic emission technique. Construction & Building Materials 112: 424-439.
18. Noorsuhada, M.N., Ibrahim, A., Muhamad, B.N., Hamidah, M.S., Soffian, N.M.S., Shahiron, S., 2014: Diagnostic of fatigue damage severity on reinforced concrete beam using acoustic emission technique. Engineering Failure Analysis 41: 1-9.
19. Noorsuhada, M.N., Muhamad, B.N., Ibrahim, A., 2013: An investigation of an acoustic wave velocity in a reinforced concrete beam from out-of plane and in plane sources. Intech 171-188.
20. Nozawa, T., Ozawa, K., Asakura, Y., 2014: Evaluation of damage accumulation behavior and strength anisotropy of NITE SiC/SiC composites by acoustic emission, digital image correlation and electrical resistivity monitoring. Journal of Nuclear Materials 455(1-3): 549-553.
21. Wu, Y., Shao, Z.P., Wang, F., 2014: Acoustic emission characteristics and felicity effect of wood fracture perpendicular to the grain. Journal of Tropical Forest Science 26(4): 522-531.
22. Yin, X.G., Li, S.L., Tang, H.Y., 2005: Study on strength fractal features of acoustic emission in process of rock failure. Chinese Journal of Rock Mechanics Engineering 24(19): 3512-3516.
23. Yoon, S.J., Chen, D., Han S.W., 2015: AE analysis of delamination crack propagation in carbon fiber-reinforced polymer materials. Journal of Mechanical Science and Technology 29(1): 17-21.
24. Zhang, S.W., Shou, K.J., Xian, X.F., 2018: Fractal characteristics and acoustic emission of anisotropic shale in Brazilian tests. Tunnelling & Underground Space Technology 71(5): 298-308.
25. Zhuoping, S., 2009: Acoustic emission characteristics of damage and fracture process of wood and felicity effect. Scientia Silvae Sinicae 45(2): 86-91.

TINGTING DENG, SHUANG JU, MINGHUA WANG, MING LI*
SOUTHWEST FORESTRY UNIVERSITY
SCHOOL OF MACHINERY AND TRANSPORTATION
KUNMING 650224, CHINA
*Corresponding author: swfu_lm@swfu.edu.cn

WOOD RESEARCH doi.org/10.37763/wr.1336-4561/66.4.528543
e-ISSN 2729-8906
66(4): 2021 528-543 pp.

EFFECT OF IMISSION TO XYLEM ANATOMY OF NORWAY SPRUCE

MARTIN LEXA[1], MONIKA VEJPUSTKOVÁ[2], ALEŠ ZEIDLER[1]
[1]CZECH UNIVERSITY OF LIFE SCIENCES PRAGUE
CZECH REPUBLIC
[2]FORESTRY AND GAME MANAGEMENT RESEARCH INSTITUTE
CZECH REPUBLIC

(RECEIVED JANUARY 2021)

ABSTRACT

The aim of this work was to analyse the relationship between anatomical parameters of spruce tracheids and climatic factors and air pollution load, in the period before, during and after the maximum air pollution load. In this study we used the method of dividing annual rings into a number of equally wide sectors, for which the average values of the tracheid dimensions, i.e., the lumen area and cell wall width, were determined. This method was compared to the classic approach, which works with the average values of parameters for the entire annual ring, or for earlywood and latewood. The study showed that the trees responded to the increased concentration of pollutants by reducing the widths of the annual rings and the values of the anatomical parameters. The higher resolution of data gives us a better insight on the influence of abiotic factors to the wood structure. The ratio of cell wall thicknesses of earlywood to latewood was also shown as a good indicator of stress.

KEYWORDS: air pollution, quaintitative wood anatomy, cell wall thickness, lumen area, Ore Mountains, *Picea abies* (L.) Karst.

INTRODUCTION

The so-called Black Triangle, which includes Northern Bohemia and the adjacent areas of Germany and Poland, was one of the most affected areas in Europe in the second half of the 20th century due to the enormous burden of fossil fuel emissions (Blažková 1996). In addition, the high level of extreme climate events has also made the situation worse. Cold winters increased the intensity of accumulation of air pollutants, and thereby subsequently in forest stands (Allen et al. 2010). From this entire area, the Ore Mountains were impacted the most (Zimermann et al. 2002) when extensive extinction of spruce stands took place (Kubelka 1992, Materna 1999). The health of the forest deteriorated rapidly

in the 1970s and 1980s. With the rapid decline of air pollution in the 1990s, the health of the surviving stands began to improve (Fiala et al. 2002, Hůnová et al. 2004). Specifically, spruces began to regenerate rapidly after deep growth depression (Sander et al. 1995, Kroupová 2002), whereas in the late 1990s the radial growth in fact exceeded the values from the pre-stress period (Rydval and Wilson 2012, Kolář et al. 2015). With the exception of a few studies (Wimmer 2002, Samusevich et al. 2017, Vejpustková et al. 2017), we have very little information about the impact that extreme pollution had on the anatomical structure of wood.

Data obtained via quantification of tracheid dimensions and their statistical processing can provide us with information about the environment in which the growth of the studied vegetation occurred (Wimmer and Grabner 1997, Olano et al. 2012, Ziaco et al. 2014). However, these anatomical characteristics may react to stress differently than the mean ring width (MRW), making them potentially suitable proxies for dendroecological studies (Kozlowski et al. 1991, Schweingruber 1996, Wimmer 2002, Vaganov et al. 2006, Puchi et al. 2020). Anatomical parameters can also be modified by air pollution (Wimmer and Halbwachs 1992, Kurczyńska et al. 1997, Samusevich et al. 2017, Vejpustková et al. 2017). Especially SO_2 load can increase sensitivity to other abiotic factors, such as frost, heat or drought (Keller et al. 1984). Unlike the mere width of the annual ring, data on the dimensions and numbers of tracheids can be investigated with a higher than annual resolution (Fonti et al. 2010), von Arx et al. 2016). One of the approaches to obtaining intra-annual resolution is to divide the annual ring into earlywood (EW) and latewood (LW) (Samusevich et al. 2020). The conditions and factors that influenced the structure and dimensions of tracheids in these two periods of the year may vary (Park and Spiecker 2005, Olano et al. 2012, Ziaco et al. 2014). The issue is that there are a large number of methods for identifying the boundary between EW and LW, such as using the Mork's index (MI) value (Denne 1989), determination via the sum of cells before and after the early and late wood boundary using the MI (Park et al. 2006), or X-ray densitometry (Koubaa et al. 2002). Although this data may provide new results (Samusevich et al. 2017, 2020, Vejpustková et al. 2017), the position of the boundary determined by the individual methods may differ and may not always respect the natural boundary between EW and LW. The primary issue of certain tree species, which also applies to the wood of the investigated spruce, is the gradual transition between EW and LW (Park et al. 2006).

We do not know exactly when a particular cell of a given annual ring is formed, but we do know their sequence. One of the new approaches is to therefore divide each annual ring into a number of equally wide sectors (Carrer et al. 2017, Puchi et al. 2020), in which the average values of the parameters of the anatomical structure – lumen area (LA) and cell wall thickness (CWT) are calculated. The relationship between anatomical parameters and pollution is then analyzed with intra-annual resolution by individual sectors, and it is thereby possible to determine which part of the annual ring was most affected by the investigated factors (Carrer et al. 2017, Pacheco et al. 2017, Castagneri et al. 2018).

The aim of the study was to analyse at the intra-annual level the effect of climate and pollution on the parameters of the anatomical structure of Norway spruce wood in the Klínovec area, i.e., the highest peak of the Ore Mountains. One of the partial goals was

to compare the method of analysis of anatomical parameters by sectors with the classic approach, which works with the average values of parameters for the entire annual ring, or for earlywood and latewood. We hypothesized hypothesised that high concentrations of pollutants have a negative effect on the values of the LA and CWT parameters, that pollution changes the nature of the relationship between climate and anatomical parameters, and that dividing the annual ring into smaller parts provides a more detailed insight into xylem growth response to abiotic factors.

MATERIAL AND METHODS

Location

For the purpose of quantitative analysis of anatomical features of wood, five cores were taken from randomly selected Norway spruce (*Picea abies* (L.) Karst) level trees in the autumn of 2015, from each of four stands (Tab. 1) in the vicinity of the highest peak of the Ore Mountains – Klínovec (1,244 m above sea level). Three stands were located at an altitude of approximately 1,000 m and the fourth at an altitude of 1,230 m nearby the hilltop. The reason for choosing this location was mainly the presence of old spruce stands, which survived the air pollution calamity. The climatic conditions are characterized by data from the nearest meteorological station, located on the German side at the top of Fichtelberg. Fig. 1 shows the average annual summer temperature (June– - August) and the annual and summer sum of precipitation (June– - August). Fig. 2 shows the average annual and winter air concentration of SO_2 represented by a combined series of measurements from the nearby Blatno and Měděnec stations. The greatest sources of pollutants in the area are the Tušimice and Prunéřov brown coal power plants, which began operating in 1964 and 1967. These power plants were completely desulphurized in the first wave of greening of coal resources from 1996 to 1999. According to a report made in 2010 by ČEZ, the company operating the power plants, the level of SO_2 concentration was reduced by 92% compared to the level at the beginning of the 1990s, NO_X by 50%, solid pollutants by 93% and CO by 77%.

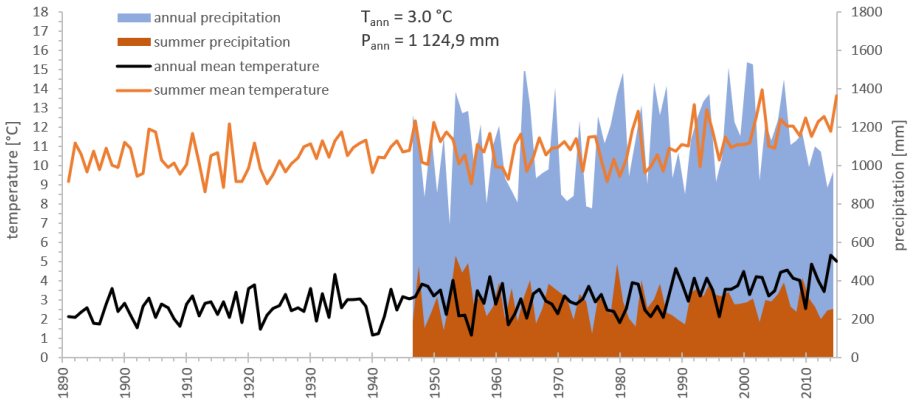

Fig. 1: Average temperatures and precipitation (at meteorological station on the Fichtelberg).

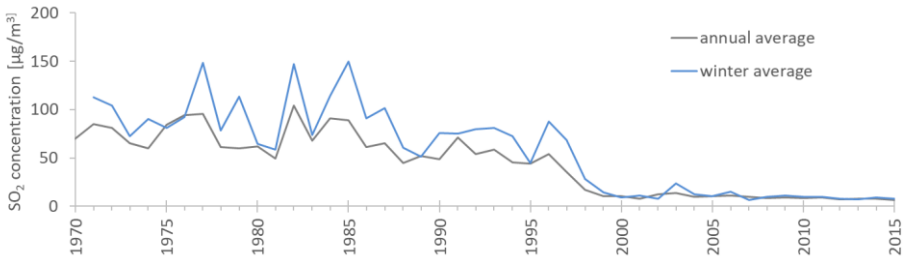

Fig. 2: Average annual and winter SO_2 concentrations (data combined from stations Blatno and Měděnec).

Tab. 1: Description of study plots.

Plot	Coordinates [WGS84]		Altitude	Exposition	Stand age
	latitude	longitude			
Sucha 1	N 50°23‘13“	E 12°59‘07“	1 030	SE	160
Sucha 2	N 50°22‘41“	E 12°57‘51“	1 009	SW	170
Loucna	N50°24‘23“	E 12°58‘14“	1 013	N	180
Klinovec	N 50°23‘40“	E 12°58‘07“	1 230	-	120

Sampling and preparation of samples

A total of 40 cores from 20 trees were collected for the purpose of cross-dating, from each tree on two cores on opposite sides in the direction of the contour line in order to eliminate the occurrence of reaction wood. First, the mean ring width (MRW) was measured using measuring table „TA“ measurement system (Velmex Inc., Bloomfield, NY, USA) with an accuracy of 0.001 mm. Cross-dating was subsequently carried out using PAST 5.1 software. A total of 20 cores, one of which each tree, were then used to create permanent microscopic slides. After dividing the cores into a length that fits on the glass slide (4–5 cm), 12 µm thick cross-cuts were made using a rotary microtome (Leica, Heidelberg, Germany). It is important to ensure that the thickness of the slide is kept constant throughout the length of the cut, as the thickness of the slide can affect the values of the measured parameters, mainly the CWT (von Arx et al. 2016). The specimens were placed on a glass slide, stained with safranin, dehydrated with series of alcohol solutions in ascending concentrating up to 100% and fixed with a synthetic resin (Eukitt, BiOptica, Milan, Italy) (Castagneri et al. 2017). At 100× optical magnification (2.9 µm/px), the specimens were scanned using a Nikon Ni-E motorized microscope. NIS-Elements software was used for capturing the composite image.

Data processing

The composite images were analyzed using software ROXAS v 3.0.1 (von Arx and Carrer 2014). For measuring parameters we used the same configuration file as Castagneri et al. (2015). The MRW, lumen area (LA) and cell wall thickness in the radial direction (CWT) were measured. For each measured cell, its relative distance from the beginning of the annual ring was recorded.

In order to find one boundary between EW and LW, each annual ring was divided into one hundred equally wide sectors, and the average value of the Mork’s index (MI) was

calculated for each of them. This value is calculated as a ratio of four times the radial thickness of the cell wall and the radial diameter of the lumen (Denne 1989). The moving average of the MI with a length of nine sectors was then calculated, and it was further ensured that this value only increased, so that if the moving average value was lower than the previous value, the previous value was recorded instead. All sectors for which the calculated MI was less than or equal to 1 were considered earlywood. In addition to earlywood and latewood, 10 equally wide sectors numbered along the direction of the wood growth were defined within each annual ring based on the relative distance of the cells from the beginning of the annual ring (Fig. 3) (Carrer et al. 2017).

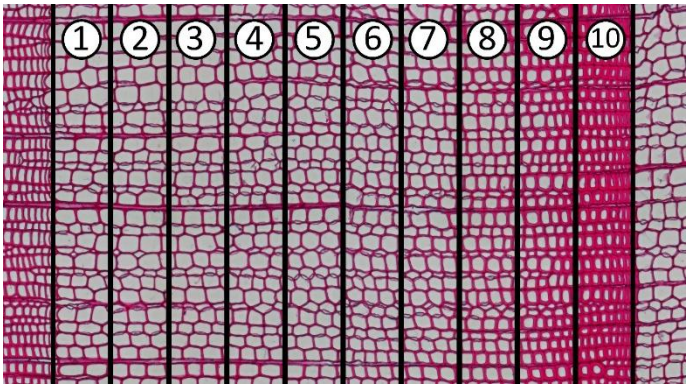

Fig. 3: Defining of ten sectors within the annual ring.

The mean value of the LA and CWT was calculated for each annual ring (RW), its earlywood and latewood, and for all ten sectors of each tree. The parameter data from the individual series were detrended using a 100 years spline, and then the average standard chronologies of all 20 trees were calculated using ARSTAN software. Furthermore, a sensitivity parameter was calculated for each chronology (Carrer and Urbinati 2006), characterizing the fluctuation of the data series, as the average absolute percentage change in the value of the relevant parameter for the annual ring compared to the value for the previous annual ring. In order to show the differences in the long-term CWT trend of earlywood and latewood, the course of CWT chronologies was approximated via a polynomial function of the sixth degree and shown in the graph.

Using XLSTAT software, a Principal Component Analysis (PCA) was carried out for all chronologies of parameters covering the common period from 1870 to 2015. The obtained chronologies were further correlated with temperature, precipitation and the SO_2 air concentrations. For the temperature, a time series with monthly averages from 1891 was available from the Fichtelberg station, whilst for precipitation the station data was from 1947, the CRU TS 4.04 (Climatic Research Unit, 2021) grid data was from 1901, and daily concentrations from 1970 were available for SO_2, which were obtained by combining data from the Blatno and Měděnec stations. The chronologies of the parameters were correlated with the monthly values of climatic parameters and the SO_2 series for the longest possible time period. In order to verify the stability of the climate–growth relationship over time, running correlations were calculated with a thirty-year window in five-year steps.

RESULTS

The strongest reaction to the air pollution stress in the 1980s is evident for MRW, where we can observe a rapid decline in values since the late 1960s, as well as increased variability (Fig. 4). The values of LA and CWT show an incomparably smaller reaction to such stress. There is only a slight decrease in the LA values.

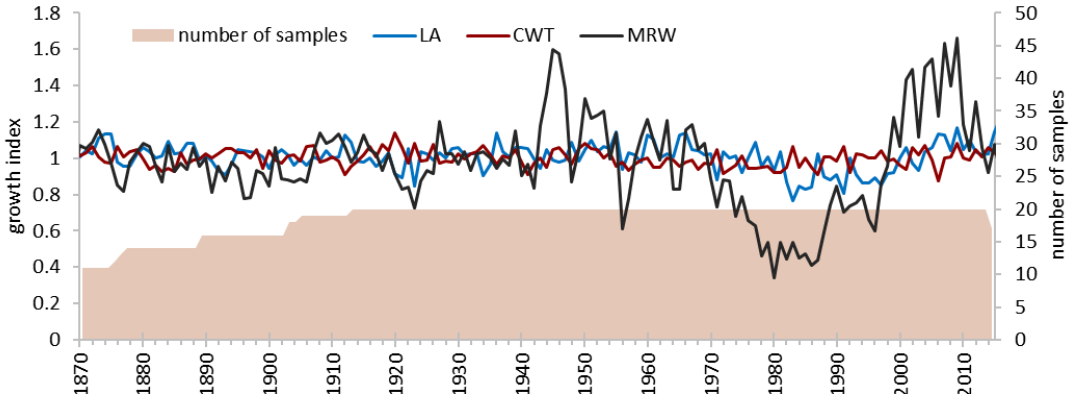

Fig. 4: Comparison of annual mean chronologies of studied parameters.

The course of the LA earlywood and latewood chronologies is very similar, but the LA latewood chronology shows higher variability (Fig. 5). The sensitivity for EW is 4.1%, and for LW 9.4%. A separate representation of the LA chronologies shows a decrease in values during the stress period.

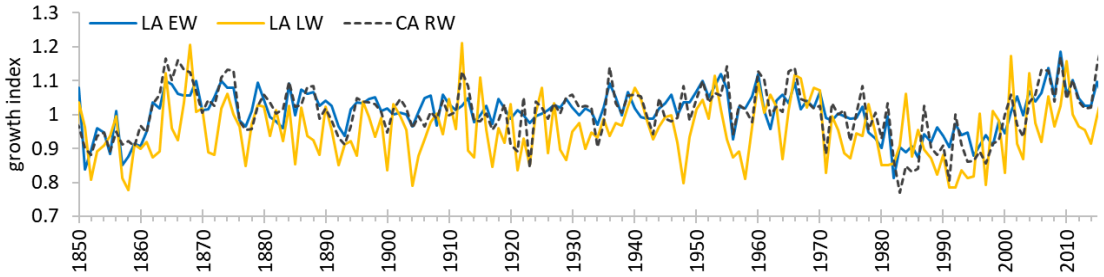

Fig. 5: Comparison of lumen area chronologies for earlywood, latewood and whole ring.

The CWT chronologies indicate similar fluctuations, but they differ in their course. Although no decrease in CWT is evident during the stress period, the course of the chronology of CWT for EW practically never exceeds the course of the chronology of the CWT for LW except for the stress period (Fig. 6). For a better representation, both chronologies in Fig. 7 are approximated by a polynomial function of the sixth degree. Herein we can better see the intersection of the CWT chronologies for early and late wood from the early 1960s to approximately the end of the millennium.

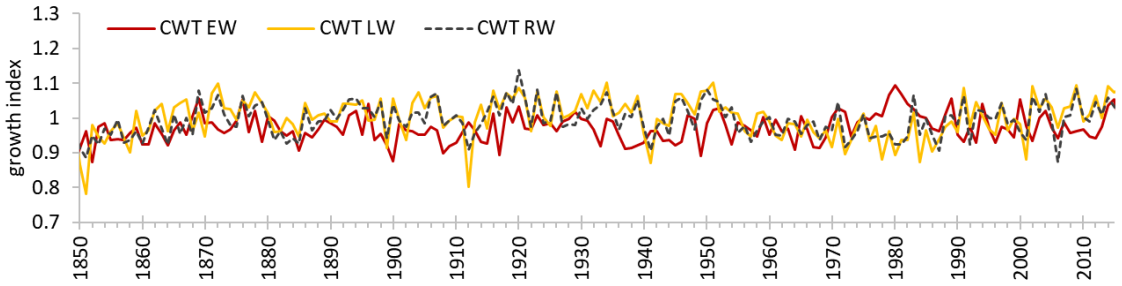

Fig. 6: Comparison of cell wall thickness chronologies for earlywood, latewood and whole ring.

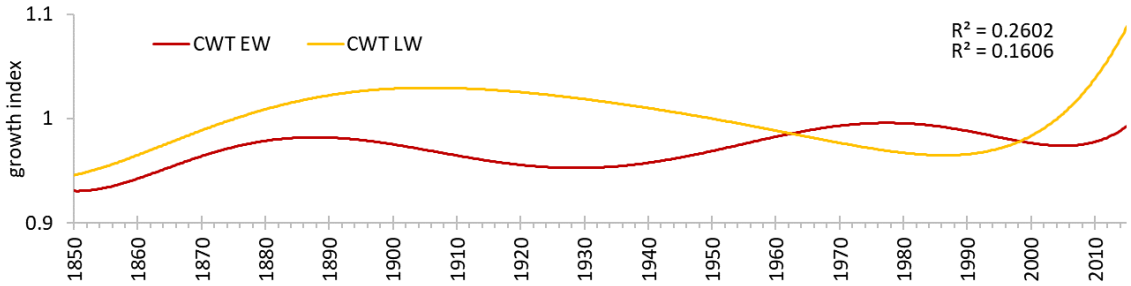

Fig. 7: Approximation of the long – term trend of cell wall thickness values for earlywood and latewood.

The LA chronology for individual sectors is shown in Fig. 8. The growth index is offset by a value of 0.5 for each subsequent chronology. It is clear that their volatility is gradually increasing. The first sector, corresponding to the beginning of xylem growth (LA1), has a sensitivity parameter of 4.8%, whereas the last (LA10) has a sensitivity parameter of 24.0%. The decrease in values during the stress period is also most evident in the last sectors.

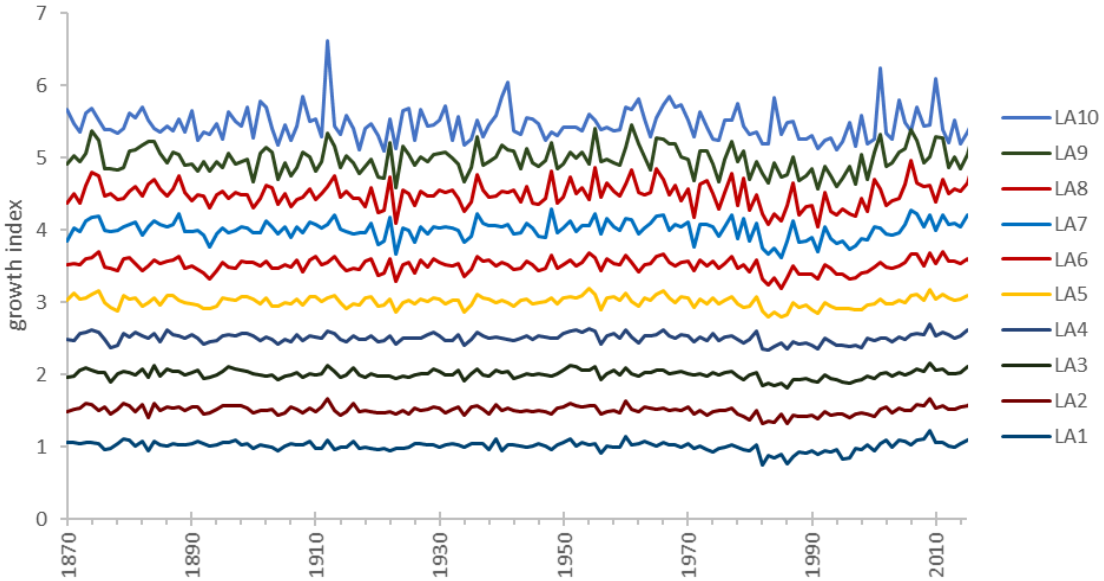

Fig. 8: Mean lumen area chronology for each of the ten sectors.

In CWT, on the other hand, the increase in sensitivity from the first to the last sectors is not as large. The first sector (LA1) has a sensitivity parameter of 2.8% and the sector with the highest value sensitivity parameter (LA8) is 9.2%. This parameter rises sharply between the sixth (LA6) and seventh (LA7) sectors from 4.7% to 8.3%. In the last sectors, there is only a slight decrease in the values of the growth index during the stress period. The growth index is offset by 0.25 for each subsequent chronology.

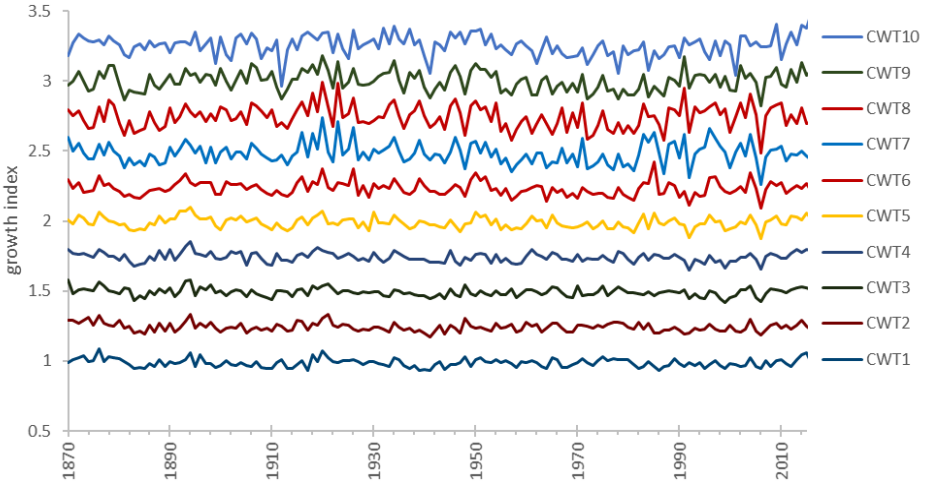

Fig. 9: Mean cell wall thickness chronology for each of the ten sectors.

The PCA shows that with regard to the LA, the adjacent sectors show a high degree of similarity (Fig. 10). With regard to CWT, the sector vectors are arranged more randomly and, unlike the LA, there is a higher similarity between more distant sectors. The MRW parameter correlates well with the first LA sectors. The first four components of the PCA analysis explain 81.2% of the data variability - the first component explains 35.8%, the second 24.7%, the third 12.1% and the fourth 8.5%.

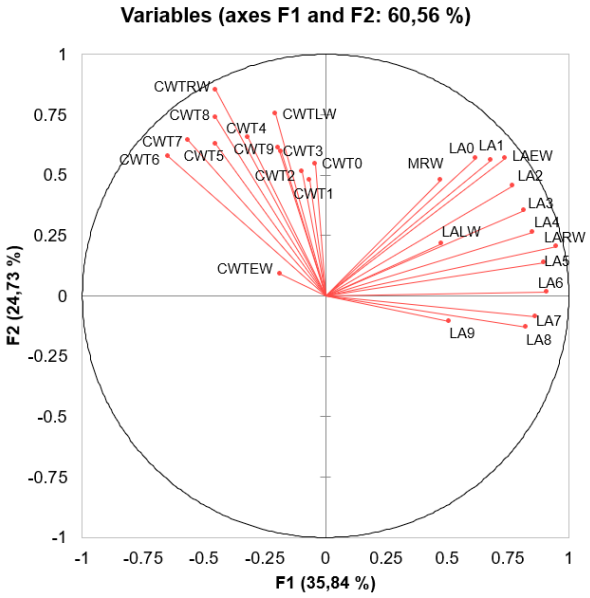

Fig. 10: Loading plot of first two components of PCA analysis.

In Fig. 11 we can see the correlations of all chronologies with SO_2 air concentrations in individual months for the period from 1970 to 2015. For comparison, the MRW chronology is plotted for both parameters, which shows high correlation with all monthly and the annual and winter average of these concentrations. We can see that the LA chronologies correlate best in the first sectors, which is also reflected in the EW and RW chronologies, and thereafter the correlation gradually weakens and no longer correlates in the final sector. We find the exact opposite with regard to correlations with the chronologies of the CWT parameter - the last sector correlates best, which is also reflected in the LW chronology.

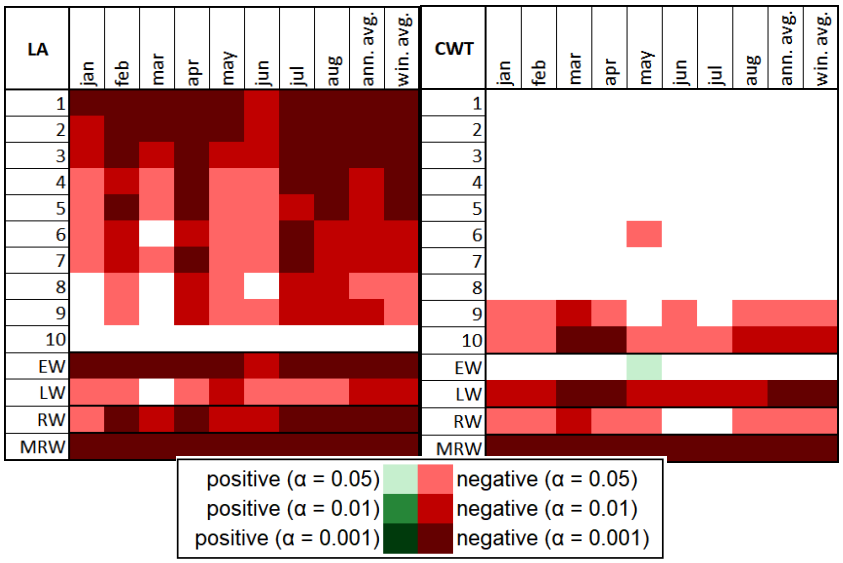

Fig. 11: Correlation of anatomical parameters chronologies with monthly, annual and winter SO_2 air concentration for the period 1970 – 2015.

Running correlations of anatomical parameters with precipitation did not show any valuable relationship. A strong negative correlation during the stress period appeared in the last few CWT sectors for LW in July, and a positive correlation during the same month with the LA in the second half of the annual ring. The running correlation of the temperature from the Fichtelberg station with the chronologies of the parameters is shown in Fig. 12. The top line always shows the middle year of the thirty-year window. For comparison, the correlation with MRW is also shown in all correlation matrices. With the exception of the post-stress period, the LA negatively correlates in the latter months (July – August) with the second half of the sectors in almost all windows. This correlation is evident at the sector level. It is also noticable in LW and RW, but not in all windows. During the stress period (1960-1990), the LA in the middle part of the annual ring correlates positively with the June temperature. For the post-stress period (1995-2015), there is only a positive correlation between the LA and the temperature in April, but in almost all of the sectors except the last, which can be seen both at the level of EW and at the level of the RW. The correlation of the CWT with the temperature in the summer months (July – August) during the stress period is also interesting. In the sectors in the first half of the annual ring the CWT correlates negatively with the temperature, whilst a positive correlation was demonstrated for the CWT in the second half of the annual ring. The second mentioned

correlation is clearly evident at the level of LW and RW, but the first correlation has not reflected into these levels. Furthermore, we can see that the CWT in the second half of the sectors correlated positively with the temperature in the first half of the last century (most strongly in the middle sectors), but in the subsequent period this relationship weakens and there is a positive correlation between temperature and the CWT in May in the last three sectors, with the strongest being in the 9th and 10th sectors. The correlation of temperatures with MRW is in most cases weaker than the correlation with anatomical parameters. However, none of the correlations of any of the parameters are stable throughout the observed period.

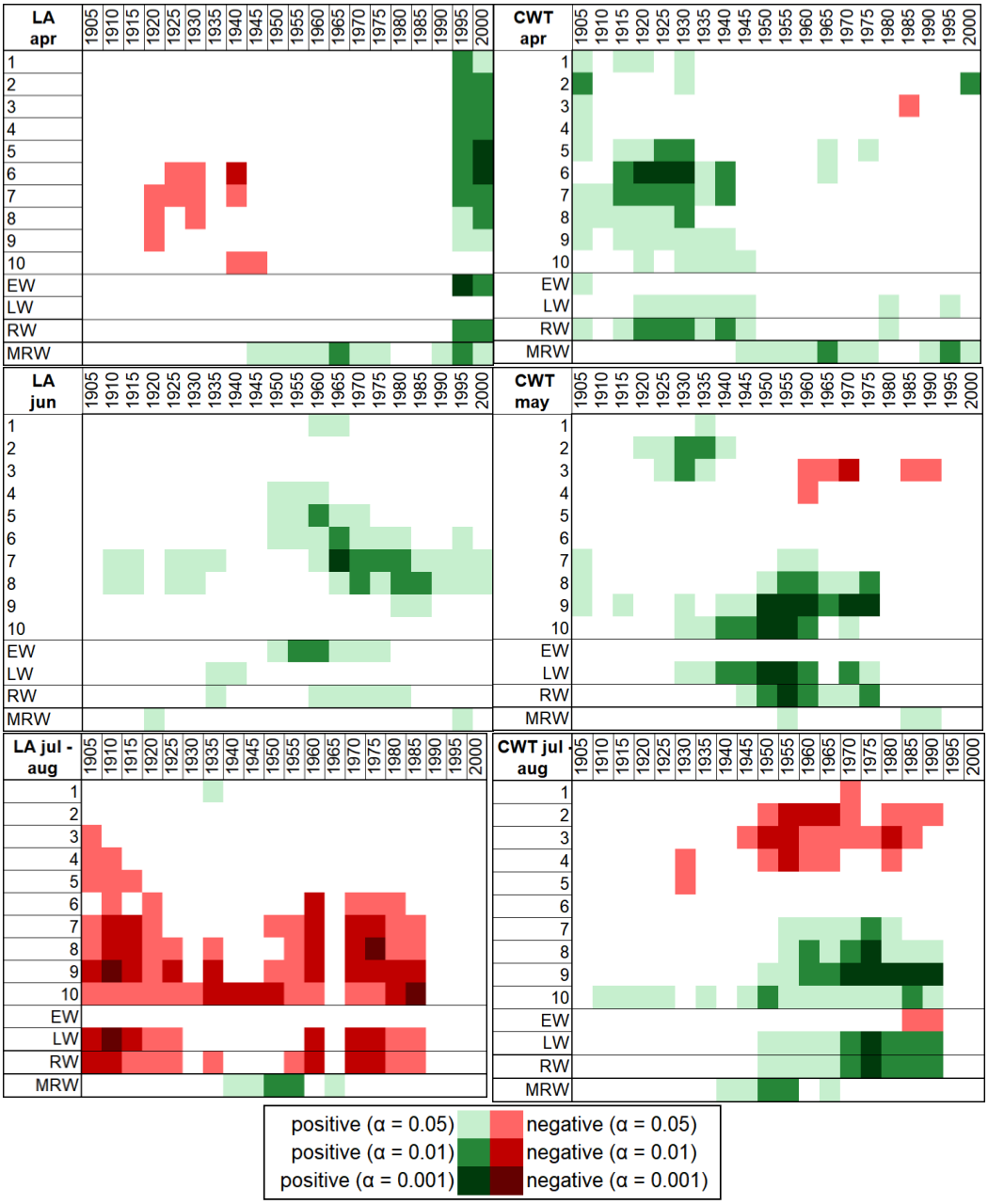

Fig. 12: Running correlation of anatomical parameters chronologies with monthly mean temperatures for the period 1891 – 2015.

Fig. 13 shows the running correlation of the LA with July and August temperatures. The sectors in the middle part of the annual ring correlate with the July temperature, whereas only the last sectors correlate with the August temperature.

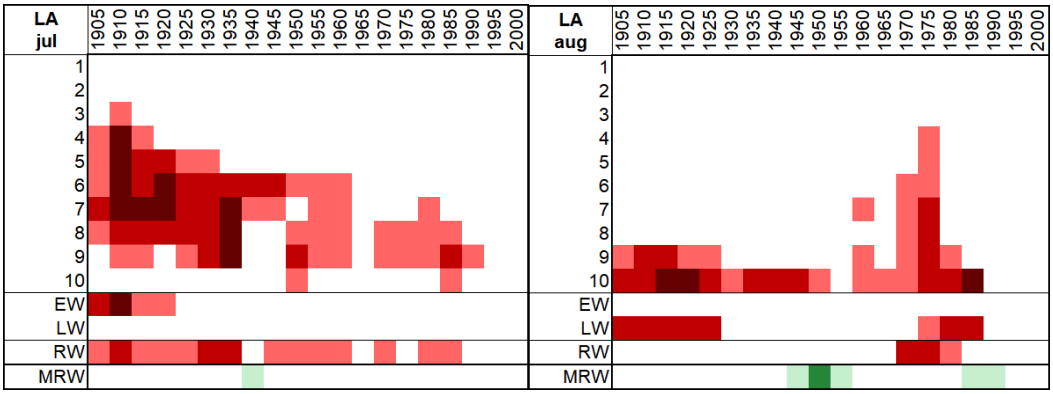

Fig. 13: Comparison of the correlation of lumen area with the mean temperature of two consecutive months.

DISCUSSION

As a traditional, quickly and easily measurable parameter, MRW is a very good indicator of stress. This is evident both from the course of the average chronology of this parameter (Fig. 4) and from the correlations with SO_2 (Fig. 11). The sharp increase of MRW values after the end of the stress impact can be due to both the effect of release (Kolář et al. 2015) and high nitrogen depositions (Lomský et al. 2013), or because of the rising temperatures in recent years due to global warming, which prolongs the growth season (Linderholm 2006, Puchi et al. 2020), or it could be a combination of these factors. This effect is also evident to a slightly lesser extent in anatomical parameters.

For the CWT values for EW and LW, approximated by the polynomial function in Fig. 4, we can see their intersection, which defines the stress period relatively accurately timewise. Likely due to the delayed initiation of cambial activity during the stress period (Rajput et al. 2008, Samusevich et al. 2017), cells with as thin cell wall as under normal circumstances are no longer formed at the beginning of the growth season, and therefore their average thickness in EW increases, and the thickness of the cell walls of the LW thin out rapidly, because during the stress period the tree does not have enough resources for the cell walls in the LW to be able to mature to full dimensions. This may be due to the fact that increased SO_2 concentrations damage the assimilation apparatus of trees, thereby reducing photosynthetic activity, which directly affects nutrient availability and the production of growth regulators (Fritts 1976, Kurczyńska et al. 1997). The same trends in the LA and CWT were also confirmed in the sectors approach (Figs. 9 and 10), where we see how their course gradually changes from the beginning to the end of the annual ring. Samusevich et al. (2017) demonstrated that, similarly to the entire MRW, the LA decreases during the stress period. Moreover, this parameter in the EW and the first sectors strongly

positively correlates with the MRW, as can be seen in the results of the PCA analysis in Fig. 10.

With regard to the effects of SO_2 (Fig. 11), the LA of EW is the most affected parameter, which is also related to the fact that this parameter strongly correlates with MRW. There is also an indication that CWT is affected only in the last two sectors, i.e., in the LW, which confirms that the maturation of the cell wall of LW cells is disrupted during the stress period. Compared to the study by Vejpustková et al. (2017), in which the EW parameters were mainly sensitive to pollution, and the study by Axelson et al. (2014), where primarily the LW parameters were sensitive, our study demonstrates that EW was more sensitive in the LA, and LW in CWT.

Due to their distribution, running correlations with precipitation are likely only anticorrelations to temperature. Precipitation is usually not a limiting factor at higher altitudes, and plant phenology is mainly controlled by temperature (Kramer et al. 2000). Interestingly, apart from the significant positive correlation of the LA with the temperature in April, no significant relationship between climatic factors and the investigated parameters was recorded in the last 2-3 correlation windows. This probably means that if a tree is not limited by precipitation or pollution and has enough nutrients and the growing season lengthens with increasing temperature (Linderholm 2006, Puchi et al. 2020), wider annual rings are formed, whose tracheids have lumens with a larger area. Adversely, during the stress and pre-stress period, the high temperature in summer months had a negative effect on the size of the LA, most likely due to the limited availability of water. During the stress period, temperature only had a positive effect on the lumen size of the middle sectors in June. Summer temperatures (July – August) also affected CWT during the stress period. They correlate positively with CWT in last sectors, which what probably means that if the temperature was higher in August, the growing season lengthened and the cells were able to mature to a greater extent. In the warmer years during the pollution period, the nature of EW cells was generally more standard – EW cells have a thinner cell wall during these years, whilst in the period of pollution load, the differences between EW and LW decrease. In this case, the increased sensitivity of the anatomical parameters with regard to temperature in the period of high SO2 concentrations was confirmed (Keller et al. 1984).

The correlation of CWT with the temperature in July to August over individual sectors shows both a positive and a negative relationship within one annual ring (Fig. 12). However, the negative correlation of CWT in the first four sectors was not reflected in the CWT relationship within the entire annual ring, nor within EW. We can therefore examine this relationship only while using the sector method, wherein the annual ring is divided into smaller parts than EW and LW. A comparison of the relationship between the LA and the temperatures of July and August once again shows the benefit of dividing the annual ring into smaller parts, because we are able to examine in detail which part of the annual ring is affected during a specific period (Puchi et al. 2020). Specifically, we can find that the cells of the last sectors were formed mainly in August over the course of the majority of the studied period.

CONCLUSIONS

Mean ring width is very sensitive to pollution. However, this study showed that the anatomical parameters were also affected by the pollution, which is evident from the significant correlations with the pollution, and from the change in the reaction to the climate during the stress and post-stress period. The relationship between earlywood and latewood cell wall thickness was shown as a sensitive indicator. The contradictory trends of these parameters in the culminating pollution period indicates the effect of the stress factor. The presence of pollutants, in particular SO_2, also affects the sensitivity of anatomical parameters to temperature. The greatest disturbance of the xylem formation occurred primarily in years with the combination of high concentrations of SO_2 with low temperature during the growing season. LW cells have thinner cell walls and the difference between CWT for EW and LW is decreasing, and during these years the LA is decreasing throughout the annual ring. Dividing of the annual ring into earlywood and latewood and into smaller sectors gives us a more detailed insight into the relationships between wood production and environmental factors with a higher than annual resolution. Although a number of relationships are already apparent from the average values of the parameters for the entire annual ring, some relationships may remain hidden without this dividing approach.

ACKNOWLEDGEMENT

The research was supported by Internal Grant Agency of the Faculty of Forestry and Wood Sciences [A17/18]. The research was also supported by the Ministry of Agriculture of the Czech Republic, institutional support MZE-RO0118.

REFERENCES

1. Allen, C.D., Macalady, A.K., Chenchouni, H., Bachelet, D., McDowell, N., Vennetier, M., Kitzberger, T., Rigling, A., Breshears, D.D., Hogg, E.H. (Ted), Gonzalez, P., Fensham, R., Zhang, Z., Castro, J., Demidova, N., Lim, J.H., Allard, G., Running, S.W., Semerci, A., Cobb, N., 2010: A global overview of drought and heat-induced tree mortality reveals emerging climate change risks for forests. Forest Ecology and Management 259(4): 660–684.
2. von Arx, G., Carrer, M., 2014: ROXAS – A new tool to build centuries-long tracheid-lumen chronologies in conifers. Dendrochronologia 32(3): 290–293.
3. von Arx, G., Crivellaro, A., Prendin, A.L., Čufar, K., Carrer, M., 2016: Quantitative wood anatomy. Practical guidelines. Frontiers in Plant Science 7: 781.
4. Axelson, J.N., Bast, A., Alfaro, R., Smith, D.J., Gärtner, H., 2014: Variation in wood anatomical structure of douglas-fir defoliated by the western spruce budworm: a case study in the coastal-transitional zone of British Columbia, Canada. Trees 28(6): 1837–1846.

5. Blažková, M., 1996: Black triangle. The most polluted part of central Europe. In: Rijtema, P.E., Eliáš, V., eds. Regional Approaches to Water Pollution in the Environment. Pp 227-249, Springer, Netherlands.
6. Carrer, M., Castagneri, D., Prendin, A.L., Petit, G., von Arx, G., 2017: Retrospective analysis of wood anatomical traits reveals a recent extension in tree cambial activity in two high-elevation conifers. Frontiers in Plant Science 8: 737.
7. Carrer, M., Urbinati, C., 2006: Long-term change in the sensitivity of tree-ring growth to climate forcing in *Larix decidua*. New Phytologist 170(4): 861–872.
8. Castagneri, D., Battipaglia, G., von Arx, G., Pacheco, A., and Carrer, M., 2018: Tree-ring anatomy and carbon isotope ratio show both direct and legacy effects of climate on bimodal xylem formation in *Pinus pinea*. Tree Physiology 38(8): 1098–1109.
9. Castagneri, D., Petit, G., Carrer, M., 2015: Divergent climate response on hydraulic-related xylem anatomical traits of *Picea abies* along a 900-m altitudinal gradient. Tree Physiology 35(12): 1378–1387.
10. Castagneri, D., Regev, L., Boaretto, E., Carrer, M., 2017: Xylem anatomical traits reveal different strategies of two Mediterranean oaks to cope with drought and warming. Environmental and Experimental Botany 133: 128–138.
11. Denne, M.P., 1989: Definition of latewood according to Mork (1928). IAWA Journal 10(1): 59–62.
12. Fiala, J., Bretschneider, B., Materna, J., 2002: Development of the atmospheric pollution and forest decline in the Czech part of the Ore Mts. In: Lomský, B., Materna, J., Pfanz, H. (eds): SO_2-pollution and forests decline in the Ore Mountains. Pp 50-85, Forestry and Game Management Research Institute, Jíloviště-Strnady, Czech Republic.
13. Fonti, P., von Arx, G., García-González, I., Eilmann, B., Sass-Klaassen, U., Gärtner, H. and Eckstein, D., 2010. Studying global change through investigation of the plastic responses of xylem anatomy in tree rings. *The New Phytologist* 185 (1): 42–53.
14. Fritts, H., 1976: Tree rings and climate. Academic Press. San Diego, California, 571 pp.
15. Hůnová, I., Šantroch, J., Ostatnická, J., 2004: Ambient air quality and deposition trends at rural stations in the Czech Republic during 1993–2001. Atmospheric Environment 38(6): 887–898.
16. Keller, T., Rutter, A.J., Elsden, S.R., Bell, J.N.B., Huttermann, A., 1984: Direct effects of sulphur dioxide on trees. Philosophical Transactions of the Royal Society of London. Series B, Biological Sciences 305(1124): 317–326.
17. Kolář, T., Čermák, P., Oulehle, F., Trnka, M., Štěpánek, P., Cudlín, P., Hruška, J., Büntgen, U., Rybníček, M., 2015: Pollution control enhanced spruce growth in the 'Black Triangle' near the Czech-Polish border. The Science of the Total Environment 538: 703–711.
18. Koubaa, A., Zhang, S.Y.T., Makni, S., 2002: Defining the transition from earlywood to latewood in black spruce based on intra-ring wood density profiles from X-ray densitometry. Annals of Forest Science 59(5–6): 511–518.
19. Kozlowski, T.T., Kramer, P.J., Pallardy, S.G., 1991: The physiological ecology of woody plants. Academic Press. San Diego, California, 657 pp.

20. Kramer, K., Leinonen, I., Loustau, D., 2000: The importance of phenology for the evaluation of impact of climate change on growth of boreal, temperate and Mediterranean forests ecosystems: an overview. International Journal of Biometeorology 44(2): 67–75.
21. Kroupová, M., 2002: Dendroecological study of spruce growth in regions under long-term air pollution load. Journal of Forest Science 48(12): 536–548.
22. Kubelka, L., 1992: Obnova lesa v imisemi poškozované oblasti severovýchodního Krušnohoří (Restoration of the imission endangered forest in the northeast Krusne hory Mts.) Arospoj, Praha, 133 pp.
23. Kurczyńska, E.U., Dmuchowski, W., Włoch, W., Bytnerowicz, A., 1997: The influence of air pollutants on needles and stems of scots pine (*Pinus sylvestris* L.) trees. Environmental Pollution 98(3): 325–334.
24. Linderholm, H.W., 2006: Growing season changes in the last century. Agricultural and Forest Meteorology 137(1–2): 1–14.
25. Lomsky, B., Sramek, V., Novotny, R., 2013: The health and nutritional status of Norway spruce stands in the Krusne hory Mts. 15 years subsequent to the extreme winter of 1995/96. Journal of Forest Science 59(9):359-369.
26. Materna, J., 1999: Development and causes of forest damage in the Ore Mts. Journal of Forest Science 45(4): 147–152.
27. Olano, J.M., Màrcia, E., García-Cervigón, A.I., Folch, M., Rozas Ortiz, V.F., 2012: Quantitative tracheid anatomy reveals a complex environmental control of wood structure in continental Mediterranean climate. International Journal of Plant Sciences 173(2): 137-149.
28. Pacheco, A., Camarero, J.J., Ribas, M., Gazol, A., Gutierrez, E., Carrer, M., 2017: Disentangling the climate-driven bimodal growth pattern in coastal and continental Mediterranean pine stands. Science of The Total Environment 615: 1518-1526.
29. Park, D., Dallaire, G., Morin, H., 2006. A method for multiple intra-ring demarcation of coniferous trees 63(1): 8-14.
30. Park, D., Spiecker, H., 2005: Variations in the tree-ring structure of Norway spruce (*Picea abies*) under contrasting climates 23(2): 93–104.
31. Puchi, P.F., Castagneri, D., Rossi, S., Carrer, M., 2020: Wood anatomical traits in black spruce reveal latent water constraints on the boreal forest. Global Change Biology 26(3): 1767–1777.
32. Rajput, K.S., Rao, K.S., Kim, Y.S., 2008: Cambial activity and wood anatomy in *Prosopis spicigera* (Mimosaceae) affected by combined air pollutants. IAWA Journal 29(2): 209–219.
33. Rydval, M., Wilson, R., 2012: The impact of industrial SO_2 pollution on north Bohemia conifers. Water, Air, & Soil Pollution 223(9): 5727–5744.
34. Samusevich, A., Lexa, M., Vejpustková, M., Altman, J., Zeidler, A., 2020: Comparison of methods for the demarcation between earlywood and latewood in tree rings of Norway spruce. Dendrochronologia 60: 125686.
35. Samusevich, A., Zeidler, A., Vejpustková, M., 2017: Influence of air pollution and extreme frost on wood cell parameters at mountain spruce stands (*Pice abies* (L.) Karst) in the Ore mountains. Wood Research 62(1): 79–90.

36. Sander, C., Eckstein, D., Kyncl, J., Dobrý, J., 1995: The growth of spruce (*Picea abies* (L) Karst) in the Krkonoše-(Giant) Mountains as indicated by ring width and wood density. Annales des Sciences Forestières 52(5): 401–410.
37. Schweingruber, F.H., 1996: Tree-rings and environment. Swiss Federal Institute for Forest, Snow and Landscape Research. Paul Haupt Verlag. Vienna, 609 pp.
38. Vaganov, E.A., Hughes, M.K., Shashkin, A.V., 2006: Growth dynamics of conifer tree rings: images of past and future environments. Springer. Berlin, 354 pp.
39. Vejpustková, M., Čihák, T., Samusevich, A., Zeidler, A., Novotný, R., Šrámek, V., 2017: Interactive effect of extreme climatic event and pollution load on growth and wood anatomy of spruce. Trees 31(2): 575–586.
40. Wimmer, R., 2002: Wood anatomical features in tree-rings as indicators of environmental change. Dendrochronologia 20(1–2): 21–36.
41. Wimmer, R., Grabner, M., 1997: Effects of climate on vertical resin duct density and radial growth of Norway spruce [*Picea abies* (L.) Karst.]. Trees 11(5): 271–276.
42. Wimmer, R., Halbwachs, G., 1992: Holzbiologische Untersuchungen an fluorgeschädigten Kiefern. Holz als Roh und Werkstoff 50(7–8): 261–267.
43. Ziaco, E., Biondi, F., Rossi, S., Deslauriers, A., 2014: Climatic influences on wood anatomy and tree-ring features of Great Basin conifers at a new mountain observatory. Applications in Plant Sciences 2(10): 140054.
44. Zimermann, F., Lux, H., Reuter, F., Wienhhaus, O., 2002: SO_2 pollution and forest decline in the Ore Mountains – historical aspects, scientific analysis, future developments. In: Lomský, B., Materna, J., Pfanz, H. (eds) SO_2-pollution and forests decline in the Ore Mountains. Pp 86-116, Forestry and Game Management Research Institute, Jíloviště-Strnady, Czech Republic.

MARTIN LEXA*, ALEŠ ZEIDLER
CZECH UNIVERSITY OF LIFE SCIENCES PRAGUE
FACULTY OF FORESTRY AND WOOD SCIENCES
DEPARTMENT OF WOOD PROCESSING AND BIOMATERIALS
KAMÝCKÁ 129
165 00 PRAHA 6 - SUCHDOL
CZECH REPUBLIC
*Corresponding author: lexa@fld.czu.cz

MONIKA VEJPUSTKOVÁ
FORESTRY AND GAME MANAGEMENT RESEARCH INSTITUTE
DEPARTMENT OF FOREST ECOLOGY
STRNADY 136
252 02 JÍLOVIŠTĚ
CZECH REPUBLIC

WOOD RESEARCH doi.org/10.37763/wr.1336-4561/66.4.544555
e-ISSN 2729-8906
66(4): 2021 544-555 pp.

COLOUR STABILITY OF STEAMED BLACK LOCUST, BEECH AND SPRUCE TIMBERS DURING SHORT-TERM PHOTODEGRADATION

DENES VARGA, LASZLO TOLVAJ, EDINA PREKLET
UNIVERSITY OF SOPRON
HUNGARY

(RECEIVED JANUARY 2021)

ABSTRACT

Black locust (*Robinia pseudoacacia* L.), beech red heartwood (*Fagus sylvatica* L.) and spruce (*Picea abies* Karst.) wood samples were treated in saturated steam at 100, 110 and 120°C then irradiated using a UV emitter mercury lamp in order to test their colour stability. Colour change was evaluated and presented in the CIE Lab colour coordinate system. Untreated black locust, beech and spruce specimens as control samples were irradiated using the same mercury lamp. Results revealed that beech produced the greatest colour stability during both steam treatment and the following UV treatment while spruce was the most sensitive species to photodegradation. Steaming reduced the colour change intensity only for black locust during photodegradation. Both redness and yellowness change demonstrate this colour stability increase. Steaming at 120°C resulted in the greatest protection against the colour alteration of black locust caused by photodegradation. The investigated thermal treatments did not change the photodegradation properties of beech and spruce specimens. A considerable increase in colour saturation of the specimens was generated by steaming, and the saturation value further increased during the UV treatment.

KEYWORDS: Steaming, UV irradiation, colour change, extractives.

INTRODUCTION

Industrial scale steam treatment of wood with the aim of colour alteration was started as early as the second half of the last century. Nevertheless, systematic research to discover the specific effects of steaming parameters has been carried out only for the last three decades. In the frame of industrial scale steam treatments, black locust and beech timbers are involved in the largest quantities. Steaming practice demonstrated that steaming of beech is uncomplicated while steaming of black locust is rather difficult due to its peculiar mechanical and anatomical properties such as the extremely high extractive content. This observation

determined that steaming of black locust was the most deeply investigated process (Horváth-Szováti 2000, Tolvaj et al. 2000, 2010, Tolvaj and Molnar 2006, Varga and Van der Zee 2008, Dzurena 2018a). At the same time, steaming behaviour of beech was also widely investigated (Tolvaj et al. 2009, Dzurenda 1013, Milić et al. 2015, Geffert et al. 2017 Dzurenda and Dudiak 2020).

There are few publications regarding the steaming properties of wood species other than beech and black locust. The possible colour variations of cherry wood generated by steam treatment were investigated by Straze and Gorisek (2008) and by Dianiskova et al. (2008). The steaming can reduce the great colour difference between sapwood and heartwood of Turkey oak (Tolvaj and Molnar 2006, Todaro et al. 2012, Csanady et al. 2015). Recently the colour change of poplar (*Populus x euramericana cv. pannonia*) by steaming was investigated to obtain attractive colour suitable for various indoor applications (Banadics and Tolvaj 2019). Steaming was found to be a proper technique to turn the naturally unattractive colour of poplar wood to a pleasant brown colour. Steam was able to double the colour saturation, which is a significant result from the perspective of industrial applications. The treatment increased both redness and yellowness values and reduced the lightness. Steaming behaviour of oak and maple wood was investigated by Dzurenda (2017, 2018b, Dzurenda et al. 2020) for getting attractive brown colour. Geffert et al. (2020) studied the colour change and chemical changes of birch wood during steaming in the 105-135°C temperature interval. Steaming properties of conifers (Scots pine, spruce, larch, sugi) were investigated in the last decade (Tolvaj et al. 2012, 2019, Preklet et al. 2019). Although, they are characterized with a rather low extractive content, depending on the applied steaming parameters, a variety of colours could be created from the initial yellowish to the modified light brown colour. These new colours were similar to the colours of aged indoor wooden constructions and furniture thus providing a fully natural alternative to chemical surface colour modification.

Objective colour measurement helps the researchers to perform exact and detailed investigation in the field of colour modification of wood. This measurement method has widely been applied in the recent past in wood research (Mitsui et al. 2001, 2004, Oltean et al. 2010, Zivkovic et al. 2014). Objective colour co-ordinates allow us to describe the behaviour of different wood species during steam treatment.

Natural wood is sensitive to weathering. Sun radiation is the main factor that induces wood photodegradation primarily through the decomposition of lignin. Although, photodegradation of natural wood is a widely studied phenomenon (Pandey 2005, Popescu et al. 2011, Persze and Tolvaj 2012, Denes and Lang 2013, Zivkovic 2013, Timar et al. 2016, Varga et al. 2017), only two papers were found dealing with the photodegradation behaviour of steamed wood. The effect of UV radiation on native and steamed maple wood was presented in a conference paper (Dzurenda et al. 2020). The change in the lightness coordinate L* was opposite for native and steamed wood. While native maple wood darkened, steamed maple wood faded. Other researchers claimed that steaming enhanced the redness stability of poplar wood against UV irradiation and slightly reduced the yellow colour sensitivity to photodegradation (Banadics et al. 2019).

Steam treated timber with an attractive brown colour is favourable used for outdoor applications. Therefore, it is considered to be important to gain information on the stability of this modified colour. The aim of this study was to discover the colour stability of steamed wood species with different extractive content during photodegradation.

MATERIALS AND METHODS

Black locust (*Robinia pseudoacacia* L.), beech red heartwood (*Fagus sylvatica* L.) and spruce (*Picea abies* Karst.) specimens were used for the tests. The specimen size was 150 × 25 × 15 mm (L × R × T). The radial surface was used for colour measurement. Initial moisture content of the specimens was between 9 and 10% before steaming. The steaming was carried out in an autoclave to keep the pressure generated by the steam. Wood specimens were placed in the autoclave with distilled water at the bottom for conditioning the air to maintain maximum relative humidity. The chosen steaming temperatures were 100°C, 110°C, and 120°C, the steaming time was 2 days.

Steamed samples were dried at room temperature up to the initial weight to generate equal moisture content for all colour measurements. Steam treated specimens were subjected to photodegradation together with the thermally untreated control specimens. UV light emitter mercury vapour lamp provided the light irradiation. The UV radiation was 80% of the total emissions (31% UV-A, 24% UV-B, and 25% UV-C). The total electric power of the applied double mercury lamps was 800 W, and the distance between the specimens and the light source was 64 cm. The light power density was 76 $J \cdot m^{-2}s^{-1}$ on the surface of the specimens. The irradiation chamber set for 60°C guaranteed ambient temperature conditions. The total irradiation time was 90 h. The irradiation was interrupted after 7, 16, 36, 60, and 90 h to measure the colour change. Colour measurements were carried out with a colorimeter (Konica-Minolta 2600d). The CIE L*, a*, and b* colour coordinates were calculated by applying the D65 illuminant and 10° standard observer with a test-window diameter of 8 mm. The colour of ten randomly chosen dots were measured and averaged for each specimen.

RESULTS AND DISCUSSION

The investigated species were chosen because of their diverse extractive content. Black locust has high extractive content covering 5-9% The main component is dihydrorobinetin covering 2-5% (Molnar and Bariska 2002). The main extractive components of black locust heartwood are the flavonoids which give 89% of the total extractive content. Within flavonoids, dihydrorobinetin is the main component covering 58% of total flavonoid content. Robinetin content covers 14% of the total flavonoid content (Sanz et al. 2011). Extractive content of beech is between 3 and 5%, while that of spruce is 2-3%. Extractive content is important because the colour of wood species is determined mainly by this chemical constituent. Most of the extractives and the hemicelluloses are sensitive to thermal treatment. Results of the thermal treatments are the darkening and the shift of the hue towards brown. The lightness change of black locust is presented in Fig. 1 generated by the applied steaming and UV treatment. The steaming caused great lightness intensity decrease which was

determined by the steaming temperature. The two-day steaming produced 20%, 38% and 54% lightness decrease generated by 100°C, 110°C and 120°C steaming temperatures, respectively. The same data for spruce (Fig. 2) were 14%, 19% and 24%. The beech showed different behaviour. The lightness change was slightly temperature dependent and the maximum lightness decrease was 15%. The reason might be that the two-day steaming was too long for beech. In industrial practice, the steaming time for beech is maximum one day. Steam generated chromophore molecules may suffer further degradation during the relatively long steaming period. The two-day steaming period was chosen as an average. (It was long for beech and short for spruce.)

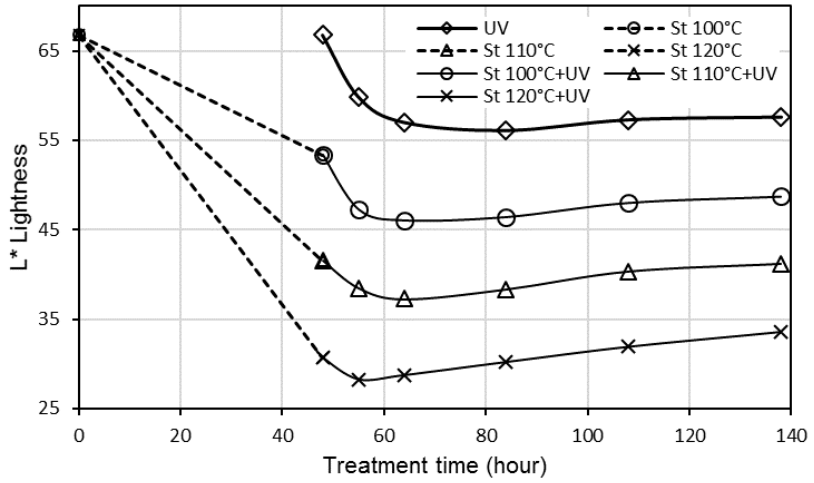

Fig. 1: Lightness change of unsteamed (UV) and steamed (St) black locust specimens caused by steaming and UV irradiation.

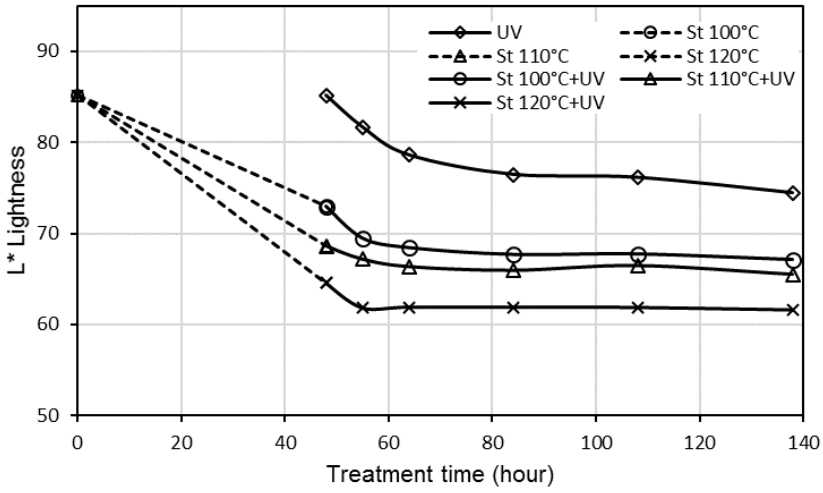

Fig. 2: Lightness change of unsteamed (UV) and steamed (St) spruce specimens caused by steaming and UV irradiation.

All of the unsteamed control specimens showed intensive lightness decrease during the first 16 hours of the UV treatment. The lightness hardly changed after this irradiation period except in the case of spruce specimens where a slow but continuous lightness decrease was observed in the 64-138-hour treatment period (Fig. 2). Steam treated specimens showed similar lightness change as the unsteamed specimens during UV irradiation. The decrease was

smaller at the beginning of the UV irradiation and also the period of the decrease became shorter. The lightness value of steamed black locust increased after 10-hour UV irradiation. The UV irradiation caused small lightening for the specimens steamed at 120°C compared to the lightness generated by the steaming. The lightness of beech and spruce samples remained constant in the 16-90-hour UV irradiation period. Results demonstrated that the steamed wood specimens were less sensitive to the darkening effect of photodegradation than the unsteamed ones.

The applied steam treatments resulted in substantial redness increase in the case of back locust and spruce specimens (Figs. 3-4). The two-day steaming produced 71%, 52% and 63% redness value increase generated by 100°C, 110°C and 120°C steaming temperatures, respectively. The same data for spruce were 153%, 172% and 181%. The redness increase of spruce followed the trend of temperature increase while no such rule could be observed in the case of black locust. Most probably this is because steam generated chromophore chemical groups in this wood species are highly sensitive to thermal degradation (Tolvaj et al. 2010). It was found that the redness of black locust timber tends to decrease after one-day steaming if the temperature is above 100°C. That is why the steaming at 100°C caused bigger redness increase than at 110°C and 120°C. The beech showed moderate redness increase during steaming and the change was hardly temperature dependent. The largest redness increase was 22% produced by steaming at 100°C.

The UV irradiation generated rapid redness increase in unsteamed black locust specimens during the first 7 hours of irradiation and the increase was moderate afterward (Fig. 3).

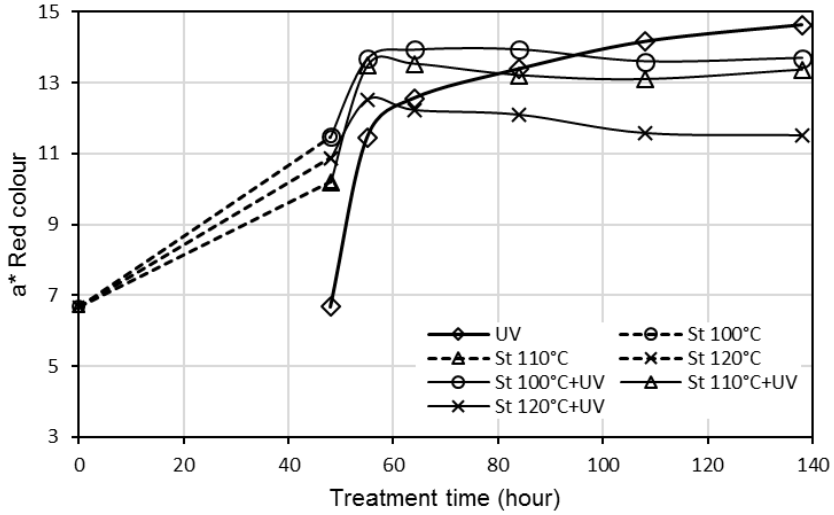

Fig. 3: Redness change of unsteamed (UV) and steamed (St) black locust specimens caused by steaming and UV irradiation.

Unsteamed beech and spruce specimens showed almost linear red colour increase during the whole 90-day UV irradiation period. Red colour values of steamed beech specimens were equal in the 84-138-hour treatment interval (UV) independently of the previous steaming process. Steamed spruce specimens presented similar photodegradation behaviour as beech regarding redness increase, with the difference that the dots representing the red colour of spruce were far from each other after steaming. Consequently, the functions of redness values

were parallel (Fig. 4). The only exception was the redness change of specimens steamed at 120°C. The redness barely changed in the 48-84-hour treatment period and moved parallel to the other lines afterwards. It can be concluded that steaming improved the redness stability only in the case of black locust. Steaming at 120°C provided the most stable red colour against UV irradiation.

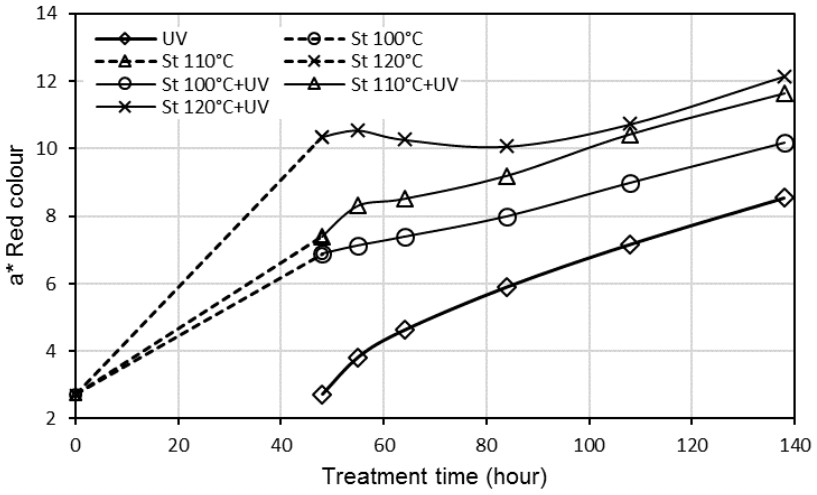

Fig. 4: Redness change of unsteamed (UV) and steamed (St) spruce specimens caused by steaming and UV irradiation.

The applied steam treatments reduced slightly the yellowness of black locust (Fig. 5). Beech specimens also suffered moderate yellowness intensity change but unlike black locust it was a temperature-independent increase (Fig. 6). Spruce specimens suffered considerable yellowness increase. The two-day steaming induced 40%, 70% and 76% yellowness value increase at 100°C, 110°C and 120°C steaming temperatures, respectively.

The UV irradiation caused rapid yellowness intensity increase during the first 7 hours of irradiation, followed by slow and linear increase afterward on the surface of all unsteamed control specimens. Comparing steamed and unsteamed black locust samples, the applied steaming reduced considerably the yellow colour coordinate increase generated by UV irradiation (Fig. 5). Moreover, steam treatment at 120°C was able to hinder further yellow colour change, so that the UV irradiation hardly influenced the yellow colour of black locust. The results showed that steaming improved the yellowness stability of black locust against UV irradiation. The yellowing effect of UV irradiation was somewhat smaller for steamed beech specimens than for unsteamed ones (Fig. 6). UV light induced yellow colour change of steamed spruce was similar to that of beech with the only difference in the starting point distribution (generated by steaming). The biggest distance between the yellowness values of unsteamed and steamed specimens (before UV irradiation) was 34 and 4 units for spruce and beech, respectively. As a consequence, trend lines were parallel and were farther to each other for spruce than for beech. These results demonstrate that preliminary steam treatment does not influence the UV irradiation induced yellow colour shift of beech and spruce specimens. UV irradiation test results showed that steaming improved the yellow colour stability of black locust. The yellowing of wood during UV irradiation is generated mainly by the degradation of lignin. Previous study demonstrated that the high extractive content of black locust partly

protected the lignin against UV degradation (Tolvaj and Varga 2012). Present results strengthen this finding as well. Unsteamed black locust, beech and spruce specimens produced 10, 14 and 23 units of yellowness increase during 90-hour UV irradiation, respectively. The order of the extractive content of the investigated species is the opposite of the order of yellowness increase. Fig. 5 demonstrates that the steaming modified new extractives are also able to protect the lignin against photodegradation. To verify this finding further chemical investigations need to be done.

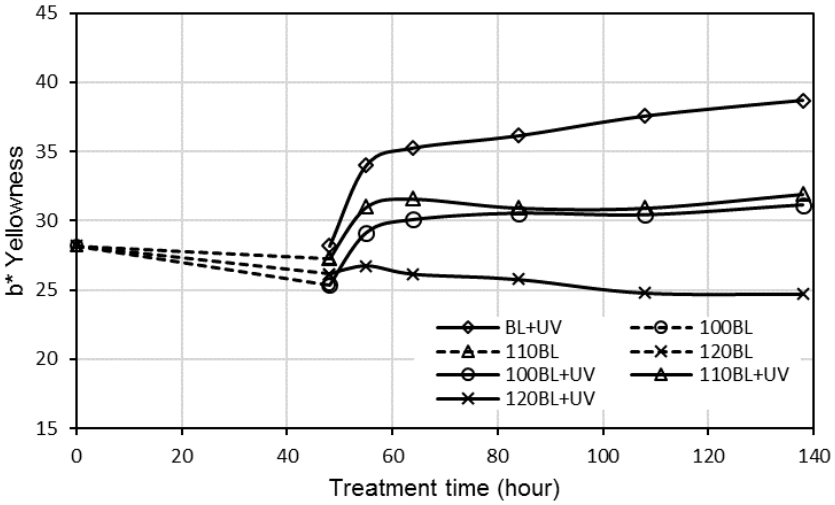

Fig. 5: Yellowness change of unsteamed (UV) and steamed (St) black locust specimens caused by steaming and UV irradiation.

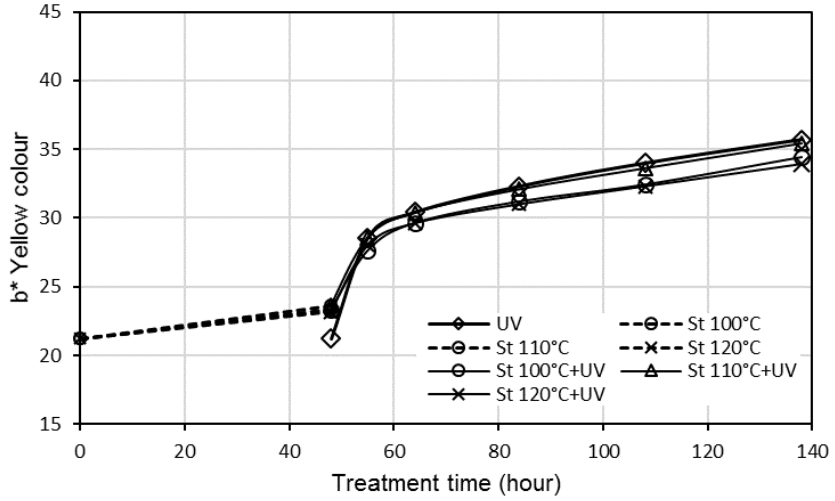

Fig. 6: Yellowness change of unsteamed (UV) and steamed (St) beech specimens caused by steaming and UV irradiation.

Shifting of colour coordinates on the a*-b* plane visualise the combined effect of steaming and UV irradiation (Figs. 7-9). This type of presentation gives the possibility to compare redness and yellowness changes. Dotted lines demonstrate the colour change caused by steaming (start and end points only), while solid lines represent the colour modification effects of the UV irradiation. The distance from the origin (0, 0) on the a*-b* plane provides the saturation value of the individual colour dots. Figs. 7-9 demonstrate that both steaming

and UV irradiation increased the saturation value considerably. The hue angle altered between 77-65°, 73-67° and 83-73° for black locust, beech and spruce, respectively. The hue alteration of black locust was twice as large as that of beech. This large hue change was generated by the steaming. The visual colour changed from the greyish yellow to chocolate brown. This alteration reflects the high sensitivity of the extractives in black locust to thermal degradation. The size of the diagram area covered by the presented colour dots represents the colour stability of the tested specimens. Small occupied area shows good colour stability. Among the investigated species, beech presented the highest colour stability against both steaming and UV irradiation (Fig. 8). Steaming did not change the sensitivity of beech to UV irradiation. Trend lines of steamed and unsteamed specimens were parallel close to each other during UV irradiation.

Unsteamed black locust produced moderate yellowness change and intensive redness value increase during the treatments. Fig. 7 presents clearly that the steaming improved the colour stability of black locust against UV treatment.

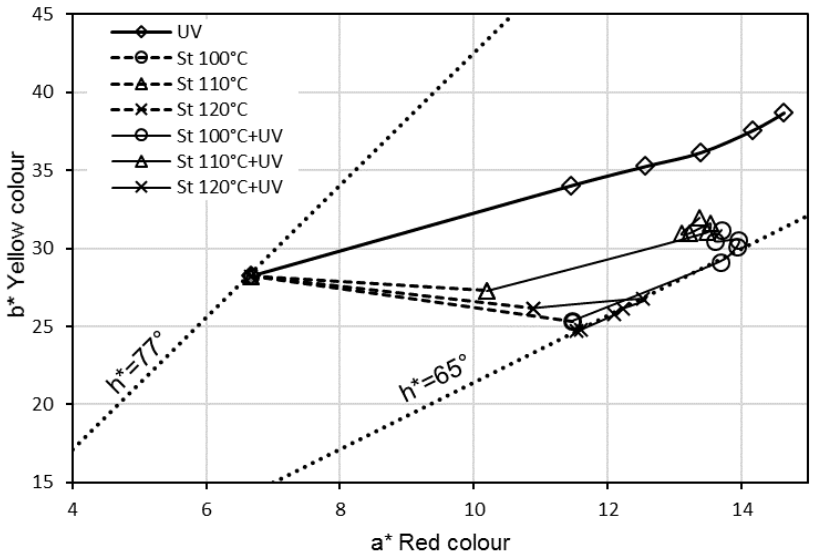

Fig. 7: Demonstration of the colour shift of black locust on the red colour (a) - yellow colour (b*) plane generated by steaming (St) and UV light irradiation.*

The colour parameters hardly changed after 7-hour UV irradiation. The colour of spruce specimens was sensitive to both steaming and UV irradiation (Fig. 9). Out of the three investigated wood species, spruce suffered the largest colour change generated by both steaming and UV irradiation. Unsteamed spruce specimens showed the highest sensitivity to UV irradiation. The low extractive content of this species was unable to reduce the effect of photodegradation. Steaming did not affect this sensitivity.

Results show that beech provided the highest colour stability during the treatments. Steaming reduced the photodegradation intensity only in the case of black locust. Spruce was the most sensitive species to photodegradation. Results strengthen the important role of extractives in photodegradation. The distance from the origin (0, 0) on the a*-b* plane provides the saturation value of the individual colour dots. Figs 7-9 demonstrate that both steaming and

UV irradiation elevated the saturation value considerably. Spruce produced the greatest and beech the smallest saturation increase.

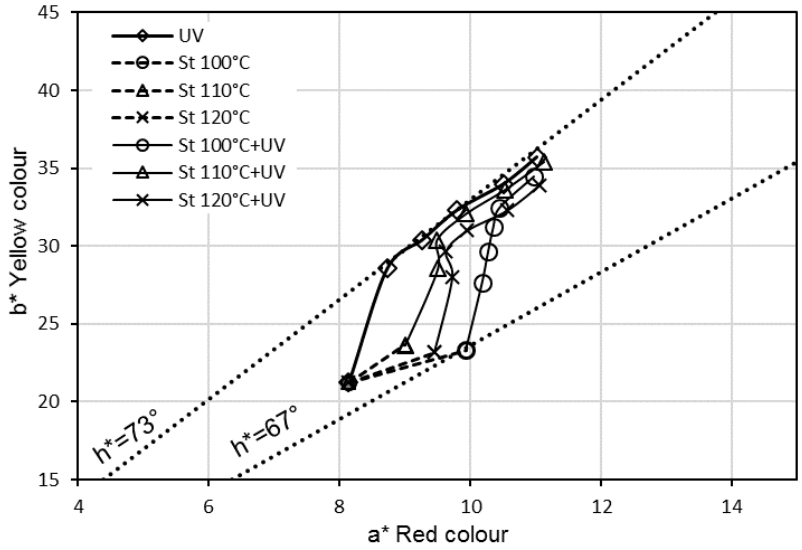

Fig. 8: Demonstration of the colour shift of beech on the red colour (a) - yellow colour (b*) plane generated by steaming (St) and UV light irradiation.*

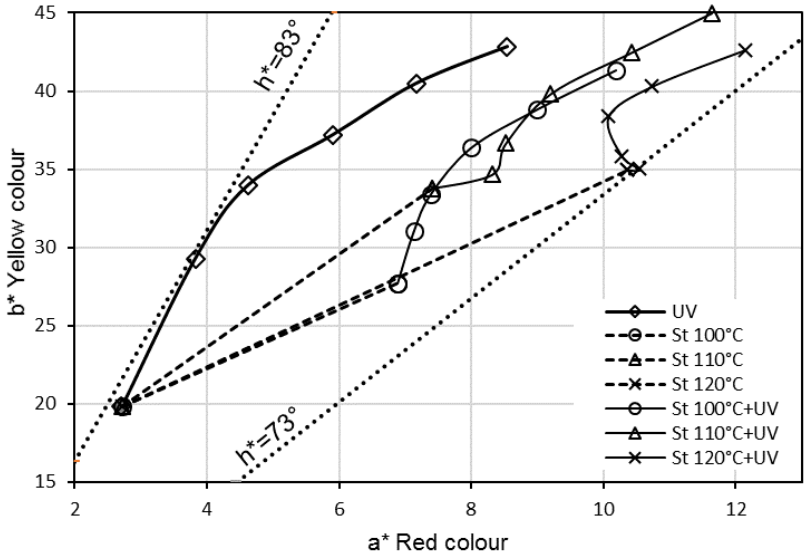

Fig. 9: Demonstration of the colour shift of spruce on the red colour (a) - yellow colour (b*) plane generated by steaming (St) and UV light irradiation.*

CONCLUSIONS

Untreated and steamed black locust, beech and spruce specimens were irradiated by UV emitter mercury lamp to test the colour stability of wood species featuring different extractive content. Colour changes were monitored by objective colour measurements and the colour data were presented in the CIE Lab system. Results revealed that beech had the greatest colour stability during the treatments while spruce was the most sensitive species to photodegradation. Steaming reduced the UV light induced colour change intensity only in the case of black locust imparting a higher colour stability thanks to its high extractive

content. Results also demonstrated that the steamed wood specimens were less sensitive to the darkening effect of photodegradation than the unsteamed ones.

Steaming reduced the sensitivity of black locust against UV irradiation concerning red colour shift. In contrast, the redness change was similar for both unsteamed and steamed beech and spruce specimens.

High extractive content of black locust was able to reduce the intensity of lignin degradation during UV irradiation monitored by the yellowness change. Steam generated extractives also showed this protecting effect in treated black locust specimens. Steaming at 120°C provided the most efficient protection.

Steaming generated considerable increases in colour saturation of the specimens, and the saturation value increased further during the UV treatment.

ACKNOWLEDGEMENT

This article was made in frame of the „EFOP-3.6.1-16-2016-00018 – Improving the role of research+development+innovation in the higher education through institutional developments assisting intelligent specialization in Sopron and Szombathely".

REFERENCES

1. Banadics, E.A., Tolvaj, L., 2019: Colour modification of poplar wood by steaming for brown colour. European Journal of Wood and Wood Products 77: 717–719.
2. Csanady, E., Magoss, E., Tolvaj, L., 2015: Quality of machined wood surfaces. Pp 171-173, Springer.
3. Denes, L., Lang, E.M., 2013: Photodegradation of heat treated hardwood veneers. Journal of Photochemistry and Photobiology B: Biology 118: 9-15.
4. Dianisková, M., Babiak, M., Tolvaj, L., 2008: Colour homogenisation of cherrywood (*Cerasus avium* L.) and black locust (*Robinia pseudoacacia* L.) during steaming. Wood Research 53(4): 45-58.
5. Dzurenda, L., 2013: Modification of wood colour of *Fagus sylvatica* L to a brown-pink shade caused by thermal treatment. Wood Research 58(3): 475-482.
6. Dzurenda, L., 2017: Modification of wood colour of *Acer platanoides* L. to a brown-red shade caused by thermal treatment. Forestry and Wood Technology 98: 26-32.
7. Dzurenda, L., 2018a: Colour modification of *Robinia pseudoacacia* L. during the processes of heat treatment with saturated water steam. Acta Facultatis Xylologiae Zvolen 60(1): 61−70.
8. Dzurenda, L., 2018b: The shades of color of *Quercus robur* L. wood obtained through the processes of thermal treatment with saturated water vapour. BioResources 13(1): 1525-1533.
9. Dzurenda, L., Geffert, A., Geffertova, J., Dudiak, M., 2020: Evaluation of the process thermal treatment of maple wood saturated water steam in terms of change of pH and color of wood. BioResources 15(2): 2550-2559.

10. Dzurenda, L., Dudiak, M., 2020: Changes in wood tree species *Fagus sylvatica* L. and characteristics of the thermal process of modifying its color with saturated water steam. Advances in Ecological and Environmental Research 5(04): 142-156.
11. Dzurenda, L., Dudiak, M., Banski, A., 2020: Influence of UV radiation on color stability of natural and thermally treated maple wood with saturated water steam. In: Tenth international scientific and technical conference "Innovations in Forest Industry and Engineering Design" – INNO 2020, 1–3 October 2020. Pp 219-224, Vitosha park hotel, Sofia, Bulgaria.
12. Geffert, A., Vybohová, E., Geffertová, J., 2017: Characterization of the changes of colour and some wood components on the surface of steamed beech wood. Acta Facultatis Xylologiae Zvolen 59(1): 49−57.
13. Geffert, A., Geffertova, J., Vybohova, E., Dudiak, M., 2020: Impact of steaming mode on chemical characteristics and colour of birch wood. Forests 11(4): 478, 12 pp.
14. Horváth-Szováti, E., 2000: A gőzölt akác világosság-változásának hőmérséklet- és időfüggése (Temperature and time dependence of lightness change of steamed black locust) (in Hungarian with English and German abstracts). SE Tudományos Közleményei 46: 179-189.
15. Milić, G., Todorović, N., Popadić, R., 2015: Influence of steaming on drying quality and colour of beech timber. Glasnik Šumarskog Fakulteta 83-96.
16. Mitsui, K., Takada, H., Sugiyama, M., Hasegawa, R., 2001: Changes in the properties of light-irradiated wood with heat treatment. Part 1. Effect of treatment conditions on the change in color. Holzforschung 55: 601-605.
17. Mitsui, K., Murata, A., Tsuchikawa, S., Kohara, M., 2004: Wood photography using light irradiation and heat treatment. Color Research Applications 29: 312-316.
18. Molnar, S., Bariska, M., 2002: Wood species of Hungary. Szaktudás Kiadó Ház, Budapest.
19. Oltean, L., Hansmann, C., Nemeth, R., Teischinger, A., 2010: Wood surface discolouration of three Hungarian hardwood species due to simulated indoor sunlight exposure. Wood Research 55: 49-58.
20. Pandey, K. K., 2005: Study of the effect of photo-irradiation on the surface chemistry of wood. Polymer Degradation and Stability 90: 9-20.
21. Persze, L., Tolvaj, L., 2012: Photodegradation of wood at elevated temperature: Colour change. Journal of Photochemistry and Photobiology B: Biology 108: 44-47.
22. Popescu, C.M., Popescu, M.C., Vasile, C., 2011: Structural analysis of photodegraded lime wood by means of FT-IR and 2D IR correlation spectroscopy. International Journal of Biological Macromolecules 48: 667-675.
23. Preklet, E., Tolvaj, L., Banadics, E.A., Alpar, T., Varga, D., 2019: Colour modification and homogenisation of larch wood by steaming. Wood Research 64(5): 811-820.
24. Sanz, M., Fernández de Simon, B., Esteruelas, E., Munoz, A.M., Cadahia, E., Hernández, T., Estrella, I., Pinto, E., 2011: Effect of toasting intensity at cooperage on phenolic compounds in acacia (*Robinia pseudoacacia*) heartwood. Journal of Agricultural and Food Chemistry 59: 3135–3145.

25. Straze, A., Gorisek, Z., 2008: Research on colour variation of steamed cherry wood (*Prunus avium* L.). Wood Research 52(2): 77-90.
26. Todaro, L., Zuccaro, L., Marra, M., Basso, B., Scopa, A., 2012: Steaming effects on selected wood properties of Turkey oak by spectral analysis. Wood Science Technology 46(1-3): 89-100.
27. Tolvaj, L., Horváth-Szováti, E., Safar, C., 2000: Colour modification of black locust by steaming. Wood Research 45(2): 25-32.
28. Tolvaj, L., Molnár S., 2006: Colour homogenisation of hardwood species by steaming, Acta Silvatica et Lignaria Hungarica 2: 105-112.
29. Tolvaj, L., Nemeth, R., Varga, D., Molnar S., 2009: Colour homogenisation of beech wood by steam treatment. Drewno 52: 5-17.
30. Tolvaj, L., Molnár, S., Németh, R., Varga, D., 2010: Colour modification of black locust depending on the steaming parameters. Wood Research 55(2): 81-88.
31. Tolvaj, L., Papp, G., Varga, D., Lang, E., 2012: Effect of steaming on the colour change of softwoods. BioResources 7(3): 2799-2808.
32. Tolvaj, L., Banadics, E.A., Tsuchikawa, S., Mitsui, K., Preklet, E., 2019: Color modification and homogenization of sugi wood by steaming. Asian Journal of Forestry 3(1): 20-24.
33. Varga, D., Van der Zee, M.E., 2008: Influence of steaming on selected wood properties of four hardwood species. Holz als Roh-und Werkstoff 66(1): 11-18.
34. Zivkovic, V., Arnold, M., Radmanovic, K., Richter, K., Turkulin, H., 2014: Spectral sensitivity in the photodegradation of fir wood (*Abies alba* Mill.) surfaces: colour changes in natural weathering. Wood Science and Technology 48: 239–252.

DENES VARGA, LASZLO TOLVAJ*, EDINA PREKLET
UNIVERSITY OF SOPRON
INSTITUTE OF PHYSICS AND ELECTROTECHNICS
BAJCSY ZS. U. 4
HU-9400 SOPRON
HUNGARY
*Corresponding author: tolvaj.laszlo@uni-sopron.hu

WOOD RESEARCH doi.org/10.37763/wr.1336-4561/66.4.556568
e-ISSN 2729-8906
66(4): 2021 556-568 pp.

DECAY RESISTANCE, DIMENSIONAL STABILITY AND MECHANICAL STRENGTH OF POPLAR WOOD MODIFIED WITH PLANT-DERIVED COMPOUNDS

JIAPENG WANG[1], ZHENJU BI[1], ZHANGJING CHEN[1,2], LI YAN[1], YAFANG LEI[1]
[1]NORTHWEST A&F UNIVERSITY
P. R. CHINA
[2]VIRGINIA TECH UNIVERSITY
USA

(RECEIVED AUGUST 2020)

ABSTRACT

The cinnamaldehyde, salicylic acid, stearolic acid and citric acid were plant-derived organic compounds that can be activated to fungi, that could degrade the wood in long term. The compounds with concentrations of 3%, 5% and 7% assisted by different dispersants were impregnated into poplar (*Populus nigra L.*) specimens by the vacuum-pressure method. After that, weight percentage gain (WPG), decay resistance against white-rot fungi (*Trametes versicolor*) and brown-rot fungi (*Gloeophyllum trabeum*), color change, dimensional stability and mechanical properties including modulus of elasticity (MOE) and modulus of rupture (MOR) were measured. The results indicated that cinnamaldehyde impregnated poplar showed antifungi activity against both *G. trabeum* and *T. versicolor*, and citric acid impregnated poplar showed antifungi activity against *G. trabeum*. The color of poplar specimens before and after impregnated cinnamaldehyde and citric acid had a little change, dimensional stability had been improved and mechanical properties especially for MOR increased significantly.

KEYWORDS: Wood preservatives, natural organic compounds, decay resistance, dimensional stability, MOE, MOR.

INTRODUCTION

Wood is a useful natural resource. It can be recycled and reused and plays a significant role in human activities (Teng et al. 2018). For applications, wood is expected to possess certain durability against fungal attacks, as well as a good dimensional stability (Coggins 2008, Ali et al. 2011, Aydin et al. 2015). The application of preservative chemicals is one of the most common wood preservation methods (Mubarok 2019).

The current inorganic preservatives pose the potential risks to the environment and human health (Borges et al. 2000, Khan et al. 2006, Nkansah et al. 2015, Brocco et al. 2017). The safer alternatives have been sought by many researchers. More and more researches on finding nuisance-free wood preservatives have been done. Many plants produced potent natural compounds which might be used as alternatives to protect wood or wood-based materials (Mohammed et al. 2016, Tchinda et al. 2018).

The plant-derived chemicals have low harmful environmental impact. For example, several plant-derived origin compounds have been found to be effective against wood-decaying fungi, such as essential oils (Kartal et al. 2006, Xie et al. 2017), tannins (Anttila et al. 2013, Tondi et al. 2015), flavonoids (Treutter 2006), alkaloids (Wang et al. 2012) and extracts of konjac flying powder (Bi et al. 2019) and coconut shell (Shiny 2018), Cameroonian woods (Tchinda et al. 2018) and eucalyptus (Gonzalez-Laredo et al. 2015).

The four natural organic compounds (cinnamaldehyde, salicylic acid, stearolic acid and citric acid) were selected. They are biodegradable and environment-friendly compared to traditional inorganic preservative. For example, cinnamaldehyde is major compound in the cinnamon essential oil and can be extracted from bark and leaves of cinnamon trees. Salicylic acid was found in willow bark and other plants as endogenous plant hormone (Asghari et al. 2010). Stearic acid can be extracted from palm oil. And citric acid is also distributed in nature widely in the citric trees. These four natural organic compounds have been used in food and cosmetics industries as preservative, or additive in pharmaceutical industry. For example, the cinnamaldehyde could be approved for apply a food flavoring and also had antimicrobial properties to extend food shelf-life (Nostro et al. 2012).

In this study, cinnamaldehyde, salicylic acid, stearolic acid and citric acid were chosen to treat poplar wood to increase the decay resistance of against white-rot fungi (*Trametes versicolor*) and brown-rot fungi (*Gloeophyllum trabeum*). The color change, dimensional stability and mechanical property of treated poplar specimens were recorded. The results of this study can provide the guidance for the natural organic plant-derived compounds as eco-friendly wood preservatives.

MATERIALS AND METHODS

Sample preparation

Poplar (*Populus nigra L.*) log with a height of 180 cm and a diameter of 20 cm at breast height was obtained from poplar plantations in Jiaozuo city, Henan Province, China. Wood specimens were cut into wood blocks. Six repetitions sized 20 mm (R) × 20 mm (T) × 10 mm (L) were chosen for detecting wood decay resistance study, six repetitions sized 20 mm (R) × 20 mm (T) × 20 mm (L) for detecting color and dimensional stability study and ten repetitions sized 20 mm (R) × 20 mm (T) × 300 mm (L) for detecting mechanical property study. The specimens were oven dried at 60°C until constant mass (M_0) which their moisture content reached 8%.

Preparation of impregnated wood

The vacuum-pressure method was used to infuse the solution into wood, using

capsule-shaped vacuum-pressure equipment. Dispersants and dissolution methods of cinnamaldehyde, salicylic acid, stearolic acid and citric acid were listed in Tab. 1. The mixed solutions are formulated into concentrations of 3%, 5% and 7% respectively to impregnate specimens under vacuum condition (-0.08 MPa) for 30 min, followed by 15-min pressure treatment (0.8 MPa). After treatment all specimens were kept in solution for 12 hours. The treated poplar specimens were then oven dried at 60°C until constant mass (M_1).

Tab. 1: Dispersants and dissolution methods for natural organic compounds.

Organic compounds	Dispersant	Solvent	Dissolving temperature	Dissolving method
Cinnamaldehyde	Cetyltrimethylammonium bromide	Water	Room temperature	Ultrasonic processing
Salicylic acid	Sodium lignosulfonate	Water	Room temperature	Ultrasonic processing
Stearolic acid		70% alcohol	60°C	Heat dissolved
Citric acid		Water	Room temperature	Ultrasonic processing

Weight percentage gain (WPG) of poplar samples after impregnation

The WPG was calculated based on the variations in the weight before and after impregnation according to Eq. 1:

$$WPG = (M_1 - M_0) / M_0 \times 100\% \quad (1)$$

where: M_0 - constant mass of poplar specimen before impregnation, (g)
M_1 - constant mass of poplar specimen after impregnation, (g).

Decay resistance determination

Decay resistance of impregnated poplar specimens was evaluated after the treated samples exposed to the white-rot fungus (*Trametes versicolor*) or the brown-rot fungus (*Gloeophyllum trabeum*). The culture bottles were filled with 150 g river sand, 75 g saw-dust, 4.3 g corn flour, 0.5 g brown sugar. 9.4 g maltose was dissolved in 100ml water and it was poured into the culture bottles slowly. Two poplar (*Populus tomentosa*) feeder blocks with dimensions of 22 mm (R) × 22 mm (T) × 3 mm (L) were placed into culture bottles. Culture bottles were then sterilized at 121°C for 1 hour, after prepared. The fungi having grown on potato dextrose agars for 7 days were inoculated on culture bottles. The culture bottles were incubated in darkness at 28°C and 80% relative humidity for 7 days until the feeder blocks full with fungal mycelium.

Impregnated poplar specimens were sterilized at 105°C for 30 min and placed onto feeder blocks in culture bottles. Each culture bottle contained two specimens. Then culture bottles with impregnated poplar specimens were incubated at 28°C and 80% relative humidity for 12 weeks. Six replicates with dimensions of 20 mm (R) × 20 mm (T) × 10 mm (L) were done in each group. After incubation in 12 weeks period, poplar specimens were taken out. The mycelium of fungi wiped off and the samples were dried at 60°C to obtain constant mass (M2). The mass loss (ML) caused by fungi was calculated using Eq. 2, and the decay resistance was determined according to the ASTM rating (ASTM, 2005) (Tab. 2).

$$ML = (M_1 - M_2) / M_1 \times 100\% \quad (2)$$

where: ML - mass loss after decay test, (%)
M_1 - mass of specimen the after impregnation, (g)
M_2 - mass of specimen after decay test, (g).

Tab. 2: Natural decay resistance rating standard of wood established by the ASTM D2017 standard.

Class of decay resistance	Mass loss (%)
Highly resistant	0 - 10
Resistant	11 - 24
Moderately resistant	25 - 44
No resistant	≥ 45

Scanning electron microscopy of decayed wood

A scanning electronic microscope (SEM, Hitachi S-4800, Japan) was used to observe mycelial distribution and the degradation of wood structure caused by fungi. The microscope was operated at acceleration voltage of 20 kV. Small samples sized 10 × 10 × 1 mm^3 were cut from the untreated poplar and decayed poplar and coated with a layer of platinum about 20 nm thick before observation. SEM images of poplar samples impregnated with concentrations of 7% natural organic compounds were chosen in the SEM study.

Color measurement

The surface color measurements of poplar specimens before and after impregnation were recorded with Spectrophotometer CS-820. The color of cross directions was measured. Six clear wood samples without any defects were used as replicates in each concentration of each compound. The L* describes the lightness, a* and b* describe the chromatic coordinates on the green-red and blue-yellow axis, resp. From the L*a*b* values, the difference in the lightness (ΔL*) and chroma coordinates (Δa* and Δb*), and total color difference (ΔE) were calculated using the following Eq. 3 (Bekhta et al. 2003):

$$\Delta E^* = [(\Delta L^*)^2 + (\Delta a^*)^2 + (\Delta b^*)^2]^{1/2} \quad (3)$$
$$\Delta L^* = Li^* - L0^*$$
$$\Delta a^* = ai^* - a0^*$$
$$\Delta b^* = bi^* - b0^*$$

where: ΔE* - the total color difference, ΔL* - the lightness difference before and after impregnation, Δa*- the difference of chromatic coordinates on the green-red axis before and after impregnation, Δb* - the difference of chromatic coordinates on the blue-yellow axis before and after impregnation.

Determination of wood dimensional stability

Poplar specimens with dimensions of 20 mm (R) × 20 mm (T) × 20 mm (L) were divided into treated groups and control groups. Six replicates were chosen in each concentration of each

compound. Treated groups and control groups were oven dried at 60°C until a constant weight. The dimensions of three sections (radial, tangential and cross) were measured and volumes were calculated (V_0). Poplar specimens with a constant weight were respectively stored in a temperature and humidity controlled incubator at 30°C and 65%, 70%, 80%, 85%, 80%, 70%, 65% relative humidity to reach the equilibrium moisture content (EMC). Dimensions of three sections and calculate volumes at above-mentioned different relative humidity were measured (Vw). Volume increase rate was calculated according to Eq. 4:

$$\Delta V = (V_w - V_0) / V_0 \times 100\% \quad (4)$$

where: V_0 - the initial volume of the specimen, (mm^3)

V_w - the volume of the specimen after conditioning, (mm^3).

Mechanical property tests

According to ASTM Standard D143, impregnated poplar specimens with dimensions of 20 mm (R) × 20 mm (T) × 300 mm (L) were tested to failure in third point loading by using a loading speed of 3 $mm \cdot min^{-1}$. Distance between two supports was set to 240 mm. And ten clear poplar specimens were chosen as replicates. Treated groups were impregnated through the above step and oven-dried at 60°C which their moisture content reached 8%. Modulus of elasticity (MOE) and modulus of rupture (MOR) of impregnated specimens and blank control groups were determined using a universal testing machine. Experimental results were statistically analyzed by SPSS Version 17 software (IBM Corp., Armonk, NY, USA). Two-way analysis of variance (ANOVA) and were applied to determine the significant differences at a significance level of $p < 0.05$.

RESULTS AND DISCUSSION

Weight percentage gain (WPG)

WPG of the impregnated poplar specimens were was presented in Fig. 1.

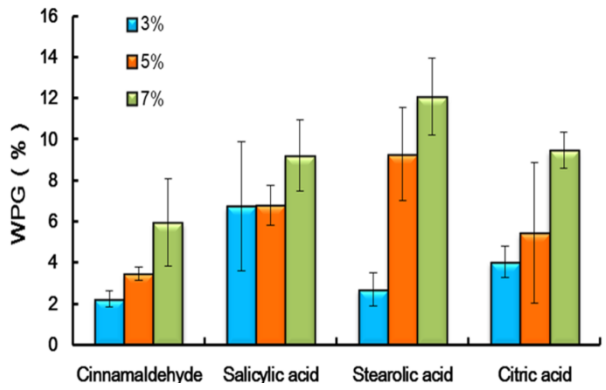

Fig. 1: WPG of the specimens which were impregnated with different concentration of natural organic compounds.

The specimens impregnated with 7% concentration stearolic acid have maximum weight increasing, with their WPG about 12.08%. Specimens impregnated with 3% cinnamaldehyde have the lowest weight gain, and their WPGs were 2.24%. Generally, as the concentration of the compounds raised, the WPGs of the specimens also increased.

Decay resistance and SEM observation of the impregnated poplar

The mass losses and decay rating of impregnated poplar wood attached by *G. trabeum* and *T. versicolor* were presented in Tab. 3. Mass losses in the control group reached 31.93% and 55.98% against *G. trabeum* and *T. versicolor.* These losses would cause considerable reductions in wood properties (Wilcox 1978). Mass losses of poplar specimens impregnated with concentration of 5%, 7% cinnamaldehyde under the culture conditions for *T. versicolor* reached 5.02% and 1.63% respectively. Excellent decay resistances of cinnamaldehyde against both *G. trabeum* and *T. versicolor* were showed, the results were consistent with Yang et al. (2017) who reported that decay resistance rating reached highly resistant for *Populus ussuriensis* Kom. impregnated with 50 $mg \cdot ml^{-1}$ cinnamaldehyde.

At the concentrations of 5% and 7% cinnamaldehyde, the treated wood against *G. trabeum* reached the high decay resistance rating. And mass losses of poplar specimens impregnated with concentration of 3%, 5% and 7% cinnamaldehyde against *G. trabeum* were less than 3%. For citric acid, the effects of decay resistances for *T. versicolor* were not very effective. However, poplar specimens impregnated with citric acid had better decay resistances against *G. trabeum*. And the effects of decay resistance treated by cinnamaldehyde and citric acid increased as impregnation concentration increased. The effect of salicylic acid and stearolic acid on the growth of *G. trabeum* and *T. versicolor* were not significant. And their antifungal activity was much weaker than that of cinnamaldehyde or citric acid.

For salicylic acid, it showed antifungi activity against both *G. trabeum* and *T. versicolor* in five-week decay resistant research reported by Bi et al. (2019), however it did not inhibit or even promote the growth of fungi. The results of this experimental phenomenon need further tests to better understand antifungi mechanism for salicylic acid as wood preservative. The mass losses of stearolic acid impregnated poplar specimens might reflect solubility issues.

The SEM images of poplar specimens impregnated with 7% concentration after 12 weeks of exposure to *G. trabeum* and *T. versicolor* were presented in Fig. 2. From blank control samples as well as samples treated by 7% salicylic acid and stearolic acid, severe damage to the poplar cell wall occurred, which were consistent with Cai et al. (2020). Mycelia were full in shape. However, mycelia were slim and were inhibited in Fig. 2d and Fig. 2j (marked with circles). And the cell wall was practically intact (marked by a rectangle). The cinnamaldehyde can inhibit the growth of for *G. trabeum* and *T. versicolor,* and the citric acid can inhibit the growth of *G. trabeum* through the SEM observation.

Tab. 2: Natural decay resistance rating standard of wood established by the ASTM D2017 standard after exposed to G. trabeum or T. versicolor.

Fungi	Types of preservatives	Concentration	Mass loss (%)	Rating
G. trabeum	Blank control		31.93 (7.42)	
	Cinnamaldehyde	3%	2.84 (2.43)	Highly resistant

		5%	2.32 (0.48)	Highly resistant
		7%	0.21 (3.15)	Highly resistant
	Salicylic acid	3%	37.04 (3.06)	Moderately resistant
		5%	40.59 (4.73)	Moderately resistant
		7%	47.67 (4.09)	No resistant
	Stearolic acid	3%	40.82 (3.31)	Moderately resistant
		5%	41.77 (4.36)	Moderately resistant
		7%	40.37 (6.39)	Moderately resistant
	Citric acid	3%	24.31 (3.20)	Moderately resistant
		5%	17.87 (5.04)	Resistant
		7%	10.53 (5.29)	Resistant
T. versicolor	Blank control		55.99 (4.49)	
	Cinnamaldehyde	3%	22.68 (10.92)	Resistant
		5%	5.02 (2.20)	Highly resistant
		7%	1.63 (2.02)	Highly resistant
	Salicylic acid	3%	41.36 (8.55)	Moderately resistant
		5%	48.97 (5.17)	No resistant
		7%	45.74 (6.83)	No resistant
	Stearolic acid	3%	50.46 (4.02)	No resistant
		5%	46.37 (2.56)	No resistant
		7%	50.28 (7.09)	No resistant
	Citric acid	3%	65.41 (5.53)	No resistant
		5%	66.38 (4.05)	No resistant
		7%	57.34 (6.08)	No resistant

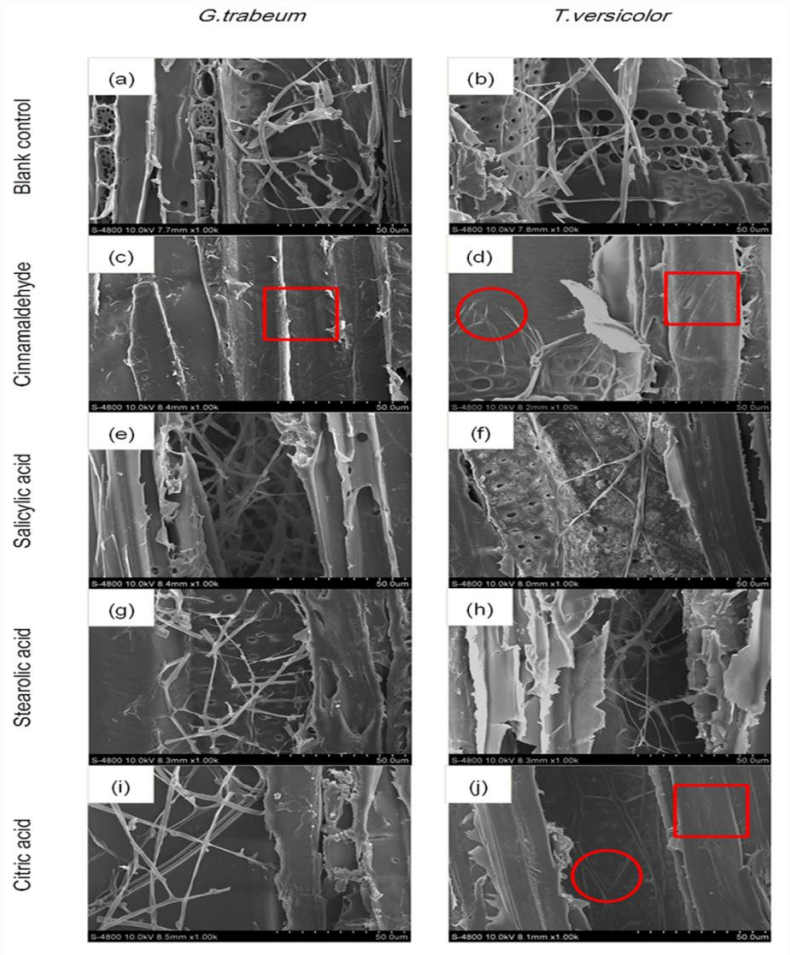

Fig. 2: SEM images of poplar samples impregnated with 7% natural organic compounds after the decay test.

Wood color change of after impregnation

The color change of poplar specimens before and after they were impregnated with various compounds were presented in Fig. 3. The L *, a *, b * and ΔE* were showed in Fig. 4. The L*, a *and b * parameters did not change much after treatment. ΔE* were remained within 10%. L* parameters of poplar samples impregnated with salicylic acid was less than that of blank control groups and other treated groups and showed darkness in wood. The color changed more as the concentration of the compounds increased.

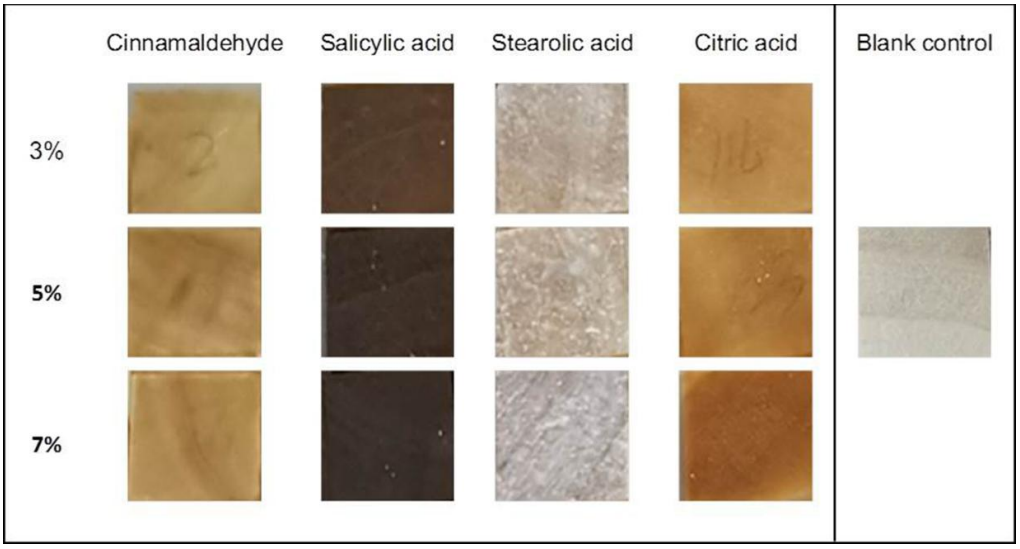

Fig. 3: The color of poplar specimens after impregnated with different compounds.

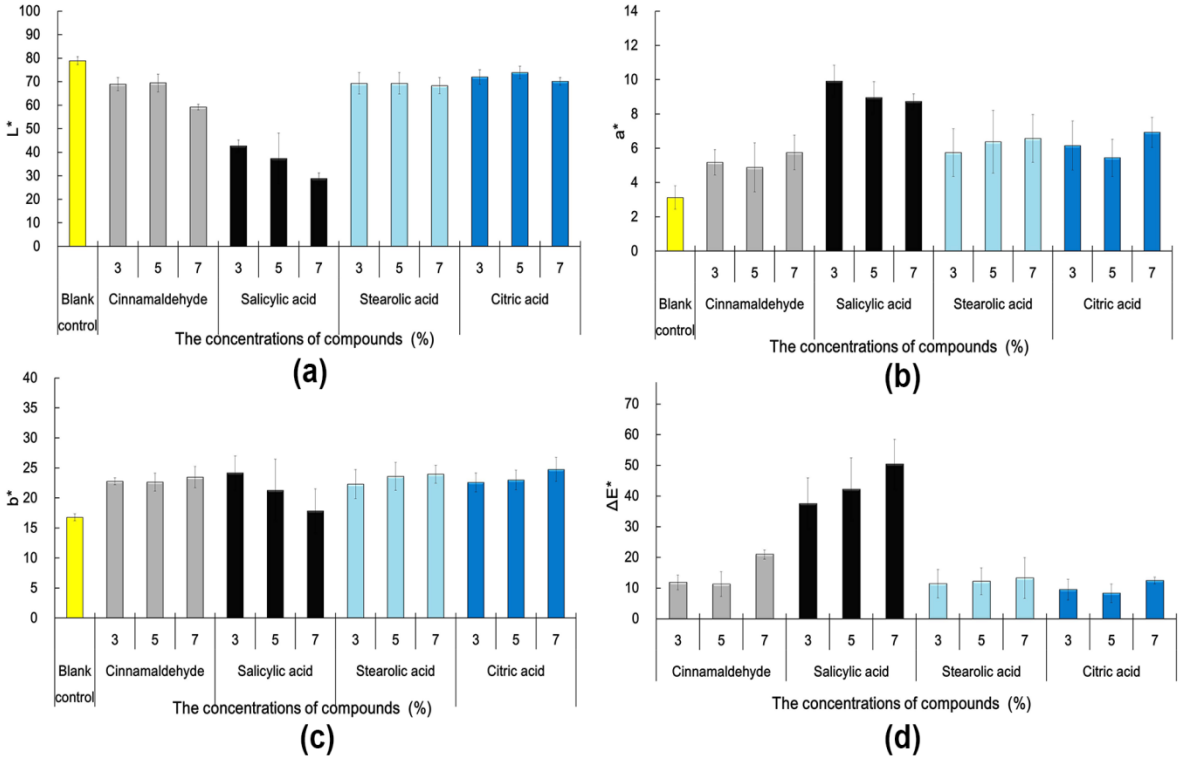

*Fig. 4: L *, a *, b * and ΔE* in poplar specimens changed after impregnated with different compounds.*

Dimensional stability of the impregnated poplar

Volume change of impregnated poplar specimens with cinnamaldehyde, salicylic acid, stearolic acid and citric acid, respectively and blank control groups were presented in Fig. 5. Volumes of specimens increased most when they were stored in a 30°C and 85% relative humidity (RH) compared to other temperature and RH. Volume increase of untreated poplar specimens reached 6.13%. Volume increase of poplar specimens impregnated with cinnamaldehyde and citric acid had a significant reduction compared to the blank control group, close to 2%. And concentration of impregnated cinnamaldehyde and citric acid had little effect on reduction of volume increase rates in poplar specimens. This result showed that wood impregnated with cinnamaldehyde or citric acid has better dimensional stability.

Natural organic compounds might be impregnated into vessel and they would block the passages of water transport (He 2019), thus dimensional stability of impregnated poplar specimens were improved.

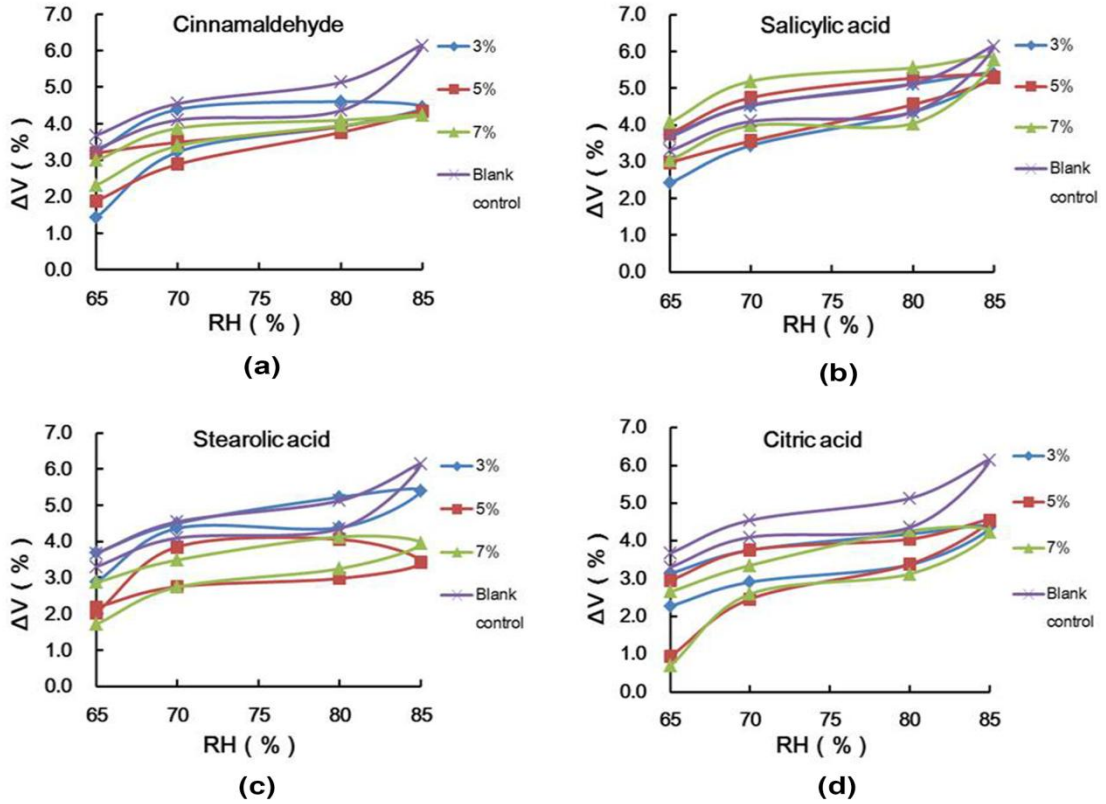

Fig. 5: Volume increase (ΔV) of poplar specimens after impregnated with different compounds.

Mechanical properties after impregnation

Mechanical properties, including modulus of elasticity (MOE) and modulus of rupture (MOR) after impregnation was presented in Fig. 6. For MOE (Fig. 6a), blank control groups reached 6291 MPa. Compounds type and compounds concentration had no significant effects on MOE ($p = 0.08$ and 0.06, resp.). MOE of other poplar specimens impregnated with four natural organic compounds was improved differently, and MOE of 3% cinnamaldehyde impregnated poplar specimens decreased slightly. MOEs of impregnated specimens were

positive correlation with concentration of cinnamaldehyde, salicylic acid, stearolic, however, citric acid group had opposite result. MOR of 7% cinnamaldehyde and 7% salicylic acid impregnated specimens reached 7339 MPa and 8241 MPa, improving 16% and 30% respectively compared to blank control groups.

For MOR (Fig. 6b), blank control groups reached 89 MPa. Compounds type and compounds concentration had significant effects on MOR (p-value = 0.006 and 0.018 resp.). MORs of treated groups all improved compared to blank control groups. MORs of impregnated specimens were positive correlation with concentration of impregnated compounds. Cinnamaldehyde and salicylic acid impregnated specimens promoted the highest among four kinds of natural organic compounds, and MOR of 7% cinnamaldehyde and 7% salicylic acid impregnated specimens reached 107 MPa and 114 MPa, improving 20% and 28% respectively compared to blank control groups.

MOR and MOE of four kinds of natural organic compounds were improved maybe it was because compounds get into the cell and strengthened the cell wall, it was consistent with the research of Bian et al. (2019).

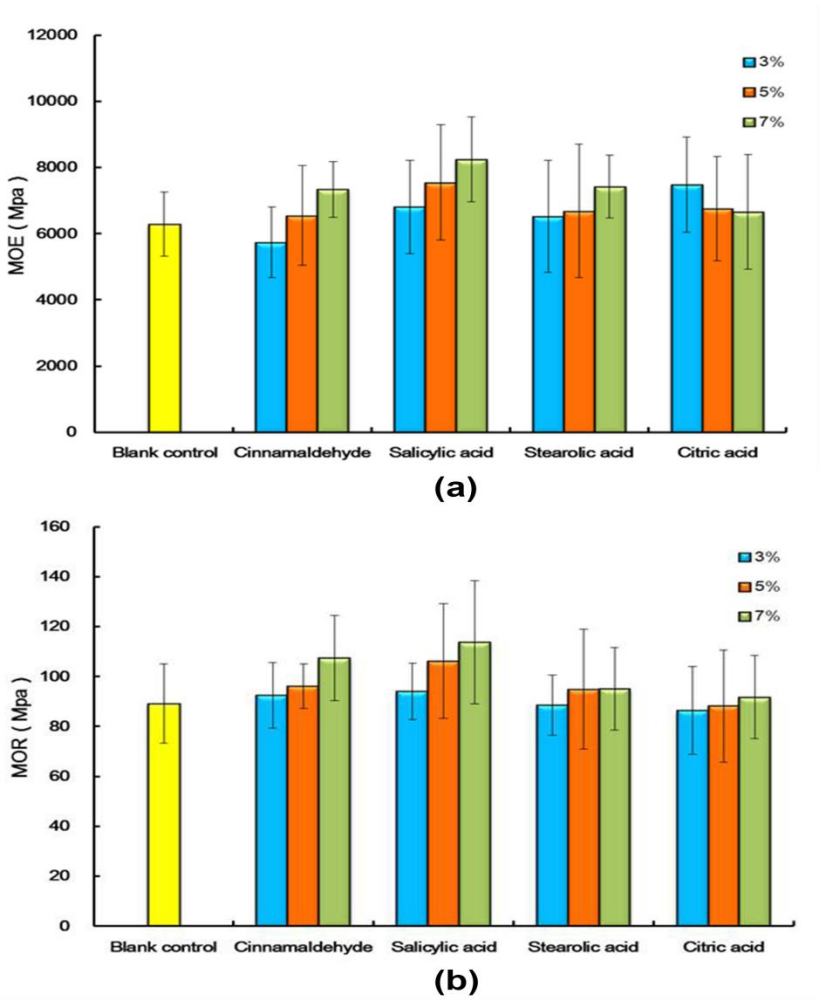

Fig. 6: Mechanical properties of poplar specimens after impregnated with different compounds: (a) MOE, (b) MOR.

CONCLUSIONS

Cinnamaldehyde, salicylic acid, stearolic acid and citric acid as active substances were impregnated into poplar wood using the vacuum-pressure method. WPG of impregnated specimens improved as the concentration increased. Wood impregnated with cinnamaldehyde showed the antifungi activity against both *G. trabeum* and *T. versicolor*, and impregnated poplar with citric acid showed the antifungi activity against *G. trabeum*. The impregnation of cinnamaldehyde, stearolic acid and citric acid did not cause large color change. Cinnamaldehyde and citric acid decreased volume increase rates thus improved dimensional stability. Mechanical properties of impregnated specimens had been improved, and compounds type and compounds concentration had no significant effects on MOE, however, they had significant effects on MOR.

ACKNOWLEDGEMENTS

The authors are very grateful for financial support from the National Key Research and Development Program of China (2017YFD0600203) and National Natural Science Foundation of China (31971590).

REFERENCES

1. Ali, A.C., Uetimane, E., Råberg, U., Terziev, N., 2011: Comparative natural durability of five wood species from Mozambique. International Biodeterioration & Biodegradation 65(6): 768-776.
2. Anttila, A.K., Pirttila, A.M., Haggman, H., Harju, A., Venalainen, M., Haapala, A., Holmbom, B., Julkunen-Tiitto, R., 2013: Condensed conifer tannins as antifungal agents in liquid culture. Holzforschung 67(7): 825–832.
3. Asghari, M., Aghdam, M.S., 2010: Impact of salicylic acid on post-harvest physiology of horticultural crops. Trends in Food Science & Technology 21(10): 502–509.
4. ASTM D2017, 2005: Standard method for accelerated laboratory test of natural decay resistance of woods. ASTM International, West Conshohocken, PA.
5. ASTM D143-09, 2011: Standard test methods for small clear specimens of timber. ASTM International, West Conshohocken, PA.
6. Aydin, E., Baysal, E., Toker, H., Turkoglu, T., Deveci, I., Ozcifci, A., Peker, H., 2015: Decay resistance, physical, mechanical, and thermal properties of heated oriental beech wood. Wood Research 60(6): 913-928.
7. Bekhta, P., Niemz, P., 2003: Effect of high temperature on the change in color, dimensional stability and mechanical properties of spruce wood. Holzforschung 57(5): 539–546.
8. Bi, Z.J., Yang, F.X., Lei, Y.F., Morrell, J.J., Yan, L., 2019: Identification of antifungal compounds in konjac flying powder and assessment against wood decay fungi. Industrial Crops and Products 140: 111650.
9. Bian, X.T., Cai, Y.C., Kong, F.X., Chai, H.J., 2019: Properties of fast-growing poplar wood by impregnation strengthening of furfuryl alcohol resin. Journal of Northeast Forestry University 47(2): 74-80.

10. Borges, M.H., Soares, A.M., Rodrigues, V.M., Andrião-Escarso, S.H., Diniz, H., Hamaguchi, A., Quintero, A., Lizano, S., JoséM. Gutierrez, J.M., Giglio, J.R., 2000: Effects of aqueous extract of *Casearia sylvestris* (*Flacourtiaceae*) on actions of snake and bee venoms and on activity of phospholipases A (2). Comparative Biochemistry and Physiology B-biochemistry & Molecular Biology 127(1): 21-30.
11. Brocco, V.F., Paes, J.B., da Costa, L.G., Brazolin, S., Arantes, M.D.C., 2017: Potential of teak heartwood extracts as a natural wood preservative. Journal of Cleaner Production 142(4): 2093-2099.
12. Cai, L.L. , Lim, H., Kim, Y., Jeremic, D., 2020: β-Cyclodextrin-allyl isothiocyanate complex as a natural preservative for strand-based wood composites. Composites part B: Engineering 193: 108037.
13. Coggins, C.R., 2008: Trends in timber preservation – a global perspective. Journal of Tropical Forest Science 20: 264–272.
14. Gonzalez-Laredo, R.F., Rosales-Castro, M., Rocha-Guzman, N.E., Gallegos-Infante, J.A., Moreno-Jimenez, M.R., Karchesy, J.J., 2015: Wood preservation using natural products. Madera Bosques 21: 63–75.
15. He, Z.B., Qian, J., Qu, L.J., Yan, N., Yi, S.L., 2019: Effects of Tung oil treatment on wood hygroscopicity, dimensional stability and thermostability. Industrial Crops and Products 140: 111647.
16. Kartal, S.N., Hwang, W.J., Imamura, Y., Sekine, Y., 2006: Effect of essential oil compounds and plant extracts on decay and termite resistance of wood. Holz als Roh-und Werkstoff 64(6): 455-461.
17. Khan, B. I., Solo-Gabriele, H. M., Townsend, T. G., Cai, Y., Townsend, 2006: Release of arsenic to the environment from CCA-treated wood. 1. Leaching and speciation during service. Environmental Science & Technology 40: 988-993.
18. Mohammed, S.A., Madhan, B., Demissie, B.A., Velappan, B., Tamil Selvi, A., 2016: Rumexabyssinicus (mekmeko) Ethiopian plant material for preservation of goat skins: approach for cleaner leather manufacture. Journal of Cleaner Production 133(1): 1043–1052.
19. Mubarok, M., Dumarcay, S., Militz, H., Candelier, K., Thévenon, M.F., Gérardin, P., 2019: Non-biocide antifungal and anti-termite wood preservation treatments based on combinations of thermal modification with different chemical additives. European Journal of Wood and Wood Products 77: 1125–1136.
20. Nkansah, K., Adedipe, O., Dawson-Andoh, B., Atta-Obeng, E., Slahor, J., Osborn, L., 2015: Determination of concentration of ACQ wood preservative components by UV-Visible spectroscopy coupled with multivariate data analysis. Chemometrics and Intelligent Laboratory Systems 120: 157-166.
21. Nostro, A., Scaffaro, R., D'Arrigo, M., Botta, L., Filocamo, A., Marino, A., Bisignano, G., 2012: Study on carvacrol and cinnamaldehyde polymeric films: mechanical properties, release kinetics and antibacterial and antibiofilm activities. Applied Microbiology and Biotechnology 96(4): 1029–1038.
22. Shiny, K.S., Sundararaj, R., Vijayalakshmi, G., 2018: Potential use of coconut shell

pyrolytic oil distillate (CSPOD) as wood protectant against decay fungi. European Journal of Wood and Wood Products 76: 767–773.
23. Tchinda, J.B.S., Ndikontar, M.K., Belinga, A.D.F., Mounguengui, S., Njankouo, J.M., Durmacay, S., Gerardin, P., 2018: Inhibition of fungi with wood extractives and natural durability of five Cameroonian wood species. Industrial Crops and Products 123: 183–191.
24. Teng, T.J., Arip, M.N.M., Sudesh, K., Nemoikina, A., Jalaludin, Z., Ng, E.P., Lee, H.L., 2018: Conventional technology and nanotechnology in wood preservation: A review. Bioresources 13(4): 9220-9252.
25. Tondi, G., Hu, J., Thevenon, M., 2015: Advanced tannin based wood preservatives. Forest Products Journal 65(3-4):S26–S32.
26. Treutter, D., 2006: Significance of flavonoids in plant resistance: a review. Environmental Chemistry Letters 4(3): 147-157.
27. Xie, Y.J., Wang, Z.J., Huang, Q.Q., Zhang, D.Y., 2017: Antifungal activity of several essential oils and major components against wood-rot fungi. Industrial Crops and Products 108: 278–285.
28. Yang, D.M., Wang, H., Li, S.J., Yuan, H.J., 2017: Decay and mould resistance of cinnamaldehyde and its derivatives. Croatian Journal of Forest Engineering 2(1): 46–50.
29. Wang, Y.M., Li, X.Q., Wang, X.M., 2012: Sophoraflavescens inhibit wood white-rot fungi. Journal of Inner Mongolia Agricultural University 33(4): 184-188.
30. Wilcox, W.W., 1978: Review of the literature on the effects of early stages of decay on wood strength. Wood and Fiber Science 9(4): 252–257.

JIAPENG WANG, ZHENJU BI, LI YAN, YAFANG LEI*
NORTHWEST A&F UNIVERSITY
COLLEGE OF FORESTRY
YANGLING, SHAANXI 712100
CHINA
*Corresponding author: leiyafang@sina.com

ZHANGJING CHEN[1,2]
[1] NORTHWEST A&F UNIVERSITY
COLLEGE OF FORESTRY
YANGLING, SHAANXI 712100
CHINA
[2] VIRGINIA TECH UNIVERSITY
DEPARTMENT OF SUSTAINABLE BIOMATERIALS
BLACKSBURG, VA 24061
USA

WOOD RESEARCH doi.org/10.37763/wr.1336-4561/66.4.569581
e-ISSN 2729-8906
66(4): 2021 569-581 pp.

PERMEABILITY AND MECHANICAL BEHAVIOUR OF MICROWAVE PRE-TREATED NORWAY SPRUCE RIPEWOOD

HESS DOMINIK, PAŘIL PETR, DÖMÉNY JAKUB, BAAR JAN
MENDEL UNIVERSITY IN BRNO
CZECH REPUBLIC

(RECEIVED JANUARY 2021)

ABSTRACT

This is a study of the influence of microwave (MW) pre-treatment on the permeability of Norway spruce ripewood (*Picea abies* L. Karst) as it affects its mechanical properties. Specimens were treated under variable moisture content, MW intensity, and impregnation processes. According to the results, the specimens with an initial moisture content of 45–65% exhibited the highest permeability values compared to reference samples. An insignificant difference was found between MW pre-treatments at 2 and 3 kW. Statistically significant results were found after long-time (24h) vacuum-pressure impregnation (LP). The average retention value following LP was 132 $kg \cdot m^{-3}$, which is almost three times greater than the MW-treated groups impregnated in a short-time vacuum-pressure process. The average depth of penetration after LP was 2.0 mm and the proportion of the impregnation area following LP was 17.6%. MW pre-treatment had no effect on the impregnability or the mechanical properties of the wood; other MW regimes are open for further examination.

KEYWORDS: Norway spruce, ripewood, vacuum-pressure, permeability, microwave pre-treatment, retention, mechanical properties.

INTRODUCTION

Norway spruce (*Picea abies* L. Karst.) is one of the most important wood species in Europe for both its economic and ecological aspects, with a long tradition of cultivation and use (Caudullo et al. 2016). These days, its timber is used to manufacture wooden shingles, a traditional roof and walls covering on historical wooden buildings. Nowadays, there is great awareness about our connections with the environment and their impact on our quality of life. There is a trend to make more contact with nature, which has seen a revival of the use of traditional wooden building materials, including wooden shingles (Policinska-Serwa and Jakimowicz 2013). Historically, fir wood was used to manufacture shingles, while larch and spruce are preferred today. Shingles are exposed to continuous action and degradation by

biotic and abiotic factors. When Norway spruce is used it is vacuum-pressure impregnated due to its low natural durability. A crucial disadvantage of the wood is its low permeability, which causes many problems during impregnation. The problem occurs mainly due to the aspiration of bordered pits during drying, when the free water is removed (Fujii et al. 1997, Hacke et al. 2004, Alfredsen et al. 2007, Lehringer 2011, Durmaz et al. 2015). Several modifications to the method, such as bio-incising, mechanical incising, drilling techniques, and steaming have been applied to improve the impregnation properties of wood species that are hard to impregnate (Schwarze et al. 2006, Lehringer et al. 2009, Dashti et al. 2012, Pánek et al. 2013). In order to increase the permeability of various wood species, microwave treatment has been studied by several researchers (Trajkovic 1994, Torgovnikov and Vinden 2009, Brodie 2009, Vinden et al. 2011, Yu et al. 2011, Terziev and Daniel 2013, Dömény et al. 2014). Microwave treatment is based on the principles of electromagnetic radiation and its interaction with polar substances, such as water. The presence of water in wood has a fundamental influence on its dielectric properties (Torgonikov 1993, Paz 2010, Dömény 2017). After felling, the inner non-conductive part of Norway spruce, called ripewood, has an average moisture content of around 34–41%, while the sapwood moisture content is substantially higher. Ripewood is more or less indistinct inner wood of spruce wood, in which the sapwood has aged and presumably died with little of any deposition of the substances associated with heartwood (Haygreen and Bowyer 1982, Glass and Zelinka 2010). According to Li et al. (2009), Torgovnikov and Vinden (2009), Yu et al. (2011), Zhang et al. (2013), and Dömény et al. (2014), microwave treatment increases the permeability by raising water vapor pressure, which delaminates cell walls. Micro- or macro-cracks (depending on the radiation intensity) are formed in the wood structure, and these influence the properties of the wood – increasing its volume and changing its mechanical properties. Treu et al. (2008) increased the permeability of Scots pine heartwood and Norway spruce by MW irradiation using high intensity and 3–14 s exposure. The author stated that the longer exposure caused larger cracks in the wood structure. The effect was more pronounced for pine than for spruce wood specimens. He et al. (2014) and Ramezanpour et al. (2014) found the optimal MW parameters for improving the impregnability of fir wood. Many studies have reported that over-intensive MW treatment causes deterioration in the mechanical properties of wood (Oloyede and Groombridge 2000, Hong-Hai et al. 2005, Machado 2006, Torgovnikov and Vinden 2009). Vinden et al. (2011) irradiated railway sleepers made of pine (*Pinus radiata*) with the aim of increasing the permeability of the wood. However, after MW treatment they recorded a reduction of its bending strength. Koiš et al. (2014) modified Norway spruce (*Picea abies* L.) using MW radiation at various power levels. The results showed that the wood structure of the samples was extensively damaged by high intensities and selected conveyor speeds. Only samples treated with 3 kW MW at 0.4 $m \cdot min^{-1}$ had modulus of elasticity (MOE) and modulus of rapture (MOR) values comparable to the reference specimens. Gezer et al. (2017) enhanced the impregnation properties of spruce wood by specific MW treatment. Nevertheless, the applied MW pre-treatment reduced the MOR, MOE and compressive strength parallel to the grain by 16–18% compared to reference specimens.

None of the published studies state whether the specimens tested were from sapwood or ripewood. The goal of this study was to contribute to the knowledge of MW pre-treatment

in increasing the permeability of Norway spruce ripewood in the lateral direction. The specific objective of the study was to investigate the effect of MW power and the initial MC of ripewood on improving the permeability of wood without significantly changing its mechanical properties. The results obtained by MW pre-treatment were compared to control specimens impregnated by short-time and long-time vacuum-pressure impregnation.

MATERIALS AND METHODS

Specimens were taken from one-meter-long logs of Norway spruce (*Picea abies* L. Karst.) cut from five trees (Czech Republic; diameters 25–35 cm). The sapwood boundary was marked on the logs while still fresh and the specimens were further cut only from ripewood (RW), which is more difficult to impregnate than sapwood. The dimensions of specimens for MW treatment were determined based on the technical parameters of the microwave device. Specimens from each log with dimensions 45 × 45 × 300 mm (R×T×L) were divided into eight groups to maintain maximum homogeneity with the same density and early and late wood width (Tab. 1); each group contained ten specimens.

Tab. 1: Wood specimens sorted into groups according to MW regime and impregnation cycle (groups 1 and 2 were reference groups).

Group	**1**	**2**	**3**	**4**
Moisture content (%)	35 ± 2	35 ± 2	35 ± 2	35 ± 2
Microwave power (kW)	-	-	2	3
Conveyor speed ($m \cdot min^{-1}$)	-	-	0.4	0.4
Microwave application (s)	-	-	90	90
Microwave energy ($kWh \cdot m^{-3}$)	-	-	41.2	61.7
Impregnation cycle	SP	LP	SP	SP

Microwave treatment Part 1

The specimens were MW treated in a continuous laboratory device that operated at a frequency of 2.45 GHz and provided adjustable power from 0.6 to 5.0 kW, under conditions stated in Tab. 1, which were chosen on the basis of preliminary tests done by Koiš et al. (2014). In the preliminary test it was found that MW power higher than 4 kW visibly damaged the structure of the tested specimens and, according to Treu and Gjolsjo (2008), MW energy of more than 50 $kWh \cdot m^{-3}$ at a frequency of 2.45 GHz could significantly increase the uptake of preservative after wood modification.

Specimens were MW treated with a single dose of radiation (one passage through the modification chamber). The surface temperature of the MW-treated specimens was measured by contactless infrared thermometer (IR-380, Volcraft, Czech Republic). After MW pre-treatment, cross sections of the specimens were covered with two layers of two-component epoxy resin (Epolex S1300/S7300) to prevent preservative flow in the longitudinal direction. The moisture content was measured by dielectric hygrometer (Wagner L 601-3), giving an MC of 35 ± 2%.

Microwave treatment Part 2

In groups 1–4, with initial moisture content 35 ± 2%, MW pre-treatment, and impregnation, better impregnability was not proven. Therefore, the initial moisture content was increased for groups 5–8. Specimens were immersed in water, and their weight was regularly measured until their moisture content reached the values given in Tab. 2. Subsequently, the same MW treatment was applied as in Part 1.

Tab. 2: Wood specimens sorted into groups according to MC and MW regime.

Group	**5**	**6**	**7**	**8**
Moisture content (%)	45–65	45–65	75–100	75–100
Microwave power (kW)	2	3	2	3
Conveyor speed ($m \cdot min^{-1}$)	0.4	0.4	0.4	0.4
Microwave application (s)	90	90	90	90
Microwave energy ($kWh \cdot m^{-3}$)	41.2	61.7	41.2	61.7
Impregnation cycle	SP	SP	SP	SP

Vacuum-pressure impregnation

The wood preservative applied was a 5% solution of Bochemit Forte Profi based on $Cu_2(OH)_2CO_3$. The impregnation process was similar to Melcher and Zwiefelhofer (2013) for possible comparison of the results. It was carried out using the Bethell method in a laboratory vacuum-pressure impregnation plant (JHP-1-0072) in two steps as shown in Tab. 3.

Tab. 3: Impregnation process – under short-time (SP) and long-time (LP) vacuum pressure.

Impregnation process steps	1. Short-time vacuum pressure (SP)	2. Long-time vacuum pressure (LP)
Total duration (min)	225	1,440
Course of action (time and pressure)	90 min vacuum (10 kPa)	225 min short-time process
	120 min overpressure (900 kPa)	90 min vacuum (10 kPa)
	15 min vacuum (20 kPa)	900 min overpressure (900 kPa)
	-	225 min short-time process

After this impregnation process, the specimens were removed and weighted. Retention R ($kg \cdot m^{-3}$) values were used as an indicator of wood preservative uptake according to Eq. 1:

$$R = \frac{(m_{after\ impregnation} - m_{before\ impregnation})}{V_{before\ impregnation}} \quad (1)$$

Lateral penetration depth and impregnated area

The lateral penetration depth in the treated specimens was indicated by the reaction of copper with dithiooxamide (5% concentration in ethanol) in a gaseous ammonium environment. Impregnated specimens were cut at the middle of their length, the cross sections were coated with dithiooxamide solution and placed in a desiccator with 25% ammonium hydroxide for 10 min. A dark blue color indicated the impregnated area.

The impregnated area as a percentage of the total was measured using the software Image J as follows. The total cross-sectional area of the specimen surface was measured and

converted into 8-bit color depth; using the thresholding method, the impregnated area of the specimens was measured. The impregnated area was calculated thus:

$$n = \frac{S_i}{S} \times 100\ (\%) \qquad (2)$$

where: n is the impregnated area (%), S_i is impregnated cross-sectional area of the specimen (mm^2), and S is total cross-sectional area of the specimen (mm^2).

The measurement of penetration depth (mm) was taken using software Image J. Ten measurements were taken of each specimen and averaged.

Mechanical properties

After testing, the treated specimens were cut into samples with dimensions 20 × 20 × 30 mm (R × T × L) and conditioned in a climate chamber at 20°C and 65% relative humidity. A compression test parallel to the grain was performed using a Zwick Z050/TH 3A Universal Testing Machine (Zwick Roell AG, Ulm, Germany). The Young's modulus of elasticity was obtained from the ratio of the stress (σ) to the strain (ε) in the linear elastic range bounded by 10% and 40% of the sample strength. The strain was determined based on the change of distance between two isolated points mechanically tracked by clip-on extensometers (Zwick Roell AG, Ulm, Germany) related to their initial distance (10 mm). The ultimate strength (σ_{max}) was calculated from the maximum load (F_{max}) at the point of failure related to the cross-sectional area (A) of the unloaded sample.

Statistical analysis

The measured data were processed using Statistica 12 software (StatSoft Inc., USA), evaluated using one-factor analysis of variance ANOVA, and completed with Tukey's honest significance test (HSD test).

RESULTS AND DISCUSSION

Retention

In this experimental study, the main indicator of wood permeability change due to treatment was the uptake of preservative solution in the transversal direction of Norway spruce ripewood. All groups of specimens exposed to various MW treatments exhibited a retention of preservative solution comparable to the reference group (Fig. 1).

Based on one-factor analysis of ANOVA, completed with Tukey's HSD test, variability was found to be not statistically significant. The only statistically significant difference in retention was found for the LP group. Wood specimens treated by MW power of 2 and 3 kW at MC 35 ± 2% showed a slight retention reduction of between 18% and 20.4% compared to the reference group. Specimens with a higher MC of 75–100%, MW-treated at the same power, similarly showed about 4.1% to 13.6% lower retention than the reference group. The specimens with a MC of 45–65% had a slightly increased retention level by 9.5%.

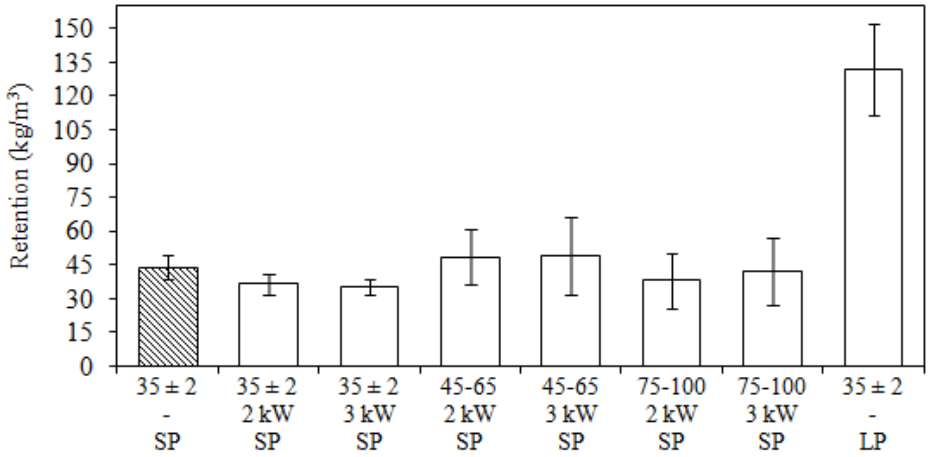

Fig. 1: Preservative solution retention of all groups treated under different conditions: moisture content, MW treatment intensity, impregnation process – short (SP) and long (LP).

The low efficacy of MW treatment was reported earlier by Treu et al. (2008) who exposed Norway spruce specimens to MW treatment repeatedly for short time periods. Even after five iterations, specimens showed no pronounced differences. He et al. (2014) found an input MC of 40–60% the optimal parameter for MW pre-treatment. The microscopic structure of wood after treatment revealed micro-cracks at the intercellular layer of the ray cells and longitudinal tracheids. Among the leading causes of a positive outcome might have been sufficient water vapor pressure in the wood structure, which was able to delaminate cell walls (Li et al. 2009, Yu et al. 2011, Zhang et al. 2013). The effect of a MC higher than 75% on MW radiation on wood may be to facilitate the absorption of microwaves and thus increase evaporation without the pressure necessary for cell-wall delamination. Treu et al. (2008) reported that the use of higher MW power and shorter exposure to MW irradiation could be more effective in producing a retention increase.

Lower initial wood MC before vacuum-pressure impregnation should be considered as it might increase retention. Many authors used an initial MC of around 12% for impregnated specimens, which caused cracks in the wood structure and e.g., altered its mechanical properties. In practice, the vacuum-pressure impregnation process uses the wood MC near the fiber saturation point (FSP) – approximately 30% (Konopka et al. 2018). Most of the authors cited did not address the difference between the sapwood and ripewood of Norway spruce during their experiments, which could be a significant reason for such high retention levels of the preservative solution after MW treatment. The density, hygroscopicity, and especially the permeability of ripewood have been reported to be quite different from those of sapwood (Kollmann and Côté 1968, Kärkkäinen, 2003).

No visible checks or cracks were observed in tested specimens with MC of 35 ± 2% after exposure to MW pre-treatment at 2 and 3 kW power, but MW power of 3 kW caused slight flow of resin to the surface. The surface temperature of specimens exposed to 2 kW was from 62 to 66°C and the 3 kW group had surface temperatures from 80 to 86°C. The temperature decreased slightly with specimens' increasing initial MC. These temperatures of treated wood specimens might have caused softening of the resins inside the wood structure and blocked the conductive paths in the lateral direction of treated wood.

Since resins are naturally present in a semi-liquid state in the wood, they can become less viscous and move – especially when the surface is heated.

The preservative retention of the ripewood was improved only by prolongation of the impregnation process to 24 hours. The average retention value of the LP group was 132 $kg \cdot m^{-3}$, which represents an almost three-fold increase in preservative solution retention over the reference group. A similar experiment was performed by Melcher and Zwiefelhofer (2013), who tried to determine the retention level and the penetration of different refractory wood species impregnated by means of two vacuum-pressure processes in which the SP lasted 2 h and LP lasted 24 h. Their findings were concordant with our experiment. The results of this work showed the dependence of treatment time on the retention of impregnating solution. According to Reinprecht (2008) the retention increase of the impregnating solution over time does not have a linear, but an exponential, dependence, which is produced by compressing the air in the treated wood when it is fully immersed (vacuum-pressure impregnation technology, dipping, immersion, etc.). Consequently, the pressure of the air in the cells of the wood increases and grows over time.

Lateral penetration depth and impregnated area

By vacuum-pressure impregnation using a water-soluble solution it's possible to impregnate spruce sapwood to a depth of 10–20 mm in the radial direction (Paserin 1970), while ripewood has a significantly lower liquid permeability and is classified in the 4th impregnability class (EN 350) as extremely difficult to impregnate with a penetration depth of several millimeters only. The results of lateral penetration depth of all groups after vacuum-pressure impregnation are observed in Fig. 2.

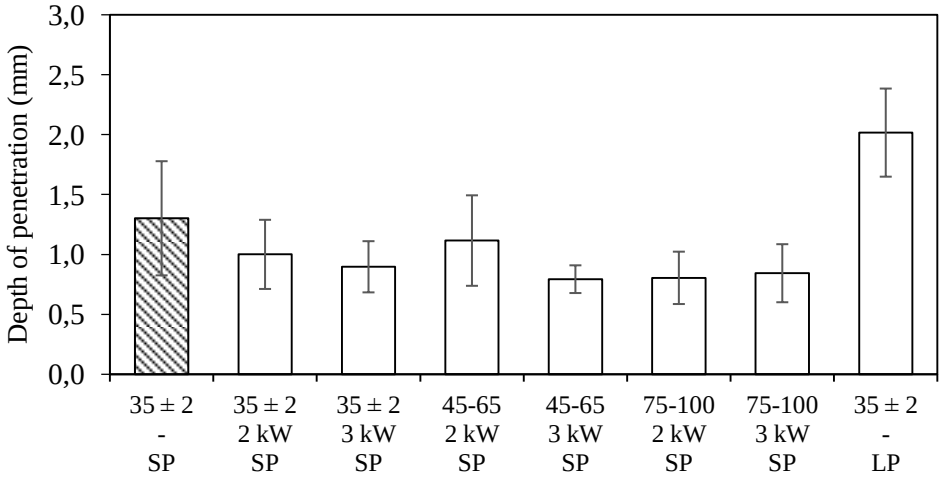

Fig. 2: Depth of penetration of all groups treated under different conditions: moisture content, MW treatment intensity, impregnation process – short (SP) and long (LP).

The only statistically significant lateral penetration depth, according to Tukey's HSD test, was found for the group of specimen's vacuum-pressure impregnated by LP cycle for 24 hours. The penetration depth of LP group was statistically significant in the case of all other groups. The average penetration depth of the LP group was 2.0 mm, which is twice as high as the other groups. All MW treated groups showed less penetration depth of

the preservative solution than the reference group. The control group impregnated with the SP cycle had an average penetration depth of 1.3 mm. The improvements in penetration depth and impregnated area by MW pre-treatment have not been demonstrated in this experiment.

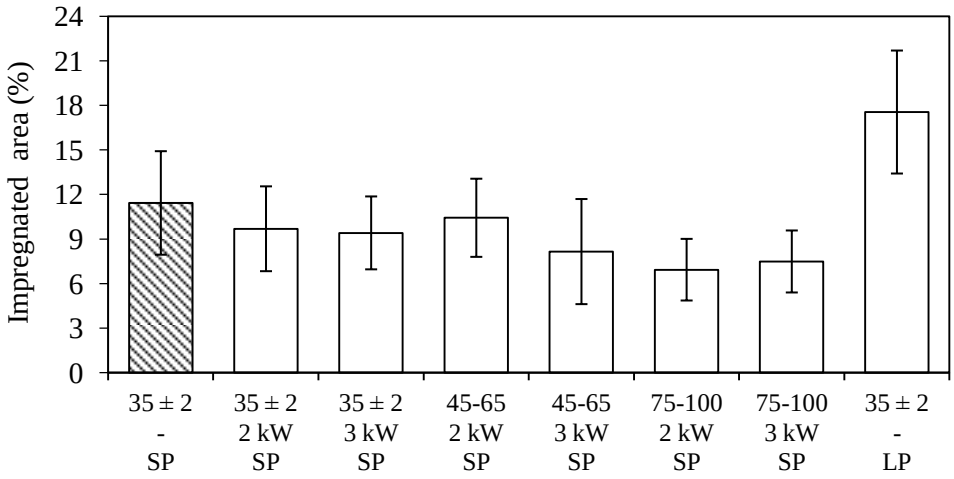

Fig. 3: Impregnated area of all groups treated under different conditions: moisture content, MW treatment intensity, impregnation process – short (SP) and long (LP).

As well as retention and penetration depth, the extent of the impregnation area was most influenced by the modification of the vacuum-pressure impregnation process. The results are observed in Fig. 3. The only statistically significant difference in impregnated area was found for the LP impregnated specimens, which differed from all other groups. The mean values of all MW-treated groups were in the range 9.7–10.0%, while specimens impregnated by LP showed twice the average value of 17.6%. From the obtained results we can say that the rate of impregnated area increase depended on the length of the impregnation process. The difference can be seen in Fig. 4.

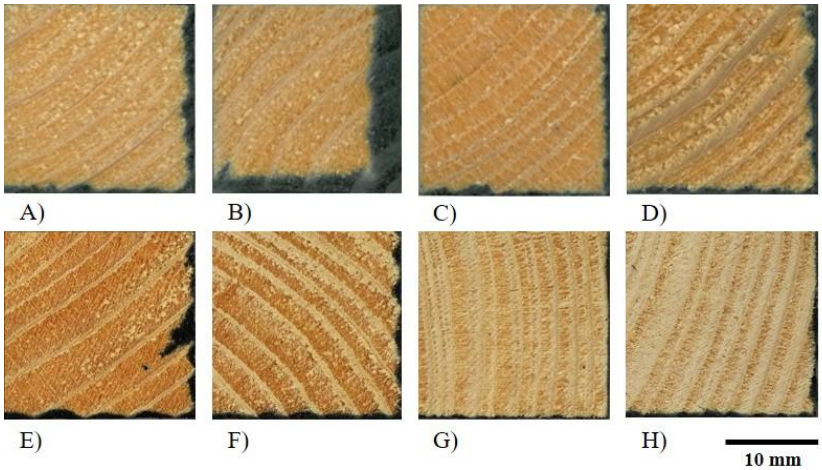

Fig. 4: Cross-sections of impregnated specimens: A) Reference (SP), B) Long process (LP), C) 2kW_MC35_SP, D) 3kW_MC35_SP, E) 2kW_MC40-60_SP, F) 3kW_MC40-60_SP, G) 2kW_MC75-100_SP, H) 3kW_MC75-100_SP.

Mechanical properties

Using a higher MW intensity or prolonged exposure to MW radiation could lead to increased permeability of Norway spruce ripewood. However, it could lead to a significant change in the mechanical properties of the wood. Mechanical testing in compression parallel to the grain was performed only for groups with an input MC of 35 ± 2%, because of statistically insignificant differences in the permeability change in groups with higher initial MC. The results of compression strength (CS) and modulus of elasticity (MOE) can be observed in Tab. 4. The mean values of CS of all groups exposed to a MW intensity of 2 and 3 kW were in the range 45.7–47.6 MPa. The CS was 0.5–4.0% less than the reference group. According to statistical analysis, the influence of MW pre-treatment or impregnation modification (LP) on the mechanical properties of Norway spruce is not statistically significant. Koiš et al. (2014) reported that the wood structure of Norway spruce was destroyed after exposure to MW with an intensity of 3–5 kW and conveyor speed of 0.2 - 0.4 $m \cdot min^{-1}$. Oloyede and Groombridge (2000) examined the effect of MW pre-treatment on Caribbean pine. The specimens were exposed to MW with an intensity of 1.6 kW at frequency 2.45 GHz for two intervals. They found that the CS was reduced by 17%. Vinden et al. (2007) increased retention by MW pre-treatment of Sitka spruce wood that significantly reduced the MOR.

When a MW intensity of 2 kW at frequency 2.45 GHz was used, the Young's modulus of elasticity (MOE) increased by 7.3% compared to the reference specimens. The use of higher MW intensity (3 kW) decreased MOE by 12.4%. According to Torgovnikov and Vinden (2009), the high absorption of MW energy by the wood can create an overpressure of water vapor, which leads to the formation of cracks in the cell wall and weakening of the material strength. The authors confirmed this theory during their experiment in which they MW-treated *Pinus radiata* and caused a reduction of wood strength of 4–26 %.

Tab. 4: The compression strength (CS) and the Young´s modulus of elasticity (MOE) of the MW treated and impregnated groups with MC of 35 ± 2 %.

Group	**Reference**	**2 kW + SP**	**3 kW + SP**	**SP**	**LP**
No. of specimens	50	50	50	50	50
MOE (GPa)	15.4[a] (5.4)	16.6[a] (5.4)	13.50[a] (4.0)	15.5[a] (6.7)	14.6[a] (5.2)
CS (MPa)	47.6[a] (7.8)	47.3[a] (7.0)	45.7[a] (7.5)	46.3[a] (7.4)	45.7[a] (6.5)

*Average standard deviation in parentheses; different letters indicate significant differences among the means according to Tukey's HSD.

CONCLUSIONS

(1) It was found that selected MW pre-treatment and different MC did not have a significant effect on the permeability of shingles made of spruce ripewood. *(2)* When a long-time process of impregnation was applied, in comparison with all MW-treated groups the retention level was three times higher. The results and statistical evaluation of retention, penetration depth, and level of impregnation area showed a dependency on adjusted time modification of vacuum-pressure impregnation. *(3)* The MW-treated and reference specimens underwent mechanical testing in which compression strength (CS) parallel to the grain and

Young's modulus of elasticity (MOE) were measured. No statistically significant differences were found. *(4)* MW treatment did not change the mechanical properties of the wood specimens; however, the retention increase remained unchanged. Modification of the impregnation process had a positive outcome; however, this method of production could be considered economically ineffective.

ACKNOWLEDGEMENTS

This work was supported by the Internal Grant Agency (IGA) of the Faculty of Forestry and Wood Technology, Mendel University in Brno, (project no. LDF_VP_2018035).

REFERENCES

1. Alfredsen, G., Flate, P.O., Evans, F.G., 2007: Comparison of four methods for natural durability classification. In: Workshop COST Action E37, Brasov, Romania, 23 pp.
2. Brodie, G., 2009: Innovative wood drying: applying microwave and solar technologies to wood drying. VDM Verlag, Saarbrucken, Germany, 120 pp.
3. Caudullo, G., Tinner, W., Daniele, R., 2016: *Picea abies* in Europe: distribution, habitat, usage, and threats. In: European atlas of forest tree species (eds. San-Miguel-Ayanz, J., de Rigo, D., Caudullo, G., Houston Durrant, T., Mauri, A.). Pp 114-116, Publication Office of the European Union. Luxemburg.
4. Dashti, H., Tarmian, A., Faezipour, M., Hedjazi, S., Shahverdi, M., 2012: Effect of microwave radiation and pre-steaming treatments on the conventional drying characteristics of fir wood (*Abies alba* L.). Lignocellulose 1: 166-173.
5. Dömény, J., Koiš, V., Dejmal, A., 2014: Microwave radiation effect on axial fluid permeability in false heartwood of beech (*Fagus sylvatica* L.). BioResources 9(1): 372-380.
6. Dömény, J., Čermák, P., Koiš, V., Tippner, J., Rousek, R., 2017: Density profile and microstructural analysis of densified beech wood (*Fagus sylvatica* L.) plasticized by microwave treatment. European Journal of Wood and Wood Production 76: 105-111.
7. Durmaz, S., Yildiz, U.C., Yildiz, S., 2015: Alkaline enzyme treatment of spruce wood to increase permeability. BioResources 10(3): 4403-4410.
8. EN 350, 2016: Durability of wood and wood-based products. Testing and classification of the durability to biological agents of wood and wood-based materials.
9. Evans, P.D., Beutel, P.J., Donnelly, C.F., Cunningham, R.B., 1994: Fire resistance of preservative treated fence posts. The Int. Res. Group on Wood Pres., Stockholm, Doc. N° IRG/WP/94-30033, 9 pp.
10. Fujii, T., Suzuki, Y., Kuroda, N., 1997: Bordered pit aspiration in the wood of *Cryptomeria japonica* in relation to air permeability. IAWA Journal 18(1): 69-76.
11. Gezer, E., Kuştaş, S., Durmaz, S., 2017: The effects of pre-microwave treatment on retention levels and some mechanical properties of spruce wood treated with CCA. 48. The International Research Group on Wood Protection, Ghent, Belçika, Pp.1-8

12. Haygreen, J.G., Bowyer, J.L., 1982: Forest products and wood science, an introduction. Iowa State University Press, Ames, IA. 495 p.
13. Hacke, U.G., Sperry, J.S., Pittermann, J., 2004: Analysis of circular bordered pit function II. Gymnosperm tracheids with torus-margo pit membranes. American Journal of Botany 91(3): 386-400.
14. He, S., Lin, L., Fu, F., Zhou, Y., Fan, M., 2014: Microwave treatment for enhancing the liquid permeability of Chinese fir. BioResources 9(2): 1924-1938.
15. Hong-Hai, L., Qing-Wen, W., Lin, Y., Tao, J., Ying-Chun, C., 2005: Modification of larch wood by intensive microwave irradiation. Journal of Forestry Research 16(3): 237-240.
16. Glass, V.G., Zelinka, L.S., 2010: Moisture relations and physical properties of wood. In: Wood handbook (chapter 4) (eds. Ross, J.). Pp 4.1 - 4.19, Forest Products Laboratory. Madison USA.
17. Kärkkäinen, M., 2003: Puutieteen perusteet (Principles of wood science) (in Finnish). Karisto Oy, Hämeenlinna. 451 p.
18. Kollmann, F., Côté, W., 1968: Principles of wood science and technology. I. Solid wood. Springer-Verlag, Berlin. 592 pp.
19. Koiš, V., Dömény, J., Tippner, J., 2014: Microwave device for continuous modification of wood. BioResources 9(2): 3025-3037.
20. Konopka, A., Barański, J., Orłowski, K., Szymanowski, K., 2018: The effect of full-cell impregnation of pine wood (*Pinus sylvestris* L.) on changes in electrical resistance and on the accuracy of moisture content measurement using resistance meters. BioResources 13(1): 1360-1371.
21. Lehringer, C., Richter, K., Schwarze, F.W., Militz, H., 2009: A review on promising approaches for liquid permeability improvement in softwoods. Wood and Fibre Science 41(4): 373-385.
22. Lehringer, C., 2011: Permeability improvement of Norway spruce wood with the white rot fungus *Physisporinus vitreus*. Doctoral dissertation, Georg-August University Göttingen, Germany, 32 pp.
23. Li, J., Zhang, L.P., Peng, F., Bian, J., Yuan, T.Q., Xu, F., Sun, R.C., 2009: Microwave-assisted solvent-free acetylation of cellulose with acetic anhydride in the presence of iodine as a catalyst. Molecules 14(9): 3551-3566.
24. Machado, J.P., 2006: Effect of microwave treatment on oak compression strength. Silva Lusitana 14(1): 51-58.
25. Melcher, E., Zwiefelhofer, J., 2013: Investigations concerning liquid absorption of six heartwood species. Pp 1-13. In: Proceedings IRG Annual Meeting. Stockholm: IRG Secretariat.
26. Oloyede, A., Groombridge, P., 2000: The influence of microwave rating on the mechanical properties of wood. Journal of Material Processing Technology 100(1): 67-73.
27. Paserin, V., 1970: Impregnation of spruce and fir wood. ŠDVÚ, Bratislava, 26 pp.
28. Paz, A.M., 2010: The dielectric properties of solid biofuels (doctoral thesis). Mälardalen University, 64 pp.

29. Pánek, M., Reinprecht, L., Mamoňová, M., 2013: *Trichoderma viride* for improving spruce wood impregnability. BioResources 8(2): 1731-1746.
30. Policinska-Serwa A., Jakimowicz, M., 2013: Wood shingles in modern construction industry. Annals of Warsaw University of Life Sciences – SGGW Forestry and Wood Technology (84): 170-175.
31. Ramezanpour, M., Tarmian, A., Taghiyari, H.R., 2014: Improving impregnation properties of fir wood to acid copper chromate (ACC) with microwave pre-treatment. iForest - Biogeosciences and Forestry 8(1): 89-94.
32. Reinprecht, L., 2008: Wood protection (Ochrana dreva). Technical University, Zvolen, 453 pp.
33. Samani, A., Ganguly, S., Kanyal, R., Tripathi, S., 2019: Effect of microwave pre-treatment on preservative retention and treatability of *Melia composita* wood. Journal of Forest Science 65: 391-396.
34. Schwarze, F.W.M.R., Landmesser, H., Zgraggen, B., Heeb, M., 2006: Permeability changes in heartwood of *Picea abies* and *Abies alba* induced by incubation with *Physisporinus vitreus*. Holzforschung 60: 450-454.
35. Trajkovic, J., 1994: The influence of microwave drying on the permeability of fir wood. Sumarski fakultet, Zagreb, Croatia. Drvna Industrija 119-123.
36. Treu, A., Rieche, H., Militz, H., 2008: Spruce and pine heartwood treatment by means of microwave radiation. The International Research Group on Wood Protection, 39th Annual Meeting, Istanbul, Türkei, IRG/WP 08-40411, 10 pp.
37. Treu, A., Gjolsjo, S., 2008: Spruce impregnation, finally a breakthrough by means of microwave radiation. In: Proceedings of the "4th Meeting of the Nordic Baltic Network in Wood Material Science & Engineering (WSE)". Pp 42-48, Copenhagen University.
38. Torgovnikov, G.I., 1993: Dielectric properties of wood and wood-based materials. Springer-Verlag, Berlin, 195 pp.
39. Torgovnikov, G.I., Vinden, P., 2009: High intensity microwave wood modification for increasing permeability. Forest Products Journal 59(4): 84-92.
40. Terziev, N., Daniel, G., 2013: Application of high frequency treatments for improved permeability of Norway spruce (*Picea abies* Karst.) wood. In: Wood the Best Material for Mankind. J. Kúdela & M. Babiak (eds.). Pp 43-48, Arbora Publishers, Zvolen.
41. Vinden, P, Torgovnikov, G, Hann, J., Shaginov, A., 2007: Microwave modification of *Picea sitchensis* (Sitka spruce). In: e-Proceedings of the Third European conference on Wood Modification. Publication City/Country Bangor, United Kingdom Pp 287-290.
42. Vinden, P., Torgovnikov, G. I., Hann, J., 2011: Microwave modification of radiata pine railway sleepers for preservative treatment. European Journal of Wood and Wood Products 69(2): 271-279.
43. Yu, J., Li, H., Sun, B., Duo, H., 2011: Effects of the Conditions on the Temperature Changes inside the Wood during Microwave Heating. Advanced Materials Research, vol. 327, Trans Tech Publications, Ltd. Pp. 100-104.
44. Zhang, Y., Jia, K., Cai, L., Shi, S. Q., 2013: Acceleration of moisture migration in larch wood through microwave pre-treatments. Drying Technology 31(6): 666-671.

DOMINIK HESS*, PETR PAŘIL, JAKUB DÖMÉNY, JAN BAAR
MENDEL UNIVERSITY IN BRNO
FACULTY OF FORESTRY AND WOOD TECHNOLOGY
DEPARTMENT OF WOOD SCIENCE AND TECHNOLOGY
ZEMĚDĚLSKÁ 3, 613 00 BRNO
CZECH REPUBLIC
*Corresponding author: dominik.hess@mendelu.cz

WOOD RESEARCH doi.org/10.37763/wr.1336-4561/66.4.582594
e-ISSN 2729-8906
66(4): 2021 582-594 pp.

INFLUENCE OF STIFFNESS RELATED TO THE C40 STRENGTH CLASS OF THE HARDWOOD GROUP ESTABLISHED BY THE BRAZILIAN STANDARD IN THE DESIGN OF TIMBER STRUCTURES

FRANCISCO ANTONIO ROCCO LAHR
UNIVERSITY OF SÃO PAULO
BRAZIL

VINICIUS BORGES DE MOURA AQUINO
FEDERAL UNIVERSITY OF SOUTHERN AND SOUTHEASTERN PARÁ
BRAZIL

FELIPE NASCIMENTO ARROYO
FEDERAL UNIVERSITY OF SÃO CARLOS
BRAZIL

HERISSON FERREIRA DOS SANTOS
FEDERAL INSTITUTE OF RONDONIA
BRAZIL

SERGIO AUGUSTO MELLO SILVA
SÃO PAULO STATE UNIVERSITY
BRAZIL

ANDERSON RENATO VOBORNIK WOLENSKI
FEDERAL INSTITUTE OF SANTA CATARINA
BRAZIL

CARLOS MAVIAEL DE CARVALHO
FEDERAL UNIVERSITY OF SOUTHERN AND SOUTHEASTERN PARÁ
BRAZIL

JOÃO PAULO BOFF ALMEIDA, ANDRÉ LUIS CHRISTOFORO
FEDERAL UNIVERSITY OF SÃO CARLOS
BRAZIL

(RECEIVED AUGUST 2020)

ABSTRACT

The Brazilian standard ABNT 7190 (1997) establishes the strength classes C20, C30, C40 and C60 for the proper framework of the different wood types in the group of hardwoods. Associated with the strength class, which is based on the compressive strength characteristic value parallel to the fibers ($f_{c0,k}$), the standard stipulates the respective values representing the stiffness (E_{c0}), with 19500 MPa being the reference value for the class C40, essential variables in structural design. For being the C40 class is the one with the greatest amplitude (20 MPa), it is possible that the value 19500 MPa is not the best representation of stiffness. This work aimed to verify the representativeness the stiffness value established by the Brazilian standard for C40 wood. The result obtained from the average confidence interval indicates the value of 14110 MPa as being the most representative, which may imply structures that are supposedly more rigid than they really are.

KEYWORDS: Wood, native forests, hardwoods, strength classes.

INTRODUCTION

One of the materials most used by man throughout history, wood is directly related to the problems solution such as housing; crossing natural and/or artificial obstacles; the vehicles construction for the different means of transport; agricultural products storage; the manufacture of furniture and packaging, among others (Coimbra et al. 2018, Almeida et al. 2019, Wolenski et al. 2020a).

Wood versatility has always been fundamental for meeting human needs. Similarly, Brazil experiences this situation (Segundinho et al. 2017, Silva et al. 2018, Wolenski et al. 2020b, Jankowska and Kozakiewicz 2014). Wood availability made its employment experience a wide expansion (Guntekin and Aydin 2016), covering more and more new possibilities of application in the structure's construction: roofs, bridges, walkways, silos, shoring and shoring (Vieira et al. 2016, Lahr et al. 2017, Guntekin and Aydin 2016, Derkowski et al. 2015, Ihnát et al. 2018).

Brazil is the second country in relation to the area of forests in the world, behind only Russia (Beech et al. 2017). The certified areas of the Amazon Forest have 1.26 million hectares (in Brazil, 6.30 million hectares of forests are certified) (Lentini et al. 2012). There is no consensus regarding the number of tree species contained in the Amazon Forest, the most recent estimate being around 16 thousand species (Ter Steege et al. 2016). These data show the importance of Brazil in relation to the forest potential and, in addition, it highlights the importance of studies for the identification and technological characterization of species from the Amazon rainforest.

In Brazil, the design and dimensioning of timber structures follows the premises and calculation methods of the normative document ABNT NBR 7190 (1997), which has

the strength (f_{c0}) and stiffness (E_{c0}) properties to compression in the parallel direction as the reference for structural design.

The Brazilian standard ABNT NBR 7190 (1997) also specifies the test methods as well as the strength classes, which fit the different wood species based on the characteristic values of the compressive strength in the direction parallel to the fibers ($f_{c0,k}$). For hardwoods, the strength classes are C20 ($20 < f_{c0,k} \leq 30$ MPa), C30 ($30 < f_{c0,k} \leq 40$ MPa), C40 ($40 < f_{c0,k} \leq 60$ MPa) and C60 ($f_{c0,k} > 60$ MPa), as shown in Tab. 1.

Tab. 1: Strength classes of hardwoods. Source: Adapted from ABNT NBR 7190 (1997).

Classes	**$f_{c0,k}$ (MPa)**	**$E_{c0,m}$ (MPa)**	**$\rho_{12\%}$ (kg·m^{-3})**
C20	20	9500	650
C30	30	14500	800
C40	40	19500	950
C60	60	24500	1000

Associated with the strength classes, standard also establishes reference values for the elasticity modulus in the compression parallel to the fibers (E_{c0}) (Tab. 1), it should be noted that the C40 class is the one with the greatest range of values (20 MPa), being the amplitude other classes of 10 MPa.

Due to the greater amplitude related to the C40 strength class, the wood species diversity existing in Brazil and the 23 years since the standard publication, it is possible that the value of E_{c0} = 19500 MPa is not an effective representative of stiffness, which can lead to less secure projects if the most appropriate value is less than 19500 MPa.

This research aimed, with the help of twenty-one species of wood from native forests and categorized in class C40 of hardwoods group, in Brazilian standard ABNT NBR 7190 (1997), of the confidence interval of the average (p = 5%) and the Bootstrap resampling technique for simulating the mean confidence interval (100 to 1000000 simulations), investigate whether the reference value of 19500 MPa proposed by the standard is effectively a representative quantity of the respective strength class, since, with the most representative value being less than that, structural projects can be developed in an unfavorable way to safety.

MATERIAL AND METHODS

The twenty-one species of wood from native forests listed in Tab. 2 were used to verify the representativeness of the reference value of 19500 MPa for the modulus of elasticity (E_{c0}) in the parallel compression to fibers for class C40 wood proposed by the Brazilian standard ABNT NBR 7190 (1997).

Tab. 2: Names of tropical forest species evaluated.

Common name	**Scientific name**
Angelim-amargoso	*Votairea fusca*
Angelim-araroba	*Vataireopsis araroba*
Angelim-pedra	*Hymenolobium petraeum*
Angelim-saia	*Votairea sp*

Angico-preto	*Piptadenia macrocarpa*
Branquinho	*Sebastiania commersoniana*
Cafearana	*Andira stipulacea*
Canela Sassafrás	*Ocotea odorifera*
Castelo	*Calycophyllum multiflorum.*
Catanudo	*Calophyllum sp*
Copaíba	*Copaifera cf. ret*
Cutiúba	*Goupia paraensis*
Goiabão	*Planchonella pachycarpa*
Guaiçara	*Luetzelburgia sp*
Louro-preto	*Ocotea sp*
Mandioqueira	*Qualea paraensis*
Parinari	*Parinari excelsa*
Piolho	*Tapirira sp*
Rabo-de-arraia	*Vochysia haenkeana*
Tatajuba	*Bagassa guianensis*
Umirana	*Qualea retusa*

The wood from homogeneous lots was properly stored, resulting in a moisture content close to 12%, as recommended by the Brazilian standard ABNT NBR 7190 (1997). The assumptions and test methods of the Brazilian standard were followed to obtain the values of resistance (f_{c0}) and stiffness (E_{c0}) to compression in the direction parallel to the fibers as well as the values of apparent density ($\rho_{12\%}$).

Also as recommended by the Brazilian standard, twelve specimens per species were manufactured and tested in parallel compression (Fig. 1) as well as twelve others for determining apparent density values, resulting in 756 experimental determinations in all.

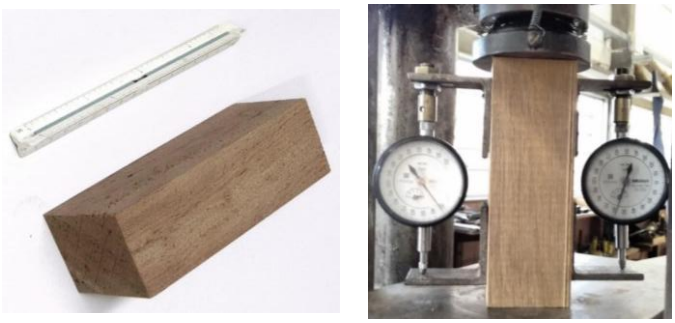

(a) (b)

Fig. 1: Standardized specimen 5 × 5 × 15 cm according to ABNT NBR 7190 (1997) (a), and the apparatus used to perform the compression tests in the direction parallel to the fibers (b).

When the specimens were broken in the universal testing machine (AMSLER, 25 tons), their moisture content (U) at the time of the tests was obtained using the Marrari M5 contact humidity meter ($10.76\% \leq U \leq 12.96\%$). With the moisture content in the samples, the values of resistance (f_{c0}) and elasticity modulus (E_{c0}) to compression in the direction parallel to the fibers were corrected to the moisture content of 12% ($f_{c0,12}$, $E_{c0,12}$) with the aid of Eqs. 1 and 2 according to ABNT NBR 7190 (1997), resp., in which f_{c0}, U and E_{c0}, U consist of the samples strength and stiffness associated with the moisture content U.

$$E_{c0,12} = E_{c0,U} \cdot \left[1 + \frac{2 \cdot (U - 12)}{100}\right] \text{ (MPa)} \quad (1)$$

$$f_{c0,12} = f_{c0,U} \cdot \left[1 + \frac{2 \cdot (U - 12)}{100}\right] \text{ (MPa)} \quad (2)$$

Based on the corrected values of compressive strength in the direction parallel to the fibers ($f_{c0,12}$), Eq. 3 according to ABNT NBR 7190 (1997) was used to determine the characteristic value ($f_{c0,k}$) for the wood categorization (Tab. 1), where f_1, f_2 to f_n denote the compressive strength values ($f_{c\,0.12}$) in ascending order of the n test specimens tested (n = 12).

$$f_{c0,k} = Max\left\{\begin{array}{c} f_1 \\ 0.7 \cdot \dfrac{\sum_{i=1}^{n} f_i}{n} \\ 1.1 \cdot \left[2 \cdot \left(\dfrac{f_1 + f_2 + f_3 + \ldots + f_{(n/2)-1}}{(n/2) - 1}\right) - f_{n/2}\right] \end{array}\right. \quad (3)$$

The mean confidence interval (variation inference in the population mean value based on the sample), at the 95% reliability level, was used to calculate the mean value as well as the lower (2.5%) and upper (97.5%), and the Anderson-Darling test (p = 5%) was used to assess the normal distribution of E_{c0} values considering the set of 21 wood species. For the assumptions assumed in the normality test, p-value equal to or greater than the level of significance implies normality in the E_{c0} distribution, which validates the results obtained from the confidence interval. In order to increase the results reliability, the Bootstrap resampling technique was used to simulate the average confidence intervals (95% reliability), with 100 to 1000000 simulations being considered.

Based on the literature (Almeida et al. 2016), the increase in density implies a tendency to increase the wood strength and stiffness. As density is a property of easy experimental determination, it was used as an resistance and stiffness estimator to compression in the direction parallel to the wood fibers by the linear regression model evaluated by analysis of variance (ANOVA), at the level of p = 5%, allowing to judge, in addition to the quality of the fit (adjusted determination coefficient - R^2_{adj}), also the significance of the models, which allows to identify whether increases in apparent density effectively imply increases in the values of mechanical properties.

RESULTS AND DISCUSSION

Tab. 3 shows the average values of apparent density ($\rho_{12\%}$), strength (f_{c0}) and stiffness (E_{c0}) to compression in the direction parallel to the fibers, as well as the characteristic value $f_{c0,k}$ (Eq. 3) of the referred strength property.

Tab. 3: Results of the physical and mechanical properties of the wood species evaluated.

Species	$\rho_{12\%}$ (kg·m^{-3})	f_{c0} (MPa)	$f_{c0,k}$ (MPa)	E_{c0} (MPa)
Angelim-amargoso	772	60	47.7	15940
Angelim-araroba	674	50	45.3	12587
Angelim-pedra	663	58	44.5	11990
Angelim-saia	764	63	51.1	24081
Angico-preto	888	73	55.6	15375
Branquilho	810	49	45.6	13813
Cafearana	678	58	42.4	14185
Casca-grossa	788	57	44.5	17936
Castelo	759	55	54.5	11105
Catanudo	804	51	51.0	13029
Copaíba	695	50	44.1	14012
Cutiúba	1152	79	55.3	18238
Goiabão	938	49	43.1	18717
Guaiçara	995	66	58.9	14027
Louro-preto	680	55	42.1	13536
Mandioqueira	855	71	59.2	19274
Parinari	792	60	56.2	21881
Piolho	828	62	43.7	13404
Rabo-de-arraia	729	60	48.7	14411
Tatajuba	945	79	55.0	18574
Umirana	705	54	52.1	10178

The variation coefficients (CV) for $\rho_{12\%}$, f_{c0} and E_{c0} varied in the ranges from 4.31 to 8.22%, from 10.22 to 16.73% and from 12.73 to 19.15%, respectively, and it is worth noting that the maximum value of CV for f_{c0} (16.73%) was lower than the 18% CV established as a limit for normal requests by the Brazilian standard ABNT NBR 7190 (1997).

As expected, the average property values of some species of wood (Tab. 3) were close to the values obtained in the studies by Nogueira, Nogueira and Lahr (2001), Christoforo et al. (2017), Aquino et al. (2018a,b), Lima et al. (2018) and Morando et al. (2019), it should be noted that the lowest value of E_{c0} obtained (Tab. 3) was equal to 10178 MPa (Umirana wood), about 52% lower than the reference value (19500 MPa) established by ABNT NBR 7190 (1997), and the largest (24081 MPa for Angelim-saia wood) is approximately 23.49% higher than the representative value of the C40 resistance class.

Fig. 2 illustrates the result of the Anderson-Darling normality test for apparent density, fundamental for validating the mean confidence interval. Tab. 4 shows the mean confidence intervals (95% reliability) obtained considering the 21 species (T-test) as well as the confidence intervals extrapolated by the Bootstrap technique.

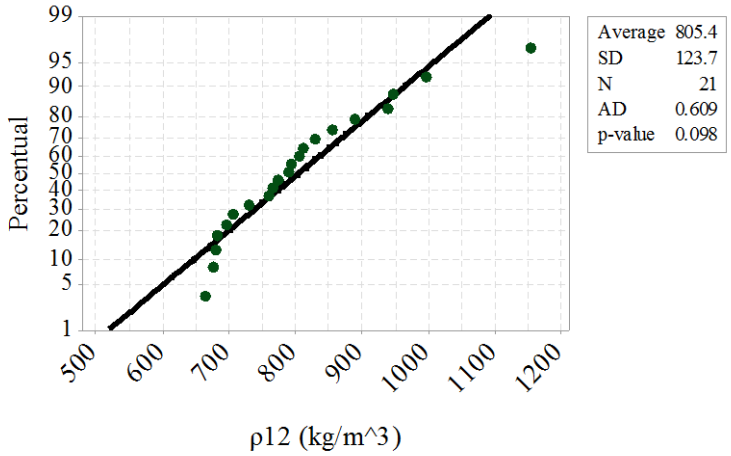

Fig. 2: Result of the Anderson-Darling normality test (p =5%) regarding the apparent density values.

Tab. 4: Confidence intervals results of the mean (CI) for the apparent density (kg·m⁻³).

Methods	CI (95% reliability)		
	Inferior limit	Average	Upper limit
T-test	749	805	862
Bootstrap - 100 simulations	755	804	850
Bootstrap - 500 simulations	752	805	850
Bootstrap - 1000 simulations	756	805	852
Bootstrap - 5000 simulations	757	805	850
Bootstrap - 10000 simulations	757	806	852
Bootstrap - 50000 simulations	757	805	851
Bootstrap - 100000 simulations	757	805	850
Bootstrap - 500000 simulations	757	805	851
Bootstrap - 1000000 simulations	757	805	851

From Fig. 3, the p-value of the Anderson-Darling normality test was higher than the level of significance adopted (p = 5%), showing the normality in the density values distribution, which validates the results of the mean confidence interval.

By the Bootstrap technique, there was a convergence of both the lateral limits and the average value between 500000 and 1000000 simulations, and for this reason, 805 kg·m^{-3} consists of the representative value of the apparent density for class C40 of the Brazilian standard ABNT NBR 7190 (1997). It should be noted that the reference value for the current standard is 950 kg·m^{-3} (Tab. 1), a value 18% higher than that found in the present study. As there is a tendency for denser woods to show greater resistance and stiffness (Almeida et al. 2016), it is very likely that the wood species used in the generation of resistance classes for the hardwood group by the current Brazilian norm (about 23 years since the last update) presented values of stiffness higher than those found in this work.

The results of the Anderson-Darling normality test and the mean confidence intervals (T-test and Bootstrap simulation) for the compression elasticity module in the direction parallel to the wood fibers are shown in Fig. 3 and Tab. 5, respectively.

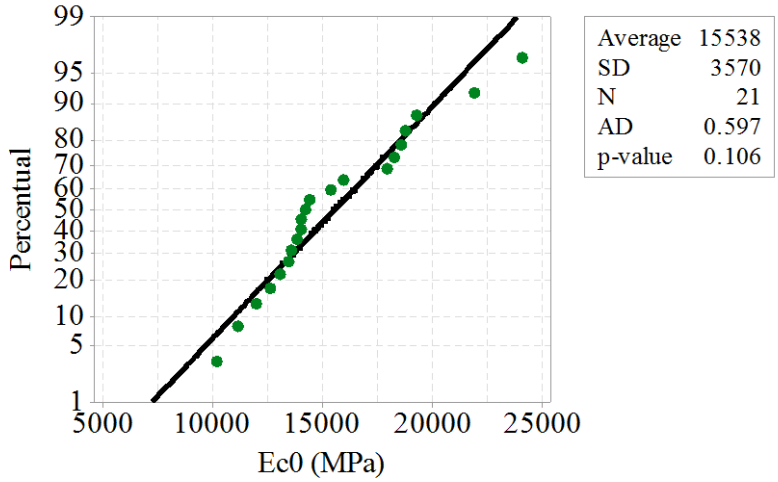

Fig. 3: Result of the Anderson-Darling normality test (p = 5%) for the elasticity modules in parallel compression.

Tab. 5: Confidence intervals results of the mean (CI) for the elasticity modulus in the compression parallel to the fibers (MPa).

Methods	**CI (95% reliability)**		
	Inferior limit	**Average**	**Upper limit**
T-test	13913	15536	17163
Bootstrap - 100 simulations	13848	15642	16881
Bootstrap - 500 simulations	14063	15510	16825
Bootstrap - 1000 simulations	14126	15537	16865
Bootstrap - 5000 simulations	14126	15554	16829
Bootstrap - 10000 simulations	14118	15540	16809
Bootstrap - 50000 simulations	14101	15536	16817
Bootstrap - 100000 simulations	14111	15539	16819
Bootstrap - 500000 simulations	14110	15538	16820
Bootstrap - 1000000 simulations	14110	15538	16820

As the distribution of E_{c0} values is normal, the confidence intervals (CI) results of the mean (95% reliability) are accepted. As in the case of apparent density, there was convergence in the elasticity modulus results in the compression parallel to the fibers between 500000 and 1000000 of simulations. Thus, the E_{c0} average value consisted of 15538 MPa, and the lower and upper limits of the average value by the CI were equal to 14110 and 16820 MPa, respectively.

Based on the average value obtained for E_{c0} with 500000 or 1000000 simulations, the reference value (19500 MPa, class C40) (Tab. 1) established by the current Brazilian legislation ABNT NBR 7190 (1997) is 25.5% higher than the average value obtained of E_{c0} in the present study and 38.2% higher than the lower limit of the average value obtained from the CI, which implies that the reference value stipulated by the aforementioned standard is unfavorable to security for allegedly considering more rigid structures.

For a better understanding of the impact of adopting the modulus of elasticity value to compression in the direction parallel to the fibers (E_{c0} = 19500 MPa) (Tab. 1) of the C40 strength class established by the Brazilian standard ABNT NBR 7190 (1997), be it the beam illustrated in Fig. 4, subject to the action of permanent (g) and accidental (q) distributed forces,

span L and b and h measures for the base and the height of the rectangular cross section, respectively.

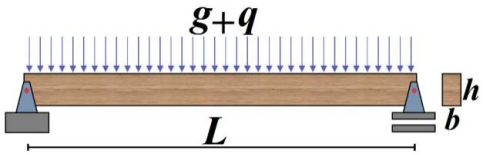

Fig. 4: Structure considered for the analysis of the effects of adopting the value of E_{c0} = 19500 MPa referring to class C40 of the Brazilian standard ABNT NBR 7190 (1997).

For structural scheme illustrated in Fig. 4, the maximum displacement occurs in the middle of the span (*L/2*), and is determined using Eq. 4:

$$\delta_{max} = \frac{5 \cdot (g+q) \cdot L^4}{32 \cdot E_{c0} \cdot b \cdot h^3} \tag{4}$$

For the limit state condition of use, the Brazilian standard establishes maximum value of vertical displacement equal to *L/200*. Assuming the values of b = 60 mm, h = 150 mm, L = 3000 mm and E_{c0} = 19500 MPa according to ABNT NBR 7190 (1997), for a maximum displacement of 15 mm (*L*/200) and making use of Eq. 4, the value resulting from the sum of the distributed forces (g + q) is equal to 4.68 kN·m^{-1}.

Considering the load of 4.68 kN·m^{-1}that meets the service limit state, but now using the values of the confidence interval of the mean (Tab. 5, last line) of the elastic modulus in the direction parallel to the fibers (E_{min} = 14110 MPa, E_{med} = 15538 MPa, E_{max} = 16820 MPa), the maximum displacements result in 20.73 mm, 18.83 mm and 17.39 mm. This implies that the displacements calculated with the E_{c0} of the present work are 38.2%, 25.5% and 15.7% higher than the displacement value of the service condition calculated based on the E_{c0} established in the C40 resistance class of the Brazilian standard. It should be noted that such excessive displacements can promote the manifestation of diverse pathologies in timber structures (Andrade et al. 2014).

Fig. 5 presents the regression models results for the mechanical properties estimates (f_{c0}, E_{c0}) as a function of apparent density.

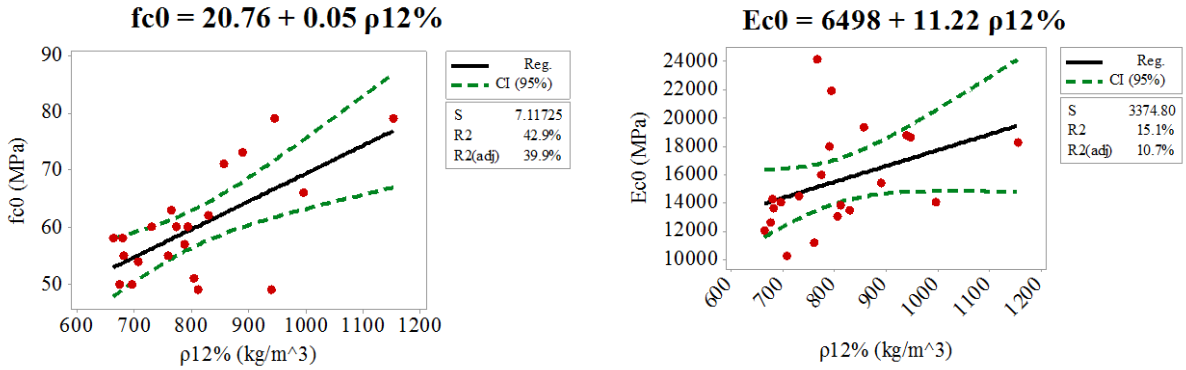

Fig. 5: Regression models.

By the adjusted determination coefficients obtained from the regression models presented in Fig. 4, it is concluded that the apparent density was not a good estimator of the strength and stiffness properties in the direction parallel to the wood fibers, however, for the estimate of the f_{c0}, it is worth noting that the model was considered significant by ANOVA (p = 5%), and this implies that increases in density promote increases in compressive strength in the direction parallel to the wood fibers (behavior trend). Such a result is justified, since the woods are both belonging to the same strength class (40 MPa $\leq f_{c0,k} <$ 60 MPa) and with densities ranging between 663 and 1152 $kg \cdot m^{-3}$ (large amplitude). To obtain more accurate models, other strength classes must be considered together (Almeida et al. 2017) as well as the adoption of chemical constituents of wood (Duarte et al. 2020) also as estimators.

CONCLUSIONS

The results of this research make it possible to conclude that: *(1)* The elasticity modulus value of 19500 MPa in compression parallel to the fibers (E_{c0}) considered by the current Brazilian standard ABNT NBR 7190 (1997) for the C40 resistance class of the hardwood group is 38.2% higher than the lower limit of the value mean (14110 MPa) obtained from the mean confidence interval (CI - 95% reliability) extrapolated by the Bootstrap technique (1000000 simulations). *(2)* From the example of the bi-supported beam under uniform loading, the adoption of the lower limit of the average value of the CI for E_{c0} (extrapolated by the Bootstrap technique) resulted in a displacement 38.2% higher than the value of the limit displacement established for the service condition by Brazilian standard. *(3)* Based on the experimental results of the 21 wood species evaluated, the apparent density ($\rho_{12\%}$) was not a good estimator of the values of resistance and stiffness to compression in the direction parallel to the fibers, which highlights the need for the incorporation of wood species of other resistance classes as well as considering the use of chemical components of wood as estimators in addition to $\rho_{12\%}$.

The results of the present research are important since the structural projects, elaborated on the premises of the Brazilian standard in force ABNT NBR 7190 (1997), may be subject to excessive displacements, which can compromise the structural integrity because it is a potential source of pathologies in the future.

ACKNOWLEDGMENTS

For all the support provided during the production of this research, the authors thank the Coordination for the Improvement of Higher Education (CAPES) and the National Council for Scientific and Technological Development (CNPq).

REFERENCES

1. ABNT, 1997: Projeto de estruturas de madeira ABNT- Técnicas NBR 7190 (Timber structures design). Associação Brasileira de Normas Técnicas.

2. Almeida, T.H., Almeida, D.H., Araujo, V.A., Silva, S.A.M., Christoforo, A.L., Lahr, F.A.R., 2017: Density as estimator of dimensional stability quantities of Brazilian tropical woods. BioResources 12(3): 6579-6590.
3. Almeida, T.H., Almeida, D.H., Arroyo, F.N., Araujo, V.A., Chahud, E., Branco, L.A.M. N., Pinheiro, R.V., Christoforo, A.L., Rocco Lahr, F.A., 2019: Time of exposure at 60^{o}C service temperature: influence on strength and modulus of elasticity in compression parallel to the grain of hardwood species. BioResources 14(1): 207-219.
4. Almeida, T.H., Almeida, D.H., Christoforo, A.L., Chahud, E., Branco, L.A.M.N., Rocco Lahr, F.A., 2016: Density as estimator of strength in compression parallel to the grain in wood. International Journal of Materials Engineering 6(3): 67-71
5. Andrade Jr., J.R., Almeida, D.H., Almeida, T.H., Christoforo, A.L., Rocco, F.A.L., 2014: Avaliação das estruturas de cobertura em madeira de um galpão de estoque de produtos químicos (Evaluation of wood roof structures of industrial shed for chemicals stock). Ambiente Construído 14(3): 75-85.
6. Aquino, V.B.M., Almeida, J.P.B., Almeida, D.H., Almeida, T.H., Panzera, T.H., Christoforo, A.L., Lahr, F.A.R., 2018a: Physical and mechanical characterization of Copaifera sp. wood specie. International Journal of Materials Engineering 8(3): 55-58.
7. Aquino, V.B.M., Panzera, T.H., Magalhães, L.N., Christoforo, A.L., Lahr, F.A.R., 2018b: Physical and mechanical characterization of Ocotea sp. wood specie. Construindo 10(2): 31-40.
8. Beech, E., Rivers, M., Oldfield, S., Smith, P.P., 2017: GlobalTreeSearch: The First complete global database of tree species and country distributions. Journal of Sustainable Forestry 36(5): 454-489.
9. Christoforo, A.L., Arroyo, F.N., Silva, D.A.L., Panzera, T.H., Rocco Lahr, F.A., 2017: Full characterization of *Calycophyllum multiflorum* wood specie. Engenharia Agricola 37(4): 637-643.
10. Coimbra, P.R.S., Almeida, A.S., Almeida, T.H., Almeida, D.H., Chahud, E., Christoforo, A.L., Rocco Lahr, F.A., 2018: Stress distribution in Tauari wood beam. International Journal of Materials Engineering 8(1): 5-11.
11. Derkowski, A., Mirski, R., Majka, J., 2015: Determination of sorption isotherms of scots pine (*Pinus sylvestris* L.) wood strands loaded with melamine-urea-phenol-formaldehyde (MUPF) resin. Wood Research 60(2): 201-210.
12. Duarte, B.B., Rocco Lahr, F.A., Curvelo, A.A.S., Christoforo, A.L., 2020: Influence of Physical and chemical components on the physical-mechanical properties of ten Brazilian wood species. Materials Research 23(2).
13. Güntekin, E., Aydin, T.Y., 2016: Prediction of bending properties for some softwood species grown in Turkey using ultrasound. Wood Research 61(6): 993-1002.
14. Ihnát, V., Lubke, H., Russ, A., Pazitiny, A., 2018: Waste agglomerated wood materials as secondary raw material for chipboards and fibreboards. Part II. Preparation and characterzation of wood fibres in terms of their reuse. Wood Research 63(3): 431-442.
15. Jankowska, A., Kozakiewicz, P., 2014: Comparison of outdoor and artificial weathering using compressive properties. Wood Research 59(2): 245-252.

16. Lahr, F.A.R., Christoforo, A.L, Varanda, L.D., Araujo, V.A., Chahud, E., Branco, L.A.M.N., 2017: Shear and longitudinal modulus of elasticity in wood: relations based on static bending tests. Acta Scientiarum-Technology 39(4): 433-437.
17. Lima, T.F.P., Almeida, T.H., Almeida, D.H., Chritoforo, A.L., Lahr, F.A.R., 2018: Propriedades físicas e mecânicas da madeira Tatajuba (*Bagassa guianensis*) proveniente de duas diferentes regiões brasileiras. Materia 23.
18. Morando, T.C., Christoforo, A.L., Aquino, V.B.M., Rocco Lahr, F.A., Rezende, G.B.M., Ferreira, R.T.L., 2019: Characterization of the wood species *Qualea albiflora* for structural purposes. Wood Research 64(5): 769-776.
19. Nogueira, M.C.J.A., Nogueira, J.S., Rocco Lahr, F.A., 2001: Avaliação da Itaúba e do Angelim Pedra para uso na construção civil (Evaluation of Itauba and Angelim Pedra wood species for use on civil construction). Revista Agricultura Tropical 5(1): 107-115.
20. Segundinho, P.G.A., Carreira, M.R., Regazzi, A.J., Dias, A.A., 2017: Influência do teor de umidade na determinação do módulo de elasticidade de vigas de *Pinus* sp (Influence of moisture content on the determination of the modulus of elasticity of *Pinus* sp. beams). Ambiente Construído 17(3): 319-329.
21. Silva, C.E.G., Almeida, D.H., Almeida, T.H., Chahud, E., Branco, L.A.M.N., Campos, C.I., Lahr, F.A.R., Christoforo, A.L., 2018: Influence of the procurement site on physical and mechanical properties of cupiúba wood species. BioResources 13(2): 4118-4131.
22. Ter Steege, H., Vaessen, R.W., Cárdenas-Lópes, D., Sabatier, D., Antonelli, A., Oliveira, S.M., Pitman, N.C.A., Jorgensen, P.M., Salomão, R.P., 2016: The discovery of the Amazonian tree flora with an update checklist of all known tree taxa. Scientific Reports 6(29549): 1-15.
23. Vieira, M.C.S., Gesualdo, F.A.R., 2016: Efeitos produzidos por entalhes nos terços extremos do vão de vigas estruturais de madeira (Effects produced by notches in the outer thirds of the span of structural timber beams). Ciência & Engenharia 25(1): 66-77.
24. Wolenski, A.R.V., Peixoto, R.G., Fedotova, V., Christoforo, A.L., Lahr, F.A.R., 2020a: Shear strength estimation model for tropical wood species. Wood Research 65(1): 175-182.
25. Wolenski, A.R.V., Peixoto, R.G., Aquino, V.B.M., Christoforo, A.L., Lahr, F.A.R., Panzera, T.H., 2020b: Evaluation of mechanical strengths of tropical hardwoods: proposal of probabilistic models. European Journal of Wood and Wood Products 79: 1-10.

FRANCISCO ANTONIO ROCCO LAHR
UNIVERSITY OF SÃO PAULO
DEPARTMENT OF STRUCTURAL ENGINEERING
SÃO CARLOS, SÃO PAULO
BRAZIL

VINICIUS BORGES DE MOURA AQUINO*
FEDERAL UNIVERSITY OF SOUTHERN AND SOUTHEASTERN PARÁ
TECHNOLOGY FACULTY

SANTANA DO ARAGUAIA, PARÁ
BRAZIL
*Corresponding author: aquino.vini@hotmail.com

FELIPE NASCIMENTO ARROYO
FEDERAL UNIVERSITY OF SÃO CARLOS
DEPARTMENT OF CIVIL ENGINEERING
SÃO CARLOS, SÃO PAULO
BRAZIL

HERISSON FERREIRA DOS SANTOS
FEDERAL INSTITUTE OF RONDONIA
DEPARTMENT OF AGRONOMICAL ENGINEERING
ARIQUEMES, RONDONIA
BRAZIL

SERGIO AUGUSTO MELLO SILVA
SÃO PAULO STATE UNIVERSITY
DEPARTMENT OF CIVIL ENGINEERING
ILHA SOLTEIRA, SÃO PAULO
BRAZIL

ANDERSON RENATO VOBORNIK WOLENSKI
FEDERAL INSTITUTE OF SANTA CATARINA
DEPARTMENT OF CIVIL ENGINEERING
SÃO CARLOS, SANTA CATARINA
BRAZIL

CARLOS MAVIAEL DE CARVALHO
FEDERAL UNIVERSITY OF SOUTHERN AND SOUTHEASTERN PARÁ
TECHNOLOGY FACULTY
SANTANA DO ARAGUAIA, PARÁ
BRAZIL

JOÃO PAULO BOFF ALMEIDA, ANDRÉ LUIS CHRISTOFORO
FEDERAL UNIVERSITY OF SÃO CARLOS
DEPARTMENT OF CIVIL ENGINEERING
SÃO CARLOS, SÃO PAULO
BRAZIL

WOOD RESEARCH doi.org/10.37763/wr.1336-4561/66.4.595605
e-ISSN 2729-8906
66(4): 2021 595-605 pp.

TRACE ELEMENT ANALYSIS OF TROPICAL WOODS USING PARTICLE INDUCED X–RAY EMISSION (PIXE) METHODS FROM WESTERN NIGERIA

CHARITY ADAEZE ONUMEJOR
COVENANT UNIVERSITY
NIGERIA

FATAI AKINTUNDE BALOGUN, SEJLO TEMIDAYO GBENU
OBAFEMI AWOLOWO UNIVERSITY
NIGERIA

MOJISOLA RACHAEL USIKALU, THEOPHILUS AANUOLUWA ADAGUNODO, AKINWUMI AKINPELU, JUSTINA ADA ACHUKA, THEOPHILUS EMUOBOR ARIJAJE
COVENANT UNIVERSITY
NIGERIA

(RECEIVED JULE 2020)

ABSTRACT

Trace element investigation and its corresponding concentration level in selected tropical woods from western Nigeria was done using PIXE-particle induced X-ray emission methods. Fifteen selected tropical woods were analyzed and twenty-seven trace elements were identified and quantified. The identified trace elements are Na, Mg, Al, Si, P, S, Cl, K, Ca, Ti, V, Cr, Mn, Fe, Co, Ni, Cu, Zn, Se, Br, Rb, Sr, Y, Zr, Ba, Pb and Bi. Calcium concentration were 2835, 3195, 4923, 5608, 7770, 5110, 2743, 5092 and 3451 ppm in samples 2, 5, 6, 10, 11, 12, 13, 14 and 15, respectively. Potassium recorded 2838, 4811, 3184, and 2021ppm in samples 1, 3, 8 and 9, respectively. Silicon recorded 5206 ppm for sample 4 and 5253 ppm for sample 7. Calcium and potassium were observed to have concentration level that is greater than 1000 ppm in all the studied samples, hence it can be said that calcium and potassium are major trace element of wood. The concentrations of the elements identified have no immediate health concern on environment and human, therefore the studied tropical woods safe for use as fuel and other purposes.

KEYWORDS: Wood elemental composition, wood elemental constituents, Particle induced X-ray emission method (PIXE), trace element analysis, Ion beam analysis (IBA).

INTRODUCTION

Particle induced X-ray emission (PIXE) is one of the Ion beam analytical (IBA) methods that detect elements with high atomic number $Z \geq 11$ in samples based on atomic fluorescence. In general, IBA methods are used to study materials of complex elemental matrix, based primarily on interaction between the samples elemental constituent and accelerated charged particle. Study samples are bombarded with charged particle to induce such interaction. Other IBA techniques are Particle induced gamma-ray emission (PIGE), Nuclear reaction analysis (NRA), and Rutherford backscattering spectrometry (RBS). PIGE and NRA are based on nuclear reactions while RBS is based on ion beam scattering techniques (Beck 2005). Many thin film composition analysis, optical coatings and depth profiling primarily make use of RBS. Many researches on elemental composition of materials (samples) employs destructive methods or digestion processes for the elemental analysis. Only every few research go for non-destructive analytical methods such as those of ion beam analytical techniques (Okochi 2007, Onumejor et al. 2018). This informed the use of Particle induced X–ray emission (PIXE) methods for trace element analysis of tropical wood from Western Nigeria. The knowledge of elemental constituents of any material serves as foundation for other numerous scientific findings about that sample material and their possible contribution to background environmental health or radioactivity (Xinwei 2006, Felix et al. 2013, Usikalu et al. 2018, Orosun et al. 2019, Joel et al. 2018, Adagunodo 2018). Therefore, knowing the elemental constituents of tropical woods will tell a lot about its other scientific usefulness. Woods are popularly used as fuel and furniture. Scientists have found other uses of wood that are of immerse benefit to humans, especially in the medical field. Bradley et al. (1991) worked on the photon attenuation potentials of tropical hardwoods and linked his findings to uses of woods in medicine. Scientists Zhang et al (2010), Constantinou (1982), White (1977) and Požgaj (1977) did some studies on the dosimetric usefulness of woods; its property, as combustible heat source and as medical phantom in radiotherapy. Tajuddin et al. (1996) reported the scattering investigation and radiographic properties of Rhophoraspp hardwood, its suitability as phantom material for dosimetric study. The value of woods and possible scientific uses all began with the simple knowledge of elemental composition. This prompted scientist in African region with rich tropical wood territory to conduct elemental studies and publish their discoveries. Aggrey-Smith (2015), measured the elemental compositions of some tropical wood species from pra-anum forest in Ghana using Instrumental neutron activation analysis (INAA). Zafar (2010) and Sakina (2013) also highlighted the importance of elemental analysis of wood/herbs for medicinal purposes. The present study will give details of trace elemental constituent of fifteen tropical woods from Western Nigeria using particle induce X-ray emission (PIXE) method. Recent research works on use of hardwood in other field of studies such as engineering (Haradhan and Chun, 2020, Sarmad et al. 2020, Chu et al. 2020) arts (Yasuji et al. 2020), medicine (Sachithrani et al. 2020, Assai et al. 2020), agriculture (Dora et al. 2020, Dominik et al. 2020), environmental management (Tejedor et al. 2020, Achim et al. 2020, Warlen et al. 2020), technology (Mátyás et al. 2020, Erchiqui et al, 2020),

communication (Qian et al. 2020, Yuming et al. 2020), reveals the diverse ways that wood analysis can be manipulated to serve multiple purposes.

MATERIAL AND METHODS

Sample preparation

A total of 15 tropical woods were selected for this study, from the western part of Nigeria, as shown in Tab. 1. Identification and collection of wood samples was done in collaboration with trained personnel from FRIN-Forest Research Institute of Nigeria, Ibadan. Selection criteria were based on availability, easy access, abundance and possibility of cultivation. The harvested wood samples were cut into small pieces, peeled, sun dried and grinded. Sun drying lasted for 14 weeks. 2 mm mesh size sieved was used for wood powders sieving after grinding. The wood powders were pelletized at pressing pressure of 8 metric tons gauge readings using hydraulic press at the Center for Energy Research and Development (CERD) measurement laboratory, Obafemi Awolowo University, Ile-Ife, Ogun State, Nigeria. Sample pellets weight ranged from 250 mg to 350 mg. Each wood sample pellet was placed in properly labeled dispensary bags and taken to the PIXE laboratory at CERD for elemental analysis. GupixWin software program was used for PIXE Spectrum analysis, The PIXE results were obtained in PPM (part per million) (Futatukawa 2000).

Tab. 1: Wood sample IDs, botanical and common names (Onumejor et al. 2018).

Sample ID	Botanical names	Local or common names
1	*Treculia africana*	Afon
2	*Triplochiton scleroxylon*	Arere (Obeche)
3	*Albizia zygia*	Aynure-white or Ayunre
4	*Albizia gummifera*	Aynure or Ayunre-yellow
5	*Cedrella odorata*	Cidrela
6	*Basella alba*	Efo-onibo
7	*Anadelphia afzeliana*	Bere
8	*Gmelina arborea*	Gmelina
9	*Funtumia spp elastic*	Ire
10	*Milicia excels*	Iroko
11	*Blahia sapida*	Isin
12	*Celtis spp*	Ita
13	*Irvingia grandifolia*	Kara koro
14	*Senna siamea*	Kasia
15	*Mansonia altissima*	Masonia

Description of accelerator facility for PIXE analysis

The accelerator facility used for this research is NEC 5SDH 1.7 MV Accelerator machine model at the Center for Energy Research and Development (CERD), Obafemi Awolowo University Ile-Ife. The ion beam analytical processes are situated inside the accelerator close to the radiofrequency (RF) charge exchange ion source. The helium and proton ions that are used to bombard research samples are generated from the ion source chamber. The accelerator facility has five ion beam lines, but only one beam line with multipurpose end station is active.

This end station has four functional IBA techniques that it can run. The IBA that the accelerator facility can run techniques includes Particle induced gamma ray emission (PIGE), Elastic recoil detection analysis (ERDA), Rutherford backscattering spectrometry (RBS) and Particle induced X-ray emission (PIXE). Each are stationed at 225^o, 30^o, 165^o and 135^o respectively. The window for beam size and position observation is at 0^o. In PIXE technique, only the top area of the sample, about 10-50 μm deep is probed by the incident charge ion beam. The profiling depth depends on the energy of the incident beam and the type of sample material. Usually the bombarded sample area for PIXE analysis is a circular section of the sample that is about 1-10mm in diameter. Therefore, the small area must be a complete representation of the whole sample, hence the pulverization (grinding) and pelletizing of the wood samples used for this study was done (Mingay 1983, Ishii 1990, Mandó 1994).

PIXE detector calibrations

Commercially available standards were used for PIXE detector calibrations. The thin mylar foils and Hey types of micromatter standards used for this study has compound/element deposits of known concentration. These micromatter standards were first analyzed using the PIXE setup process before analyzing the study samples. Results of the standards obtained were checked and compared with stated concentration on purchase specification within error margin of five percent as state by Mingay (1983), Ishii (1990) for X-ray detector calibrations. In calibrating the system, the 0.6 - 3.5 MeV energy ranges of the $4He^+$ particles were used to bombard the standard samples. The choice of commercial standard selected are such that provide a representation of the entire spectrum needed for the analysis.

Applications of PIXE to elemental analysis

Collimator was positioned in front of the target, and the beam spot was resized to 1mm. When beam hits the target, the X-ray detector collects and measure X-ray from target (study samples) by analyzing the energy spectrum using equation 1. Obtained counts $N_x(Z)$ and atomic number Z of the characteristic X-rays for each detected element were automatically substituted and analyze with GUPIXWIN software.

Mounting a sample uniformly on a thin polyethylene film, we obtain the quantity NZ ($g \cdot cm^{-2}$) for element Z as follows:

$$N_Z = N_X(Z)\frac{4\pi m_Z z_p e}{\sigma_Z^X d\Omega e f f_Z Q N_{Av.}} \quad (1)$$

where: dΩ, ef, f_Z, Q, z_P and N_{Av}. are the solid angle of the X-ray detector, the detector efficiency, integrated projectile charge, projectile charge, and Avogadro's number respectively.

In the case of a thick target, the effect of the reduction due to the X-ray self-absorption and projectile energy loss in the target should be considered when applying the above formula. (Keizo 2019, Ishii 2019).

RESULTS AND DISCUSSION

Study samples were analyzed under the same experimental procedures as those of the micromatter commercial standards used for calibration. Micromatter standards has certified values used to validate the PIXE procedure. GUPIXWIN spectrum analysis software was used for identification of characteristic X-rays through their energies and quantitative analysis of their subsequent elemental concentrations. A total of 27 trace elements were identified and quantified in part per million concentration levels as shown in Tab. 2.

Tab. 2: PIXE elemental concentrations of selected samples 1 to 15 ($\mu g.g^{-1}$).

Elements	Sample ID														
	1	**2**	**3**	**4**	**5**	**6**	**7**	**8**	**9**	**10**	**11**	**12**	**13**	**14**	**15**
Na	389	0	65.35	0	68.03	0	245.8	125.8	0	48.95	0	0	0	125	0
Mg	2653	33.41	536	294.3	1178	1198	719.1	1508	1075	1504	683.6	187.8	742.3	474	930.9
Al	268.7	158.1	368	85.4	338.4	667.5	262.2	337.9	296.5	483.9	452.2	258.2	301.6	130.5	435.3
Si	441	276	645.8	5206	512.9	1509	5253	543.3	342	795.3	615.1	458.3	713.6	318.7	430.8
P	201.9	52.32	99.61	252.6	0	342.5	275.5	57.88	286.1	0	397.3	93.1	301.4	186.9	381.3
S	697.8	220.3	714.5	1171	214.8	718.5	278.3	61.29	694.1	95.19	605.8	218.2	666.8	188.4	210.1
Cl	146.9	227.8	84.33	511.3	57.56	35.16	2768	2.996	31.63	87.36	38.41	80.8	68.42	75.23	48.38
K	2838	1925	4811	1489	1096	2001	3487	3184	2021	2362	2139	1364	1106	2331	1809
Ca	1524	2835	2082	846.1	3195	4923	3192	2857	1996	5608	7770	5110	2743	5092	3451
Ti	7.6	2.619	9.945	2.345	0	10.82	2.386	11.28	0	7.632	10.51	2.745	9.618	8.532	13.65
V	5.504	2.523	0	3.437	0	1.763	3.702	0	0	0	5.534	0	4.152	0.5542	0
Cr	6.477	2.913	0	0	1.935	4.565	5.887	0	0.8619	0	0	0	2.184	0	4.591
Mn	17.29	1.592	19.97	10.89	0	9.832	8.443	2.833	14.64	8.742	24.64	7.324	60.33	3.817	0
Fe	18.26	75.99	109.5	1851	36.81	209.6	21.59	833.3	22.11	68.39	91.98	26.86	34.21	15.29	28.99
Co	6.656	0	0.9216	36.67	6.369	0	10.1	8.867	0	9.798	0	0	0.2863	4.786	5.281
Ni	0	0	0	9.541	4.08	10.7	1.377	0.8991	0	0	0	0	2.622	2.328	0
Cu	2.077	6.352	2.606	8.026	0	1.443	0	0	7.7	4.93	5.892	2.867	1.287	11.24	1.962
Zn	40.08	3.43	11.57	0	1.762	45.96	8.786	22.4	19.64	1.156	31.81	10.33	11.65	4.664	0
Se	5.636	0	0	0	0	0	0	0	2.971	0	0	0	0	0	0
Br	0	3.015	0	50.75	5.844	5.061	0	3.164	0	2.829	0	13.46	6.253	0	4.803
Rb	25.65	15.94	0	18.12	10.94	13.77	0	0	0	0	12.18	37.97	0	8.996	0
Sr	0	33.35	22.65	0	37.17	0	0	0	0	158.5	160.3	96.88	20.29	75.11	27.82
Y	0	0	16.62	25.35	14.57	0	0	14.65	0	29.65	0	0	0	0	14.72
Zr	0	69.71	0	70.92	0	0	61.02	70.82	13.75	0	0	35.68	35.66	0	0
Ba	0.6211	3.804	0.6734	0	0	8.03	6.138	7.411	0.8325	12.42	3.085	4.512	7.527	0	0.3293
Pb	1.258	1.149	0.362	8.189	1.76	0.6914	0	0	1.225	1.015	0	0	0	0	0
Bi	3.543	0	0	5.518	0.7421	0.8008	0	0	0.9968	0	0.358	0	0	0	0.4648

The identified trace elements are Na, Mg, Al, Si, P, S, Cl, K, Ca, Ti, V, Cr, Mn, Fe, Co, Ni, Cu, Zn, Se, Br, Rb, Sr, Y, Zr, Ba, Pb and Bi. Silicon Si, Potassium K and Calcium Ca, Magnisium Mg, recorded the highest in several sample. Calcium had the highest concentration values in 9 different samples, Potassium in 4 and Silicon in 2 samples. Calcium had 2835, 3195, 4923, 5608, 7770, 5110, 2743, 5092 and 3451 ppm in samples 2, 5, 6, 10, 11, 12, 13, 14 and 15, respectively. Potassium had 2838, 4811, 3184, and 2021 ppm in samples 1, 3, 8 and 9, respectively. Silicon has 5206 ppm in sample 4 and 5253 ppm in sample 7. To better identify the major trace element in studied samples, a cumulative distribution pattern plot of trace

element was done as shown in Fig. 1. The lines with label 1000 to 8000 represents trace elements concentration levels in ppm, the digits 1 (one) to 15 (fifteen) on the concentration line edges represents the 15 (fifteen) studied samples. Each identified and quantified trace element were represented with several colored lines as shown on the legend in Fig. 1. The four noticeable patterns above the 1000 ppm concentration line, represents the major trace element measured in studied samples. Calcium Ca, with grey colored line, formed the largest pattern, its highest concentration level points to 11 as shown in Fig. 1.

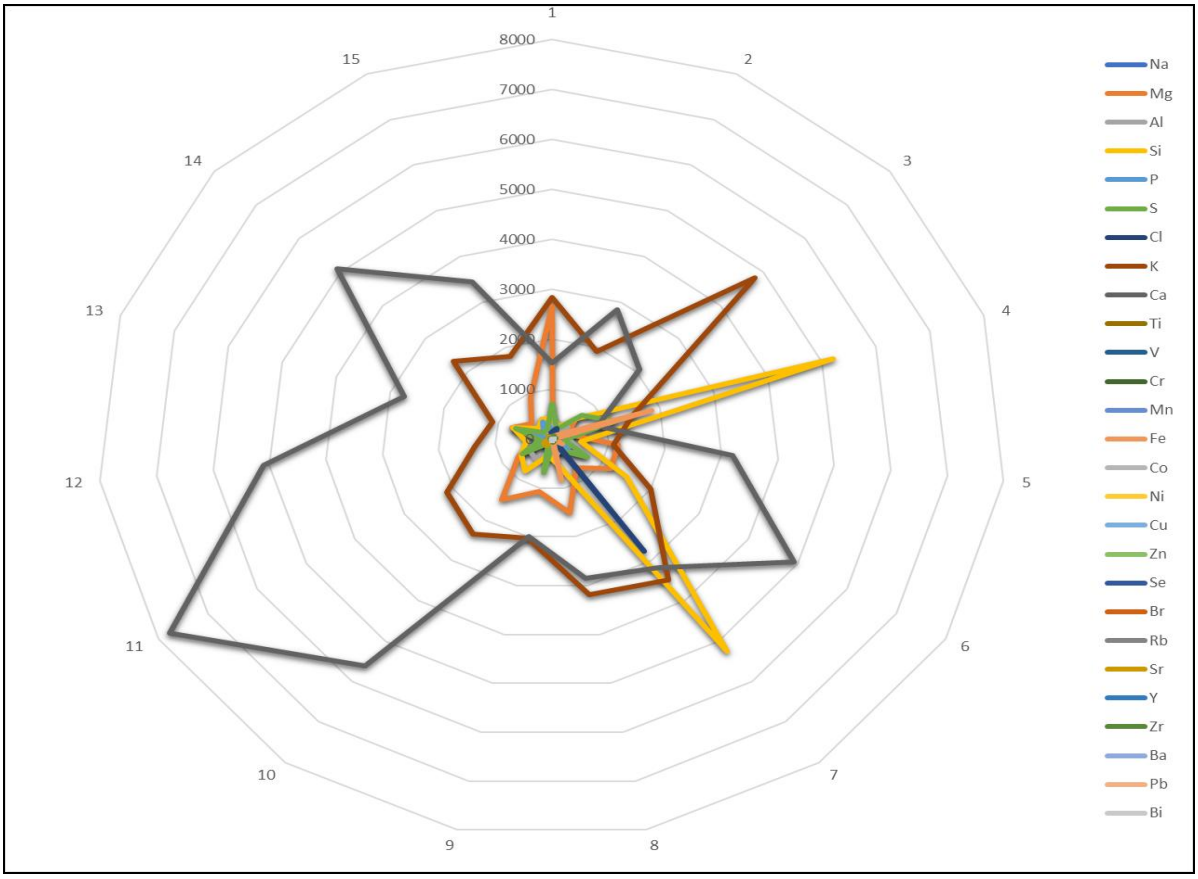

Fig. 1: Radar plot of cumulative distribution pattern of trace element in studied samples.

Next large pattern observed was Potassium K, with red colored line and highest trace element concentration points edge is on 3 (sample 3). The yellow colored line pattern with point edges on samples 4 and 7 stands for Silicon Si distribution. Magnesium Mg, with orange colored line was the fourth noticeable pattern with highest concentration edge point on sample 1. Other trace element distribution patterns were clustered below the 1000 ppm concentration line. Hence, it can be said that Calcium Ca, Potassium K, Silicon Si, and Magnesium Mg, were the major trace element of studied wood samples. Other elements that can be included as major trace elements are those present in all studied samples. They are Al, P, S, Cl, Mn, Fe, and Zn. This implies that Calcium Ca, Potassium K, and Silicon Si are the major trace elements of the studied wood samples, having concentration levels > 1000 ppm. Fig. 2, revealed that the detected trace elements clustered around Na to Ca, as shown on the x-axis (trace element axis) position 1 to 9. The observed concentration order were Ca < K < Si < Mg < others.

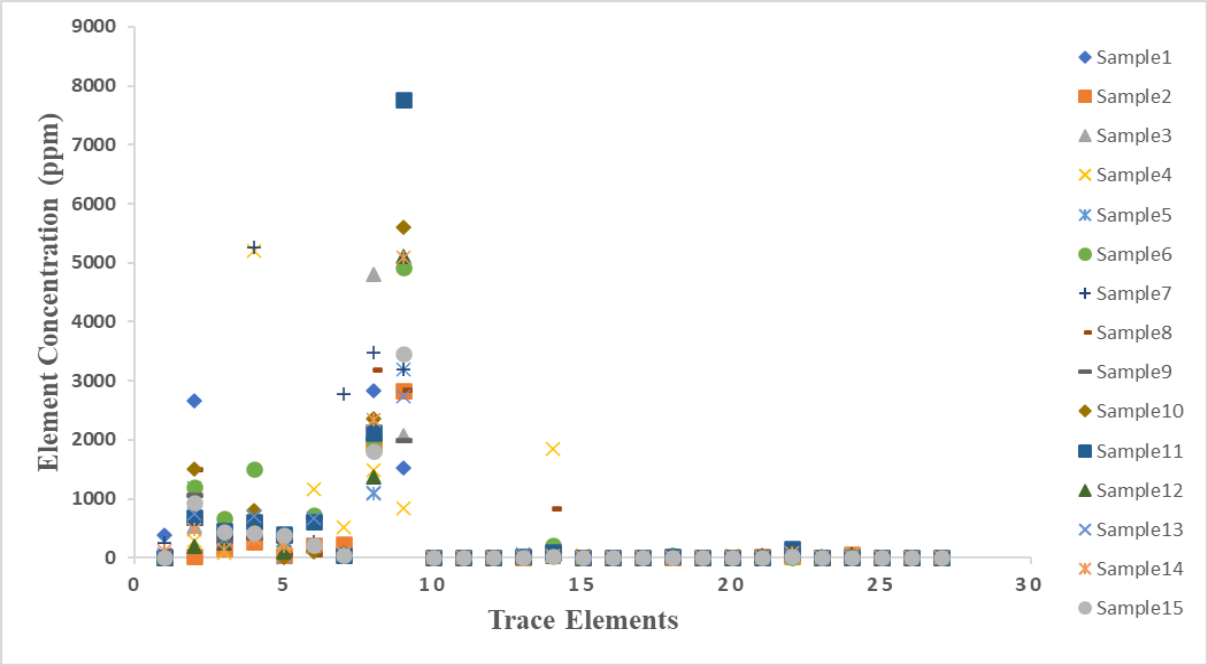

Fig. 2: Trace elemental concentration of samples.

CONCLUSIONS

Fifteen different types of tropical wood were studied using particle induce X-ray emission (PIXE) method of ion beam analytical techniques, for identification of constituent elements and its corresponding concentration level in ppm. Elements identifies with varying concentration levels are Na, Mg, Al, Si, P, S, Cl, K, Ca, Ti, V, Cr, Mn, Fe, Co, Ni, Cu, Zn, Se, Br, Rb, Sr, Y, Zr, Ba, Pb and Bi. Calcium had 2835, 3195, 4923, 5608, 7770, 5110, 2743, 5092 and 3451 ppm in samples 2, 5, 6, 10, 11, 12, 13, 14 and 15 respectively. Potassium had 2838, 4811, 3184, and 2021 ppm in samples 1, 3, 8 and 9 respectively. Silicon has 5206 ppm for sample 4 and 5253 ppm for sample 7. Many elements were below detection limit and were reported to have zero concentration values in the result tables. Calcium and potassium were observed to have concentration level that is greater than 1000 ppm in all the studied samples, hence it can be said that calcium and potassium are major trace element of wood. The concentrations of the elements identified have no immediate health concern and is therefore safe for use as fuel and other purposes.

ACKNOWLEDGMENTS

We appreciate the management of Covenant University, Nigeria for the publication support received from them.

REFERENCES

1. Beck, L., 2005: Improvement in detection limits by using helium ions for particle-induced X-ray emission. X-Ray Spectrom 34: 393–399.
2. Okochi, T., Hoshino, Y., Fujii, H., Mitsutani, T., 2007: Nondestructive tree-ring measurements for Japanese oak and Japanese beech using micro-focus X-ray computed tomography. Dendrochronologia (online) 24(2-3): 155-164.
3. Onumejor, C.A., Balogun, F.A., Akinpelu, A., Arijaje, T.E., Usikalu, M.R., 2018: Rutherford backscattering spectrometry (RBS) method for the determination of elemental constituent of tropical wood matrices from Western Nigeria. IOP Conf. Series: Earth and Environmental Science 173: 1-4.
4. Xinwei, L., Zhang, X., 2006: Measurements of natural radioactivity in sand collected from the Baoji Weihe Sands Park, China. Environmental Geology 50: 977-982.
5. Olise, F.S., Onumejor, C.A., Akinlua, A., Owoade, O.K., 2013: Geochemistry and health burden of radionuclides and trace metals in shale samples from the North-Western Niger Delta Journal of Radioanalytical and Nuclear Chemistry 295: 871–881.
6. Usikalu, M.R., Onumejor, C.A., Akinpelu, A., Achuka, J.A., Omeje, M., Oladapo, O.F., 2018: Natural radioactivity concentration and its health implication on dwellers in selected locations of Ota. IOP Conf. Series: Earth and Environmental Science 173: 1-8.
7. Orosun, M.M., Usikalu, M.R., Oyewumi, K.J., Adagunodo, A.T., 2019: Natural radionuclides and radiological risk assessment of Granite mining field in Asa, North-Central Nigeria. MethodsX 6: 2504-2514.
8. Joel, E.S., Maxwell, O., Adewoyin, O.O., Ehi-Eromosele, C.O., Embong, Z., Oyawoye, F., 2018: Assessment of natural radioactivity in various commercial tiles used for building purposes in Nigeria. MethodsX 5: 8-19.
9. Adagunodo, T.A., George, A.I., Ojoawo, I.A., Ojesanmi, K., Ravisankar, R., 2018: Radioactivity and radiological hazards from a kaolin mining field in Ifonyintedo, Nigeria. MethodsX 5: 362–374.
10. Bradley, D.A., Tajuddin, A.A., Sudin, C.W.A.C.W., Bauk, S., 1991: Photon attenuation studies on tropical hardwoods. International Journal of Radiation Applications and Instrumentation. Part A. Applied Radiation and Isotopes 42771-773.
11. Zhang, X., Chen, Q., Bradford, R., Sharifi, V., Swithenbank, J., 2010: Experimental investigation and mathematical modelling of wood combustion in a moving grate boiler. Fuel Processing Technology 91(11): 1491-1499.
12. Constantinou, C., 1982: Phantom materials for radiation dosimetry, I. liquids and gels. British Journal of Radiology: 52217-224.
13. White, D.R., 1977: An analysis of the Z-dependence of photon and electron interactions. Physics in Medicine and Biology 22(1977b): 219-228.
14. Požgaj, A., Chovanec, D., Kurjatko, S., Babiak, M., 1997: Structure and properties of wood (in Slovak). Príroda a.s., Bratislava, 485 pp.

15. Tajuddin, A.A., Sudin, C.W.A.C.W., Bradley, D.A., 1996: Radiographic and scattering investigation on the suitability of *Rhizophora* spp. as tissue-equivalent medium for dosimetric study. Radiation Physics and Chemistry 47: 739-740.
16. Aggrey-Smith, S., Preko, K., Wilson, F., Gbadago, J., 2015: Measurement of elemental compositions of selected tropical wood species – a case study of Pra Anum Forest, Ghana. International Journal of Biomedical Science and Engineering 3(3): 34-43.
17. Zafar, A.M, Mohammad, S, Saad Bin, Z.M, Mahwish, A.K., 2010: Herbal treatment for cardiovascular disease. The evidence-based therapy. Pakistan Journal of Pharmaceutical Sciences 23(1): 119-124.
18. Sakina, M.Y., Alia, E.A.R., Gihan, O.M.E., Abdelhafeez, M.A.M., 2013: Elemental analysis of ten Sudanese medicinal plants using X-ray fluorescence. Journal of Applied and Industrial Sciences 1(1): 49-53.
19. Futatukawa, S., 2000: Bio PIXE theory and applications. Chapter 2. Sample preparation for the quantitative analysis of biological materials. Sample preparation method of biological materials by Nitric Acid ashing using a Microwave Oven. Radioisotopes 49: 447–450.
20. Mingay, D., 1983: Calibration of micromatter co. Standards used for the calibration of PIXE analysis systems. Journal of Radioanalytical Chemistry, (Foils manufactured by Micromatter Co., Deer Harbor, WA.) 78: 127.
21. Ishii, K., Morita, S., 1990: Bio-PIXE at the Takizawa facility (Bio-PIXE with a baby cyclotron). International Journal of PIXE 1: 1–29.
22. Mandó, P.A., 1994: Advantages and limitations of external beams in applications to arts & archeology, geology and environmental problems. Nuclear Instruments and Methods B 85: 815–823.
23. Keizo, I., 2019: PIXE and its applications to elemental analysis. Quantum Beam Science 3(2): 12.
24. Ishii, K., Terakawa, A., Ushijima, H., Hitomi, K., Nagano, N., Nogami, M., 2019: Application of a medical PET cyclotron to PIXE analysis. In: Proceedings of the 16th International Conference on Particle Induced X-ray Emission. Pp 39-40, vol. 39, Caldas da Rainha, Portugal.
25. Haradhan, K., Chun W.K., 2020: High acoustic absorption properties of hackberry compared to nine different hardwood species: a novel finding for acoustical engineers. Applied Acoustics 169: 1-8.
26. Sarmad, S., Luigi, F., Raffaele L., 2020: Behavior factor evaluation of CFS wood sheathed shear walls according to FEMA P695 for Eurocodes. Engineering Structures 221: 2-8.
27. Chu, P., Ashraf, A.D., Ahmed, M.A.H., 2020: Simplified numerical approach for the lateral load analysis of light-frame wood shear wall structures. Engineering Structures 219: 1-7.
28. Yasuji, K., Shigeru, Y., Tsutomu, T., Yoichi, S., 2020: Coloring mechanisms of ancient buried wood: Japanese cedar trees excavated from the foothills of Mt. Chokai. Journal of Wood Science 66: 1-7.
29. Sachithrani, K., Sachinthani, K., Lahiru, R., Kalpani, A., Disnie, R., Hashan, J., Cholani, W., Suneth, S., 2020: Assessment of the applicability of wood anatomy and DNA

barcoding to detect the timber adulterations in Sri Lanka. Pp. 5-10, Scientific Reports, vol. 10.
30. Assai, H., Paul, H., Hussam, M., 2020: Structural performance of a wood-sand-wood wall for blast protection. Engineering Structures 219: 1- 9.
31. Dora, N., Sibylle, F., Rainer, G.J., 2020: Characterization of charcoal and firewood ash for use in African peri-urban agriculture. Chemical and Biological Technologies in Agriculture 7: 1-8.
32. Dominik, T., Andreas, S., Julius, S., Jonas, H., Jörg, M., Rupert, S., 2020: Effects of disturbance patterns and deadwood on the microclimate in European beech forests. Agricultural and Forest Meteorology 291: 1-10.
33. Tejedor, J., Cóndor, V., Almeida-Naranjo, C.E., Guerrero, V.H., Villamar, C.A., 2020: Performance of wood chips/peanut shells biofilters used to remove organic matter from domestic wastewater. Science of The Total Environment 738: 3-5.
34. Achim, B., Marek, W., Andreas L., Doris, G., Michał, W., 2020: Petrological and geochemical characteristics of xylites and associated lipids from the First Lusatian lignite seam (Konin Basin, Poland): Implications for floral sources, decomposition and environmental conditions. Organic Geochemistry 147: 3-7.
35. Warlen, S. C., Maura, D.C., Pablo, J.F., Pena, R., Marianade, A.I., Fernando, V., Claudia, F.B., 2020: Intraspecific variation in functional wood anatomy of tropical trees caused by effects of forest edge. Forest Ecology and Management 473: 1-11.
36. Mátyás, B., Róbert. N., Jakub, S., Anna, S., 2020: FTIR analysis of chemical changes in wood induced by steaming and longitudinal compression. Cellulose 27: 6811-6829.
37. Erchiqui, F., Kaddami, H., Dituba-Ngoma, G., Slaoui-Hasnaoui, F., 2020: Comparative study of the use of infrared and microwave heating modes for the thermoforming of wood-plastic composite sheets. International Journal of Heat and Mass Transfer 158: 1-9.
38. Qian, H., Tianyi, Z., Haiyang, Z., Zehui, J., Lu, H., Xiaoning, L., 2020: Prediction of stiffness and strength distributions in laminated-wood treated by high voltage electrostatic field (HVEF). Materials Today Communications 24: 1-11.
39. Yuming, X.Y., Huanga, X., Menga, F., Wangb, L., Wana, Z., Donga, J.C., 2020: Friction rivet joining towards high-performance wood-metal hybrid structures. Composite Structures 247: 1-7.

CHARITY ADAEZE ONUMEJOR*, MOJISOLA RACHAEL USIKALU, THEOPHILUS AANUOLUWA ADAGUNODO, AKINWUMI AKINPELU, JUSTINA ADA ACHUKA, THEOPHILUS EMOBOR ARIJAJE
COVENANT UNIVERSITY
DEPARTMENT OF PHYSICS
P.M.B 1023
OTA, OGUN STATE
NIGERIA
*Corresponding author: charity.onumejor@covenantuniversity.edu.ng

FATAI AKINTUNDE BALOGUN, SEJLO TEMIDAYO GBENU
OBAFEMI AWOLOWO UNIVERSITY
CENTRE FOR ENERGY RESEARCH AND DEVELOPMENT
P.M.B. 13
ILE-IFE, OSUN STATE
NIGERIA

WOOD RESEARCH doi.org/10.37763/wr.1336-4561/66.4.606620
e-ISSN 2729-8906
66(4): 2021 606-620 pp.

PERFORMANCE OF COATED TUNGSTEN CARBIDE IN MILLING COMPOSITE BOARDS

KIDUNG TIRTAYASA PUTRA PANGESTU, WAYAN DARMAWAN, DODI NANDIKA, IMAM WAHYUDI
BOGOR AGRICULTURAL UNIVERSITY
INDONESIA

LUMONGGA DUMASARI
PURWOKERTO MUHAMMADIYAH UNIVERSITY
INDONESIA

HIROSHI USUKI
THE UNIVERSITY OF TOKYO
JAPAN

(RECEIVED JULY 2020)

ABSTRACT

The purpose of this research was to analyze the performance (wear resistance, surface roughness, chip formation, and noise level) of AlCrN, TiN, and TiAlN coated tungsten carbides in cutting composite boards. The composite boards of wood plastic composite, laminated veneer lumber, and oriented strand board were cut by the coated tungsten carbide tools in a computer numerical control router. The results show that the differences in structure among the composite boards resulted in the difference in clearance wear, chip formation, surface roughness, and noise level phenomenon. The abrasive materials in wood plastic composite generated the highest clearance wear on the coated carbide tools tested. TiAlN coated carbide tool provided better wear resistance, smoother composite boards surfaces, and lower noise levels.

KEYWORDS: Chip formation, clearance wear, coated tungsten carbide tool, composite board, noise level, surface roughness.

INTRODUCTION

Composite board industries manufacturing wood plastic composite (WPC), laminated veneer lumber (LVL), and oriented strand board (OSB) are developing rapidly in various countries (Antov et al. 2020). They have high ratio of the tensile strength of the material to its density (Kulman et al. 2019). These composite boards have been widely used for decorative and building construction purposes (Ribeiro and del Menezzi 2019). In the secondary wood manufacturing industry, where the composite boards are machined using a cutting tool, the wear of cutting tool edge, in addition to the cutting force (Koleda et al. 2019, Kopecký et al. 2019) and friction coefficient (Li and Zhang 2019), is one of the imperative productivity parameters in the machining. Darmawan and Tanaka (2004), Darmawan et al. (2009, 2011) reported that the wear of cutting tool affects the noise level and the surface quality. The high heterogeneity in structure of composite board compared to metal and wood would be predicted to result in the complexity of cutting tool wear problem. Therefore, the elucidation of the wear phenomenon of cutting tools is considered to be necessary in an effort to find better choices of cutting tool materials used in cutting composite boards.

At present, a cutting tool material that dominates in the wood working industry is tungsten carbide. Tungsten carbide is a good selection for many wood machining processes because of its toughness and hardness. Darmawan et al. (2012) reported that the wear resistance of tungsten carbide tool was much higher than high speed steel tools for cutting tapi-tapi wood and composite boards (cement board, particle board, and fiber board) in the same cutting condition, as a result of the higher hardness of tungsten carbide tool (1450 HV) compared to high speed steel tool (815 HV). Though tungsten carbide tool has been widely used for machining solid wood, however previous studies reported that machining of composite boards using tungsten carbide tools has been limited due to relatively high rate of wear caused by combination of abrasion, high-temperature oxidation, and inorganic content such as silica in composite boards (Darmawan et al. 2012). In addition, Ratnasingam et al. (2010) noted that machining of particleboard caused carbide cutting tool to wear out much faster than cutting of solid woods. Therefore, a need for cutting tool with longer life and better performance exists especially for cutting composite boards.

Other cutting tool materials that were produced for the secondary wood manufacturing industry are ceramic, cubic boron nitride, and polycrystalline diamond cutting tool. However, the cost of these cutting tools seems to very high, and the difficulty in creating cutting tools of complex shapes and tool size limits for the composite board machining application (Darmawan 2017). An alternative, deposition of hard coating materials onto the surface of tungsten carbide tools has been recently promoted for cutting composite boards. The effects on cutting tool wear of adding hard coating materials onto the surface of tungsten carbide tools are reported in the literatures. Titanium nitride (TiN), titanium carbon nitride (TiCN), and chromium nitride (CrN) coating films were deposited on tungsten carbide tools by physical vapor deposition (PVD) method (Darmawan et al. 2001). It was noted in the work that these coated carbide tools were advantageous in reducing the progression of wear, in retaining lower

noise level and normal force in cutting hardboard and wood-chip cement board compared to uncoated carbide tool. TiCN coating thin film deposited on tungsten carbide tools has increased microhardness, reduced the coefficient of friction, and subsequently improved cutting tool life as compared to uncoated carbide tool (Talib et al. 2013). In addition, depositioning TiCN coating film on tungsten carbide tools has reduced the thermal conductivity of cutting tool from 80.20 $kW \cdot m^{-1} \cdot K^{-1}$ to 0.10 $kW \cdot m^{-1} \cdot K^{-1}$. This reduction results in the prevention of cobalt oxidation during cutting at high temperature (Talib et al. 2013). In contrast, Sheikh-Ahmad and Stewart (1995) noted that TiN and titanium aluminium oxide nitride (TiAlON) coated carbide tools did not provide any improvement in wear resistance compared to uncoated carbide tool when cutting particleboard, and the titanium carbide (TiC) coated carbide tool provided only a slight improvement.

Depositions of a newly coating material of aluminium chromium nitride (AlCrN) and commercially coatings of TiN and titanium aluminium nitride (TiAlN) onto tungsten carbide tools in the field of composite boards machining are little known concerning their performance. These coating materials have high hardness, better oxidation resistance, and lower friction coefficient. The ongoing research was proposed to achieve better performance of the AlCrN, TiN, and TiAlN coated tungsten carbide tools in cutting composite boards of WPC, LVL, and OSB. The performance investigated were wear resistance, surface roughness, chip formation, and noise level.

MATERIAL AND METHODS

General specification of the tungsten carbide tools tested and the composite boards machined are shown in Tab. 1 and Tab. 2, respectively.

Tab. 1: Specification of tungsten carbide tools tested.

Coatings	Film thickness (μm)	Hardness (HV)	Oxidation temperature (^oC)	Friction coefficient
Uncoated	-	1400	Start at 700	0.8
AlCrN	3	2800	Start at 1000	0.6
TiN	3	2200	Start at 600	0.7
TiAlN	3	2800	Start at 800	0.8

Film thickness, hardness, oxidation temperature, and friction coefficient values were measured according to ASTM B568, ASTM E2546, ASTM G111, and ASTM G99, respectively.

Tab. 2: Specification of composite boards machined.

Composite boards	Moisture content (%)	Density ($kg\ m^{-3}$)	Modulus of rupture (MPa)	Hardness ($N\ m^{-2}$)	Silica content (%)
WPC	2.1	135	28	3.64	5.09
LVL	10.4	83	80	5.23	0.73
OSB	11.2	59	20	1.41	0.01

Moisture content and density values were measured according to BS 373, Modulus of rupture and hardness values were measured according to ASTM D143, silica content was measured according to TAPPI T211 om-02.

The K10 carbide tool (90% WC and 10% Co) used as a substrate was in 6.40 mm long, 4.30 mm wide, and 2.45 mm thick with a clearance angle of 5^o and a rake angle of 13^o. This

geometry is now being commercially produced to prevent chipping of the cutting edge when using in abrasive work materials machining. The tungsten carbide tools were coated with monolayer coatings of AlCrN, TiN, and TiAlN by the arc-ion plating method on both clearance and rake faces.

Cutting test was set up on the computer numerical control (CNC) router with condition as shown in Tab. 3. The composite board samples were prepared in rectangular form. A piece of work material was placed on the table of the CNC router and locked by vacuum machine. Cutting tool edge was held rigidly in a cutting tool holder with diameter of cutting circle of 12 mm. Cutting test was performed along the edge of the board with spindle rotation set in the clockwise direction. The coated carbide tools were inspected with an optical video microscope before cutting test for any surface defects and cracks of the coating film on both clearance and rake faces. The cutting was stopped at every specified linear cutting length of 100 m, at which the cutting tool wear, surface roughness, chip formation, and noise level were investigated. The cutting tools wear was inspected using an optical video microscope to obtain the amount of edge recession and delamination wear (Fig. 1).

Tab. 3: Specification of cutting conditions.

Variable	Condition
Cutting speed (m s^{-1})	6.3
Feed rev (mm rev^{-1})	0.2
Spindle speed (rev min^{-1})	10000
Feed speed (mm min^{-1})	2000
Cutting width (mm)	1
Cutting depth (mm)	2

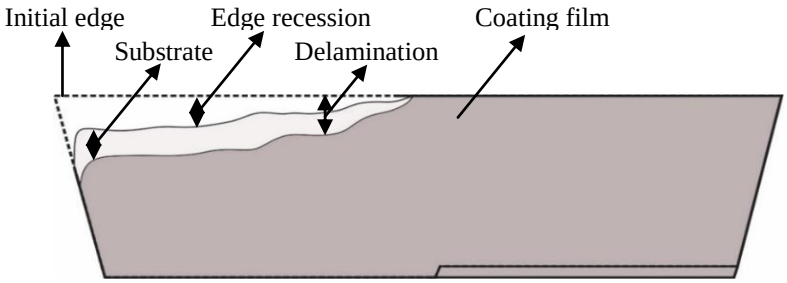

Fig. 1: Schematic wear measurement on the clearance face of coated carbide tools.

The machined surface was evaluated in the Ra value of surface roughness. The surface roughness tester SJ-210 was used to measure the roughness on the surface of the machined composite boards. The Ra was measured across the cutting direction of samples with a diamond tip radius of 5 μm. The tracing length was 15 mm and the cut off was 2.5 mm. Five points for roughness measurement were diagonally marked on the surface of the samples. Investigation of the chips was carried out by mesh analysis of the formed chips. The deposited chips on the table. of the machine were collected and documented. The chip shapes in this work were classified according to the method suggested by Su et al. (2003). The collected chips were sieved by steel screens of 10 mesh (diameter of holes 2.0 mm), 20 mesh (diameter of holes 0.8 mm), 40 mesh

(diameter of holes 0.4 mm), and 80 mesh (diameter of holes 0.2 mm). The sieved chips were analyzed according to the type of chip and the weight percentage of each screened chip. A precision sound level meter Sanfix 356 was used for measurement of the sound level of the audible cutting noise on the A scale, which is usually used for measuring the peak of sound pressure level. The sound level meter was set up at the height of the cutting tool edge (about 1 m above ground level) and at a distance of about 1 m along a straight line extending from the cutting tool edge. The noise level was recorded per 5 second at every cutting test, and the values was transferred to a computer for analysis.

RESULTS AND DISCUSSION

Edge recession and delamination

The amount of edge recession increased with increasing in cutting length (Fig. 2). The gradual progression of wear on the surface of cutting tool was reported to be resulted from the cutting heat friction between the cutting tool and workpiece (Wei et al. 2018). The coated carbide tools provided better performance, especially in reducing the progression of edge recession than the uncoated carbide tool when cutting WPC, LVL, and OSB. The phenomenon was caused by a remarkable enhancement in hardness of coated carbide tools after coated with a coating film (Tab. 1).

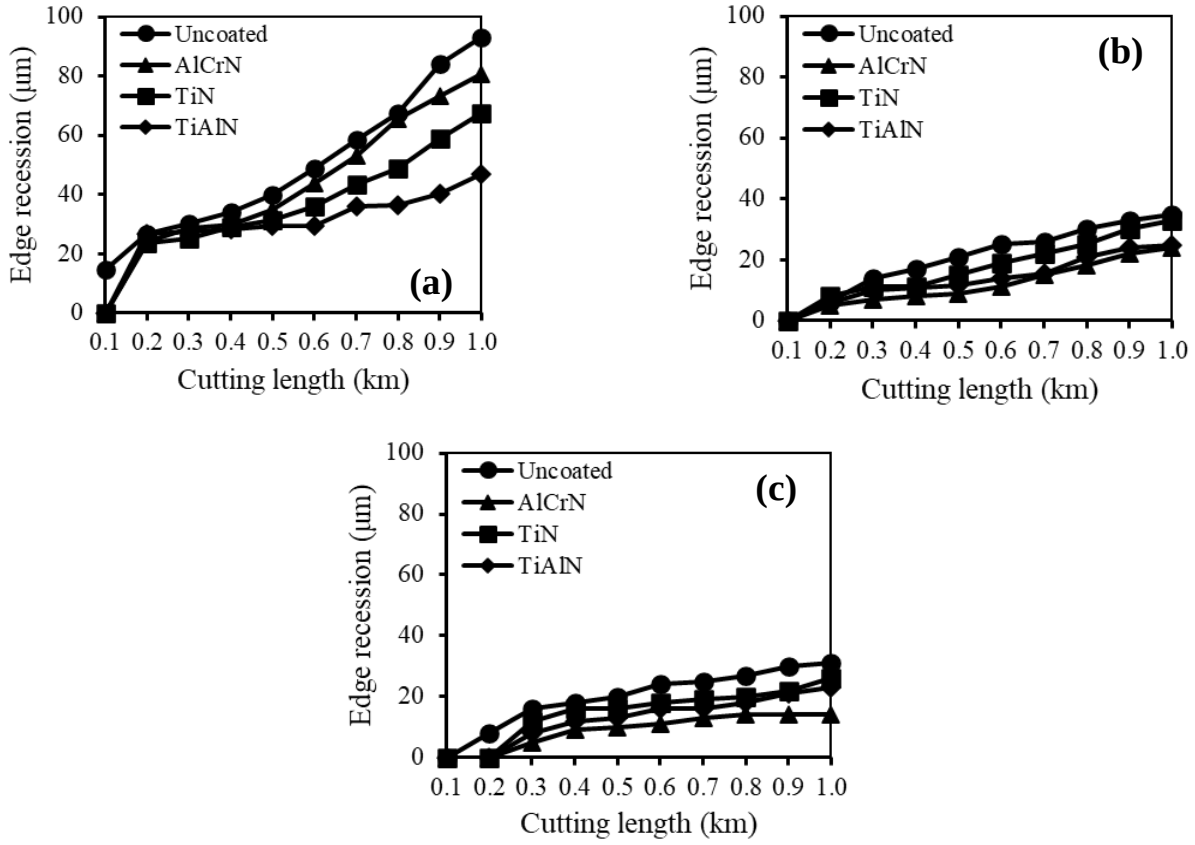

Fig. 2: Edge recession behaviours of tungsten carbide tools in cutting: (a) WPC, (b) LVL, (c) OSB.

The AlCrN, TiN, and TiAlN coated carbide tools showed similar edge recession progress near the beginning of cutting the composite boards, however the progression was gradually different among these coated carbide tools at the end of cutting. The AlCrN coated carbide tools generated the lowest edge recession in cutting LVL and OSB, however it generated the highest edge recession among the coated carbide tools tested when cutting WPC. Though the AlCrN coated carbide tool had a superior specification compared to the other coated carbide tools (Tab. 1), however it could not be superior for cutting abrasive material of WPC. WPC was higher in density and silica content compared to LVL and OSB (Tab. 2). The TiAlN coated carbide tool provided a lower edge recession than AlCrN coated carbide tool when cutting WPC. Moreover, the AlCrN coated carbide tool provided only a slight difference in edge recession compared to TiAlN coated carbide tool when cutting LVL and OSB. It was also noted in other studies that AlCrN coated carbide tool with high hardness, low friction coefficient, and high oxidation temperature generate lower amount of coating film delamination and lower edge wear in cutting metal compared to the TiAlN coated carbide tool (Kumar et al. 2014, Chandrashekhar et al. 2016, Mo et al. 2007).

The reason for the above phenomenon could be due to the higher brittleness of the AlCrN coating, which caused the coating film to crack and to detach (Fig. 3) from the surface of the tungsten carbide substrate, especially when cutting abrasive composite board (WPC). The AlCrN coated tool micrograph (Fig. 3a) shows a crack on the coating film near the cutting edge without any friction marks on the AlCrN coating film. Though the AlCrN coated carbide tool was the lowest in friction coefficient (0.6) among the coated carbide tools tested, however its high brittleness could promote the presence of the cracks followed by delamination of the coating film without abrasion. TiN coating film shows friction marks on the coating film near the cutting edge with a small cracking. Otherwise, TiAlN coating film shows friction marks without any cracks along the coating film near the cutting edge because of its highest friction coefficient (0.8) among the coated carbide tools.

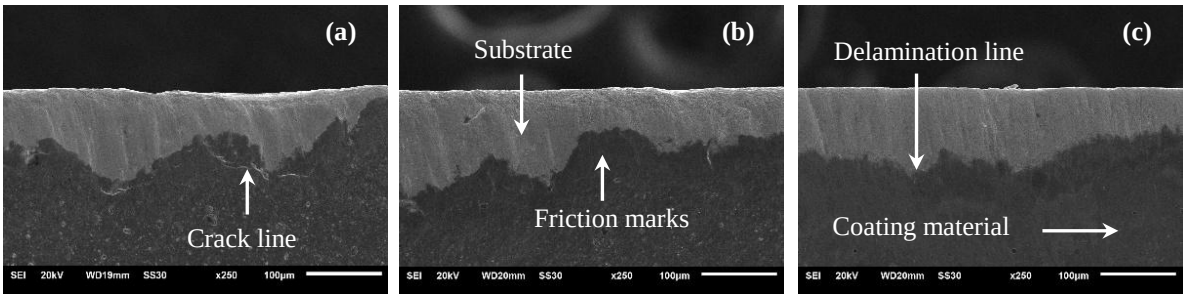

Fig. 3: SEM micrograph of the worn clearance face of (a) AlCrN, (b) TiN, and (c) TiAlN coated carbide tools at the end of cutting WPC.

It also appears in Fig. 2 that there was a considerable difference in amount of edge recession of coated carbide tools among the composite boards machined. The result shows that the coated carbide tools suffered more wear when cutting WPC compared to LVL and OSB. The higher density, MOR, hardness, silica content (Tab. 2), and a high amount of inorganic

matters in WPC could be the reason for this phenomenon. The presences of abrasive and additives materials in the WPC led to severe mechanical wearing on the cutting tool edge tested. The main components of WPC were plastic polymer, lignocellulose materials, fillers (mostly crystalline silicates, titanium dioxide, and other heavy metals), stabilizers, pigments, and other additives (Niska and Sain 2008, Saloni et al. 2011). It was confirmed in previous studies that the high amount of inorganic matters contained in the composite boards, combined with plastic polymer cause severe abrasive wear to the cutting tool (Saloni et al. 2011). On the other hand, the lowest density, hardness, MOR, and silica content of the OSB compared to other composite boards generated the lowest edge recession wear on the coated carbide cutting tools tested. The edge recession wear on coated carbide tools could be attributed by the amount of delamination of coating films. It was reported by Fahrussiam et al. (2016) that there was a strong linear relationship between delamination and edge recession wear when cutting composite boards using coated carbide tools. The result shows the progression of coating films delamination of the coated carbide tools, in which delamination increased with the increase in cutting length (Fig. 4). The higher delamination of the coating films resulted in the higher edge recession wear during the cutting. It could be considered that the cutting edge would be more susceptible to wearing, since the coating film had been delaminated from the surfaces of the cutting edge. AlCrN coated carbide tool generated the highest delamination wear when cutting the WPC, whereas TiAlN coated carbide tool generated lowest delamination wear when cutting the WPC.

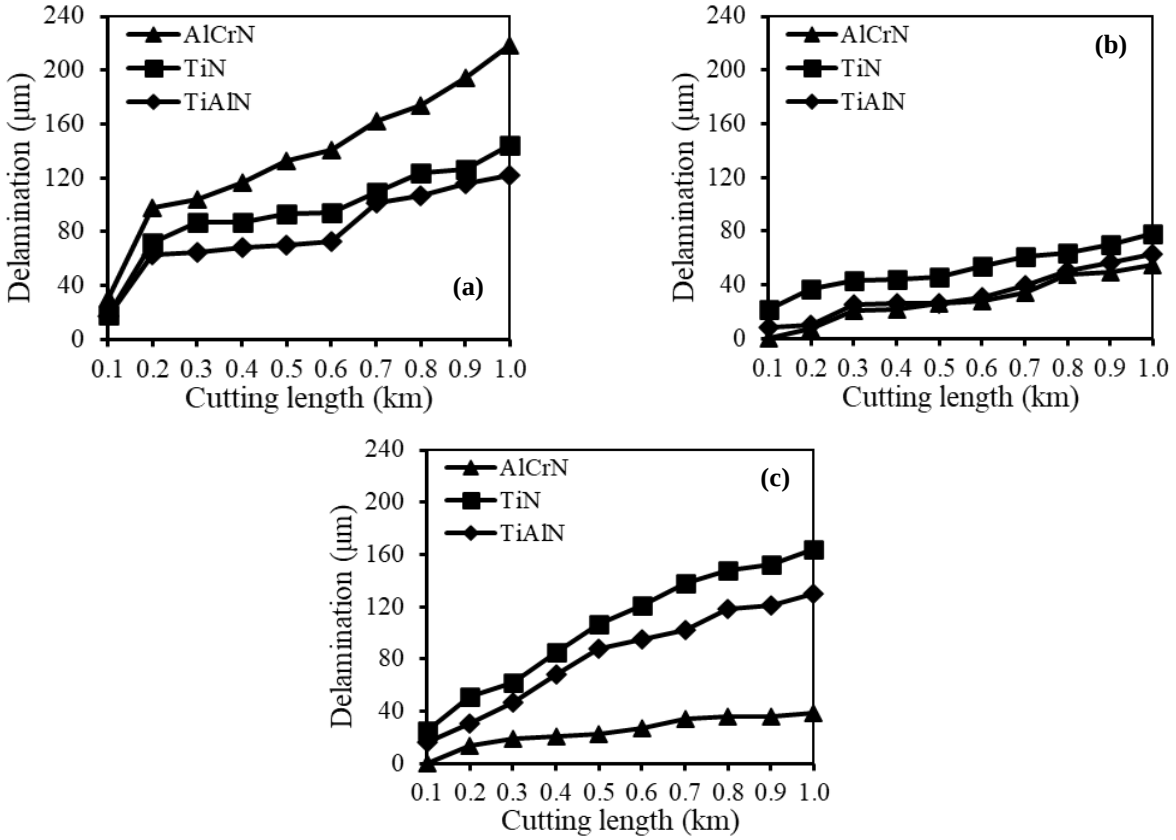

Fig. 4: Delamination behaviours of coated carbide tools in cutting (a) WPC, (b) LVL, and (c) OSB.

The reason for above phenomenon could be due to weak adhesion between AlCrN coating film and tungsten carbide substrate. The formation of weak adhesion bond is considered as a result from the following reasons. First, high residual stress on AlCrN coating film results in the formation of weak adhesion bond between the coating film and the tungsten carbide substrate, which cause the higher delamination (Yang et al. 2008, Zhu et al. 2015). Zhu et al. (2015) and Pham et al. (2010) noted that the lower chromium (Cr) and the higher aluminum (Al) content of the coating film will cause the higher residual stress on the cutting edge of the coated carbide tool. Kumar et al. (2014) and Adesina et al. (2019) found a low Cr content (18.6% - 22.2%) in AlCrN coating film. Higher Al content (38.1%) in AlCrN coating film compared to Al content (20.4%) in TiAlN coating film was also reported in these studies. Second, AlCrN coating film was found to be poor in adhesion with the tungsten carbide substrate because of the poor thermal conductivity (Dumkum et al. 2018). In addition, Lee et al. (2009) noted that the low thermal conductivity of AlCrN coating film may be a reason to raise the cutting temperature at the cutting tool interface, and causes the delamination wear as well as the built-up edge formation. It also appears in Fig. 4 that TiN and TiAlN coated carbide tool generated a higher delamination in cutting OSB than in cutting LVL. This fact could be attributed to the rigid behavior of the strands on the OSB. The strands were incompletely severed from the board. The strands led to rub against the coated carbide tools continuously, and in turn generated a higher delamination of TiN and TiAlN coating film.

Chip formation

Investigation of chips generated during cutting of the WPC, LVL, and OSB shows that both uncoated and coated carbide tools produced similar type and size of chips. The chip shapes were determined as spiral chip, splinter chip, flow chip, thin chip, and granule chip (Fig. 5). The spiral and splinter chips were netted on 10 mesh sieve, flow and thin chips were netted on 20 mesh sieve, and granule chips passed through 20 mesh sieves.

It also appears in Fig. 5 that the composite boards generated different chip shapes. The difference in chip shapes was caused by the difference in structure among the composite boards. WPC and LVL chips were classified as spiral chip, splinter chip, and flow chips (Fig. 5.1a-c and Fig. 5.3a-c, resp.). The OSB chips were classified as spiral chip, splinter chip, thin chip, and granule chip (Fig. 5.4a and 5.4c-e, resp.).

The spiral chip was found in all composite boards machined. The spiral chip was formed from incompletely severed chips through compression. Flow chips were only found in cutting WPC and LVL. Su et al. (2003) noted that the flow chips match to the theoretical shape of milling model. The absent of flow chips in cutting OSB was caused by its frangible structures. It was reported that the frangible structure allows chip separation through tension perpendicular to the grain (Darmawan et al. 2019). The instantaneous impact between cutting tool edge and the frangible structure of OSB resulted in the formation of splinter, thin, and granule chips during cutting OSB. Splinter chips were block chips torn along the grain. Thin chips were almost the same as the flow chip but a little smaller. Granule chips were generated from broken pieces. Granule chip was generated in all composite boards machined.

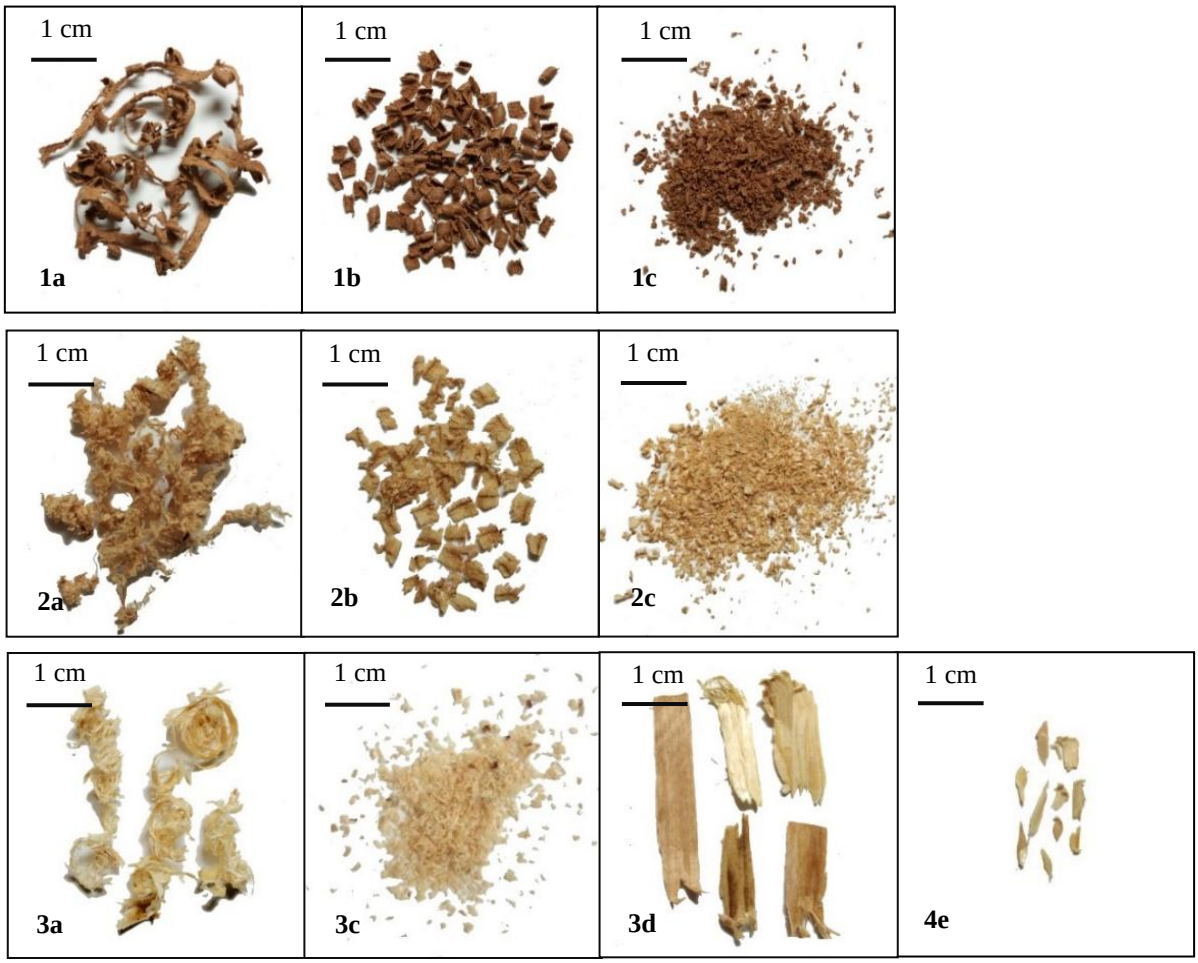

Fig. 5: Classification of chips in five shapes: (a) spiral, (b) flow, (c) granule, (d) splinter, and (e) thin, generated during cutting (1) WPC, (2) LVL, and (3) OSB.

The chip distributions were similar among the tungsten carbide tools tested for all composite boards machined (Tab. 4).

Tab. 4: Weight percentage of chips generated during cutting composite boards.

Composite boards	Tungsten carbide tool	Weight percentage (%)				
		10 mesh (> 2 mm)	20 mesh (0.8-2 mm)	40 mesh (0.4-0.8 mm)	80 mesh (0.2-04 mm)	> 80 mesh (< 0.2 mm)
WPC	Uncoated	3.7	93.2	1.2	1.0	0.8
	AlCrN	4.5	92.6	1.1	1.0	0.8
	TiN	2.6	94.6	1.4	0.8	0.7
	TiAlN	5.9	92.3	0.6	0.7	0.5
LVL	Uncoated	1.3	31.4	34.6	23.6	9.1
	AlCrN	0.5	35.5	34.1	21.2	8.6
	TiN	0.5	33.7	36.5	20.8	8.5
	TiAlN	1.1	39.7	30.5	20.8	7.8
OSB	Uncoated	8.3	18.9	34.6	22.3	15.7
	AlCrN	11.6	19.1	34.0	24.5	10.8
	TiN	12.1	18.9	34.0	24.2	10.8
	TiAlN	12.4	18.9	35.0	23.5	10.2

The similar distribution was caused by the same geometry used for the cutting tool tested. The similarities in cutting tool geometry was reported to produce a similar chip type and distribution (Su et al. 2003, Wyeth et al. 2009, Darmawan et al. 2019). The results in Tab. 4 show that the chip distributions were different among the composite boards machined. It was found that the chips of WPC were more uniform in size compared to the chips of LVL and OSB, because of its fine structures. Cutting of WPC generated mostly flow chip (93%). A large amount of fine granule chips of OSB (through 80 mesh sieve) was observed to produce serious air pollution in the work area.

Surface roughness

The results show that the Ra value of composite boards tended to increase with increasing in cutting length (Fig. 6). The coated carbide tools generated smoother composite board surfaces than uncoated carbide tool. The AlCrN coated carbide tool tended to generate the smoothest surface in cutting LVL and OSB, whereas the TiAlN coated carbide tool tended to generate smoothest surface in cutting WPC. These facts could be attributed to the wear phenomenons. The mechanical abrasion occured during cutting resulted in an irregularity on the cutting edge of the cutting tools, which led to irregularities on the surface of the composite boards machined.

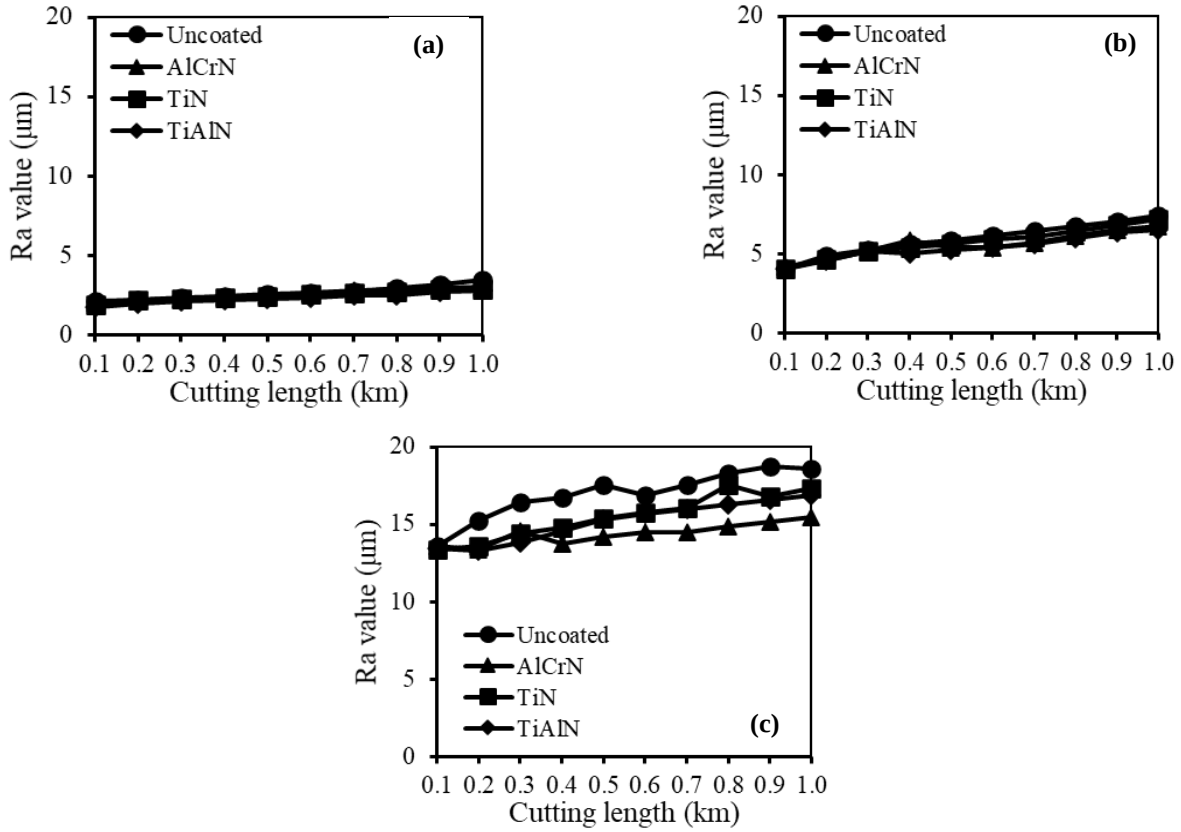

Fig. 6: Surface roughness behaviours of tungsten carbide tools in cutting: (a) WPC, (b) LVL, (c) OSB.

It was confirmed in Fig. 3 that higher irregularity on the cutting edge of AlCrN coated carbide tool compared to TiAlN coated carbide tool caused the higher surface roughness of WPC machined by the AlCrN coated tool. The same phenomenon was also reported by Wei et al. (2018). It was reported that there was a noticeable and similar tendency between surface roughness and cutting tool wear, which explain that cutting tool wear provided great influence on machining quality.

There was a considerable difference in surface roughness among the composite boards machined. The highest and the lowest surface roughness were retained by OSB and WPC, respectively for all tungsten carbide tools tested. The difference in surface roughness among the composite boards was caused by their structures. The highest surface roughness of OSB was caused by the high porosity due to the irregular orientations and sizes of the strands in the board. Conversely, WPC was form by mechanical compaction of very fine matters structure which was led to smoothest surfaces. Moreover, the difference in moisture content of OSB and WPC (11.2% and 2.1%, respectively) would also affect the surface roughness of the board. It was reported by Cleverson et al. (2015) that the increase in the moisture content causes an increase in the surface roughness.

Noise level

There was not prominent difference in noise level between uncoated and coated carbide tools for all composite boards machined (Fig. 7). The average noise level in cutting the composite boards using uncoated carbide tool, AlCrN, TiN, and TiAlN coated carbide tool was observed to be 78.5 dB, 78.4 dB, 78.2, and 78.0 dB, respectively. It could be noticed that the uncoated carbide tool tended to produce slightly higher noise compared to the coated carbide tools. TiAlN coated carbide tool generated the lowest noise level among the coated carbide tools tested. This could be due to the lower amount of wear attained by the TiAlN cutting tool edge. Since the wear occurred on the cutting tool edge due to abrasion, it would expand the contact area between the worn cutting edge and the composite boards, which led to produce the higher noise during cutting. Though AlCrN coated tool showed the lowest wear among the tungsten carbide tools tested in cutting LVL and SB, it generated the highest noise level than other coated carbide tools because of its high in hardness.

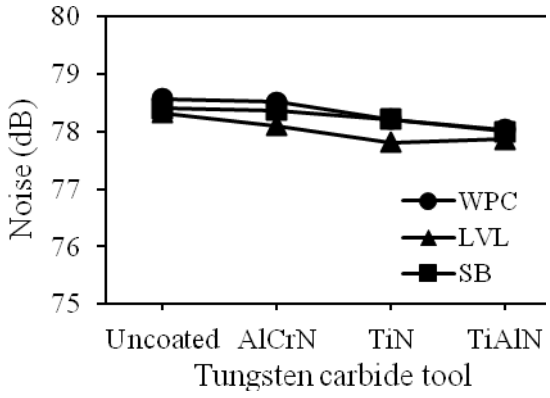

Fig. 7: Noise level in cutting composite boards using tungsten carbide tools.

The noise level was slightly different in cutting composite boards using the same tungsten carbide tools. The highest noise level was generated in cutting WPC (78.3 dB) and the lowest was in cutting LVL (78.0 dB). The difference in structure among the composite boards is considered to be the reason for this phenomenon. The high density, high hardness, high silica content, and low moisture content of WPC led to generate the highest noise during cutting compared to the other composite boards. In addition, Krilek et al. (2016) also reported the difference in structure between softwood and hardwood species generated different noise level, in which cutting of hardwood generated higher noise than softwood. Moreover, the higher moisture content of the samples was reported to reduce the emission of sound during machining (Cleverson et al. 2015).

Though LVL provided higher hardness and density compared to OSB, however cutting of OSB generated higher noise than in cutting of LVL. The noise in cutting OSB was observed to be generated from incompletely severed strands on the board. The same phenomenon was reported by Durcan and Burdurlu (2018) in cutting medium density fiberboard (MDF) of different densities. It was found that the noise level increased with decreasing of density. Decreasing density caused a reduction in elements of the cell wall or amount of substance that responding to the cutting force decreases and more breaking and crushing effect reveal.

The average noise level generated from cutting composite boards using tungsten carbide tools tested was 78.3 dB, with the maximum noise level was 81.2 dB. As recommended by ACGIH (2012), the maximum noise threshold limit value for workers is 85 dB for total duration of 8 hours per day. Therefore, cutting the composite boards using both uncoated and the coated tungsten carbide tools could be under control.

CONCLUSIONS

The coated carbide tools provide better wear resistance, smoother composite boards surfaces, and lower noise level compare to uncoated tungsten carbide tool in cutting WPC, LVL, and OSB. The difference in cutting tool tested does not provide significant difference in chip size and type. TiAlN coated carbide tool shows a better cutting performance and is suggested for machining the composite boards, especially in cutting an abrasive composite board. The abrasive materials contained in the composite boards are notable in wearing the tungsten carbide tools. The surface roughness of composite boards and the noise level increase due to increasing in the wear and could be a good indication for the wear of the tungsten carbide tools. The structure of the composite boards is observed more important than the wear of the tungsten carbide tools in determining the chip formation and surface roughness.

ACKNOWLEDGMENTS

The authors would like to thank Directorate of Higher Education (DIKTI), Ministry of Research, Technology, and Higher Education of the Republic of Indonesia for its financial

support under grant number 3/E1/KP.PTNBH/2019. The authors also thank to IPB University for the assistance in this research.

REFERENCES

1. Adesina, A.Y., Iqbal, Z., Al-badour, F.A., Gasem, Z.M., 2019: Mechanical and tribological characterization of AlCrN coated spark plasma sintered W–25% Re–Hfc composite material for FSW tool application. Journal of Materials Research and Technology 8(1): 436-446.
2. ASTM B568, 2009: Standard test method for measurement of coating thickness by X-ray spectrometry.
3. ASTM D143, 2005: Standard test methods for small clear specimens of timber.
4. ASTM E2546, 2009: Standard practice for instrumented indentation testing.
5. ASTM G111, 2006: Standard guide for corrosion tests in high temperature or high-pressure environment.
6. ASTM G99, 2010: Standard test method for wear testing with a pin-on-disk apparatus.
7. Antov, P., Savov, V., Neykov, N., 2020: Sustainable bio-based adhesives for eco-friendly wood composites. A review. Wood Research 65(1): 51-62.
8. BS 373, 1957: Methods of testing small clear specimens of timber.
9. Chandrashekhar, A., Kabadi, V.R., Bhide, R., 2016: Scratch wear resistance of TiAlN and AlCrN coated EN-353 steel. Journal of Material Science & Engineering 5(4): 251.
10. Cleverson, P., Manoel, C.S.A., Simone, S.A., 2015: Moisture content and its influence on the roughness and noise emission during wood machining. Advanced Materials Research 1088: 680-685.
11. Darmawan, W., 2017: Cutting tool edge engineering for echo-machining of wood. IPB Pr. Bogor, 7 pp.
12. Darmawan, W., Azhari, M., Rahayu, I.S., Nandika, D., Putri, R.L., Nishio, S., 2019: The chips generated during up milling and down milling of pine wood by helical router-bits. Wood Research 64(4): 691-704.
13. Darmawan, W., Gottlober, C., Oertel, M., Wagenfuhr, A., Fischer, R., 2011: Performance of helical edge milling cutters in planing wood. European Journal of Wood and Wood Products 69: 565-572.
14. Darmawan, W., Quesada, J., Rossi, F., Marchal, R., Machi, F., 2009: Improvement in wear characteristics of the AISI M2 by laser cladding and melting. Journal of Laser Applications 21(4): 176-182.
15. Darmawan, W., Rahayu, I., Nandika, D., Marchal, R., 2012: The importance of extractives and abrasives in wood materials on the wearing of cutting tools. Bioresources 7(4): 4715-4729.
16. Darmawan, W., Tanaka, C., 2004: Discrimination of coated carbide tools wear by the features extracted from parallel force and noise level. Annals of Forest Science 61: 731–736.

17. Darmawan, W., Tanaka, C., Usuki, H., Ohtani, H., 2001: Performance of coated carbide tools when grooving wood-based materials: effect of work materials and coating materials on the wear resistance of coated carbide tools. Journal of Wood Science 47(2): 94-101.
18. Dumkum, C., Jaritngam, P., Tangwarodomnukun, V., 2018: Surface characteristics and machining performance of TiAlN-, TiN- and AlCrN-coated tungsten carbide drills. Journal of Engineering Manufacture 1-12.
19. Durcan, F.M., Burdurlu, E., 2018: Effect of some machining parameters on noise level in planing of some wood materials. BioResources 13(2): 2702-2714.
20. Fahrussiam, F., Praja, I.A., Darmawan, W., Wahyudi, I., Nandika, D., Usuki, H., Koseki, S., 2016: Wear characteristics of multilayer-coated cutting tools in milling wood and wood-based composites. Tribology in Industry 38(1): 66–73.
21. Koleda, P., Barcík, Š., Naščák, Ľ., Svoreň, J., Štefková, J., 2019: Cutting power during lengthwise milling of thermally modified oak wood. Wood Research 64(3): 537-548.
22. Kopecký, Z., Hlásková, Ľ., Solař, A., Nesázal, P., 2019: Cutting forces in quasi-orthogonal CNC milling. Wood Research 64(4): 879-890.
23. Krilek, J., Kováč, J., Barcík, S., Svoreň, J., Štefánek, M., Kuvik, T., 2016: The influence of chosen factors of a circular saw blade on the noise level in the process of cross cutting wood. Wood Research 61(3): 475-486.
24. Kulman, S., Boiko, L., Haláry Gurová, D., Sedliačik, J., 2019: Prediction the fatigue life of wood-based panels. Wood Research 64(3): 373-388.
25. Kumar, T.S., Prabu, S.B., Manivasagam, G., Padmanabhan, K.A., 2014: Comparison of TiAlN, AlCrN, and AlCrN/TiAlN coatings for cutting-tool applications. International Journal of Minerals, Metallurgy and Materials 21(8): 796-805.
26. Lee, S.M., Chow, H.M., Huang, F.Y., 2009: Friction drilling of austenitic stainless steel by uncoated and PVD AlCrN and TiAlN-coated tungsten carbide tools. International Journal of Machine Tools and Manufacture 49: 81–88.
27. Li, W.G., Zhang, Z.K., 2019: The effect of micro-pits texture on the coefficient of friction between wood and cemented carbide under different wood moisture content. Wood Research 64(4): 731-742.
28. Mo, J.L., Zhua, M.H., Leia, B., Lenga, Y.X., Huanga, N., 2007: Comparison of tribological behaviours of AlCrN and TiAlN coatings-deposited by physical vapor deposition. Wear 263: 1423–1429.
29. Niska, K.O., Sain, M., 2008: Wood-polymer composites. CRC Press. New York, 1 pp.
30. Pham, T.H.T., Le Bourhis, E., Goudeau, P., Guérin, P., 2010: Residual stresses in AlCrN PVD thin films. In: 14th International Conference on Experimental Mechanics. Pp 1-7, Poitiers.
31. Ratnasingam, J., Ma, T.P., Ramasamy, G., 2010: Tool temperature and cutting forces during the machining of particleboard and solid wood. Journal of Applied Science 10(22): 2881–2886.
32. Ribeiro, M.N.F., del Menezzi, C.H., 2019: Effect of the temperature and pressure on properties of densified medium density fiberboards. Wood Research 64(4): 613-624.

33. Saloni, D., Buehlmann, U., Lemaster, R.L., 2011: Tool wear when cutting wood fiber–plastic composite materials. Forest Product Journal 61(2): 149-154.
34. Sheikh-Ahmad, J.Y., Stewart, J.S., 1995: Performance of different PVD coated tungsten carbide tools in the continuous machining of particleboard. In: Proceedings of the 12th International Wood Machining Seminar. Pp 282-291, Kyoto.
35. Su, W.C., Wang, Y., Zhu, N., Tanaka, C., 2003: Effect of tool angles on the chips generated during milling wood by straight router-bits. Journal of Wood Science 49: 271-274.
36. T211 om-02, 2002: Ash in wood, pulp, paper, and paperboard: Combustion at 525^{o}C.
37. Talib, R.J., Zaharah, A.M., Selamet, M.A., Mahaidin, A.A., Fazira, M.F., 2013: Friction and wear characteristics of WC and TiCN-coated insert in turning carbon steel workpiece. The Malaysian International Tribology Conference. Procedia Engineering 68: 716-722.
38. Wei, H., Guo, X., Zhu, Z., Cao, P., Wang, B., Ekevad, M., 2018: Analysis of cutting performance in high density fiberboard milling by ceramic cutting tools. Wood Research 63(3): 455-466.
39. Wyeth, D.J., Goli, G., Atkins, A.G., 2009: Fracture toughness, chip types and the mechanics of cutting wood. A review. Holzforschung 63: 168-180.
40. Yang, S.M., Chang, Y.Y., Lin, D.Y., Wang, D.Y., Wu, W., 2008: Mechanical and tribological properties of multilayered TiSiN/CrN coating synthesized by a cathodic arc deposition process. Surface and Coating Technology 202: 2176–2181.
41. Zhu, L.H., Hu, T., Peng, X., Ni, W.Y., Liu, Y.X., 2015: Effect of Al content on adhesion strength of TiAlN coatings. Transaction of Mater and Heat Treatment 36(3): 154-158.

KIDUNG TIRTAYASA PUTRA PANGESTU, WAYAN DARMAWAN*,
DODI NANDIKA, IMAM WAHYUDI
BOGOR AGRICULTURAL UNIVERSITY
FACULTY OF FORESTRY
DEPARTMENT OF FOREST PRODUCTS
16680 BOGOR, INDONESIA
*Corresponding author: wayandar@indo.net.id

LUMONGGA DUMASARI
PURWOKERTO MUHAMMADIYAH UNIVERSITY
53182 PURWOKERTO, INDONESIA

HIROSHI USUKI
THE UNIVERSITY OF TOKYO
INSTITUTE OF INDUSTRIAL SCIENCE
DEPARTMENT OF MECHANICAL AND BIOFUNCTIONAL SYSTEM
153-8505 TOKYO, JAPAN

WOOD RESEARCH doi.org/10.37763/wr.1336-4561/66.4.621629
e-ISSN 2729-8906
66(4): 2021 621-629 pp.

EFFECTS OF HEAT TREATMENT ON SOME CHEMICAL COMPOUND AND MECHANICAL PROPERTIES OF BLACK PINE WOOD

SAHIN AKYUREK, MURAT AKMAN, MURAT OZALP
KUTAHYA DUMLUPINAR UNIVERSITY
TURKEY

(RECEIVED OCTOBER 2020)

ABSTRACT

In this study, effects of heat treatment on bending strength, compression strength, chemical compound and solubility of Black pine wood (*Pinus nigra* J.F. var. seneriana) was examined. For this purpose, Black pine wood samples were kept in temperature of 250°C for 2 hours. Test results of heat-treated Black pine wood and control samples indicated that mechanical characteristics including compression strength and bending strength were affected negatively with heat treatment. Bending strength of heat treated and non-treated test samples were 129 and 76 $N \cdot mm^{-2}$, respectively. Compression strength of heat treated and non-treated test samples were 53 and 43 $N \cdot mm^{-2}$, resp. In addition, level of extractives, cellulose and hemicellulose decreased while lignin content increased with percentage of 40%. Significant decreases occurred in all chemical solubility values.

KEYWORDS: Bending strength, heat treatment, Anatolian black pine, compression strength, lignin, cellulose, hemicellulose.

INTRODUCTION

In the heat treatment application, temperature generally varies depending on type of wood material, dimensions, initial moisture percentage, material expectation, mechanical characteristics, dimensional stability and resistance to biotic and abiotic attacks. Temperature generally varies between 180ºC and 280ºC, while heat treatment time is applied between 15 min and 24 hours (Kamdem et al. 2002).

Today, heat treatment is applied in many countries in Europe under different commercial brands and performed with different methods. Some of these methods include the Finnish process (Heat treatment) method using steam for heating wood material, Plato method with

Dutch steam and hot air, French method using an inert gas (Rectification), and German (OHT) method using hot oil (Mayes and Oksanen 2002).

Rozsa and Fortes (1989) investigated the effect of heat treatment on pressure resistance of *Quercus suber* wood heat-treated at 100°C and 300°C. The study stated that resistance losses were higher in samples under heat treatment in a water vapor environment at 300°C than in the control samples due to thermal decomposition of wood material under heat. Viitaniemi (1997) investigated the bending strength of pine wood subjected to heat treatment under water vapor protection at 180°C to 250°C. As a result, there were losses of bending resistance at certain rates compared to control samples under the heat treatment,

It was specified that there was a decrease in elasticity modulus in bending, especially at 150°C above in both tree species in experimental investigations of pine and beech sapwood exposed to heat treatment at different temperatures and periods. However, pressure resistance is slightly affected, while shock resistance is more affected (Schneider 1971). Impacts of heat treatment on resistance characteristics of Eucalyptus (*Eucalyptus saligna*) wood were investigated (Vital and Lucia 1983). The samples were heat-treated at 105°C to 155°C for 10 to 160 hours. The experiment with increasing temperature and time reported a significant decrease in bending resistance, modulus of elasticity in bending, pressure, and shear resistance parallel to fibers. Modification and degradation of hemicellulose are primarily responsible for initial losses in bending strength, not degradation or depolymerization of lignin and cellulose during heat treatment. The bending resistance is reduced more considering heat treatment time and temperature. It was stated that the load sharing capacity of hemicellulose in the lignin-hemicellulose matrix is broken, causing loss of resistance. Another reason is a decrease in the degree of hemicellulose polymerization due to disruption of the spine of hemicellulose (LeVan et al. 1990). Degradation of hemicelluloses results in cross-linking reactions between components of the material, crystallization of microfibrils, and a reduction in the accumulation of tension in microfibrils (Dwianto et al. 1996). It was reported that bending resistance decreases between 4% and 49% depending on different wood species and heat treatment conditions (Esteves et al. 2007, Shi et al. 2007). Changes in pressure value are related to the method and application parameters of heat treatment and chemical structure that change. It has more lignin ratio and less acid number in heat-treated wood species than the normal material has, which indicates that hemicelluloses and some extractives are degraded (Nuopponen et al. 2005). Hemicellulose, which constitutes the structure of wood material, changes at 180°C, lignin at 200°C, and cellulose at 210°C leading to the start of decomposition. As seen here, the first deteriorating structure in wood material is followed by hemicellulose containing acetyl group, followed by lignin, and finally cellulose structure (Jeske et al. 2012, Ndiaye and Tidjani 2012, Tufan et al. 2015).

The aim of this study is to examine the effects of heat treatment on bending strength, compression strength, chemical compositions, and solubility of black pine (*Pinus nigra* J.F. var. seneriana) wood.

MATERIAL AND METHODS

Samples of Anatolian Black pine used in this study were obtained from Domanic Forest Management Directorate Ala Goz Forest Management Department of Kutahya, in 104 sections, in the north of Karakiran hill at 1025 m altitude. In the bending strength tests, TS 2474 (1976) rules were followed. The following equations were used to calculate bending strength (σ_e):

$$\sigma_e = \frac{3 \cdot F_{max} \cdot L}{2 \cdot b \cdot h^2} \quad (N \cdot mm^{-2}) \qquad (1)$$

where: σ_e is bending strength ($N \cdot mm^{-2}$), b is the width of sample piece (mm), h is the thickness of sample piece (mm), F_{max} is the maximum force at breaking point (N), and L is the distance between supports (mm).

Compression strength tests were carried out according to TS 2595 (1976) standards. The following equations were used to calculate compression strength parallel to grain ($\sigma_{c//}$):

$$\sigma_{c//} = \frac{F_{max}}{b \cdot h} \quad (N \cdot mm^{-2}) \qquad (2)$$

where: F_{max} is the maximum force at breaking point (N), b is the width of sample (mm), h is the thickness of the sample (mm).

Air-dried Black pine chips were ground to 60 mesh fractions using a mill and were chosen to determine chemical components in accordance with relevant TAPPI Standard methods. Humidity, lignin, ashes, and α-cellulose values were determined using the standards Tappi T 264 om-88, Tappi T 222 om-88, Tappi T 211 om-85, and Tappi T 203 os-71, respectively. Solubility in NaOH 1% and water was determined using Tappi T 207 om-88, resp. Cellulose and holocellulose contents were determined according to Kurschner Hoffer nitric acid and Wise's chlorite methods, respectively (Browning 1967, Wise and Karl 1962, Kurschner and Hoffer 1993). Based on the methods listed above, three replicates were performed for each experiment. Chemical analyzes were carried out in Forest Products Chemical and Technology Laboratory, Kahramanmaras University, Forest Industry Engineering Department. Black pine wood was used in all sample experimental studies. Black pine wood samples used in this study were kept at 250°C for 2 hours.

RESULTS AND DISCUSSION

Chemical and mechanical tests were performed on wood samples of black pine (*Pinus nigra* ssp. Pallasiana var. seneriana) before and after heat treatment. The findings are given below.

Bending strength results

The bending strength data for heat treated and non-treated pine wood were given in Tab. 1 (Akman et al. 2018). When the data in Tab. 1 are analyzed, it can be easily seen that heat treatment affected the bending strength of the wood. The percentage of the bending strength decreased approximately by 41%. In previous studies, some researchers reported that heat treatment affects the mechanical properties of the wood. For example, Esteves et al. (2014) investigated sapwood and heartwood samples of *Pinus pinaster* treated at 190 and 200ºC and reported the decreased bending strength by 50 and 30% for sapwood and heartwood, respectively. Similar results on bending strength were reported by Bekhta and Niemz (2003) related to spruce wood treated at high temperatures. Bal (2014) reported that heat treatment had lower effects on the mechanical properties such as modulus of rupture, modulus of elasticity, and IB of juvenile wood than of mature wood. Xie et al. (2020) determined similar results about reducing the bending strength of the heat-treated *Toona sinensis* wood.

Tab. 1: Bending strength results ($N \cdot mm^{-2}$).

Samples	**Bending strength results**	
	Non-treatment	**Heat treatment (**250°C, 2 hours)
1	165.22	100.28
2	142.62	71.71
3	174.70	83.40
4	107.15	69.24
5	116.88	76.45
6	98.81	65.15
7	108.33	62.11
8	69.91	82.00
9	150.86	81.09
10	163.50	72.65
Average	129.80	76.41
Standard deviation	34.48	11.01

Heat treatment negatively affected the bending strength properties of Anatolian black pine wood. The interaction between these obtained values was examined with variance analysis, and obtained results are given in Tab. 2.

Tab. 2: Variance analysis results of bending strength.

Variance source	**Df**	**Sum of squares**	**Mean squares**	**F test**	**P**
Heat treatment	1	14252.461	142461.461	21.754	0.000
Error	18	11792.958	655.164		
Corrected total	19	26045.418			

According to the results of the conducted variance analysis, the effects of heat treatment on the bending strength of black pine wood were found significant with a 5% of error.

Compression strength results

Test results of compression strength are given in Tab. 3. When the data in Tab. 3 are analyzed, it can be shown that heat treatment affect the compression strength of pine wood.

The compression strength of heat treated samples is greater than that of non-treated samples. Similar results were obtained in previous studies conducted by some researchers. For example, Yıldız et al. (2006) reported the decreases of compression strength of spruce wood treated with four different temperatures. Bal and Bektaş (2013) noted that compression strength of juvenile and mature wood of *Eucalyptus grandis* decreased in different proportions. Xie et al. (2020) determined compressive strength decreased by 33.84% at the temperature 220ºC compared to control samples. But, conversely, Some researchers reported that heat treatment increased the compression strength of the heat treated wood (Kol 2010, Perçin et al. 2016).

Tab. 3: Compression strength results ($N \cdot mm^{-2}$) (Akman et al. 2018).

Samples	**Compression strength results**	
	Non-treatment	**Heat treatment** (250°C, 2 hours)
1	52.68	36.06
2	42.14	46.57
3	56.95	47.36
4	55.85	42.20
5	56.61	47.44
6	62.92	46.02
7	56.56	38.78
8	54.17	42.26
9	58.23	41.38
10	54.24	49.21
11	57.05	37.05
12	48.64	47.70
13	57.60	34.06
14	39.63	50.68
15	55.08	48.91
Average	53.89	43.71
Standard deviation	6.12	5.30

Heat treatment negatively affected the compression strength properties of black pine wood. The interaction between these obtained values was examined with variance analysis, and the obtained results are given in Tab. 4.

Tab. 4: Variance analysis results of compression strength.

Variance source	**Df**	**Sum of squares**	**Mean squares**	**F test**	**P**
Heat treatment	1	776.938	776.938	23.734	0.000
Error	28	916.571	32.735		
Corrected total	29	1693.509			

According to the results of variance analysis conducted, effects of heat treatment on compression strength of black pine wood were found significant with 5% of error.

Chemical compositions results

Values of chemical composition results for black pine wood are given in Tab. 5. The amount of extractive agent after heat treatment decreased more than that of the holocellulose and cellulose. Since gelling occurs during heat treatment, alpha-cellulose

content could not be measured after heat treatment. After heat treatment, a decrease in ash value was also observed. The amount of lignin increased after heat treatment. Extractive, holocellulose, cellulose, and ash amount decreased after heat treatment in different proportions. Conversely, lignin content increased after heat treatment. Similar results were reported in previous studies on chemical compositions of heat-treated wood (Yıldız et al. 2006, Brito et al. 2008, Xie et al. 2020).

Tab. 5: The chemical compositions of black pine (Akyurek 2019).

Chemical compositions	**Standards**	**Non-treatment**	**Heat treatment** (250°C, 2 hours)
Extractives (%)	ASTM D1107-96	8.71 ± 0.35	0.61 ± 0.1
Holocellulose (%)	Wise et al. (1946)	64.67 ± 0.36	51.76 ± 0.23
Cellulose (%)	Kurschner and Hoffer (1993)	48.27 ± 1.61	39.35 ± 1.39
Alfa Cellulose (%)	TAPPI T203 om-93	40.10 ± 0.24	*
Lignin (%)	TAPPI T222 om-98	34.32 ± 0.82	48.21 ± 0.03
Ash (%)	TAPPI T211 om-02	0.60 ± 0.07	0.33 ± 0.06

± - standard deviation, *- alpha cellulose content could not be determined because gelling occurred during determination of alpha cellulose of heat-treated wood sample.

Chemical solubility results

The values of chemical solubility results for black pine wood are given in Tab. 6 (Akyurek 2019). After heat treatment, solubility values significantly decreased. Chemical solubility and compositions of some pine wood species are given in Tab. 7.

Tab. 6: The chemical solubility of black pine.

Chemical solubility	**Standards**	**Non-treatment**	**Heat treatment** (250°C, 2 hours)
% 1’ NaOH (%)	TAPPI T212 om-02	19.75 ± 0.55	1.66 ± 0.07
Hot water (%)	TAPPI T207 om-93	8.68 ± 0.26	2.12 ± 0.07
Cold water (%)	TAPPI T207 om-93	7.42 ± 0.24	0.94 ± 0.12

Tab. 7: Chemical solubility and of components some type of tree.

		Pinus brutia Gultekin (2014)	***Pinus sylvestris*** Gultekin (2014)	***Pinus nigra*** Kılıc et al. (2010)
Chemical components	**Holocellulose (%)**	74.7	75.4	-
	Cellulose (%)	53.7	56.0	-
	Extractives (%)	-	-	-
	Lignin (%)	25.1	26.1	-
	Ash (%)	0.39	0.27	0.19
	Alfa cellulose (%)	70.5	69.7	50.41
Solubility	**1% NaOH (%)**	15.0	10.8	12.76
	Hot water (%)	5.09	5.3	4.18
	Cold water (%)	3.39	1.97	2.11

CONCLUSIONS

After heat treatment of Black pinewood material, decreases in bending resistance and compressive strength values were observed in proportion to temperature and time. Bending

resistance decreased more than the pressure resistance. This may be due to greater and earlier degradation of cellulose than those of lignin.

After chemical analysis of cell wall components of black pine, it was found that the amount of extractive material was 8.71% without heat treatment and 0.61% with heat treatment. The amount of holocellulose was 64.67% without heat treatment and 51.76% with heat treatment. The amount of cellulose was 48.27% without heat treatment and 39.35% with heat treatment. The amount of alpha-cellulose was 40.10% without heat treatment. The amount of lignin was 34.32% without heat treatment and 48.21% with heat treatment; the amount of ash was 0.60% without heat treatment and 0.33% with heat treatment. Although alpha-cellulose was measured as 40.1% without heat treatment, the value after heat treatment could not be measured due to gelling. An increase in the amount of lignin may be due to faster and earlier degradation of other components. The reason is that lignin appears to be proportionally high due to later degradation rather than an increase.

After chemical analyses of solubility values of black pine, it was detected that 1% NaOH solubility was 19.75% without heat treatment and 1.66% with heat treatment. Hot water solubility was 8.68% without heat treatment and 2.12% heat treatment. Cold water solubility was 7.42% without heat treatment and 0.94% without heat treatment. Significant reductions occurred in all solubility values after heat treatment.

ACKNOWLEDGEMENT

Some test results of this present study was presented in International Conference on Science and Technology (ICONST 2018) September 5-9 in Prizren, Kosovo.

REFERENCES

1. Akman, M., Ozalp, M., Cerçioğlu, M., 2018: The effects of heat treatment on some mechanical properties Anatolian black pine (*Pinus nigra* J.F. var. seneriana) and investigation of soil properties. ICONST-International Conference on Science and Technology, Proceeding Book, Pp 438-447, September 5-9, Prizren, Kosovo.
2. Akyurek, S., 2019: The study on effect of heat treatment on the wood cell wall components of Black pine (*Pinus Nigra J. F. Var. Seneriana)* and Its Chemical Resolutions. Kutahya Dumlupinar University, Graduate School of Natural and Applied Sciences, M.Sc. Thesis, Kutahya.
3. Bal, B.C., 2014: Some physical and mechanical properties of thermally modified juvenile and mature black pine wood. European Journal of Wood and Wood Products 72: 61–66.
4. Bal, B.C., Bektaş, İ., 2013:The effects of heat treatment on some mechanical properties of juvenile wood and mature wood of *Eucalyptus grandis*. Drying Technology 31(4): 479-485.
5. Bekhta, P., Niemz, P., 2003: Effect of high temperature on the change in color, dimensional stability and mechanical properties of spruce wood. Holzforschung 57(5): 539-546.

6. Brito, J.O., Silva, F.G., Leão, M.M., Almeida, G., 2008: Chemical composition changes in eucalyptus and pinus woods submitted to heat treatment. Bioresource Technology 99(18): 8545-8548.
7. Browning, B.L., 1967: Methods of wood chemistry. Vol. 1, Interscience Publishers, New York. Pp 287-289.
8. Dwianto, W., Tanaka, F., Inoue, M., Norimoto, M., 1996: *Fagus orientalis* changes of wood by heat or steam treatment. Wood Research 83: 47-49.
9. Esteves, B.M., Domingos, I.J., Pereira, H.M., 2007: Pine wood modification by heat treatment in air. Biroresources 3(1): 142-154.
10. Esteves, B., Nunes, L., Domingos, I., Pereira, H., 2014: Comparison between heat treated sapwood and heartwood from *Pinus pinaster*. European Journal of Wood and Wood Products 72(1): 53-60.
11. Gultekin, G., 2014: Determination of chemical, morphological, anatomical, physical and mechanical properties of sapwood and heartwood of some softwood and hardwood. Kahramanmaras Sutcu Imam University, Graduate School of Natural and Applied Sciences, Ph.D. Thesis.
12. Jeske, H., Schirp, A., Cornelius, F., 2012: Development of a thermogravimetric analysis (TGA) method for quanti analysis of wood flour and polypropylene in wood plastic composites (WPC). Thermochimica Acta 543: 165-171.
13. Kamdem, D.P., Pizzi, A., Jermannuad, A., 2002: Durability of heat-treated wood. Holz als Roh und Werkstoff 60:1-6.
14. Kılıc, A., Sariusta, S.E., ve Hafizoglu, H., 2010: Chemical structure of compression wood of *Pinus sylvestris, P. nigra* and *P. brutia*, Journal of Forestry 12(8): 33-39.
15. Kol, H.S., 2010: Characteristics of heat-treated turkish pine and fir wood after thermo wood processing. Journal of Environmental Biology 31(6): 1007-1011.
16. Kurschner, K., Hoffer, A., 1993: Cellulose and cellulose derivative. Fresenius Journal of Analytical Chemistry 92(3): 145-154.
17. LeVan, S.L., Ross, R.J., Winandy, J.E., 1990: Effects of fire retardant chemicals on bending properties of wood at elevated temperatures. Res. Pap. FPL-RP498, USDA Forest Service Forest Products Laboratory, Madison, WI-USA, 24 pp.
18. Mayes, D., Oksanen, O., 2002: ThermoWood handbook. Finnforest 3, Finland. Pp 5-15.
19. Ndiaye, D., Tidjani, A., 2012: Effects of coupling agents on thermal behavior and mechanical properties of wood flour/polypropylene composites. Journal of Composite Materials 46(24): 3067–3075.
20. Nuopponen, M., 2005: FT-IR and UV Raman spectroscopic studies on thermal modification of scotch pine wood and its extractable compounds. Helsinki University of Technology, Espoo, Finland: 29 pp.
21. Percin, O., Peker, H., Atilgan, A., 2016: The effect of heat treatment on the some physical and mechanical properties of beech (*Fagus orientalis* Lipsky) wood. Wood Research 61(3): 443-456.
22. Rozsa, M.E., Fortes, M.A., 1989: Effects of water vapor heating on structure and properties of cork. Wood Science Technology 23(2): 27-34.

23. Schneider, A., 1971: Investigations on the influence of heat treatment in the temperature range 100-200°C on modulus of elasticity. Holz Roh-u Werkstoff 29(11): 431-440.
24. Shi, J.L., Kocaefe, D., Zhang, J., 2007: Mechanical behaviour of Québec wood species heat-treated using ThermoWood process. Holz als Roh-und Werkstoff 65: 255-259.
25. TAPPI, 2013: Viscosity of pulp (capillary viscometer method). TAPPI test methods, standard methods for pulp and paper, technical association of pulp and paper industry. Tappi Press, Atlanta.
26. TS 2474, 1976: Wood-determination of ultimate strength in static bending. Ankara.
27. TS 2595,1976: Wood-determination of ultimate stress in compression parallel to grain. Ankara.
28. Tufan, M., Gulec, T., Cukur, U., Akbas, S., Imamoglu, S., 2015: Some properties of wood plastic composites produced from waste cups. Kastamonu University. Journal of Forestry Faculty 15(2): 176-182.
29. Viitaniemi, P., 1997: Decay resistant wood created in a Heating process. Industrial Horizons.
30. Vital, B.R., Lucia, M.D., 1983: Effect of heating on some properties of *Eacalyptus saligna* wood. Revista-Arvore 7(2): 136-146.
31. Wise, E.L., Karl, H.L., 1962: Cellulose and hemicelluloses in pulp and paper science and technology. New York: Vol. 1. Pulp, Edited by C. Earl Libby, McGraw HillBook Co.
32. Xei, J., Chen, L., Shao, H., He, L., Jiang, Y., Lu, D., Xiao, H., Chen, Y., Huang, X., Hao, J., Tu, L., Lin, T., Xiao, Y., Chen, G., Qi, J., 2020: Changes in physical-mechancal properties and chemical compositions of *Toona sınensıs* wood before and after thermal treatment. Wood Research 65(6): 877-884.
33. Yildiz, S., Gezer, E.D., Yildiz, U.C., 2006: Mechanical and chemical behavior of spruce wood modified by heat. Building and Environment 41(12): 1762-1766.

SAHIN AKYUREK, MURAT AKMAN
KUTAHYA DUMLUPINAR UNIVERSITY
GRADUATE SCHOOL OF NATURAL AND APPLIED SCIENCES
43000 KUTAHYA
TURKEY

MURAT OZALP*
KUTAHYA DUMLUPINAR UNIVERSITY
FACULTY OF SİMAV TECHNOLOGY
DEPARTMENT OF WOOD WORKS INDUSTRIAL ENGINEERING
43500 SİMAV, KUTAHYA
TURKEY
*Corresponding author: murat.ozalp@dpu.edu.tr

WOOD RESEARCH doi.org/10.37763/wr.1336-4561/66.4.630642
e-ISSN 2729-8906
66(4): 2021 630-642 pp.

INFLUENCE OF ULTRA LOW AND HIGH TEMPERATURE ON ENZYMATIC PRETREATMENT OF BEECH BRANCHES WOOD

MICHAL HALAJ, ŠTEFAN BOHÁČEK, ANDREJ PAŽITNÝ, VLADIMÍR KUŇA, JOZEF BALBERČÁK
PULP AND PAPER RESEARCH INSTITUTE
SLOVAKIA

(RECEIVED DECEMBER 2020)

ABSTRACT

The publication is focused on the effect of ultra low and high temperature on enzymatic pretreatment of beech wood (*Fagus sylvatica* L.). Two fractions < 0.7 mm and 1.0 – 2.5 mm of disintegrated branches sawdust were used for experiments. Glucose and xylose yields were measured after 24, 48, and 72 hours of enzymatic hydrolysis with 15 % load of the enzyme measured to total cellulose content. The influence of freezing under -80°C and boiling under pressure at +160°C on samples before enzymatic hydrolysis was observed. Mutual combination of boiling under pressure to obtain the maximum water uptake and subsequent freezing was used to better understand the process of cell destruction. The results show that the boiling pretreatment has a positive influence on the total monosaccharide yields and the subsequent freezing may slightly increase these yields even further. The maximum monosaccharide conversion (73.24%) was achieved using the fraction < 0.7 mm.

KEYWORDS: Enzymatic pretreatment, freezing, boiling under pressure, *Fagus sylvatica* L., glucose, xylose, wood fractions.

INTRODUCTION

Due to a rising global demand for wood consumption, which leads to degradation of environment, the emphasis is put on the use of secondary wood resources. Recycling of waste wood (Ihnát et al. 2020), including wood-based composites (Lübke et al. 2020), has become more important, or alternative sources are sought instead of wood raw material (Lübke et al. 2014). Unprocessed wood residues after harvesting come into consideration, which can be processed by known chemical (Balberčák et al. 2017, 2018) or enzymatic

procedures (Pažitný et al. 2020). The main utilization of less valuable wood sources still targets to liquid biofuels, mainly to most promising bioethanol (Cheah et al. 2020, Prasad et al. 2016). Bioethanol shows high oxygen content, that results to better combustion efficiency, and also has a higher octane number allowing operation at high compression ratios (Branco et al. 2019). So, pretreatment methods of agricultural, municipal lignocellulosic wastes or even still considered microalgae (Sankaran et al. 2020, Halaj et al. 2019) play important roles in practical application.

Forest residues after wood harvesting remain underutilized due to economic and operational barriers caused by high cost of collecting, treatment, and transportation (Han et al. 2010). Most residues of the tree logs remain as land cover. Significant research has focused on tree residues as potential source of energy biomass (He et al. 2014). The mass distribution of wood in deciduous trees at harvesting time is to be 68% in stems, 10-19% in crowns and branches, and 8-25% in roots. After harvesting, about 35 to 50% of wood biomass stays in the forests as stumps and branches (Okai and Boateng 2007). The number of publications on wood characteristics in branch parts of the hardwood species is still low. The differences in chemical compositions between trunk and branches were observed in wood e.g. *Alianthus altissima* (Samariha and Kiaei 2011), birch (*Betula pendula*) (Krutul et al. 2014).

Pretreatments using high temperatures are well known, but research that focused in freezing is still evolving. The principle of freezing methods is a volume change of water by approximately 9% during freezing. The biomass impregnated with water is subjected to be completely frozen. The volume expansion of water during freezing results to open channels of wood and leads to disruption cell wall or lignocellulosic material structure loose. The freeze-damaged material has an increased surface for enzymatic hydrolysis (Rooni et al. 2017, Zhu et al. 2020). According to literature the main source of suitable material for cryolysis is agricultural waste, like barley straw (Rooni et al. 2017), rice straw (Chang et al. 2011, Deng et al. 2018), wheat straw (Wang et al. 2013, Ihnát et al. 2015, Pažitný et al. 2019a, Sasaki et al. 2021), corncobs and corn stalks (Echeverria et al. 2018, Yuan et al. 2019, Li et al. 2019a), sugarcane bagasse (Farghaly et al. 2021). Another substances were also used for cryolysis, such as rush (*Juncus maritimus*) (Smichi et al. 2016), switchgrass (*Panicum virgatum*) (Yang et al. 2009), poplar wood (Zhu et al. 2020, Boháček et al. 2020), and waste cotton towels (Sasaki et al. 2020). Base on the fact that wood material is denser, more publications show combination of freezing with another methods of pretreatment. Data show this combination with only chemical pretreatment, such as Jeong et al. (2016) observed the effect of freezing on Mongolian oak (*Quercus mongolica*) after impregnation with 1% H_2SO_4, on the other hand, alkaline co-pretreatment published Li et al. (2019b) as combination of freezing-thawing (from -20 up to 20°C) with addition of ammonia, or with NaOH (Su and Fang 2017, Sasaki et al. 2021).

The aim of this paper is to evaluate the effects of pretreatment of branch beech wood (*Fagus sylvatica* L.) in a wide range of temperature conditions. Limits, as deep freezing at -80°C and boiling under pressure at 160°C were selected as borders for experiments. A mutual combination of these extreme methods was considered, as well.

MATERIAL AND METHODS

Material

The beech (*Fagus sylvatica* L.) was collected in the region of Bratislava, Slovak Republic. The enzyme complex Cellic®CTec3 was purchased from Novozymes A/S (Bagsværd, Denmark). The enzyme activity was determined as 1700 BHU (Biomass Hydrolysis Units)/g. The range of the diameter of branches was from 2.0 to 4.5 cm.

Methods

Preparation of fractions

Leaves and other impurities were removed from the timber and debarked by a single-knife laboratory disc chipper. The wood was shredded for smaller parts, then dry milled in a Brabender mill (Brabender®, GmbH & Co. KG, Germany) with used bottom sieve 2.5 mm mesh. The fraction was purified by sieve 1.0 mm mesh in a sieve tester after 5 min of sieving. The material passed through 1.0 mm sieve was milled again in a Brabender mill with bottom sieve 0.7 mm to prepare two size fractions: 1.0-2.5 mm and < 0.7 mm.

Water impregnation

An absolute dry weight of the both fractions was determined by moisture analyzer Denver IR35 with use infrared heating to be 91.76 % for 1.0-2.5 mm and 93.1 % for < 0.7 mm fraction. The samples of both fractions for only blank and deep freezing for saturation by water as 12.5 g of absolute dry weight of the material + 87.5 mL of distilled water were prepared separately. The other samples of fractions used for boiling at higher pressure and combination of boiling at higher pressure and deep freezing, were prepared together at 2.5-times higher dose to be in extent as 31.25 g of absolute dry weight + 218.75 mL of distilled water. The impregnation was performed in closed PET bags in orbital shaker-incubator 24 hours at 60°C.

Pretreatment of samples

The impregnated blank samples were placed into a kitchen freezer until the other fractions were pretreated. The single deep freezing was performed in a laboratory ultra low freezer at -80°C, for 4 days. In order to avoid the protection effect of ice surrounding of the sawdust particles, the water was decanted into flasks before the freezing pretreatment and kept in a freezer. The boiling under higher pressure was performed at 2 L stainless steel batch reactor for steam explosion pretreatment (Amar Equipments Pvt. Ltd., India). The boiling was carried out at temperature of 160°C, pressure 5.5 bar for 30 min. Before the thermal treatment, 50 mL of distilled water was added into the impregnated fractions as the excess to ensure the material to be all the time under water, the suspension was poured into aluminum beverage can, and placed into the reactor in a water bath. The thermally pretreated fractions were divided into sample only thermally pretreated and sample with combination of thermal pretreatment with following deep freezing. The only thermally pretreated samples were immersed in water in a concentration of 12.5 % w/w of absolute dry weight. From the samples with combination of

thermal pretreatment and deep freezing, the water was also decanted into flasks and kept in a freezer as the thermally untreated samples.

Enzymatic hydrolysis

Before the enzymatic hydrolysis of the pretreated samples by thermal degradation and subsequent deep freezing, was the absolute dry weight again determined, and the decanted water was added into the material to prepare the suspension of consistency 12.5 % w/w. To the samples treated by only deep freezing, the water after decantation before treatment was added, too. The enzymatic hydrolysis was carried out using Cellic CTec3 at 15 % w/w (g Cellic CTec3/100 g suspension) in orbital shaker-incubator ES-20/60 (BioSan Ltd., Republic of Latvia) at temperature 50°C for 96 hours. The pH was adjusted to 5.0 and regulated during the hydrolysis by 0.1 N sulphuric acid or 0.1 N sodium hydroxide. The collecting of samples from the hydrolysates to determine the content of monosaccharides was performed after 24, 48, 72, and 96 hours.

The conversion of glucan to glucose after enzymatic hydrolysis was calculated by the ratio of glucose concentration that was released during enzymatic hydrolysis to the glucose in the beech sawdust and was calculated according to the Eq. 1:

$$Glucan\ conversion\ (\%) = \frac{glucose \times V \times 0.9}{glucan\ content \times m} \times 100 \quad (1)$$

where: glucose is concentration of glucose in enzymatic hydrolysis liquor ($g \cdot L^{-1}$); V is the volume of the hydrolytic liquor (L); glucan content in beech sawdust, *m* is mass of o.d. beech sawdust (g), and 0.9 is the conversion factor for glucose to glucan. The xylan conversion was calculated analogously, with the use of conversion factor of 0.88 for xylan to xylose (Stankovská et al. 2018).

Analyses

Determination of *ash content* was performed according to ISO 1762. The content of *extractives in dichloromethane* was determined according to Tappi T 204 cm-94, and content of *extractives in hot water* according to Tappi T 207 cm-08. *Klason lignin* content was found out according to Tappi T 222 om-98 and *acid-soluble lignin* content according to Tappi UM 250.

P*olysaccharide* glucan, xylan, mannan, galactan and arabinan were evaluated after calculations of the concentrations of glucose, xylose, mannose, galactose and arabinose in hydrolyzate after determination of lignin. The hydrolysis was carried out with 4% H_2SO_4 at 121°C for 2 hours, to hydrolyze the oligosaccharides, following by neutralization with $BaCO_3$. The monosaccharide concentration after hydrolysis was determined by HPLC with Rezex ROA H^+ column. The mobile phase was 0.005 N H_2SO_4 at a flow rate of 0.5 $mL.min^{-1}$, and temperature 30°C. The samples were cleaned from solid impurities by 22 μm filter. The tests were conducted in two parallels.

Inorganic elements in ash

The content of Na, K, Ca, Mg, Fe, Mn, Zn, Cu elements in the wood was determined by atomic absorption spectrometry (AAS) using flame atomization according to the method Tappi T 266. The soluble part of the ash in hydrochloric acid was used for determination of them. The concentration of P element was determined by spectrometry using ammonium molybdate according to standard STN EN ISO 6878. The concentration of Si in the branch wood was calculated by gravimetrical determination of SiO_2 content in the insoluble ash residue after treatment by hydrofluoric acid.

RESULTS AND DISCUSSION

Beech wood belongs to the most utilized hardwood in Europe. The waste obtained from processing this hardwood is promising feedstock for production of 2G bioethanol. Biorefinery is capable to treat 400,000 dry metric tons of this wood into products as polymer-grade ethylene, organosolv lignin and biofuels (Budzinski & Nitzsche 2016, Nagarajan et al. 2017, Pažitný et al. 2019b). In Slovakia, beech represents 29% of wood in forests and together with oak are the most widespread hardwood trees in the country (Dittmar et al. 2003, Pajtík et al. 2011, Marková et al. 2018).

Tab. 1 shows the chemical composition of the beech wood determined by chemical analyses according to the appropriate methods. The content of extractives was 3.7%, lignin in this wood occupied 21.5%, and content of polysaccharides almost 69%, the glucan content in the polysaccharide part represented 64.1%. Literature data show, that the range of cellulose content is 41 to 50%, the total lignin content 22-30%, extractives up to 15%, the total content of polysaccharides ranges from 70 to 77%. Further the ash content differs from 0.72% to 1.1% (González-Peña et al. 2009, Miklečić & Jirouš-Rajković 2016, Demirbaş 2005, de Wild et al. 2009). The chemical composition approximately corresponds to the literature data. The content of inorganic elements is shown in Tab. 2. The analyses by de Wild et al. (2009), showed that calcium, potassium, and magnesium were also the first dominant elements in the beech wood.

Tab. 1: Chemical composition of branch wood of beech.

Ash (%)		0.57
Extractives (%)	Dichloromethane	0.29
	Hot water	3.44
	Total	3.73
Lignin (%)	Klason*	17.1
	Acid-soluble	4.45
	Total	21.55
Polysaccharides (%)	Glucan	44.2
	Xylan	22.3
	Mannan	1.26
	Galactan	0.76
	Arabinan	0.41
	Total	68.93

Tab. 2: Inorganic elements concentration in branch wood of beech.

Inorganic elements (mg.kg^{-1})									
Ca	K	Mg	P	Si	Na	Mn	Fe	Zn	Cu
1010	783	192	181	29	77.5	120	8.58	4.77	1.66

The dependence of yields on used methods of pretreatment

The yields after 24; 48; 72 and 96 h hydrolysis of the variously pretreated fractions of beech sawdust are shown in Tab. 3. The yields of total monosaccharides after the hydrolysis of thermally untreated smaller fraction samples decrease after 48 h (maximal yields 25.6 g·L^{-1} for blank – hydrolysis after water impregnation without any pretreatment, and 24.5 g·L^{-1} for deeply frozen), the yields of the larger fraction decrease after 72 h (maximal yields 20.7 g·L^{-1} for blank, and 22.3 g·L^{-1} for deeply frozen). After 96 h hydrolysis of the untreated samples were the yields lower, than those after 24 h hydrolysis, in a range from 8% for blank of the larger fraction to 41% for blank of the smaller fraction.

Tab. 3: The monosaccharide yields and conversions of variously pretreated fractions of beech sawdust.

Sample	**Time of hydrolysis** (h)	**Glucose** (g·L^{-1})	**Glucose conversion** (%)	**Xylose** (g·L^{-1})	**Xylose conversion** (%)	**Total monosaccharides** (g·L^{-1})	**Total monosaccharides conversion** (%)
0.7 Bl[1]	24	19.50	31.76	4.83	15.25	24.32	25.40
0.7 F[2]	24	19.18	31.24	4.69	14.81	23.86	24.92
0.7 Bo[3]	24	35.51	57.84	18.71	59.07	54.21	56.62
0.7 Fbo[4]	24	36.28	59.10	19.47	61.47	55.75	58.23
1.0 - 2.5 Bl	24	15.82	25.77	3.25	10.26	19.08	19.93
1.0 - 2.5 F	24	17.50	28.51	3.58	11.30	21.08	22.02
1.0 - 2.5 Bo	24	27.67	45.07	11.83	37.35	39.50	41.26
1.0 - 2.5 Fbo	24	27.08	44.11	12.49	39.43	39.57	41.33
0.7 Bl	48	20.50	33.39	5.14	16.23	25.64	26.78
0.7 F	48	19.56	31.86	4.91	15.50	24.47	25.56
0.7 Bo	48	40.68	66.27	20.82	65.73	61.50	64.24
0.7 Fbo	48	42.65	69.48	22.14	69.89	64.79	67.68
1.0 - 2.5 Bl	48	16.23	26.44	3.81	12.03	20.30	21.20
1.0 - 2.5 F	48	18.01	29.34	3.73	11.78	21.74	22.71
1.0 - 2.5 Bo	48	32.24	52.52	13.96	44.07	46.20	48.26
1.0 - 2.5 Fbo	48	31.77	51.75	13.64	43.06	45.40	47.42
0.7 Bl	72	15.84	25.80	4.16	13.13	20.01	20.90
0.7 F	72	18.04	29.39	4.84	15.28	22.87	23.89
0.7 Bo	72	43.24	70.44	21.72	68.57	64.96	67.85
0.7 Fbo	72	45.52	74.15	23.39	73.84	68.91	71.98
1.0 - 2.5 Bl	72	17.13	27.90	3.58	11.30	20.71	21.63
1.0 - 2.5 F	72	18.40	29.97	3.84	12.12	22.25	23.24
1.0 - 2.5 Bo	72	33.40	54.41	14.55	45.93	47.95	50.09
1.0 - 2.5 Fbo	72	34.08	55.51	14.64	46.22	48.72	50.89
0.7 Bl	96	10.91	17.77	3.46	10.92	14.37	15.01
0.7 F	96	13.81	22.50	3.91	12.34	17.72	18.51
0.7 Bo	96	44.17	71.95	22.46	70.91	66.62	69.59
0.7 Fbo	96	45.99	74.92	24.13	76.18	70.12	**73.24**
1.0 - 2.5 Bl	96	14.55	23.70	2.99	9.44	17.54	18.32

1.0 - 2.5 F	96	15.07	24.55	3.27	10.32	18.34	19.16
1.0 - 2.5 Bo	96	34.01	55.40	14.90	47.04	48.91	51.09
1.0 - 2.5 Fbo	96	34.03	55.43	14.79	46.69	48.82	50.99

[1]Bl = blank; [2]F = deep freezing at -80°C; [3]Bo = boiling at 160°C; [4]Fbo = boiling at 160°C, subsequent deep freezing at -80°C.

On the other hand, the yields of thermally treated samples are the highest after 96 h of the hydrolysis, for the smaller fraction, 66.6 $g \cdot L^{-1}$ for only thermally degraded sample, 70.1 $g \cdot L^{-1}$ (Fig. 1), the maximum yield achieved in this study, for deeply frozen material after thermal degradation, and for the larger fraction, 48.9 $g \cdot L^{-1}$ for only thermally degraded material, for material with combination of thermal degradation with subsequent deep freezing 48.8 $g \cdot L^{-1}$. The effect of thermal degradation, to compare the maximal yield of thermally untreated sample, 25.6 $g \cdot L^{-1}$ (smaller fraction, blank) and for thermally treated sample, 66.6 $g \cdot L^{-1}$ (smaller fraction, only thermal degradation), the thermal degradation increased the maximum yields in this study by 160%.

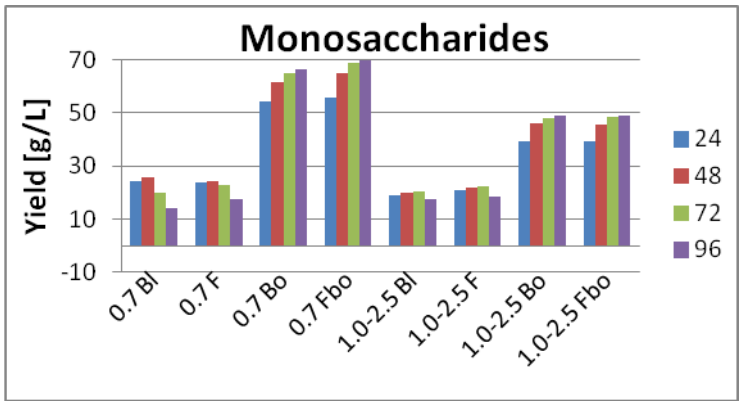

Fig. 1: The yields of total monosaccharides of pretreated branch wood beech fractions in dependence of time of enzymatic hydrolyses. Bl = blank; F = deep freezing at -80°C; Bo = boiling at 160°C; Fbo = boiling at 160°C and subsequent deep freezing at -80°C.

The maximum yield of glucose for thermally untreated samples was 20.5 $g \cdot L^{-1}$ (smaller fraction, blank), and for thermally degraded was 46 $g \cdot L^{-1}$ (Fig. 2). The thermal degradation showed a more significant effect for the yields of xylose, the maximal yield for non-thermally treated samples was 5.1 $g \cdot L^{-1}$, and for thermally treated samples was 24.1 $g \cdot L^{-1}$, which is 4.73-times higher to compare the effect of the thermal degradation of glucose, 2.24-times higher (Fig. 3).

To compare the dependence of particle size on the yield showed, that the maximum yield achieved using the smaller fraction, < 0.7 mm, was the mentioned maximum yield in this paper, 70.1 $g \cdot L^{-1}$, for the larger fraction the maximum yield was 48.9 $g \cdot L^{-1}$ (larger fraction, only thermal pretreatment), that was higher by 43%. The effect of deep freezing in the thermally degraded smaller fraction was shown as 5.2% to compare the yield after only thermal pretreatment and the yield after the combination of thermal pretreatment with subsequent deep freezing. The efficiency of the observed factors in this study is in order deep freezing < particle size < thermal degradation. To compare the yield of blank sample fraction 1.0-2.5 mm after 24 h

enzymatic hydrolysis (19.1 $g \cdot L^{-1}$) and the maximal yield in this paper, 70.1 $g \cdot L^{-1}$ after 96 h of the enzymatic hydrolysis of fraction < 0.7 mm after thermal pretreatment following by deep freezing, was higher by 267%. The conversion of polysaccharides shows the efficiency of lignocellulosic biomass hydrolysis based on the pretreatment and the access of enzymes onto the biomass surface.

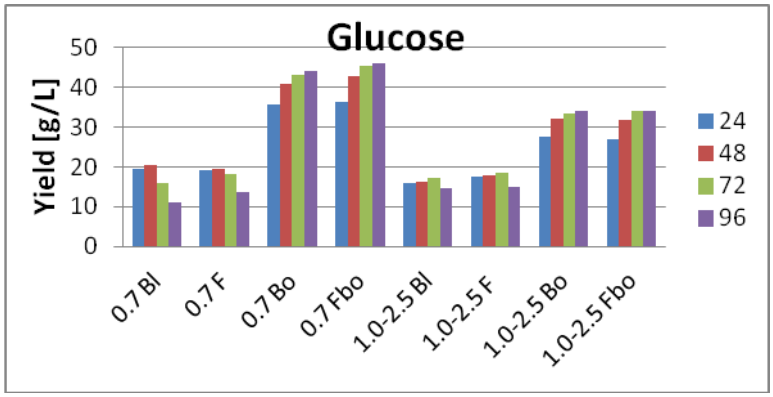

Fig. 2: The yields of glucose of pretreated branch wood beech fractions after enzymatic hydrolyses. Bl = blank; F = deep freezing at -80°C; Bo = boiling at 160°C; Fbo = boiling at 160°C and subsequent deep freezing at -80°C.

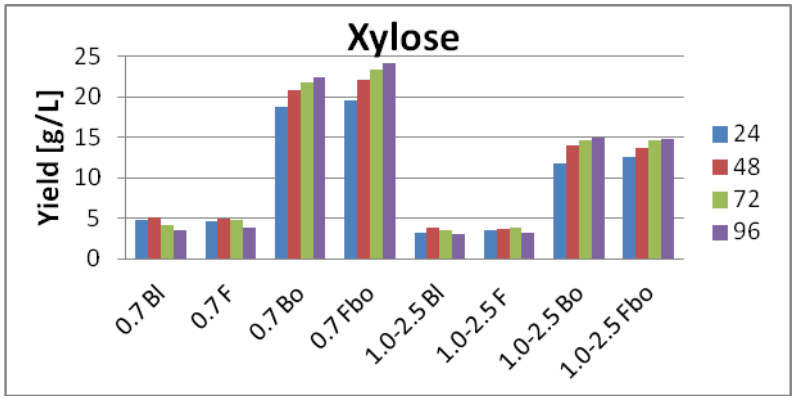

Fig. 3: The yields of xylose of pretreated branch wood beech fractions after enzymatic hydrolyses. Bl = blank; F = deep freezing at -80°C; Bo = boiling at 160°C; Fbo = boiling at 160°C and subsequent deep freezing at -80°C.

To compare the conversions, from the blank sample fraction 1.0 - 2.5 mm after 24 hours of enzymatic hydrolysis (20 %), the combination of milling, thermal pretreatment and deep freezing the conversion increased to 73.2 % after 96 h of hydrolysis for the sample fraction < 0.7 mm, thermally pretreated following by deep freezing. In study Jeong et al. (2016) the conversion more than 90% was achieved after freeze-thaw pretreatment and subsequent two-stage hydrolysis (by 1 % sulfuric acid, following by enzymatic hydrolysis). Our previous study focused on pretreatment of beech sawdust, the total monosaccharide conversion of particle size < 0.7 mm after steam explosion at 180°C for 10 min was 84.7% (Pažitný et al. 2019b). Although the deep freezing pretreatment showed no effect for thermally

untreated fraction < 0.7 mm, the maximum conversion of the total monosaccharides was 26.8% after 48 h of enzymatic hydrolysis blank sample was mildly higher as compare with blank sample (24.0% conversion) and 1st cycle (24.3%) of study focused cryolysis poplar sapwood dust, particle size < 0.7 mm, including cyclic freezing thawing (Boháček et al. 2020). On the other hand, very weak effect of deep freezing was observed on fraction 1.0 - 2.5 mm without the thermal pretreatment, the maximum yields of total monosaccharides after 72 h of enzymatic hydrolysis were increased from 20.7 $g \cdot L^{-1}$ (conversion of 21.6%) to 22.3 $g \cdot L^{-1}$ (conversion of 23.2%). Despite of that, the yields and conversions were lower, than in the previous study (Boháček et al. 2020). Zhu et al. (2020) compared the yields after freezing of poplar at -20°C and -70°C. Hemicellulose was extracted after freeze-thaw pretreatment at temperature 170°C for 1 h with wood to water ratio of 1:6 (w/w). The results showed, that from the sample without freezing was the yield of hemicelluloses of 64.9 $mg \cdot g^{-1}$, after treatment in temperature -20°C the yield increased to 85.9 $mg \cdot g^{-1}$, and the treatment at -70°C resulted in the yield of 92.1 $mg \cdot g^{-1}$ of the poplar wood.

CONCLUSIONS

Two size fractions, < 0.7 (smaller) and 1.0-2.5 (larger) mm mesh sawdust of beech (*Fagus sylvatica* L.) were subjected to observe the influence of deep freezing at -80°C, treatment in water under high pressure 5.5 bar, at temperature 160°C for 30 min (thermal treatment), and combination of these treatments to enhance enzymatic accessibility.

The maximum influence of deep freezing was observed in increasing of conversion from 69.6% (without freezing) to 73.2% (frozen) for thermally treated smaller fraction. The influence of particle size raised the maximum conversion of the larger fraction 51.1% to the highest conversion of smaller fraction 73.2%. The thermal pretreatment increased the maximum conversion from 26.8% for thermally untreated material to 69.6% for the thermally treated material without deep freezing.

The analyses showed that the influence of those factors for disruption of the lignocellulosic biomass and effect on the enzyme accessibility is in order of deep freezing < particle size < thermal degradation.

ACKNOWLEDGMENT

This work was supported by the Slovak Research Development Agency under contract No. APVV- 18 - 0533.

REFERENCES

1. Balberčák, J., Boháček, Š., Medo, P., Ihnát, V., Lübke, H., 2017: Chemical processing of waste wood based agglomerates Part I: Evaluation of properties of fluting liners made of semichemical pulp obtained by a mildly alkaline sulphur-free cooking process. Wood Research 62(5): 715-726.

2. Balberčák, J., Boháček, Š., Pažitný, A., Ihnát, V., Lübke, H., 2018: Chemical processing of waste wood based agglomerates part II: Evaluation of properties of fluting liners made of semichemical pulp obtained by an alkaline cooking process. Wood Research 63(1): 35-44.
3. Boháček, Š., Pažitný, A., Halaj, M., Balberčák, J., Kuňa, V., 2020: Freeze-thaw pretreatment of poplar sapwood dust.. Wood Research 65(6): 905-916.
4. Branco, R.H., Serafim, L.S., Xavier, A.M., 2019: Second generation bioethanol production: on the use of pulp and paper industry wastes as feedstock. Fermentation 5(1): 4.
5. Budzinski, M., Nitzsche, R., 2016: Comparative economic and environmental assessment of four beech wood based biorefinery concepts. Bioresource Technology 216: 613-621.
6. Chang, K.L., Thitikorn-Amorn, J., Hsieh, J.F., Ou, B.M., Chen, S.H., Ratanakhanokchai, K., Huang, P.J., Chen, S.T., 2011: Enhanced enzymatic conversion with freeze pretreatment of rice straw. Biomass and Bioenergy 35(1): 90-95.
7. Cheah, W.Y., Sankaran, R., Show, P.L., Ibrahim, T.N.B.T., Chew, K.W., Culaba, A., Jo-Shu, C., 2020: Pretreatment methods for lignocellulosic biofuels production: current advances, challenges and future prospects. Biofuel Research Journal 7(1): 1115.
8. de Wild, P.J., den Uil, H., Reith, J.H., Lunshof, A., Hendriks, C., van Eck, E.R., Heeres, E.J., 2009: Bioenergy II: Biomass valorisation by a hybrid thermochemical fractionation approach. International Journal of Chemical Reactor Engineering 7(1).
9. Demirbaş, A., 2005: Estimating of structural composition of wood and non-wood biomass samples. Energy Sources 27(8): 761-767.
10. Deng, Y., Qiu, L., Yao, Y., Qin, M., 2018: A technology for strongly improving methane production from rice straw: freeze-thaw pretreatment. RSC Advances (8): 22643-22651.
11. Dittmar, C., Zech, W., Elling, W., 2003: Growth variations of common beech (*Fagus sylvatica* L.) under different climatic and environmental conditions in Europe – a dendroecological study. Forest Ecology and Management 173(1-3): 63-78.
12. Echeverria, C., Bazan, G., Gonzalez, J.S., Lescano, L., Pagador, S., Linares, G., 2018: Pretreatment by acidification and freezing on corncob polymers and its enzymatic hydrolysis. Asian Journal of Scientific 11(2): 222-231.
13. Farghaly, A.M., Ahmed, K., Gad, A., 2021: Synergetic physical freezing and chemical pretreatment of lignocellulosic sugarcane bagasse followed by enzymatic hydrolysis. Preprint.
14. González-Peña, M.M., Curling, S.F., Hale, M.D., 2009: On the effect of heat on the chemical composition and dimensions of thermally-modified wood. Polymer degradation and stability 94(12): 2184-2193.
15. Halaj, M., Paulovičová, E., Paulovičová, L., Jantová, S., Cepák, V., Lukavský, J., Capek, P., 2019: Extracellular biopolymers produced by Dictyosphaerium family-Chemical and immunomodulative properties. International journal of biological macromolecules 121: 1254-1263.
16. Han, H.S., Halbrook, J., Pan, F., Salazar, L., 2010: Economic evaluation of a roll-off trucking system removing forest biomass resulting from shaded fuelbreak treatments. Biomass and Bioenergy 34(7): 1006-1016.

17. He, L., English, B.C., Daniel, G., Hodges, D.G., 2014: Woody biomass potential for energy feedstock in United States. Journal of Forest Economics 20(2): 174-191.
18. Ihnát, V., Borůvka, V., Lübke, H., Babiak, M., Schwartz, J., 2015: Straw pulp as a secondary lignocellulosic raw material and its impact on properties of properties of insulating fiberboards. Part III. Preparation of insulating fiberboards from separately milled lignocellulosic raw materials. Wood Research 60(3): 457-466.
19. Ihnát, V., Lübke, H., Balberčák, J., Kuňa, V., 2020: Size reduction downcycling of waste wood. Review. Wood Research 65(2): 205-220.
20. Jeong, H.S., Jang, S.K., Kim, H.Y., Yeo, H., Choi, J.W., Choi, I.G., 2016: Effect of freeze storage on hemicellulose degradation and enzymatic hydrolysis by dilute-acid pretreatment of Mongolian oak. Fuel 165: 145-151.
21. Krutul, D., Zielenkiewicz, T., Radomski, A., Zawadzki, J., Antczak, A., Drozdzek, M., 2014: Impact of the environmental pollution originated from sulfur mining on the chemical composition of wood and bark of birch (*Betula pendula* Roth.). Annals of Warsaw University of Life Sciences-SGGW. Forestry and Wood Technology 88: 117-125.
22. Li, J., Wachemo, A.Ch., Yuan, H., Zuo, X., Li, X., 2019a: Natural freezing-thawing pretreatment of corn stalk for enhancing anaerobic digestion performance. Bioresource Technology 288: 121518.
23. Li, J., Wachemo, A.Ch., Yu, G., Li, X., 2019b: Enhanced anaerobic digestion performance of corn stalk pretreated with freezing-thawing and ammonia: An experimental and theoretical study. Journal of Cleaner Production 247: 119112.
24. Lübke, H., Ihnát, V., Borůvka, V., 2014: Straw pulp as a secondary lignocellulosic raw material and its impact on properties of insulating fiberboards. Wood Research 59(5): 747-756.
25. Lübke, H., Ihnát, V., Kuňa, V., Balberčák, J., 2020: A multi-stage cascade use of wood composite boards. Wood Research 65(5): 843-854.
26. Marková, I., Ladomerský, J., Hroncová, E., Mračková, E., 2018: Thermal parameters of beech wood dust. BioResources 13(2): 3098-3109.
27. Miklečić, J., Jirouš-Rajković, V., 2016: Influence of thermal modification on surface properties and chemical composition of beech wood (*Fagus sylvatica* L.). Drvna industrija: Znanstveni časopis za pitanja drvne tehnologije 67(1): 65-71.
28. Nagarajan, S., Skillen, N.C., Irvine, J.T.S., Lawton, L.A., Robertson, P.K.J., 2017: Cellulose II as bioethanol feedstock and its advantages over native cellulose. Renewable and Sustainable Energy Reviews 77: 182-192.
29. Okai, R., Boateng, O., 2007: Analysis of sawn lumber production from logging residues of branchwood of *Aningeria robusta* and *Terminalia ivorensis*. European Journal of Forest Research 126(3): 385-390.
30. Pajtík, J., Konôpka, B., Priwitzer, T., 2011: Dendromass allocation in the young stands of European beech and sessile oak. Report Forest Research 56(4): 291-300.
31. Pažitný, A., Russ, A., Boháček, S., Stankovská, M., Ihnát, V., Šutý, S., 2019a: Various lignocellulosic raw materials pretreatment processes utilizable for increasing holocellulose

accessibility for hydrolytic enzymes. Part I. Evaluation of wheat straw pretreatment process. Wood Research 64(1): 13-24.
32. Pažitný, A., Russ, A., Boháček, Š., Stankovská, M., Ihnát, V., Šutý, Š., 2019b: Various lignocellulosic raw materials pretreatment processes utilizable for increasing holocellulose accessibility for hydrolytic enzymes: Part II. Effect of steam explosion temperature on beech enzymatic hydrolysis. Wood Research 64(3): 437-447.
33. Pažitný, A., Russ, A., Boháček, Š., Šutý, Š., Ihnát, V., 2020: Perspective pretreatment method of beech and poplar wood and wheat straw in 2G biofuel production processing. Nova Biotechnologica et chimica 19(1): 80-97.
34. Prasad, A., Sotenko, M., Blenkinsopp, T., Coles, S.R., 2016: Life cycle assessment of lignocellulosic biomass pretreatment methods in biofuel production. The international journal of life cycle assessment 21(1): 44-50.
35. Rooni, V., Raud, M., Kikas, T., 2017: The freezing pretreatment of lignocellulosic material: a cheap alternative for Nordic countries. Energy 139: 1-7.
36. Samariha, A., Kiaei, M., 2011: Chemical composition properties of stem and branch in *Alianthus altissima* wood. Middle East Journal of Scientific Research 8(5): 967-970.
37. Sankaran, R., Cruz, R.A.P., Pakalapati, H., Show, P.L., Ling, T.C., Chen, W.H., Tao, Y., 2020: Recent advances in the pretreatment of microalgal and lignocellulosic biomass: A comprehensive review. Bioresource technology 298: 122476.
38. Sasaki, C., Sumitomo, Y., Odashima, K., Asada, C., Nakamura, Y., 2021: Microwave-assisted hydrolysis of cellulose in towel and wheat straw using freeze-thawing with NaOH. Waste and Biomass Valorization 12(25): 1-9.
39. Smichi, N., Messaoudi, Y., Moujahed, N., Gargouri, M., 2016: Ethanol production from halophyte *Juncus maritimus* using freezing and thawing biomass pretreatment. Renewable Energy 85: 1357-1361.
40. Stankovská, M., Fišerová, M., Gigac, J., Pažitný, A., 2018: Effect of alkaline extrusion pretreatment of wheat straw on filtrate composition and enzymatic hydrolysis. Cellulose Chemistry and Technology 52(9-10): 815-822.
41. Su, T.CH., Fang, Z., 2017: One-pot microwave-assisted hydrolysis of cellulose and hemicellulose in selected tropical plant wastes by NaOH-freeze pretreatment. ACS Sustainable Chemistry & Engineering 5,6: 5166-5174.
42. Wang, X.M., Wang, L.J., Yu, M., Chen, H., 2013: Freeze-thaw and sulfuric acid pretreatment of wheat straw for fermentable sugar release. Advanced Materials Research 724-725: 257-260.
43. Yang, Y., Sharma-Shivappa, R.R., Burns, J.C., Cheng, J., 2009: Saccharification and fermentation of dilute-acid-pretreated freeze-dried switchgrass. Energy Fuels 23(11): 5626-5635.
44. Yuan, H., Lan, Y., Zhu, J., Wachemo, A.Ch., Li, X., Yu, L., 2019: Effect on anaerobic digestion performance of corn stover by freezing-thawing with ammonia pretreatment. Chinese Journal of Chemical Engineering 27(1): 200-207.

45. Zhu, H., Ma, Q., Sheng, J., Yang, R., 2020: Freeze–thaw repetition as an auxiliary method to promote efficient separation of hemicellulose from poplar. Green Chemistry 22(3): 942-949.

MICHAL HALAJ*, ŠTEFAN BOHÁČEK, ANDREJ PAŽITNÝ, VLADIMÍR KUŇA,
JOZEF BALBERČÁK
PULP AND PAPER RESEARCH INSTITUTE
DÚBRAVSKÁ CESTA 14
081 04 BRATISLAVA
SLOVAK REPUBLIC
*Corresponding author: halaj@vupc.sk

WOOD RESEARCH doi.org/10.37763/wr.1336-4561/66.4.643656
e-ISSN 2729-8906
66(4): 2021 643-656 pp.

EFFECTS OF STAND DENSITY ON TURPENTINE TERPENE COMPONENTS AND RESIN DUCT MORPHOLOGICAL STRUCTURE OF *PINUS MASSONIANA*

JIANHUA LYU, CHENG GUAN, XIANWEI LI, MING CHEN
SICHUAN AGRICULTURAL UNIVERSITY
CHINA

(RECEIVED OCTOBER 2020)

ABSTRACT

The influence of stand density on the resin duct morphological structure and terpene components of *Pinus massoniana* were studied. The resin duct morphological characteristics and the relative content of the terpene components were investigated by microscopy and gas chromatography-mass spectroscopy, respectively. The experimental results revealed that there was a specific correlation between the stand density and resin duct area, resin duct diameter, and the relative contents of main terpene components in the turpentine extracts. Additionally, the relative contents of *β*-pinene and (+)-camphene were positively correlated with stand density, with correlation coefficients of 0.8208 and 0.5539, respectively. In contrast, the relative contents of (+)-longifolene and (+)-longicyclene were negatively correlated with stand density, with correlation coefficients of -0.5750 and -0.7726, respectively, and *α*-pinene, *β*-caryophyllene, and (+)-*α*-longipinene had no correlation with stand density. The relative content of (+)-*α*-pinene was negatively correlated with the relative contents of both (+)-longifolene and (+)-longicyclene, with correlation coefficients of -0.8770 and -0.8914, respectively. There were positive correlations between the relative contents of (+)-longifolene and (+)-longicyclene with correlation coefficient of 0.9718, (+)-longifolene and (+)-*α*-longipinene with correlation coefficient of 0.8399, *β*-caryophyllene and (+)-*α*-longipinene with correlation coefficient of 0.9360, and (+)-longicyclene and (+)-*α*-longipinene with correlation coefficient of 0.8626.

KEYWORDS: *Pinus massoniana*, stand density, terpene components, resin duct morphological structure.

INTRODUCTION

Pinus massoniana Lamb., also known as Masson pine, belongs to the family Pinaceae Lindl., Pinus Linn., and is widely available in Central and Southern China. *Pinus massoniana*

is an important resin-producing tree species in China; more than 90% of the pine resin in China is tapped from *P. massoniana* (Lai et al. 2020).

A resin duct is a typical self-protective structure of Pinaceae plants and is the first line of defense against insects and pathogens (Roberds et al. 2003, King et al. 2011). Pine oleoresin secreted by the resin duct is a mixture of terpenoids, and is a transparent and colorless mucus. Pine oleoresin is the leading secondary metabolite of pine, and it can be made into rosin, turpentine, and other valuable industrial raw materials using heat and distillation to remove any impurities (Rodrigues-Corrêa et al. 2012).

Most of the research literature focuses on forest resource management, genetic breeding, and pest control (Song et al. 2005, Zeng and Tang 2012, Ali et al. 2019, Ni et al. 2019). Additionally, few of the published research discusses the relationship between the stand density, the microstructure or macrostructure of wood, and the resin yield of trees (Giagli et al. 2019, Lyu et al. 2020).

Some studies show that the chemical components of resin, the resin flow rate, the number and density of resin ducts, and other defensive characteristics of many coniferous trees are controlled by their heredity, which are the stable genetic characteristics of the trees (Roberds et al. 2003, Franceschi et al. 2005, King et al. 2011, Moreira et al. 2012).

Resin ducts and resin cells are two characteristic structures commonly found in pine needles and trunks (Berryman 1972). Wu and Hu (1995) studied the relationship between the resin duct morphological structure, resin yield, and secretion of the tree *Pinus tabulaeformis*, then clarified the mechanism for resin synthesis and secretion. Zhu and Huang (2002) found a significant positive correlation between the number of resin ducts and the resin yield of *P. massoniana*. In addition, the resin yield capacity of pine is related to the resin duct diameter: a larger resin duct diameter results in a higher flow velocity and flow amount (Phillips and Croteau 1999). Mu et al. (2012) found that the number of resin ducts and resin cells in high resin-yield trees was higher than that in low resin-yield trees, which can be used as a noticeable and valuable index for early screenings of the high resin-yielding capacity of *Pinus kesiya* var. *langbianensis* trees. A similar conclusion was reached by Lombardero et al. (2000) in which the resin yield of *Pinus yunnanensis* is closely related to the number of resin ducts in the needles, the phloem and xylem, and the area of resin ducts in the phloem. However, analyzing the factors affecting the resin yield of 79 high-yielding *P. massoniana* trees from different regions shows that the resin yield of *P. massoniana* has little relationship with the diameter and number of sapwood resin ducts and instead shows that it is related to the area of the resin ducts (Moghaddama and Farhadib 2015). Other research focused on *P. massoniana* clones has similar conclusions (Liu et al. 2013). Others have found a remarkable difference in the resin yield of *P. massoniana* with different densities. Increasing the stand density results in an increase in the resin yield per unit area of *P. massoniana* but additionally results in a decrease in the average annual yield per plant. However, increasing the stand density to a certain extent results in a decrease in the resin yield per unit area (Rodríguez-García et al. 2014, Neis et al. 2018).

The aims of this paper are: *(a)* to investigate the relationship between the stand density and the resin duct morphological structure of *P. massoniana*; and *(b)* the relationship between the stand density and the terpene components in turpentine extracts of *P. massoniana*.

MATERIAL AND METHODS

Materials

The turpentine extracts were collected from the sample trees of *Pinus massoniana* plantation, located in Damaoping area of Pingchang County (Bazhong, China) at an altitude of approximately 740 m. Four plots with an area of approximately 600 m^2 were delineated using a round quadrat method. The stand density of each sample plot was 833 plants/hm^2, 1000 plants/hm^2, 1167 plants/hm^2, and 1333 plants/hm^2, and each plot was labeled Group A, B, C, and D, respectively. Five *P. massoniana* trees with diameter at breast height (DBH) of 20 to 35 cm were randomly selected from each group and were harvested for resin at 1.2 m above the ground surface. The resin from each group was collected separately, packed in vacuum bags, and stored with no access to light. After the completion of resin tapping, all the sample trees were cut down, and the discs of corresponding resin tapping areas were collected for wood anatomical experiments. Finally, the turpentine was extracted via a steam distillation method in the laboratory.

Methods

Resin duct morphological characteristics determination experiment

Each disc was cut into five samples (10 × 10 × 10 mm) with an electric jigsaw. Samples were softened in distilled water for 6 h and then sliced into 30-μm sections by a sliding microtome on the cross-section, radial section, and tangential section. The sections were stained with 0.1% safranine for 1 to 2 min, dehydrated in graded alcohols (30%, 50%, 75%, 95%, and 100%) 5 min each, and cleaned for 5 min in fresh xylene.

The wood anatomical characteristics were determined via image analysis on histological cuts using a microscope (Leica DM500; Leica Microsystems, Wetzlar, Germany) at a magnification of 40x to 400x and analyzed with Leica Application Suite (LAS) EZ software (Leica Microsystems, Version 4.2.0, Wetzlar, Germany) (Fig. 1).

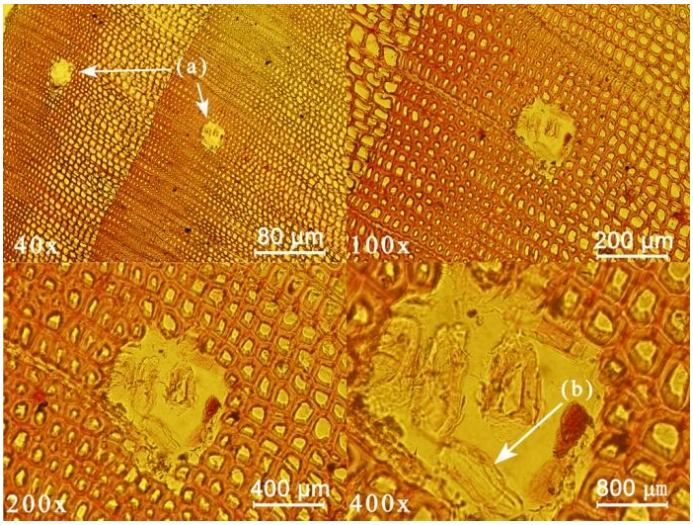

Fig. 1: Cross-section of a wood sample of P. massoniana: (a) resin ducts and (b) resin cells.

The following characteristics were measured: resin duct area (μm^2), resin duct density (cells/mm^2), the total area of resin duct per unit area ($\mu m^2/mm^2$), the length-width ratio of the resin cell, resin duct diameter (μm), and the ratio of wall-to-cavity of the resin cell.

Relative content of terpenes in turpentine extracts determination experiment

The terpenes components in the turpentine extracts were analyzed by a gas chromatograph-mass spectrometer (GCMS-QP2010 Plus; Shimadzu, Tokyo, Japan). Helium was used as the carrier gas with a flow rate of 1.2 $mL \cdot min^{-1}$. The gas chromatograph (GC) oven temperature was programmed at 50°C (held 2 min), raised to 120°C (held 2 min) at $10°C \cdot min^{-1}$, raised to 260°C at $5°C \cdot min^{-1}$, and subsequently to 290°C (held 15 min) at $10°C \cdot min^{-1}$. The injector temperature was set at 220°C, and the GC split ratio was adjusted to 10 : 1. A sample of 1.0 μL was injected using the splitless mode after being dissolved into n-hexane, and the mass conditions were as follows: electron impact ionization was employed with a collision energy of 70 eV, and the mass spectrometer ion source was maintained at 200°C, full scan mode in the m/z range 1250 with a 0.50 s/scan velocity. The relative concentration (%) was determined by integrating all peaks obtained in the total ion chromatogram (TIC) mode. The terpene components were identified via comparison of the mass spectra with the NIST08 library (NIST, Version 2.0, Gaithersburg, MD, USA).

RESULTS AND DISCUSSION

Relationship between stand density and resin duct morphological characteristics

The programming language R (R Foundation for Statistical Computing, Version 3.6.3, Vienna, Austria) was used to analyze the correlation coefficient and linear regression between the stand density and the resin duct morphological characteristics. The results from the analysis of stand density with each of the following are shown in Fig. 2, respectively: resin duct area, resin duct diameter, resin duct density, the total area of resin duct per unit area, the length-width ratio of the resin cell, and the ratio of wall-to-cavity of the resin cell.

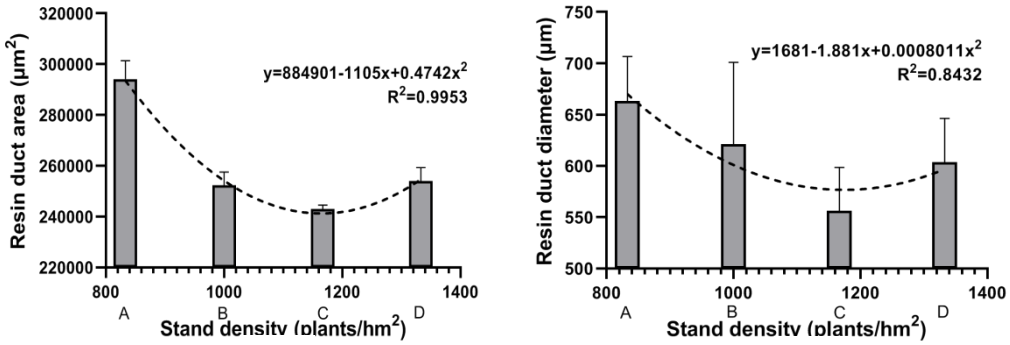

(a) **(b)**

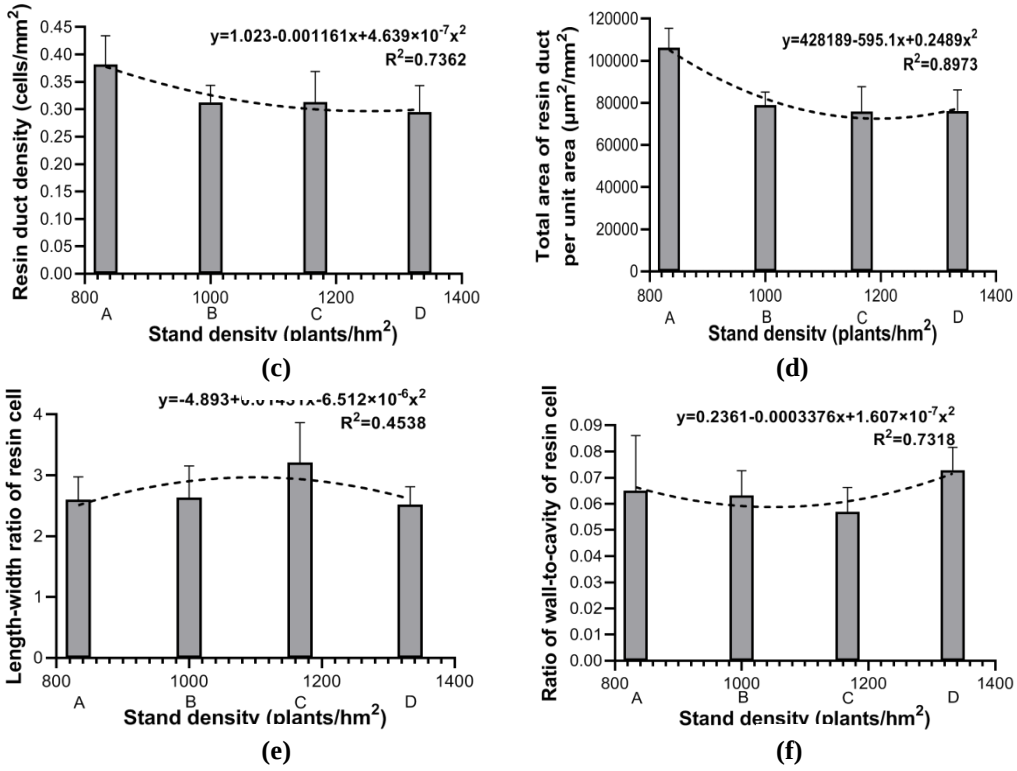

Fig. 2: Linear regression of stand density and resin ducts morphological characteristics: (a) stand density and resin duct area; (b) stand density and resin duct diameter; (c) stand density and resin duct density; (d) stand density and total area of resin duct per unit area; (e) stand density and length-width ratio of resin cell; (f) stand density and ratio of wall-to-cavity of resin cell.

Figs. 2a,b show that increasing the stand density resulted in a significant decrease in the resin duct area at a level of p = 0.05. This decrease in the resin duct area slowed after the stand density reached a level of 1167 plants/hm^2. The direct correlation between the resin duct area and the resin duct diameter showed that the changing trend of the resin duct diameter with the stand density was similar to that of the resin duct area; however, the standard deviation value for the latter was higher due to the noticeable difference within the group. When the stand density was 833 plants/hm^2, the resin duct area and resin duct diameter reached the maximum. Because of the limited environmental conditions of the sample plot, the sampling range of stand density could not be expanded, so it was impossible to determine whether the changing trend of resin duct area and resin duct diameter would rise or becomes slow. Based on relevant research reports by Lombardero et al. (2000) and Liu et al. (2013), it can be deduced that the maximum resin yield was in this study gradient at 833 plants/hm^2. Meanwhile, increasing stand density resulted in a decrease in the resin duct area and resin duct diameter, leading to the decline of resin yield per plant. This showed similar results to other studies (Rodríguez-García. 2014).

As shown in Fig. 2c,d the resin duct density and the total area of resin duct per unit area were negatively correlated with the stand density in the range of 833 to 1333 plants/hm^2 with small correlation coefficient R^2 value.

From Fig. 2e,f the standard deviation of the length-width ratio of the resin cell and the ratio of wall-to-cavity of the resin cell in the range of 833 to 1333 plants/hm^2 was too high. Additionally, the R^2 values obtained of the fitting curve was too low, so the fitting curves have no reference value. Therefore, the correlation between the stand density and the length-width ratio of the resin cell, and between stand density and ratio of wall-to-cavity of resin cell are not significant in the range of 833 to 1333 plants/hm^2.

Relationship between stand density and terpene components in turpentine extracts

Quantification was determined *via* percentage peak area calculations using gas chromatography-flame ionization detector (GC-FID). The chromatographic peaks were preliminarily identified using an automatic search of the National Institute of Standards and Technology (NIST) gas chromatograph-mass spectrometry (GC/MS) library. The obtained mass spectra were then compared with those reported in previous literature (Adams 2007, Ioannou et al. 2014, Lyu et al. 2018). The chemical compounds were analyzed qualitatively using the relative reservation index and *via* peak area normalization measurements. The total ion chromatograms (TIC) of the turpentine terpene components in stand density Groups A, B, C, and D are shown in Fig. 3.

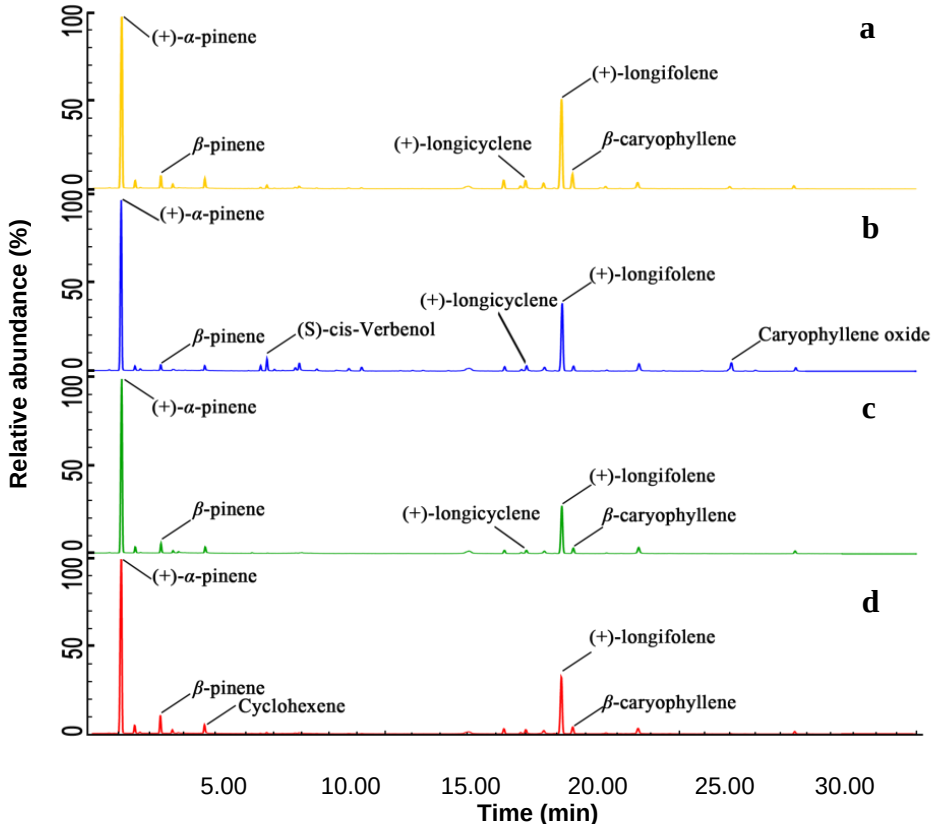

Fig. 3: Ion chromatogram of terpene components extracted from the turpentine extracts of Pinus massoniana plantations with different stand densities: (a) Group A with stand density 833 plants/hm^2; (b) Group B with stand density 1000 plants/hm^2; (c) Group C with stand density 1167 plants/hm^2; (d) Group D with stand density 1333 plants/hm^2.

The results of the relative content analysis showed that the content of (+)-*α*-pinene and (+)-longifolene were the first and second highest, which occupied 46.25% to 58.52% and 21.10% to 30.14% of total terpenes in turpentine extracts, respectively, and followed by *β*-caryophyllene in Groups A and C, in which its content was 4.12% and 3.55%, respectively. In group B, caryophyllen oxide ranked third in relative content with 3.56%, and in Group D, *β*-pinene ranked third in relative content with 4.42%. The top five relative contents of each group are marked on the graph; however, Group B shows six terpenes because the relative contents of *β*-pinene and (+)-longicyclene in Group B were both 1.86%. Other studies have shown partially similar results: (+)-*α*-pinene was also the dominant compound ranging from 34.99% to 43.60%, followed by *β*-pinene ranging from 15.29% to 29.40%, but (+)-longifolene only ranked fourth ranging from 4.39% to 6.78% (Tümen and Reunanen 2010).

Additionally, R was used to analyze the correlation coefficient and the linear regression between the stand density and relative content of the main terpene components in turpentine extracts. The results of stand density and (+)-*α*-pinene, (+)-longifolene, *β*-pinene, *β*-caryophyllene, cyclohexene, (+)-camphene, (+)-longicyclene, (+)-*α*-longipinene, and 7-methyl-3-methyleneocta-1,6-diene are shown in Fig. 4a through Fig. 4i.

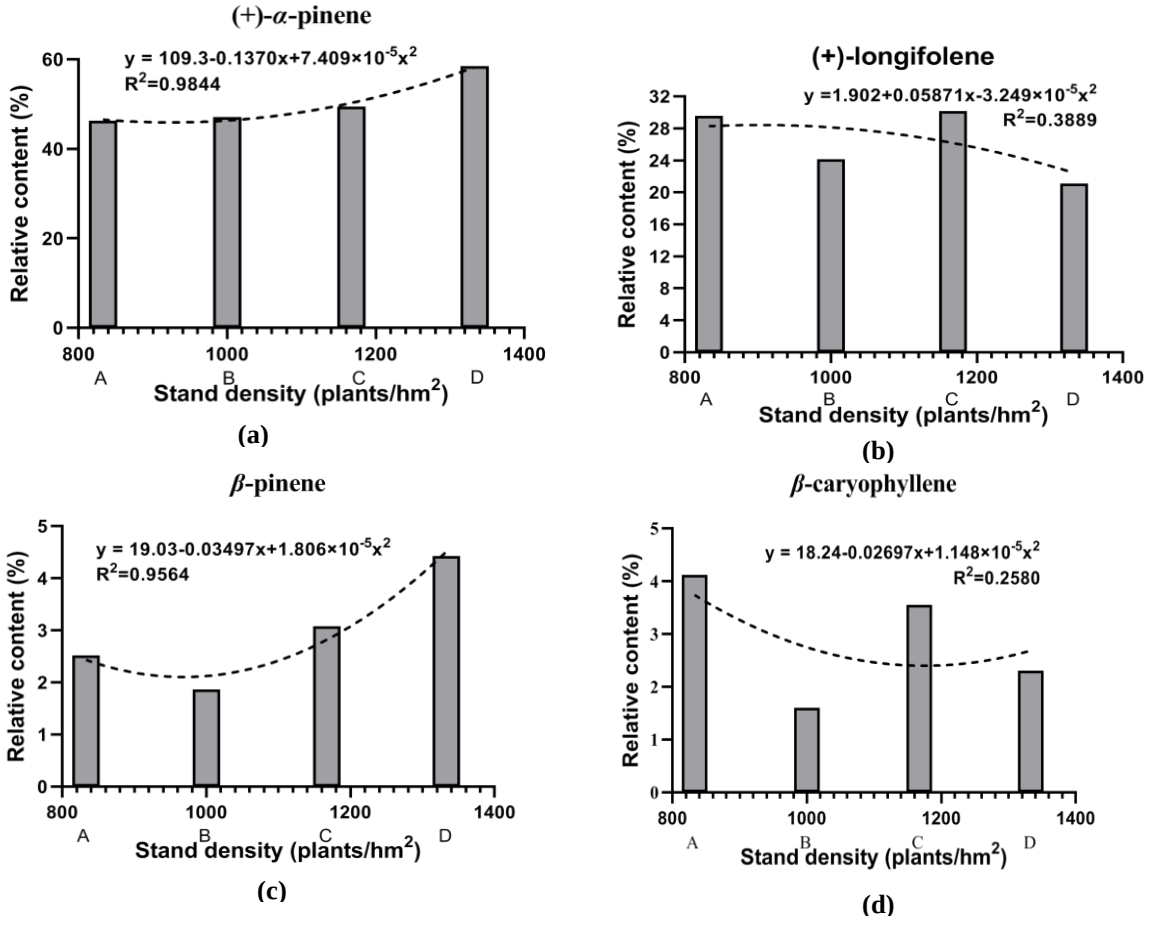

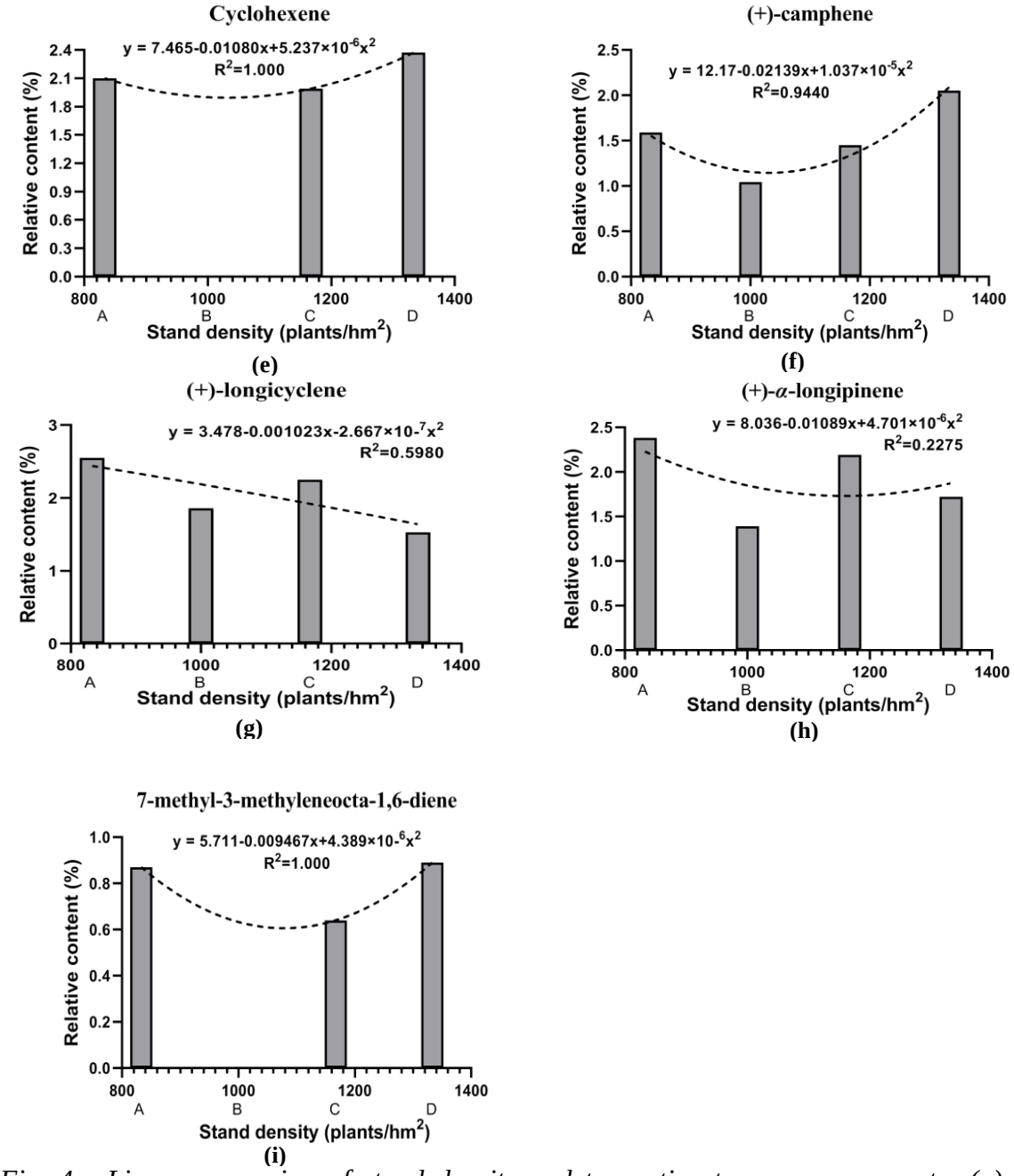

Fig. 4: Linear regression of stand density and turpentine terpene components: (a) stand density and (+)-α-pinene; (b) stand density and (+)-longifolene; (c) stand density and β-pinene; (d) stand density and β-caryophyllene; (e) stand density and cyclohexene; (f) stand density and (+)-camphene; (g) stand density and (+)-longicyclene; (h) stand density and (+)-α-longipinene; (i) stand density and 7-methyl-3-methyleneocta-1,6-diene.

According to Fig. 4a, there was a positive correlation between the relative content of *α*-pinene in the turpentine extracts with a stand density in the range of 833 to 1333 plants/hm^2. The relative content of *α*-pinene at the stand density of 1333 plants/hm^2 was positive at a p = 0.05 level when compared with the relative content at the stand density of 833 plants/hm^2. According to Fig. 4b, the relative content of (+)-longifolene at 1000 and 1333 plants/hm^2 showed significance at p = 0.05 and 0.01 level, respectively. According to

Fig. 4c, there was a positive correlation between the relative content of *β*-pinene in turpentine extracts and stand density in the range of 1000 to 1333 plants/hm^2 with R^2 = 0.9564. The *β*-pinene relative content at stand density of 1000 plants/hm^2 showed significance at p = 0.05 level, and at stand density of 1333 plants/hm^2 extremely significant at p = 0.01 level. According to Fig. 4d, the *β*-caryophyllene relative contents at stand densities of 1000 and 1333 plants/hm^2 both showed extreme significance at p = 0.01 level. According to Fig. 4e, the cyclohexene relative content in turpentine extracts at the stand density of 1333 plants/hm^2 showed significance at a p = 0.05 level. However, due to the absence of cyclohexene in Group B, although the R^2 value of the fitting curve generated by polynomial curve fitting was ideal, the positive correlation between cyclohexene and stand density in the range of 833 to 1333 plants/hm^2 could not be determined. According to Fig. 4f, there was a positive correlation between the (+)-camphene relative content and stand density in the range of 1000 to 1333 plants/hm^2. The relative content of (+)-camphene at a stand density of 1000 plants/hm^2 showed extreme significance at a p = 0.01 level, and the relative content at the stand density of 1333 plants/hm^2 showed significance at a p = 0.05 level. According to Fig. 4g, the relative contents of (+)-longicyclene at 1000 and 1333 plants/hm^2 showed extreme significance at a p = 0.01 level, but no correlation conclusion could be drawn between the relative content of (+)-longicyclene and stand density in the range of 833 to 1333 plants/hm^2, and the fitting curve here was approximate to a straight line. According to Fig. 4h, the relative content of (+)-*α*-longipinene at 1000 and 1333 plants/hm^2 showed significance at p = 0.01 and 0.05 level, respectively. According to Fig. 4(i), the relative content of 7-methyl-3-methyleneocta-1,6-diene in the turpentine extracts at a stand density of 1167 plants/hm^2 showed extreme significant correlation at a p = 0.01 level. However, it could not be determined that there was any correlation between 7-methyl-3-methyleneocta-1,6-diene and stand density in the range of 833 to 1333 plants/hm^2 because of the missing values in Group B. The reason may be due to the instability of many substances in turpentine extracts, some components in the turpentine extracts will change in the structure under conditions where there is light; additionally, as the isomer of α-pinene, β-pinene will change into D-α-pinene or L-α-pinene under the action of the external physical environment, to a certain extent. Some α-pinene will produce α-pinene oxide through an oxidation-reduction reaction in air, and (+)-longifolene will transform into (+)-longicyclene in the presence of oxidants (Wilbon et al. 2013).

Correlation analysis of terpene components in turpentine extracts

Due to the missing values of cyclohexene and 7-methyl-3-methyleneocta-1,6-diene in the turpentine extracts of Group B, the two sets of data cannot be used for multiple comparisons, which affects the results of the comparisons. Therefore, cyclohexene and 7-methyl-3-methyleneocta-1,6-diene were excluded from the terpene components of turpentine extracts in the multiple comparisons.

The Pearson multiple comparison method was used *via* the programming language R to compare the filtered data, and the scatter plot matrix method was used to establish the matrix. Based on the results of the two analyses, the correlation between the relative content of the primary terpene components in turpentine extracts were analyzed, and the correlation

analysis and curve fitting of the main selected terpene components were implemented.

The Pearson multiple comparison method was used to obtain the correlation matrix among the terpene components (Fig. 5). The results were as follows: for the relative contents of *α*-pinene and (+)-longifolene, *α*-pinene and (+)-longicyclene were significantly negatively correlated; for the relative contents of (+)-longifolene and (+)-longicyclene, (+)-longifolene and (+)-*α*-longipinene were significantly positively correlated; lastly, there was a significant positive correlation between *β*-caryophyllene and (+)-*α*-longipinene and between (+)-longicyclene and (+)-*α*-longipinene.

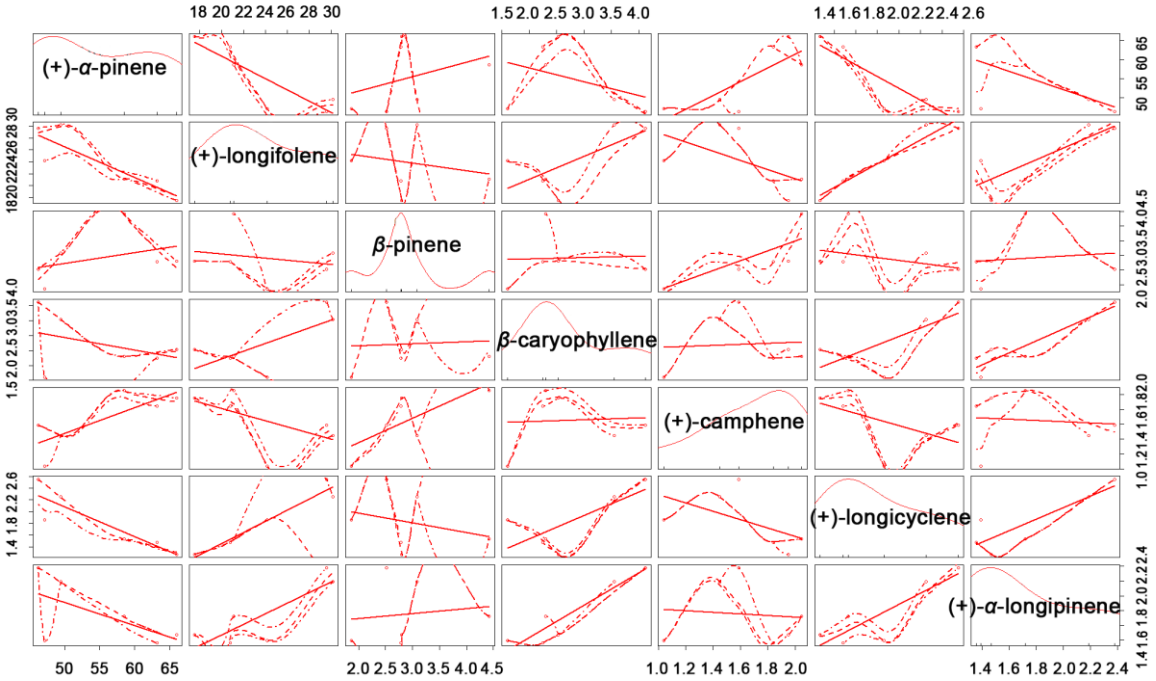

Fig. 5: Correlation matrix of the relative contents of main terpene components in turpentine extracts.

After summarizing and screening the results shown in Fig. 5, the possibly-related main terpene components were compared using analysis of variance method of the programming language R for a test on statistical significance. Then, the linear regression and binomial nonlinear regression were carried out by using the R software with function *lm()* which is used to fit linear models. Finally, the scatter diagram and regression model diagram were combined in Fig. 6.

As shown in Fig. 6, the correlation matrix and correlation analysis of six pairs of the main terpene components in the turpentine extracts have a good fitting effect, and all data showed that there was a significant correlation among them. There were linear correlations between *α*-pinene and (+)-longifolene, *α*-pinene and (+)-longicyclene, and (+)-longifolene and (+)-longicyclene, where the former two were the negative correlations and the latter was a positive correlation. In contrast, the curve correlation between (+)-longifolene and (+)-*α*-longipinene, *β*-caryophyllene and (+)-*α*-longipinene, and (+)-longicyclene and (+)-*α*-longipinene were more potent than the linear correlation. Additionally, all of them were positively correlated.

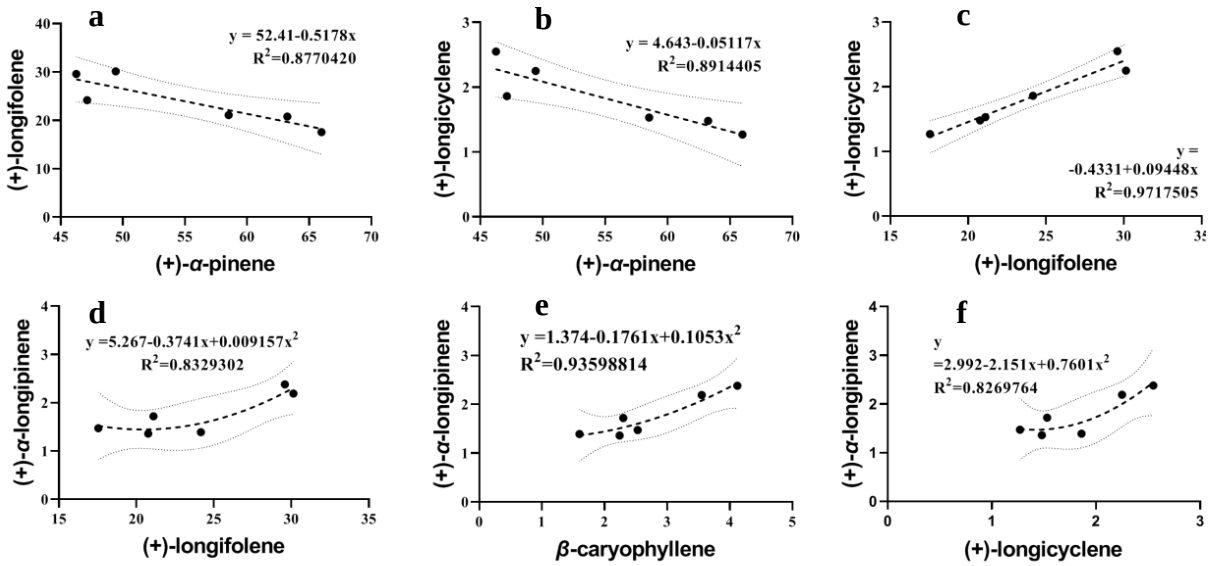

Fig. 6: Regression model between selected terpene components in turpentine extracts: (a) (+)-α-pinene and (+)-longifolene; (b) (+)-α-pinene and (+)-longicyclene; (c) (+)-longifolene and (+)-longicyclene; (d) (+)-longifolene and(+)-α-longipinene; (e) β-caryophyllene and (+)-α-longipinene; (f) (+)-longicyclene and (+)-α-longipinene.

Through the comparative analysis of the main terpene components in the turpentine extracts, it was found that some terpenes in the turpentine extracts showed a significant correlation. These correlations were a linear correlation or curvilinear correlation. The cause of the considerable relationship may be partly due to how some terpenes could be transformed into each other or were antagonistic to each other in chemical reactions. However, it may also be the stress of *P. massoniana* on the environment, which triggers gene regulation (Ren et al. 2008, Quan and Ding 2017).

CONCLUSIONS

(1) Under different stand densities, the resin duct morphological structure of *Pinus massoniana* followed a specific trend of change. The correlation factors of the resin duct morphological characteristics showed a similar trend of change. For example, the two elements with a higher correlation, i.e., the resin duct area and resin duct diameter, would be negatively correlated with the change of the stand density gradient in this study. When the stand density was 1167 plants/hm^2, the decrease in the resin duct area and resin duct diameter began to slow down. *(2)* The change of the stand density resulted in a change in the relative contents of the main terpene components in the *P. massoniana* turpentine. Some of the terpene components were positively correlated with the change of the stand density, such as *α*-pinene, *β*-pinene, and (+)-camphene, and some terpene components had no significant relationship with the evolution of the stand density, such as (+)-*α*-longipinene and *β*-caryophyllene. *(3)* Due to the absence of the two terpene components 7-methyl-3-methyleneocta-1,6-diene and cyclohexene, no relevant components were detected in Group B.

Therefore, it was impossible to determine the relationship between the changes of the two terpenes with the stand density. This may be due to the instability of many substances in the volatile oil of the turpentine extracts. A series of chemical reactions began when the resin flowed out of *P. massoniana* and was exposed to the air.

ACKNOWLEDGMENTS

The authors are grateful for the support of the Ministry of Education Humanities and Social Sciences Research Project of China (Grant No. 19YJC760009), the Key Research and Development Project of Sichuan Science and Technology Plan Projects (Grant No. 2020YFS0357), the Project of National Science & Technology Pillar Program during the 12th Five-year Plan Period (Grant No. 2011BAC09B05), German Government Loans for Sichuan Forestry Sustainable Management Project (Grant No. G1403083), the Project of Modern Design and Culture Research Center, Sichuan Key Research Base of Philosophy and Social Sciences (Grant No. MD18Z002), the Opening Foundation for Industrial Design Industry Research Center, Key Research Base of Humanities and Social Sciences, and the Sichuan Education Department (Grant No. GYSJ18-037).

REFERENCES

1. Adams, R.P., 2007: Identification of essential oils components by gas chromatography Quadrupole mass spectrometry. Allured Publishing Corporation, Carol Stream, IL, USA., 804 pp.
2. Ali, A., Dai, D., Akhtar, K., Teng, M., Yan, Z., Urbina-Cardona, N., Mullerova, J., Zhou, Z., 2019: Response of understory vegetation, tree regeneration, and soil quality to manipulated stand density in a *Pinus massoniana* plantation. Global Ecology and Conservation 20: e00775.
3. Berryman, A.A., 1972: Resistance of conifers to invasion by bark beetle-fungus associations. BioScience 22(10): 598-602.
4. Franceschi, V.R., Krokene, P., Christiansen, E., Krekling, T., 2005: Anatomical and chemical defenses of conifer bark against bark beetles and other pests. New Phytologist 167(2): 353-376.
5. Giagli, K., Vavrcik, H,. Fajstavr, M., Cerny, J., Novosadova, K., Martinik, A., 2019: Stand factors affecting the wood density of naturally regenerated young silver birch growing at the lower altitude of the Czech Republic region. Wood Research 64(6): 1011-1022.
6. Ioannou, E., Koutsaviti, A., Tzakou, O., Roussis, V., 2014: The genus *Pinus*: A comparative study on the needle essential oil composition of 46 pine species. Phytochemistry Reviews 13(4): 741-768.
7. King, J.N., Alfaro, R.I., Lopez, M.G., Van Akker, L., 2011: Resistance of Sitka spruce (*Picea sitchensis* (Bong.) Carr.) to white pine weevil (*Pissodes strobi* Peck): Characterizing the bark defense mechanisms of resistant populations. Forestry 84(1): 83-91.

8. Lai, M., Zhang, L., Lei, L., Liu, S., Jia, T., Yi, M., 2020: Inheritance of resin yield and main resin components in *Pinus elliottii* Engelm. at three locations in southern China. Industrial Crops and Products 144: 1-10.
9. Liu, Q., Zhou, Z., Fan, H., Liu, Y., 2013: Genetic variation and correlation among resin yield, growth, and morphologic traits of *Pinus massoniana*. Silvae Genetica 62(1-6): 38-43.
10. Lombardero, M.J., Ayres, M.P., Lorio Jr, P.L., Ruel, J.J., 2000: Environmental effects on constitutive and inducible resin defences of *Pinus taeda*. Ecology Letters 3(4): 329-339.
11. Lyu, J., Zhao, J., Xie, J., Li, X., Chen, M., 2018: Distribution and composition analysis of essential oils extracted from different parts of *Cupressus funebris* and *Juniperus chinensis*. BioResources 13(3): 5778-5792.
12. Lyu, J., Huang, W., Chen, M., Li, X., Zhong, S., Chen, S., Xie, J., 2020: Analysis of tracheid morphological characteristics, annual rings width and latewood rate of *Cupressus funebris* in relation to climate factors. Wood Research 65(4): 565-577.
13. Moghaddama, M., Farhadib, N., 2015: Influence of environmental and genetic factors on resin yield, essential oil content and chemical composition of *Ferula assa-foetida* L. populations. Journal of Applied Research on Medicinal and Aromatic Plants 2(3): 39-76.
14. Moreira, X., Alfaro, R.I., King, J.N., 2012: Constitutive defenses and damage in Sitka spruce progeny obtained from crosses between white pine weevil resistant and susceptible parents. Forestry 85(1): 87-97.
15. Mu, R., Wang, S., Pu, X., 2012: Anatomical comparison of the resin duct structure between the high and low resin yield trees of *Pinus kesiya* var. *langbianensis*. Journal of Forestry Engineering 26(2): 49-53.
16. Neis, F.A., de Costa, F., Füller, T.N., de Lima, J.C., da Silva Rodrigues-Corrêa, K.C., Fett, J.P., Fett-Neto, A.G., 2018: Biomass yield of resin in adult *Pinus elliottii* Engelm. trees is differentially regulated by environmental factors and biochemical effectors. Industrial Crops and Products 118(8): 20-25.
17. Ni, Z., Bai, T., Chen, Y., Huang, Y., Xu, L., 2019: Effects of parental genetic distance on offspring growth performance in *Pinus massoniana*: significance of parental-selection in a clonal seed orchard. Euphytica 215(12): 195.
18. Phillips, M.A., Croteau, R.B., 1999: Resin-based defenses in conifers. Trends in Plant Science 4(5): 184-190.
19. Quan, W., Ding, G., 2017: Dynamic of volatiles and endogenous hormones in *Pinus massoniana* needles under drought stress. Scientia Silvae Sinicae 53(4): 49-55.
20. Ren, Q., Hu, Y., Jin, Y., Deng, W., Li, Z., Yang, L., Nkoma, M.K., 2008: Rapid changes in induced non-volatile secondary metabolites in damaged *Pinus massoniana* Lamb. Frontiers of Forestry in China 3(3): 249–253.
21. Roberds, J.H., Strom, B.L., Hain, F.P., Gwaze, D.P., McKeand, S.E., Lott, L.H., 2003: Estimates of genetic parameters for oleoresin and growth traits in juvenile loblolly pine. Canadian Journal of Forest Research 33(12): 2469-2476.
22. Rodrigues-Corrêa, K.C.S., Lima, J.C., Fett-Neto, A.G., 2012: Pine oleoresin: tapping green chemicals, biofuels, food protection, and carbon sequestration from multipurpose trees. Food and Energy Security 1(2): 81-93.

23. Rodríguez-García, A., López, R., Martín, J.A., Pinillos, F., Gil, L., 2014: Resin yield in *Pinus pinaster* is related to tree dendrometry, stand density and tapping-induced systemic changes in xylem anatomy. Forest Ecology and Management 313(1): 47-54.
24. Song, J., Luo, Y., Shi, J., Yan, X., Chen, W., Jiang, A., 2005: Niche characteristics of boring insects within *Pinus massoniana* infected by *Bursaphelenchus xylophilus*. Journal of Beijing Forestry University 27(6): 108-111.
25. Tümen, İ., Reunanen, M., 2010: A comparative study on turpentine oils of oleoresins of *Pinus sylvestris* L. from three districts of Denizli. Records of Natural Products 4(4): 224-229.
26. Wilbon, P.A., Chu, F., Tang, C., 2013: Progress in renewable polymers from natural terpenes, terpenoids, and rosin. Macromolecular rapid communications 34(1): 8-37.
27. Wu, H., Hu, Z.H., 1995: The relation between the structure of resin ducts and the resin synthesis and mode of its elimination in *Pinus tabulaeformis*. Journal of Northwest University (Natural Science Edition) 25(5): 529-532.
28. Zeng, W, Tang, S., 2012: Modeling compatible single-tree aboveground biomass equations for masson pine (*Pinus massoniana*) in southern China. Journal of Forestry Research 23(4): 593-598.
29. Zhu, Q., Huang, Y., 2002: Regression analytical studies on the resin canal and resin-producing capacity of *Pinus massoniana*. Journal of Fujian Forestry Science and Technology 29(4): 15-16.

JIANHUA LYU, CHENG GUAN, XIANWEI LI, MING CHEN*
SICHUAN AGRICULTURAL UNIVERSITY
[1]COLLEGE OF FORESTRY
[2]WOOD INDUSTRY AND FURNITURE ENGINEERING KEY LABORATORY OF SICHUAN PROVINCIAL DEPARTMENT OF EDUCATION
CHENGDU, SICHUAN
CHINA
*Corresponding author: chenming@sicau.edu.cn

WOOD RESEARCH doi.org/10.37763/wr.1336-4561/66.4.657665
e-ISSN 2729-8906
66(4): 2021 657-665 pp.

AGRO-FORESTRY RESIDUES VALORIZATION BY LIGNINOSOME OF *GRIFOLA FRONDOSA*

MILICA GALIĆ, JASMINA ĆILERDŽIĆ, JELENA VUKOJEVIĆ, MIRJANA STAJIĆ
UNIVERSITY OF BELGRADE
SERBIA

(RECEIVED SEPTEMBER 2020)

ABSTRACT

Grifola frondosa HAI 1232 was tested for ligninolytic enzyme activities and for lignin, cellulose and hemicellulose degradation during cultivation on eight common agro-forestry residues in Serbia. Wheat straw was favorable lignocellulosic for the production of Mn-dependent and Mn-independent peroxidases (2513.89 and 354.17 U L^{-1}, respectively), while selected residues inhibited the synthesis of laccases. The highest lignin removal was observed during fermentation of blackberry sawdust (36.75%), while the highest selectivity index was recorded on oak sawdust (4.34). The dry matter loss varied between 8.17% in corn stalks and 14.16% in apple sawdust. According to the presented results, it can be concluded that *G. frondosa* HAI 1232 could be an important participant in various biotechnological processes due to its high capacity to selectively degrade different agro-forestry residues.

KEYWORDS: Agro-forestry residues, delignification, *Grifola frondosa*, ligninolytic enzymes.

INTRODUCTION

In the future bio-based society, global challenges such as climate changes, ecosystem degradation, associated with industrialization and growing global population, force us to find effective biological solutions. Fungi are relatively understudied, but according to Hyde et al. (2019) they are an essential and biotechnologically useful group of organisms with a remarkable potential for industrial exploitation. It is known that many modern industries are based on fungi and their metabolites and it is believed that these organisms are the future cell factories for the production of food, pharmaceuticals, enzymes and bio-control agents (Goyal et al. 2016, Lange et al. 2020, Meyer et al. 2020).

Reducing dependence on non-renewable, unsustainable resources is one of the keys for stable economic growth and sustained environmental quality (Antov et al. 2020). Industrial and

agricultural wastes, rich in lignocellulose, are produced in large tonnages and have special importance because of their renewable nature (Asgher et al. 2013). However, majority of these residues are either improperly deposited or disposed of by burning, which is not restricted to developing countries alone. Ghaffar et al. (2015) also pointed out that enormous amounts of cuttings from fruits remain unexploited and present serious ballast of the environment. Thus, based on the data from Food and Agriculture Organization, reported by Krausmann et al. (2008), 6.6 G ton of dry biomass is unused per year of which a 2.5 G ton are burned residues. Although collecting of that biomass and its conversion to valuable products will require much efforts and energy, Bos and Broeze (2020) indicate that these biotransformations may significantly contribute to sustainability goals. A good example of such a contribution is the development of the new biorefinery which was started with the conversion of highly abundant wheat straw and corn stover to biofuel, as one of the most widely used alternative energy sources (Ghaffar et al. 2015, Lange et al. 2020).

Over the last 5-10 years, fungi have taken the center role in the conversion of lignocellulosic residues into different high-value products. Physical, chemical and physico-chemical pretreatments of the residues employ methods which are cost/energy intensive, while biological one including the white-rot fungi, is mild and environment friendly. It is well known that fungal enzymes are always preferred over plant and animal ones due to wide isoforms diversity and extraordinary catalytic properties. Furthermore, their low cost, faster production and higher yield are some more of the advantages (Goyal et al. 2016). Through the action of a strong ligninolytic enzyme system, containing lignin and Mn-oxidizing peroxidases, laccases and some auxiliary enzymes, white-rot fungi can degrade lignin, the most recalcitrant polymer in biomass (Saritha and Arora 2012, Ćilerdžić et al. 2017). Because of strong bond to hollocellulose and role of protective barrier, lignin increases resistance of cell wall and complicates the accessibility of cellulolytic enzymes to cellulose which requires decomposition of the lignin network prior hydrolysis (Esteghlalian et al. 2001, Hideno et al. 2007, Dashtban et al. 2009, Saritha and Arora 2012). Controlling the number factors which affect the activities of the enzymes and lignin degradation extent, such as fungal species/strain, lignocellulose type and cultivation conditions leads to the most effective pretreatment process (Isroi et al. 2011, Ćilerdžić et al. 2017). Fungal delignification integrated with solid-state production of low-cost cellulase would result in a cost-efficient conversion of lignocellulose materials (Saritha and Arora 2012). Fungal role in biomass conversion is of great significance because they can “unlock” the full potential of the lignocellulosic biomass which expands the range of the fungal applications (Hyde et al. 2019).

Due to the unique nutritional and medicinal properties of *G. frondosa*, which have been a topic of numerous researches, this white-rot mushroom has gained popularity as a healthy food. However, not much data is available on its ligninolytic enzymes potential. Considering its availability and cultivation on a commercial scale, further research is needed to broaden the knowledge of this significant species. Therefore, the present study aimed to determine Mn-oxidizing peroxidases and laccase activity profiles in *G. frondosa* cultivated on common agro-forestry residues and its potential for delignification.

MATERIALS AND METHODS

Organism and cultivation conditions

The culture of *Grifola frondosa* HAI 1232, obtained from the Institute of Evolution, University of Haifa, Israel (HAI) and deposited in the collection of the Faculty of Biology, University of Belgrade was used in this study. The inoculum was prepared in 250 mL flasks containing 100.0 mL of synthetic glucose/ammonium nitrate/yeast extract medium inoculated with 7-days old "mother" culture. The incubation was conducted at room temperature on a rotary shaker for 7 days. Sterile distilled water (dH_2O) was used to wash the obtained biomass and its homogenization was performed in a laboratory blender (Waring, USA). Solid-state fermentation of 8 agro-forestry residues (apple-, blackberry-, grapevine-, oak-, plum-, and raspberry sawdust, corn stalks and wheat straw) was carried out in 250 mL Erlenmeyer flasks, containing 6.0 g of the residue soaked with 30.0 mL of the modified synthetic medium (without glucose) and inoculated with 9.0 mL of the homogenate. The cultivation was conducted at 25°C in the dark for 21 days. All the experiments were done in triplicates and results were expressed as mean ± standard error.

Assays of enzyme activity and total protein production

According to the method of Stajić et al. (2017), the produced ligninolytic enzymes were extracted by sample stirring with 50.0 mL of dH_2O at 4°C for 10 min. The obtained extracts were centrifugated (4°C, 3000 rpm, 15 min) and resulting supernatants were used for measurement of MnP-oxidizing peroxidases [Mn-dependent peroxidase (MnP, EC 1.11.1.13) and Mn-independent peroxidase (MnIP, EC 1.11.1.16)] and laccase (EC 1.10.3.2)], as well as total protein content by a spectrophotometer [CECIL CE2501 (BioQuest), UK]. Mn-oxidizing peroxidases activities were determined by the rate of oxidation of Phenol Red at 610 nm. The reaction mixture (V_{tot} = 1.0 mL) contained succinate buffer, sample, 2mM H_2O_2, and phenol red, with or without addition of $MnSO_4$ (for MnP and MnIP, respectively). Laccase activity was assayed in the mixture composed of phosphate buffer, ABTS (2,2'–azinobis (3–ethylbenzothiazoline–6–sulfonicacid), and sample, at 436 nm. Enzymatic activity was expressed in U L^{-1}, and the activity of 1U presents the amount of enzyme that transforms 1.0 μmol of substrate per min.

The total protein content (mg mL^{-1}) was determined by the method of Silva et al. (2005), i.e. by measurement of Bradford's reagent color change at λ = 595 nm induced by sample. The bovine serum albumin was used as the standard and further for calculation of the specific enzyme activity (U mg^{-1}).

Determination of lignin, cellulose and hemicellulose contents

The loss of substrate dry matter (%) was determined by Eq. 1:

$$(Mi - Mf)/Mi \times 100 \quad (1)$$

where: M*i* - the initial lignocellulosic mass, M*f* - the mass after fermentation.

The determination of hemicellulose, cellulose and lignin contents was carried out using the modified methods of Kirk and Obst (1988) and Van Soest et al. (1991). Dried ground sample (1.0 g) was treated with neutral detergent/Na_2SO_3 mixture aiming to remove soluble sugars, proteins, lipids, and vitamins and the obtained biomass presented neutral detergent fibers (NDF). Hemicellulose was removed with a solution of acidic detergent and the obtained mass was defined as acidic fibers (ADF). The hemicellulose amount was determined as difference between NDF and ADF. Lignin content (LC) expressed as the percentage of quantity presented in the initial sample was defined after ADF incubation with 72% H_2SO_4 at 30°C and hydrolysis at 120°C. Cellulose content represented the difference between ADF and LC. Selectivity index, *i.e*. lignin/cellulose removal ratio was used as an indicator of lignin degradation selectivity.

Statistical analyses

All the experiments were done in three replicates and the results were expressed as mean ± standard error. Assaying of any significant differences among means was performed by One-way analysis of variance (ANOVA) and Tukey`s test, using STATISTICA, version 6.0 (StatSoft, Inc., Tulsa, USA). Statistical significance was declared at $p < 0.05$.

RESULTS AND DISCUSSION

During 21 days of solid-state cultivation, *G. frondosa* HAI 1232 synthesized assayed enzymes which activity depended on the carbon source i.e., agro-forestry residues (Fig. 1). Thus, wheat straw was favorable lignocellulosic for the production of MnP by studied species as a very high activity was detected (2513.89 U L^{-1}). The moderate levels of the enzyme activity were obtained after oak sawdust and corn stalks fermentation (87.12 U L^{-1} and 60.61 U L^{-1}, respectively), while it was remarkable lower after fermentation of plum, raspberry and grapevine sawdust, ranging from 29.04 U L^{-1} to 47.98 U L^{-1} and even absent on apple- and blackberry sawdust (Fig. 1).

Regarding MnIP activity, it showed greater variation in dependence on tested residues than MnP. Although the maximum activity was also detected on wheat straw, its peak was many-fold lower (354.17 U L^{-1}) than in the case of MnP (Fig.1). Blackberry sawdust also induced MnIP (142.05 U L^{-1}), while two-fold and lower values of enzyme activity were observed on other substrates. The minimal MnIP activity was noted on apple sawdust (9.47 U L^{-1}), while grapevine sawdust inhibited the synthesis of this enzyme (Fig. 1).

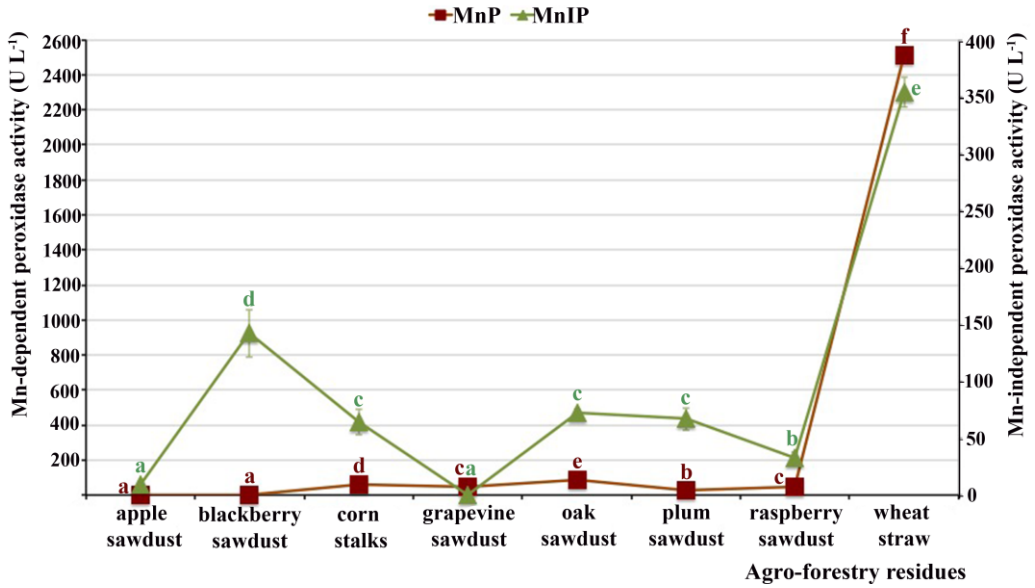

Fig. 1: Mn-dependent and Mn-independent peroxidase activity of Grifola frondosa HAI 1232 during agro-forestry residues fermentation. Values superscripted with the same letter in each values group (for each enzyme) are not significantly different ($p < 0.05$).

Contrary to Mn-oxidizing peroxidase activities, selected residues completely inhibited the laccase activity, which could be explained by strong influence of fermentation period on the activity. Total protein concentration was ranged from 0.63 mg mL^{-1} after raspberry fermentation to 2.99 mg mL^{-1} noted on corn stalks, which consequently reflected on specific enzyme activities. Thus, the maximal MnP specific activity was detected after wheat straw fermentation (2.07 U mg^{-1}), while the activities for other tested enzymes were less than 1.0 U mg^{-1}.

The lignocellulose degradation ability of *G. frondosa* HAI 1232 was also evaluated (Tab. 1). The results clearly showed that this species was good and selective degrader of most tested agro-forestry residues. Thus, the highest total dry matter loss was recorded in raspberry sawdust, even 14.16%. The reduction of dry matter was also significant in apple- and blackberry sawdust (13.83% and 13.17%, respectively), while the lowest values were obtained for corn stalks (8.17%) and oak sawdust (8.30%). Considering the laccase absence during wheat straw fermentation, Mn-oxidizing peroxidases could be responsible for lignin removal (30.82%), which degradation rate was in accordance with the activity level (Fig. 1, Tab. 1). However, this correlation was not observed for other substrates. A slightly higher delignification extent was noted during blackberry sawdust and corn stalks fermentation (36.75% and 32.26%, respectively). *G. frondosa* weakly depolymerized cellulose in these three residues which reflected on high selectivity indices descending from 3.39 in corn stalks, through 2.15 in blackberry sawdust to 1.97 in wheat straw. However, the highest selectivity index (4.34) was obtained after oak sawdust fermentation, but lignin depolymerization was not highly effective (23.85%). The lowest selectivity indices were noted during cultivation of grapevine- and plum sawdust (1.02 and 1.16, respectively) where the capacities of lignin and cellulose degradation were similar, while hemicellulose mineralization was remarkable, 46.29% in plum sawdust and 35.83% in grapevine sawdust (Tab. 1).

Tab. 1: The level of agro-forestry residues depolymerization (%) by Grifola frondosa (values superscripted with different letters in the same column are significantly different (p < 0.05).

Agro-forestry residues	Samples	Sample weight (g)	Polymers composition of samples (mg)			Dry matter loss (%)	Extent of polymers degradation (%)			Sel. index
			Lignin	Cellulose	Hemicel.		Lignin	Cellulose	Hemicel.	
Apple sawdust	Control*	6.00	1158.00	2808.00	1176.00	/	/	/	/	/
	HAI 1232	5.17	852.72	2253.25	821.71	13.83^{c}	26.36^{c}	19.76^{e}	30.13^{d}	1.33^{a}
Blackberry sawdust	Control*	6.00	1218.00	2712.00	1038.00	/	/	/	/	/
	HAI 1232	5.21	770.40	2248.56	811.98	13.17^{c}	36.75^{e}	17.09^{d}	21.77^{b}	2.15^{b}
Corn stalks	Control*	6.00	594.00	2796.00	1860.00	/	/	/	/	/
	HAI 1232	5.51	402.38	2530.11	1504.78	8.17^{a}	32.26^{d}	9.51^{b}	19.12^{b}	3.39^{c}
Grapevine sawdust	Control*	6.00	1421.41	2652.00	887.08	/	/	/	/	/
	HAI 1232	5.27	1201.79	2250.72	569.27	12.16^{b}	15.45^{a}	15.13^{c}	35.83^{e}	1.02^{a}
Oak sawdust	Control*	6.00	1530.00	2808.00	1159.00	/	/	/	/	/
	HAI 1232	5.50	1165.15	2654.57	802.42	8.30^{a}	23.85^{b}	5.49^{a}	30.82^{d}	4.34^{d}
Plum sawdust	Control*	6.00	1837.49	2544.00	1368.00	/	/	/	/	/
	HAI 1232	5.29	1464.22	2098.54	734.45	11.83^{b}	20.31^{b}	17.51^{d}	46.29^{f}	1.16^{a}
Raspberry sawdust	Control*	6.00	1200.00	2160.00	1308.00	/	/	/	/	/
	HAI 1232	5.15	875.16	1930.50	988.42	14.16^{c}	27.07^{c}	10.63^{b}	24.43^{c}	2.54^{b}
Wheat straw	Control*	6.00	666.00	2418.00	1692.00	/	/	/	/	/
	HAI 1232	5.30	460.75	2038.96	1488.18	11.66^{b}	30.82^{d}	15.68^{c}	12.05^{a}	1.97^{b}

Comparing to some previous reports, *G. frondosa* strain profiled in this study has shown a better ability to produce highly active Mn-oxidizing peroxidases. Thus, Montoya et al. (2012) reported very low MnP activity (4 U g^{-1}) after 23 days of solid-state fermentation of oak sawdust/corn bran medium by *G. frondosa* PSUMCC 922, while slightly higher activity (22.6 U L^{-1}) was observed by Mikiashvili et al. (2011) after 35 days of oak sawdust solid-state fermentation by strain MBFBL 684. However, contrary to our strain that did not produce laccases, the strains studied by other authors secreted laccase during fermentation of various lignocellulosics. Thus, strain studied by Montoya et al. (2012) produced low active laccase (12 U g^{-1}) after 23 days of oak sawdust/corn bran medium fermentation. Contrary to Xing et al. (2006) who reported activity of only 70 U L^{-1} after even 52 days of submerged cultivation in glucose/ammonium nitrate/yeast extract/asparagine monohydrate medium, strain MBFBL 596 studied by Mikiashvili et al. (2011) secreted laccase of even 703.3 U L^{-1} after only 15 days of oak sawdust solid-state fermentation. This could be explained either by the fact that laccase activity decreases with cultivation period which was already shown in previous reports (Ćilerdžić et al. 2014, Stajić et al. 2017) or by the influence of medium composition.

Despite the lack of laccase activity, *G. frondosa* HAI 1232 was more effective delignifier than other previously tested species/strains of this genus as well as other white-rot fungi. Thus, Mikiashvili et al. (2011) reported much lower lignin mineralization (< 10%) during oak sawdust

fermentation by studied *G. frondosa* strains. Although our strain was less effective in lignin removal from oak sawdust than strain tested by Montoya et al. (2012), which degraded 67% of lignin, our strain showed higher selectivity. In comparison with white rot species studied by Zhao et al. (2020), strain HAI 1232 showed higher delignification capacity and selectivity during corn stalks depolymerization. However, *Pleurotus* species studied by Ćilerdžić et al. (2017) were much better and more selective delignifiers of wheat straw than *G. frondosa* HAI 1232.

CONCLUSIONS

Although fungi are essential for matter cycling due to their degradative abilities and have so many proven uses in different biotechnological areas, their great potential needs further exploration. Screening fungi for the production of ligninolytic enzymes and consequently delignification of various agro-industrial residues has often been reported, but to date, the ligninolytic potential of *G. frondosa* has only scarcely been researched. Therefore, the presented results have clearly shown that *G. frondosa* HAI 1232 is a potent degrader of frequent agro-forestry residues. Demonstrated high capacity of studied species to selectively degrade lignocellulose also indicated its ability to potentially participate in various biotechnological processes. Since the use of fungi and fungal products is considered very important for a more sustainable future, these promising results present one more contribution to the reaching of this goal.

ACKNOWLEDGEMENTS

This study was carried out under project No. 173032, financially supported by the Ministry of Education, Science and Technological Development of the Republic of Serbia.

REFERENCES

1. Antov, P., Savov, V., Neykov, N., 2020: Sustainable bio-based adhesives for eco-friendly wood composites. A review. Wood Research 65(1): 51-62.
2. Asgher, M., Ahmad, Z., Iqbal, H.M.N., 2013: Alkali and enzymatic delignification of sugarcane bagasse to expose cellulose polymers for saccharification and bio-ethanol production. Industrial Crops and Products 44: 488-495.
3. Bos, H.L., Broeze, J., 2020: Circular bio-based production systems in the context of current biomass and fossil demand. Biofuels, Bioproducts and Biorefining 14(2): 187-197.
4. Dashtban, M., Schraft, H., Qin, W., 2009: Fungal bioconversion of lignocellulosic residues; opportunities and perspectives. International Journal of Biological Sciences 5(6): 578.
5. Esteghlalian, A.R., Srivastava, V., Gilkes, N., Gregg, D.J., Saddler, J.N., 2001: An overview of factors influencing the enzymatic hydrolysis of lignocellulosic feedstocks. In: Glycosyl hydrolases for biomass conversion (eds. Himmel, ME, Baker, W, Saddler, JN). Pp 100–111, ACS. Washington.

6. Ghaffar, S.H., Fan, M., McVicar, B., 2015: Bioengineering for utilization and bioconversion of straw biomass into bio-products. Industrial Crops and Products 77: 262-274.
7. Goyal, S., Ramawat, K.G., Mérillon, J.M., 2016: Different shades of fungal metabolites: an overview. In: Fungal metabolites (eds. Mérillon, JM, Ramawat, KG). Pp 1-29, Springer International Publishing, Cham, Switzerland.
8. Hideno, A., Aoyagi, H., Isobe, S., Tanaka, H., 2007: Utilization of spent sawdust matrix after cultivation of *Grifola frondosa* as substrate for ethanol production by simultaneous saccharification and fermentation. Food science and technology research 13(2): 111-117.
9. Hyde, K.D., Xu, J., Rapior, S., Jeewon, R., Lumyong, S., Niego, A.G.T., Chaiyasen, A., 2019: The amazing potential of fungi: 50 ways we can exploit fungi industrially. Fungal Diversity 97: 1-136.
10. Isroi, I., Millati, R., Niklasson, C., Cayanto, C., Taherzadeh, M.J., Lundquist, K., 2011: Biological treatment of Lignocelluloses with white-rot fungi and its applications. BioResources 6(4): 5224-5259.
11. Kirk, T.K., Obst, J.R., 1988: Lignin determination. In: Methods in Enzymology (eds. Colowick, SP, Kaplan, NO). Pp 87-101, Academic Press Inc. San Diego.
12. Krausmann, F., Erb, K.H., Gingrich, S., Lauk, C., Haberl, H., 2008: Global patterns of socioeconomic biomass flows in the year 2000: A comprehensive assessment of supply, consumption and constraints. Ecological Economics 65(3): 471–487.
13. Lange, L., Agger, J.W., Meyer, A.S., 2020: Fungal Biotechnology: Unlocking the full potential of fungi for a more sustainable world. In: Grand Challenges in Fungal Biotechnology (ed. Nevalainen, H). Pp 3-32, Springer Nature. Cham, Switzerland.
14. Meyer, V., Basenko, E.Y., Benz, J.P., Braus, G.H., Caddick, M.X., Wösten, H.A.B., 2020: Growing a circular economy with fungal biotechnology: a white paper. Fungal biology and biotechnology 7(5): 1-23.
15. Mikiashvili, N.A., Isikhuemhen, O.S., Ohimain, E.I., 2011: Lignin degradation, ligninolytic enzymes activities and exopolysaccharide production by *Grifola frondosa* strains cultivated on oak sawdust. Brazilian Journal of Microbiology 42(3): 1101-1108.
16. Montoya, S., Orrego, C.E., Levin, L., 2012: Growth, fruiting and lignocellulolytic enzyme production by the edible mushroom *Grifola frondosa* (maitake). World Journal of Microbiology and Biotechnology 28(4): 1533-1541.
17. Saritha, M., Arora, A., 2012: Biological pretreatment of lignocellulosic substrates for enhanced delignification and enzymatic digestibility. Indian journal of microbiology 52(2): 122-130.
18. Shimoda, T., Shirouchi, T., Suzuki, A., Morikawa, Y., Nishibori, K., 2012: Storage of maitake mushroom (*Grifola frondosa*) culture medium after harvesting fruit bodies is an effective pretreatment for ethanol conversion. Journal of wood science 58(4): 342-351.
19. Silva, C.M.M.S., Melo, S.I., Oliveira, R.P., 2005: Ligninolytic enzyme production by *Ganoderma* spp. Enzyme and Microbial Technology 37(3): 324-329.
20. Stajić, M., Ćilerdžić, J., Galić, M., Ivanović, Ž., Vukojević, J., 2017: Lignocellulose degradation by *Daedaleopsis confragosa* and *D. tricolor*. Bioresources 12(4): 7195-7204.

21. Van Soest, P.V., Robertson, J.B., Lewis, B.A., 1991: Methods for dietary fiber, neutral detergent fiber, and nonstarch polysaccharides in relation to animal nutrition. Journal of Dairy Science 74(10): 3583-3597.
22. Zhao, X., Wang, F., Fang, Y., Zhou, D., Wang, S., Wu, D., Zhong, R., 2020: High-potency white-rot fungal strains and duration of fermentation to optimize corn straw as ruminant feed. Bioresource Technology 123512.
23. Ćilerdžić, J., Vukojević, J., Stajić, M., Lončar, N., 2014: Intraspecific diversity in the production and characterization of laccase within *Ganoderma lucidum*. BioResources 9(3): 5577-5587.
24. Ćilerdžić, J., Galić, M., Vukojević, J., Brčeski, I., Stajić, M., 2017: Potential of selected fungal species to degrade wheat straw, the most abundant plant raw material in Europe. BMC plant biology 17(2): 249.
25. Xing, Z.T., Cheng, J.H., Tan, Q., Pan, Y.J., 2006: Effect of nutritional parameters on laccase production by the culinary and medicinal mushroom, *Grifola frondosa*. World Journal of Microbiology and Biotechnology 22(8): 799-806.

MILICA GALIĆ*, JASMINA ĆILERDŽIĆ, JELENA VUKOJEVIĆ, MIRJANA STAJIĆ
UNIVERSITY OF BELGRADE
FACULTY OF BIOLOGY
11000 BELGRADE
SERBIA
*Corresponding author: galic.m@bio.bg.ac.rs

WOOD RESEARCH doi.org/10.37763/wr.1336-4561/66.4.666677
e-ISSN 2729-8906
66(4): 2021 666-677 pp.

FOUR SOLVENT EXTRACTION OF *CINNAMOMUM CAMPHORA* XYLEM AND ANALYSIS OF THE ANTI-FUNGAL ACTIVITY OF THE EXTRACTIVES

QUAN LI[1,2]
[1]KAILI UNIVERSITY
CHINA
[2]FUJIAN PROVINCIAL KEY LABORATORY OF FEATURED MATERIALS IN BIOCHEMICAL INDUSTRY
CHINA

NING JI
GUIZHOU ACADEMY OF FORESTRY
CHINA

ZHANGUANG WANG
KAILI UNIVERSITY
CHINA

CUIXIANG LU
GUANGXI ZHUANG AUTONOMOUS REGION FORESTRY RESEARCH INSTITUTE
CHINA

HUI LIN
NINGDE NORMAL UNIVERSITY
CHINA

(RECEIVED SEPTEMBER 2020)

ABSTRACT

Four solvents including distilled water, acetone, ethyl acetate and petroleum ether were used to extract xylem of *C. camphora*. The differences in chemical compounds of xylem of *C. camphora* were analyzed by gas chromatography/mass spectrometry (GC/MS) and the anti-fungal activity of *C. camphora* extractives on *Coriolus versicolor* (CV), *Trametes versicolor* (TV), *Poria vaporari*a (PP) and *Gloeophyllum trabeum* (GT) were tested. The result showed that the chemical composition and relative content of the four different solvent extracts

were different. A large number of chemical compounds in the *C. camphora* extractives had a variety of biological activity and certain application value. The growth inhibitory rates of ethyl acetate extracts of *C. camphora* on PP, CV, TV and GT were 52.24%, 52.51%, 43.26%, and 54.63%, respectively. According to the concentration for 50% of maximal effect, the inhibitory order on test fungus were GT > PP > CV > TV.

KEYWORDS: *Cinnamomum camphora* extracts, Chemical compound, Soxhlet extraction, Growth inhibitory rates.

INTRODUCTION

It is generally believed that the chemical composition of the decay resistance wood determines the degree of toxicity to wood rot fungi. Extracting anti-fungi compounds with low toxicity to humans, high anti-fungal efficiency and good environmental compatibility from plant as preservative is a new approach to the research and development in the field of wood preservation. *Cinnamomum camphora* (L.) Presl is a highly decay resistance tree species, so the research and development of extracts from *C. camphora* xylem is of a great significance to wood protection. The bioactivity compounds such as camphor oil, which can be extracted from the bark, xylem, root and leaves of *C. camphora*, have the function of resisting to fungus, bacteria and insects (Chen et al. 2018). Current research showed that all kinds of wood species have nature stress response to outside stimulus in long term natural evolution process, which is due to the difference in biological organization, structure, chemical compounds and content caused by the long-term accumulation, hence the grade of natural decay resistance is different. Frizzo et al. (2000) reviewed the resource distribution, chemical compounds of leaves, bark and stem of camphor tree, but did not mention the extraction difference of different solvents from *C. camphora*. The research and application of plant extracts mainly focus on the filed of food preservation (Hao et al. 1998, Ahmadi et al. 2010, El-Nagerabi et al. 2012, Prakash et al. 2012) and antibacterial agents (Lima et al. 1993, Jamalian et al. 2012, Mishra et al. 2012). Ghaedi et al. (2015) also extend the research about natural plant-derived extracts to interdisciplinary (Scalbert et al. 1998), including life sciences, biology and chemistry (Sansone et al. 2014). With the popularity of the environmental concept, more and more scholars began to pay attention to the use of plant extracts on wood preservatives. At present, plant-derived preservatives have an obstacles to large-scale promotion and application due to the complex of separating and extracting from wood. Therefore, it is necessary to deeply analyze the effective anti-fungal compounds and anti-fungal mechanism of wood decay (Chen et al. 2013, Kumari et al. 2015), to lay the foundation for further industrial production and application of *C. camphora* extract as wood preservative. Furthermore, it is equally important to study on extracts from the xylem of *C. camphora*, which will help to get a comprehensive and in-depth understanding of the content of the chemical compositions and discussing its utilization value. This research is of great significance for the research, development, application and promotion of *C. camphora* extractives as a preservative and similar plant-derived extracts as raw material products.

MATERIAL AND METHODS

Material, reagent and equipment

C. camphora wood was 40-50 years old and was collected from the streets of Fuzhou, China. It was crushed with a grinder and filtered through a 40-mesh sieve to obtain test materials. Brown rot fungi (*Poria vaporari*a, *Gloeophyllum trabeum*) and white rot fungi (*Coriolus versicolor*, *Trametes versicolor*) were obtained from Fujian agriculture and forest university (Fuzhou, China) and were used for the anti-fungal test. Acetone, ethyl acetate and petroleum ether were analytically pure purchased from Shanghai pilot chemical corporation. Agilent 5975C/7890N gas chromatography mass spectrometer was manufactured by American Agilent company.

Extraction of *C. camphora*

The xylem of *C. camphora* was pulverized (40-60 mesh) after air drying. 50 g of *C.camphora* powder was placed in a heat reflux extraction. Distilled water, acetone, ethyl acetate and petroleum ether were used as solvents, respectively. The solvents were heated to their respective boiling point temperature and heated for 2 h with a ratio of solid/solvent ratio of 1:10 ($g \cdot mL^{-1}$), then the extractives filtered to obtain the extracted liquid. The solvent was recovered by distillation under reduced pressure, and the *C. camphora* extracts were obtained at the same time. The extracts were collected and stored in labeled brown sample bottles. The extracts obtained were analyzed by gas chromatography/mass spectrometry (GC/MS) and used for anti-fungal test.

GC/MS conditions

Chromatographic conditions: DB-17MS (30 m × 0.25 mm × 0.25 μm) column, 99.999% high purity helium carrier gas, flow rate 1.0 $mL \cdot min^{-1}$, injection volume 0.8 μL, split ratio 10:1, the inlet temperature was 280°C. Program temperature rise: 50°C (maintain 3 min), 20°C·min^{-1} rise to 80°C (maintain 3 min); 2°C·min^{-1} rise to 120°C (maintain 5 min); 1.5°C·min^{-1} rise to 130°C (maintain 5 min); 2°C·min^{-1} rose to 180°C (hold for 5 min); 5°C·min^{-1} rose to 250°C (hold for 5 min).

Mass spectrometry conditions: EI ionization source, electron energy 70 eV; ion source temperature 230°C; scan mass range: 30-600 amu; solvent delay 3 min. The mass spectra were searched using the NIST library, and compared with the manual spectrum analysis and the related literature.

Anti-fungal test

Coriolus versicolor (CV), *Trametes versicolor* (TV), *Poria vaporari*a (PP) and *Gloeophyllum trabeum* (GT) were tested by growth rate of poison medium culture method. The medium containing molten maltose in a 9 cm petri dish were added with a certain amount of extracts and mixed to obtain the final concentration of 0.5 $g \cdot L^{-1}$, 1.0 $g \cdot L^{-1}$, 1.5 $g \cdot L^{-1}$, 2 $g \cdot L^{-1}$, 2.5 $g \cdot L^{-1}$. All kinds of fungal were incubated medium at 28 ± 2°C, 75-85% relative humidity for

several days to mycelia get to petri dishes edge. All tests were performed in triplicate. The effective dose for 50% inhibition (EC_{50}) was calculated by profit analysis. The growth inhibition rates was calculated as follows:

$$\text{Growth inhibition rates (\%)} = \frac{D_0 - Dt}{D_0} \times 100\% \quad (1)$$

where: D_0 was blank control colony growth diameter with an average of three replications (mm), and D_t was preservative treatment colony growth diameter with an average of three replications (mm).

RESULTS AND DISCUSSION

The compound identification and analysis of extracts from *C. camphora* xylem

Total ion chromatogram of the water and acetone extracts of *C. camphora* xylem separated and analyzed by GC/MS was shown in Fig. 1. 41 compounds were separated from the water extracts, and 6 compounds were identified, which accounted for 11.65% of the total peak area. Among these compounds, three of them had mass fraction than 1%, and included 2-pinen-4-one (2.26%), 2,6-dimethoxyphenol (2.07%), di-2-ethylhexyl phthalate (5.34%). 208 compounds were separated from the xylem acetone extracts, and 23 compounds were identified, which accounted for 30.56% of the total peak area (Tab. 1). The compounds with a mass fraction than 1% included camphor (5.18%), tetradecanal (4.16%), myristic acid (1.48%), pentadecanoic acid (1.25%), di-2-ethylhexyl phthalate (3.55%), γ-sitosterol (3.88%), and cyclotetracosane (1.47%) (Silan et al. 2018).

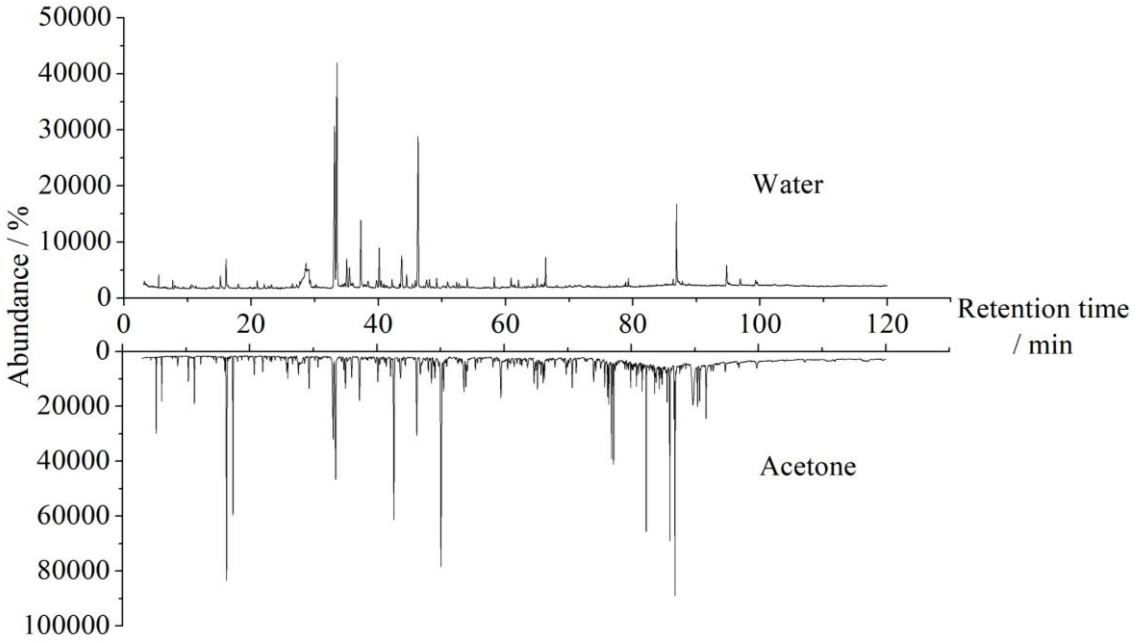

Fig. 1: Total ion chromatogram of the water and acetone extracts of C. camphora xylem.

Tab. 1: Volatile compounds and their relative area of peak extracted by water and acetone solvent extraction.

No.	Compounds	Water			Acetone		
		Retention time (min)	Relative content (%)	Matching rate (%)	Retention time (min)	Relative content (%)	Matching rate (%)
1	(1-Methylethyl)benzene	-	-	-	6.173	0.55	94
2	Linalool	-	-	-	11.315	0.91	92
3	Guaiacol	15.17	0.85	94	-	-	-
4	2-Pinen-4-one	16.076	2.26	78	-	-	-
5	Terpinen-4-ol	-	-	-	16.089	0.27	96
6	(1r,4r)-(+)-Camphor	-	-	-	16.374	5.18	98
7	1,8-Epoxy-p-menthan-2-ol	-	-	-	20.733	0.49	95
8	1,7-Dimethyl-7-(4-methyl-3-pentenyl)-tricyclo[2.2.1.0(2,6)]heptane	-	-	-	25.831	0.36	98
9	Safrole	-	-	-	25.979	0.41	98
10	L-Threitol	28.515	0.33	93	-	-	-
11	Heptadecanal	-	-	-	34.816	0.39	94
12	2,6-Dimethoxyphenol	35.475	2.07	94	-	-	-
13	d-Cadinene	-	-	-	36.045	0.61	95
14	Tetradecanal	-	-	-	42.688	4.16	99
15	2-Isopropyl-5-methyl-9-methylene–bicyclo[4.4.0]dec-1-ene	-	-	-	48.594	0.72	95
16	2-Pentadecanone	-	-	-	49.137	0.61	94
17	Myristic acid	-	-	-	53.704	1.48	99
18	4-Allyl-2,6-dimethoxyphenol	-	-	-	54.021	0.78	83
19	3,4,5-Trimethoxyphenol	58.238	0.8	86	-	-	-
20	Pentadecanoic acid	-	-	-	59.513	1.25	99
21	Palmitic acid	-	-	-	64.727	0.82	96
22	Palmitic Acid Vinyl Ester	-	-	-	65.257	0.7	87
23	1-Heptadecene	-	-	-	70.717	0.87	93
24	1-Pentadecanol	-	-	-	71.344	0.39	95
25	Linoleic acid	-	-	-	75.827	0.71	99
26	Di-2-ethylhexyl phthalate	86.882	5.34	98	86.882	3.55	98
27	γ-Sitosterol	-	-	-	89.708	3.88	95
28	Cyclotetracosane	-	-	-	91.766	1.47	96

Note: Identification was achieved using computer to match the mass spectra with the NIST library.

Total ion chromatogram of the ethyl acetate and petroleum ether extracts of *C. camphora* xylem separated and analyzed by GC/M was shown in Fig. 2. 46 compounds were separated from the ethyl acetate extracts, and 20 compounds were identified, which accounted for 48.72% of the total peak area (Tab. 2). Compounds with high content included di-2-ethylhexyl phthalate (6.04%), tetradecanal (5.32%), eucalyptol (1.18%), linalool (3.45%), terpinen-4-ol (1.02%), camphor (13.85%), safrole (1.48%), (-)-b-santalene (1.41), d-cadinene (1.03%), myristic acid (1.53%), pentadecanoic acid (1.49%), cyclopentadecane (1.19%), γ-sitosterol (3.18%), 1-triacontanol,and 1-acetate (1.82%), etc. 30 compounds were separated from the ethyl acetate extracts, and 14 compounds were identified, which accounted for 49.29% of the total peak area

(Tab. 2). Compounds with high content included linalool (2.8%), camphor (6.60%), 1,7-dimethyl-7-(4-methy-3-pentenyl) tricyclo (1.69%), safrole (1.8%), (-)-b-santalene (1.64%), d-cadinene (1.88%), myristic acid (1.49%), 2-isopropyl-5-methyl-9-methylene-bicyclo[4.4.0] dec-1-ene (1.36%), pentadecanoic acid (1.82%), cyclopentadecane (1.58%), γ-sitosterol (6.25%), α-terpineol (6.97%), cyclotetracosane (1.24%), and cyclooctacosane (2.17%), etc.

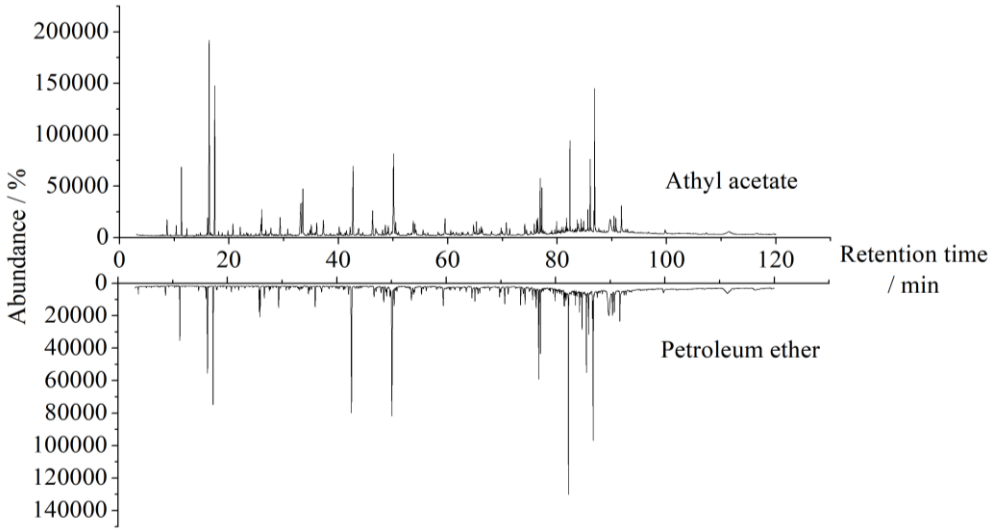

Fig. 2: Total ion chromatogram of the xylem ethyl acetate and petroleum ether extracts of C. camphora.

Tab. 2: Volatile components and their relative area of peak extracted by ethyl acetate and petroleum solvent extraction.

No.	Compounds	Ethyl acetate			Petroleum ether		
		Retention time (min)	Relative content (%)	Matching rate (%)	Retention time (min)	Relative content (%)	Matching rate (%)
1	Eucalyptol	8.682	1.18	99	-	-	-
2	Linalool	11.321	3.45	96	11.309	2.8	97
3	Terpinen-4-ol	16.108	1.02	97	-	-	-
4	(1r,4r)-(+)-Camphor	16.393	13.85	98	16.367	6.6	98
5	1,3,3-Trimethyl-2-oxabicyclo[2.2.2]octan-6-ol	20.74	0.9	97	-	-	-
6	1,7-Dimethyl-7-(4-methyl-3-pentenyl)-tricyclo[2.2.1.0(2,6)]heptane	25.843	0.77	99	25.831	1.69	99
7	Safrole	25.992	1.48	98	25.986	1.8	98
8	(-)-b-Santalene	29.362	1.41	94	29.375	1.64	96
9	d-Cadinene	36.057	1.03	96	36.051	1.88	96
10	Tetradecanal	42.701	5.32	99	42.701	10.49	99
11	2-Isopropyl-5-methyl-9-methylene-bicyclo[4.4.0]dec-1-ene	48.607	0.82	93	48.594	1.36	94
12	Myristic acid	53.717	1.53	99	-	-	-
13	Pentadecanoic acid	59.526	1.49	99	59.493	1.82	99
14	Palmitic acid	64.733	0.83	99	-	-	-
15	Palmitic acid vinyl ester	65.263	0.73	91	-	-	-
16	Cyclopentadecane	70.729	1.19	94	70.73	1.58	91
17	Linoleic acid	75.833	0.68	99	-	-	-

18	Di-2-ethylhexyl phthalate	86.888	6.04	98	-	-	-
19	γ-Sitosterol	89.715	3.18	99	89.76	6.25	97
20	α-Terpineol	-	-	-	17.389	6.97	87
21	Cyclotetracosane	-	-	-	86.746	1.24	96
22	1-Triacontanol,1-acetate	91.772	1.82	95	-	-	-
23	Cyclooctacosane	-	-	-	91.766	2.17	94

*Identification was achieved using computer matching of the mass spectra with the NIST library.

The results of GC/MS identification and analysis of *C. camphora* xylem extracts extracted by four solvents showed that the main compounds of the extracts extracted by water and acetone were similar to those of essential oil extracted from *C. camphora* leaves extracts in Australia by Stubbs et al. (2004), which were made up of camphor and various phenols. The main compounds of the extracts extracted by ethyl acetate and petroleum ether were similar to compounds of essential oil extracted from *C. camphora* leaves extracts by Guo et al. (2016), but the content was different. Pragadheesh et al. (2013) identified and classified the chemical components of essential oil obtained from *C. camphora* by steam distillation, and identified the components with certain biological activities, including linalool, safrole, camphor, α-pinene, β-phellandrene, 1,8-cineole, eugenol, etc., and concluded that *C. camphora* essential oil had strong fumigation and contact toxicity. The compounds were similar to the compounds of extracts in this experiment, which could indicate that *C. camphora* essential oil and active ingredients had the potential as nature fumigants and insecticide.

Classification analysis of extracts

It could be seen from Fig. 3 that the four extraction solvents had different effects on the extraction of various compounds in the *C. camphora* xylem (Chen et al. 2020).

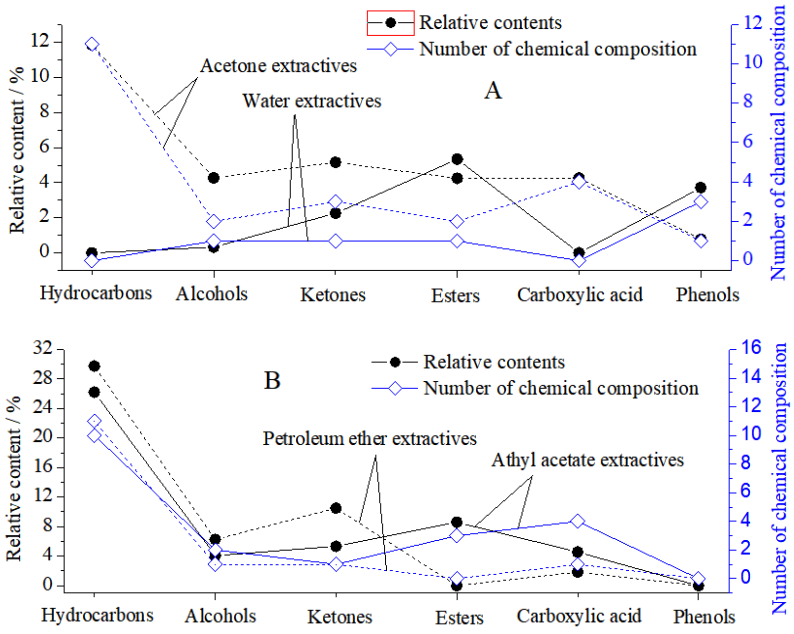

Fig. 3: Relative contents and number of chemical composition of extracts from the of C. camphora xylem by different solvent: a) water and acetone, b) ethyl acetate and petroleum ether.

The relative contents of category was shown in Fig. 3a. Water had a good effect on the extraction of esters and phenols, but it had a poor effect on hydrocarbons and carboxylic acids. The extracts mainly included alcohol (0.33%), aldehyde and ketones (2.26%), esters (5.34%), and phenols (3.72%). Using acetone as solvent to extract camphor xylem could obtain hydrocarbons (11.84%), alcohols (4.27%), ketones (5.16%), esters (4.25%), carboxylic acids (4.26%) and phenols (0.78%). The relative content could be seen from Fig. 3b. Ethyl acetate had the best effect on the extraction of hydrocarbons, while had the worst effect on ketones and phenols. Petroleum ether had a good effect on the extraction hydrocarbons and ketones, but had a poor effect on extraction of esters and phenols.

A comprehensive comparison of Fig. 3, Tab. 1 and Tab. 2 on the classification of *C. camphora* xylem extract can be found. Although water as a solvent was less effective than ethyl acetate and petroleum ether in extracting camphor, its extract had a relatively high phenolic content. Phenolic compounds are easily combined with wood rot fungal proteins at low concentrations to denature them, and can cause protein precipitation at high concentrations (Maciejewicz et al. 1999). Therefore, it can achieve a good pharmacologic effects of anti-fungi. Acetone had a good effect on the extraction of hydrocarbons and ketones, but it had a poor effect on phenols. The main hydrocarbons were terpenes, accounting for 7.46%, including camphor (5.18%), linalool (0.91%), terpinen-4-ol (0.27%), and d-cadinene (0.61%), 1,8-epoxy-p-menthan-2-ol (0.49%), and other terpenoids. Part of the chemical compounds have insecticidal, antipruritic, antibacterial and antiseptic effects (Lee et al. 2006). Ethyl acetate and petroleum ether both can be used as solvent to extract linalool, camphor, safrole, (-)-b-santalene, d-cadinene, myristic acid, pentadecanoic acid, cyclopentadecane, γ-sitosterol and other substances from *C. camphora* xylem. The most abundant component was camphor which has antibacterial and anti-inflammatory effects (Li et al. 2013). Myristic acid is used to prepare food flavors such as fat and milk, and γ-sitosterol can be used to treat diabetes (Balamurugan et al. 2011).

The inhibitory effect of the extracts against wood rot fungi

It could be seen from Fig. 4 of the growth inhibition ration results that the ethyl acetate extracts of *C. camphora* showed different degrees of inhibitory effects on the four wood rot fungi. At a concentration of 2.5 $g \cdot L^{-1}$, the growth inhibition rates of *C. camphora* extractives on PP, CV, TV and GT were 52.24%, 52.51%, 43.26%, and 54.63%, respectively. From the overall trend, the inhibitory effect of ethyl acetate extracts of *C. camphora* against wood rot fungi was positively correlated with the concentration, and the growth inhibition ration became larger as the concentration increases (Breda et al. 2016).

The toxic regression equation of ethyl acetate extracts of *C. camphora* on the growth of wood rot fungal mycelium was shown in Tab. 3. The concentration for 50% of maximal effect (EC_{50} value) of ethyl acetate extracts of *C. camphora* to wood rot fungus were 2.07-4.72 $g \cdot L^{-1}$. According to the EC_{50} value, the inhibitory order were GT > PP > CV > TV. It could be seen that the inhibitory effect of ethyl acetate extracts of *C. camphora* against brown rot fungi was better than that of on white rot fungi (Li et al. 2014, Zhang et al. 2020).

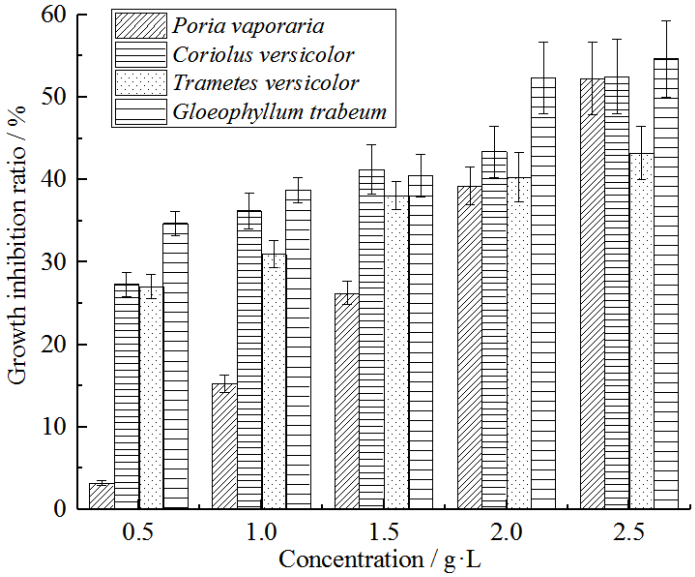

Fig. 4: Inhibitory activity of C. camphora extractives against wood rot fungi.

Tab. 3: Toxicity of C. camphora extracts against wood rot fungi.

Fungi	[a]Toxic regression equation	R^2	[a]EC_{50} /g·L^{-1}
Poria vaporaria	y = 2.6697x + 3.9474	0.9971	2.48
Coriolus versicolor	y = 0.8693x + 4.644	0.9544	2.57
Trametes versicolor	y = 0.6534x + 4.5598	0.9674	4.72
Gloeophyllum trabeum	y = 0.7414x + 4.7657	0.8331	2.07

Note: [a] Average of three replications.

CONCLUSIONS

There were some differences in the total number of compounds and relative contents of each solvent extract from *C. camphora* xylem. Compared with the *C. camphora* extracts all over the world, it was found that the origin of the *C. camphora* had little effect on its main compounds, but had a large effect on the proportion of its compounds. GC/MS analysis of the four solvent extracts of *C. camphora* xylem identified terpenoids and phenols with strong insect repellent, bacteriostatic and antiseptic effects. There were higher effect for the brow-rot fungi (GT and PP) as for the white-rot fungi (CV and TV). The research provides guidance for further development of biotic wood preservatives.

ACKNOWLEDGMENTS

The authors are grateful to the Natural Science Foundation of China (No. 31760191) for their support of this research, The Special Project of Ningde Normal University for Serving the Local Economic and Social Development (2018ZX406), Fujian Provincial Key Laboratory of Featured Materials in Biochemical Industry (FJKL_FBCM202005) and Major Research Project of Innovative Group of Guizhou Provincial Department of Education (KY [2017]048).

REFERENCES

1. Ahmadi, F., Sadeghi, S., Modarresi, M., Abiri, R., Mikaeli, A., 2010: Chemical composition, in vitro anti-microbial, antifungal and antioxidant activities of the essential oil and methanolic extract of *Hymenocrater longiflorus* Benth. of Iran. Food and Chemical Toxicology 48(5): 1137-1144.
2. Balamurugan, R., Duraipandiyan, V., Ignacimuthu, S., 2011: Antidiabetic activity of γ-sitosterol isolated from *Lippia nodiflora* L. in streptozotocin induced diabetic rats. European Journal of Pharmacology 667(1-3): 410-418.
3. Breda, C.A., Gasperini, A.M., Garcia, V.L., Monteiro, K.M., Bataglion, G.A., Eberlin, M.N., Duarte, M.C., 2016: Phytochemical analysis and antifungal activity of extracts from leaves and fruit residues of Brazilian savanna plants aiming its use as safe fungicides. Natural Products and Bioprospecting 6(4): 195-204.
4. Chen, J., Tang, C., Zhang, R., Ye, S., Zhao, Z., Huang, Y., Yang, D., 2020: Metabolomics analysis to evaluate the antibacterial activity of the essential oil from the leaves of *Cinnamomum camphora* (Linn.) Presl. Journal of Ethnopharmacology 253: 112652.
5. Chen, S., Zheng, T., Ye, C., Huannixi, W., Yakefu, Z., Meng, Y., Yang, Y., 2018: Algicidal properties of extracts from *Cinnamomum camphora* fresh leaves and their main compounds. Ecotoxicology and Environmental Safety 163: 594-603.
6. Chen, Y., Zeng, H., Tian, J., Ban, X., Ma, B., Wang, Y., 2013: Antifungal mechanism of essential oil from *Anethum graveolens* seeds against *Candida albicans*. Journal of Medical Microbiology 62(8): 1175-1183.
7. El-Nagerabi, S.A., Al-Bahry, S.N., Elshafie, A.E., Al-Hilali, S., 2012: Effect of *Hibiscus sabdariffa* extract and *Nigella sativa* oil on the growth and aflatoxin B1 production of *Aspergillus flavus* and *Aspergillus parasiticus* strains. Food Control 25(1): 59-63.
8. Frizzo, C.D., Santos, A.C., Paroul, N., Serafini, L.A., Dellacassa, E., Lorenzo, D., Moyna, P., 2000: Essential oils of camphor tree (*Cinnamomum camphora* Nees & Eberm) cultivated in Southern Brazil. Brazilian Archives of Biology and Technology 43(3): 313-316.
9. Ghaedi, M., Naghiha, R., Jannesar, R., Mirtamizdoust, B., 2015: Antibacterial and antifungal activity of flower extracts of *Urtica dioica*, *Chamaemelum nobile* and *Salvia officinalis*: Effects of $Zn(OH)_2$ nanoparticles and Hp-2-minh on their property. Journal of Industrial and Engineering Chemistry 32: 353-359.
10. Guo, S., Geng, Z., Zhang, W., Liang, J., Wang, C., Deng, Z., Du, S., 2016: The chemical composition of essential oils from *Cinnamomum camphora* and their insecticidal activity against the stored product pests. International Journal of Molecular Sciences 17(11): 1836.
11. Hao, Y.Y., Brackett, R.E., Doyle, M.P., 1998: Efficacy of plant extracts in inhibiting *Aeromonas hydrophilaand* and *Listeria monocytogenesin* refrigerated, cooked poultry. Food Microbiology 15(4): 367-378.
12. Jamalian, A., Shams-Ghahfarokhi, M., Jaimand, K., Pashootan, N., Amani, A., Razzaghi-Abyaneh, M., 2012: Chemical composition and antifungal activity of *Matricaria*

recutita flower essential oil against medically important dermatophytes and soil-borne pathogens. Journal de Mycologie Medicale 22(4): 308-315.

13. Kumari, S., Jain, P., Sharma, B., Kadyan, P., Dabur, R., 2015: In vitro antifungal activity and probable fungicidal mechanism of aqueous extract of *Barleria grandiflora*. Applied Biochemistry and Biotechnology 175(8): 3571-3584.
14. Lee, H.J., Hyun, E.A., Yoon, W.J., Kim, B.H., Rhee, M.H., Kang, H.K., Yoo, E.S., 2006: In vitro anti-inflammatory and anti-oxidative effects of *Cinnamomum camphora* extracts. Journal of Ethnopharmacology 103(2): 208-216.
15. Li, Q., Lin, J.G., Liu, J., 2013: Decay resistance of wood treated with extracts of *Cinnamomum camphora* xylem. BioResources 8(3): 4208-4217.
16. Li, Q., Wang, X., Lin, J., Liu, J., Jiang, M., Chu, L., 2014: Chemical composition and antifungal activity of extracts from the xylem of *Cinnamomum camphora*. Bioresources 9(2): 2560-2571.
17. Lima, E.D.O., Gompertz, O.F., Giesbrecht, A.M., Paulo, M.D.Q., 1993: In vitro antifungal activity of essential oils obtained from officinal plants against dermatophytes: Antimyzetische Aktivität ätherischer Öle von Heilpflanzen in vitro gegen Dermatophyten. Mycoses 36(9-10): 333-336.
18. Maciejewicz, W, Meresta, T., 1999: Quantitative determination of the bacteriostatic activity against *Staphylococcus aureus* of certain flavonoids, phenolic acids and esters occurring in propolis. Bulletin of the Veterinary Institute in Pulawy 43: 71-76.
19. Mishra, P.K., Shukla, R., Singh, P., Prakash, B., Kedia, A., Dubey, N.K., 2012: Antifungal, anti-aflatoxigenic, and antioxidant efficacy of Jamrosa essential oil for preservation of herbal raw materials. International Biodeterioration & Biodegradation 74: 11-16.
20. Pragadheesh, V.S., Saroj, A., Yadav, A., Chanotiya, C.S., Alam, M., Samad, A., 2013: Chemical characterization and antifungal activity of *Cinnamomum camphora* essential oil. Industrial Crops and Products 49: 628-633.
21. Prakash, B., Singh, P., Kedia, A., Dubey, N.K., 2012: Assessment of some essential oils as food preservatives based on antifungal, antiaflatoxin, antioxidant activities and in vivo efficacy in food system. Food Research International 49(1): 201-208.
22. Sansone, F., Picerno, P., Mencherini, T., Porta, A., Lauro, M. R., Russo, P., Aquino, R.P., 2014: Technological properties and enhancement of antifungal activity of a Paeonia rockii extract encapsulated in a chitosan-based matrix. Journal of Food Engineering 120: 260-267.
23. Scalbert, A., Cahill, D., Dirol, D., Navarrete, M.A., De Troya, M.T., Van Leemput, M., 1998: A tannin/copper preservation treatment for wood. Holzforschung-International Journal of the Biology, Chemistry, Physics and Technology of Wood 52(2): 133-138.
24. Silan, C., Tiefeng, Z., Chaolin, Y., Wulan, H., Zumulati, Y., Yiyu, M., Xin P., Zhengfeng T., Junhao W., Yuandan M., Youyou Y., Zhongqing M., Zhaojiang Z. 2018: Algicidal properties of extracts from *Cinnamomum camphora* fresh leaves and their main compounds. Ecotoxicology and Environmental Safety 163: 594-603.

25. Stubbs, B.J., Specht, A., Brushett, D., 2004: The essential oil of *Cinnamomum camphora* (L.) Nees and Eberm.- variation in oil composition throughout the tree in two chemotypes from eastern Australia. Journal of Essential Oil Research 16(1): 9-14.
26. Zhang, H., Kai, T.U., Hou, Q., Lin, H., Quan, L.I., 2020: The physiological and biochemical mechanisms of *Cinnamomum camphora* xylem extracts inhibit wood-decay fungi. Wood research 65(4): 531-542.

QUAN LI[1,2]
[1]KAILI UNIVERSITY
KAILI 556011, GUIZHOU, P. R. CHINA
[2]FUJIAN PROVINCIAL KEY LABORATORY OF FEATURED MATERIALS IN BIOCHEMICAL INDUSTRY
NINGDE 352106, FUJIAN, P. R. CHINA

NING JI
GUIZHOU ACADEMY OF FORESTRY
FORESTRY INDUSTRY RESEARCH INSTITUTE
GUIYANG 550000, GUIZHOU
P.R. CHINA

ZHANGUANG WANG
KAILI UNIVERSITY
KAILI 556011, GUIZHOU
P. R. CHINA

CUIXIANG LU*
GUANGXI ZHUANG AUTONOMOUS REGION FORESTRY RESEARCH INSTITUTE
NANNING 530002, GUANGXI
P. R. CHINA
*Corresponding author: 48002809@qq.com

HUI LIN*
[1]NINGDE NORMAL UNIVERSITY
COLLEGE OF CHEMISTRY AND MATERIALS
FUJIAN PROVINCIAL KEY LABORATORY OF FEATURED MATERIALS IN BIOCHEMICAL INDUSTRY
[2]FUJIAN PROVINCE UNIVERSITY
KEY LABORATORY OF GREEN ENERGY AND ENVIRONMENT CATALYSIS
NINGDE 352100, FUJIAN
P. R. CHINA
*Corresponding author: linhui@ndnu.edu.cn

WOOD RESEARCH doi.org/10.37763/wr.1336-4561/66.4.678688
e-ISSN 2729-8906
66(4): 2021 678-688 pp.

APPLICATION OF PHOTOMETRY IN DETERMINING THE DUST MASS CONCENTRATION OF HARDWOODS

ANKA OZANA ČAVLOVIĆ
UNIVERSITY OF ZAGREB
CROATIA

IVAN BEŠLIĆ
INSTITUTE FOR MEDICAL RESEARCH AND OCCUPATIONAL HEALTH
CROATIA

(RECEIVED JULY 2020)

ABSTRACT

Given the carcinogenicity of hardwood dust, the aim of this study was to determine the effectiveness of the photometric method for different types of woodworking machines and its application in determining the mass concentration of inhalable dust for raw and dry hardwoods. In addition to the optical part of the device, the input part of the measuring device contains the Institute of Occupational Medicine (IOM) inhalable dust filter holder. This correlation of gravimetric and photometric methods in determining the dust mass concentration showed that photometry underestimates the mass concentration measured gravimetrically. The results of this study recommend the application of a correction factor 2 for a timber band saw and a correction factor 3 for circular saws in determining the mass concentration of hardwood dust by the photometric method. It was showed that photometry can be used if the correction factor of the optical device has been previously tested for specific wood processing place.

KEYWORDS: Photometry, correction factor, inhalable dust, hardwoods, carcinogenicity.

INTRODUCTION

In 1994 IARC (International Agency for Cancer Research) researchers classified wood dust into the first group of carcinogenic substances and they found that higher risk was caused by hardwood dust than by softwood dust (Kos et al. 2004). Based on many scientific researches of professional diseases and classifications of the IARC in 1999 the European Union declared

wood dust as carcinogenic substances (Klein et al. 2001, Kauppinen et al. 2006, Llorente et al. 2009, Douwes et al. 2017, Holm and Festa 2019). Latest European Directive 2017/2398 on the protection of workers from the risks related to exposure to carcinogens or mutagens at work prescribe the limit values of 2 $mg \cdot m^{-3}$ (3 $mg \cdot m^{-3}$ until 17 January 2023) which refer to mass concentration of inhalable dust of hardwood species measured or calculated in relation to a reference period of 8-hour exposure of workers. Since 1999, many EU countries have applied a lower exposure limit to wood dust than the prescribed EU Directive (Spee et al. 2006, Campopiano et al. 2016).

Many authors have investigated the possibility of applying photometry as a real-time method that lasts shorter than working shift, in addition to the most reliable application of the gravimetric method for determining the mass concentration of wood dust in worker exposure studies (Koch et al. 1999, Koch et al. 2002, Tatum et al. 2002, Rando et al. 2005a,b). The mentioned authors presented the development and application of the RespiCon (TSI, Inc.) optical device, with the simultaneous selective collection of the inhalable, thoracic and respirable fraction of floating particles. The advantage of measuring worker exposure with a direct reading monitor is that it allows graphical display of worker activity and identification of peak exposure and underlying determinants in real time (Rosén et al. 2005). Continuous optical measurement provides detailed information on personal exposure and real-time work tasks, secondary sources and specific worker behaviors. The mass concentration of inhalable wood dust in full shift was determined by a video exposure monitoring system that includes video cameras, a real-time Split2 dust monitor connected to an IOM sampling head (Douwes et al. 2017). Thorpe and Walsh (2007) were compared the optical instruments' responses of the Split2 (SKC Ltd) and Microdust Pro (Casella Ltd) with the reference IOM inhalable dust samplers. The conical inhalable filter holder (CIS) and IOM inhalable filter holder with porous foam inserts were tested as optical device inlet adaptor. Measurements using the Split2 with IOM adaptor showed better agreement with the reference IOM inhalable dust sampler compared to the Microdust Pro device with CIS inlet adaptor. The main difference between IOM and CIS samples is in the size and shape of the orifices and the concentration measurements showed larger differences for larger particles in laboratory tests and field research (Campopiano et al. 2016). Baltrenas and Kvasaukas (2005) using Microdust Pro optical method determined 4,6% higher values of wood dust mass concentration by than gravimetric method. Thorpe and Walsh (2013) concluded that in order to obtain an accurate measure of airborne particle concentration, the aerosol monitor should always be compared to a reference gravimetric dust sampler to determine an average calibration factor. The optical device uses the principle of near-forward light scattering of an infrared radiation to immediately and continuously measure the concentration in $mg \cdot m^{-3}$ of airborne dust particles. As the particle passes between the lenses, the light intensity decreases, and an output signal proportional to the value of the mass concentration of suspended particles from the working atmosphere is recorded. In order to determine the predictable correction factor for different levels of dust concentration related to photometric and gravimetric measurements of wood dust, the sensitivity of the photometer in relation to the particle size distribution, particle density and its refractive index was analysed (O'Shaughnessy et al. 2002, Dado et al. 2017). A significant

influence of the relative humidity of the surrounding air on the results of the photometric method was also observed (Thomas and Gerbhart 1994, Lanki et al. 2002). The density of wood particles varies depending on the species of wood and the moisture content in the wood, but also the shape and size of the particles due to the mechanical processing in which they are formed. Therefore, photometer mass concentration measurements additionally require an assessment of the effectiveness in a specific wood environment. According to theoretical predictions, previous studies have shown lower photometry efficiency at higher mass concentrations of inhalable dust (Čavlović et al. 2009). This is supported by the results of research that increasing the mass concentration of total particles does not increase proportionally and the mass fraction of respirable particles (Kos et al. 2004). In this regard, it is known complete photometric and gravimetric stacking results (correction factor of about 1) for particles up to 10 μm. The best photometer sensitivity for particles of 0.6 μm was found at constant mass concentration (Čavlović et al. 2009).

The correction factor for any type of aerosol is determined from the ratio of mass concentrations measured by the gravimetric method and mass concentrations measured by infrared radiation during photometer measurements (NIOSH Manual for analytical methods). The correction factor needs to be calculated due to the influence of the physical properties of the particles (type and size of the particles, refractive indexes and light scattering properties of particles) on the sampling efficiency. However, previous studies of dust exposure at workplace have shown that other influencing factors need to be taken into account and that the type of wood machining has a significantly greater impact on the mass concentration than the wood species and the quality of exhaustion (Kos et al. 2002). The authors Palmqvist and Gustafsson (1999) analysed the influencing factors on the emission of wood dust, namely the influence of mechanical processing (average chip thickness and rake angle) and the influence of wood properties (moister content in wood and the wood fibers direction). It has been shown that the average chip thickness of sawdust has the greatest influence (fi = -5.7) on the emission of particles into the surrounding air, while the moisture content in wood has a significantly smaller impact (fi = -2.0). In other studies of wood dust emissions from different working machines, the reduction of the average chip thickness significantly increased the wood dust emissions in the working environment (Kos et al. 2004). The aim of this research was to determine the efficiency of the photometric method by obtaining a correction factor for different types of woodworking machines and its application in determining the mass concentration of inhalable dust for raw and dry hardwood (beech and oak wood).

MATERIAL AND METHODS

Determination of wood dust mass concentration by photometric and gravimetric method was made at different wood machining places, during processing raw and dry hardwood species (oak and beech wood) in sawmill (band saw and circular saw) and in wooden floor production plant (four side planer and circular saw). The optical device the Split2 model manufactured by SKC (Dorset, UK, 2006), for continuous measurement of mass concentration of floating

particles, consists of a device for data processing and a display, an input part consists of the inhalable dust IOM filter holder and an optical part of the device (Fig. 1).

The optical part of the device uses an infrared light source located at an angle of 90° to the photodetector. The optical device operated actively connected to a Casella pump (Bedford, UK, 2001), set to an air flow of 2 $l \cdot min^{-1}$ (EN ISO 10882-1: 2001). The air sample passes through an optical detector (photometric) and then through a filter holder (gravimetric). The correction factor for continuous determination of mass concentration was obtained as the ratio of mass concentration determined by gravimetric and photometric methods.

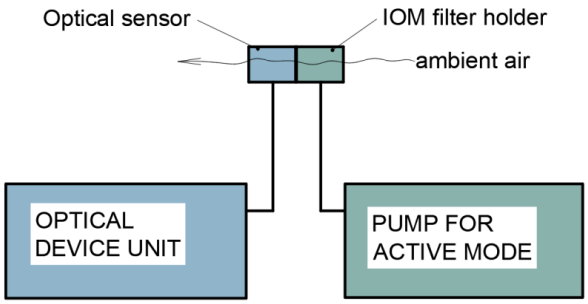

Fig. 1: Optical device connected to the pump and optical input part with IOM filter holder.

The instructions of NMAM Method 0600 (NIOSH Manual of analytical methods, National Institute for Occupational Safety and Health) were applied in calibration of device for continuous determination of mass concentration. Conducting continuous measurements for at least 30 min is a condition for determining short-term exposure. Wood dust samples were collected on average 40 min in dry wood processing and 110 min in raw wood processing. To achieve the reliability of continuous measurement with this device, the correction factor is determined from the mean value obtained from at least10 repetitions.

The mass concentration of inhalable dust was determined by gravimetric method (according to the standard ZH 1/120.41: 1989). The 25 mm quartz filters (Whatman QM-A) were conditioned in the desiccator on (20 ± 1) °C and (50 ± 5)% relative humidity 24 h before and after weighing and before and after the sampling. The weighing was carried out on a micro scale, type METTLER-TOLEDO MX-5 (Greifensee, Switzerland), which is capable of reading values at 10^{-6}, with the measuring deviation of 10^{-4} g. The stationary method of collecting samples was chosen due to the required precision of the optical part of the very sensitive device. HRN CEN /TR 15230: 2007 states that it is possible to use personal samplers for stationary collection.

Statistical differences in correction factors between samples obtained during processing with different machines were tested by the Student's test. The Mann-Whithey u-test was used when the condition of homogeneity of variance was not fulfilled. Descriptive statistics of variables and statistical analyses were performed using statistical software - STATISTICA 13.4.0.14.

RESULTS AND DISCUSSION

The arithmetic average values of calculated correction factor for different woodworking machines, timber band saw, circular saw and four side planer, from the results of determining the mass concentration of inhalable wood dust by gravimetric and photometric method, are shown in Tab. 1. The geometric mean as a better indicator of dust emission was selected to show the average values of the wood dust mass concentration for all group of samples.

Tab. 1: Gravimetrically and photometrically determined mass concentration of inhalable dust and correction factors.

Wood processing machine	**Wood dust**	**Number of samples**	**Mass concentration**[a] , ($mg \cdot m^{-3}$)		**Correction factor**[b], c_g/c_{ph}
			Gravimetric method, c_g	**Photometric method, c_{ph}**	
Timber band saw	Raw oak wood	10	0.818	0.502	2.24 ± 1.35
	Raw beech wood	13	0.661	0.442	1.84 ± 1.16
Circular saw	Raw oak wood	11	0.962	0.344	3.18 ± 1.45
	Dry beech wood	11	0.171	0.093	2.88 ± 2.37
Four side planer	Dry oak wood	13	0.754	0.314	3.10 ± 1.96
	Dry beech wood	10	3.297	1.052	3.74 ± 1.89

a - geometric mean; b - arithmetic mean and standard deviation.

From the range of the mean values of the correction factors for individual machine types it is obviously that it is not enough to distinguish correction factors according to the wood species, entirely. The obtained correction factors represent the low efficiency of the photometric method which underestimates the mass concentrations values obtained gravimetrically. Stacking the measured values by the two methods, photometric and gravimetric, shown in Fig. 2.

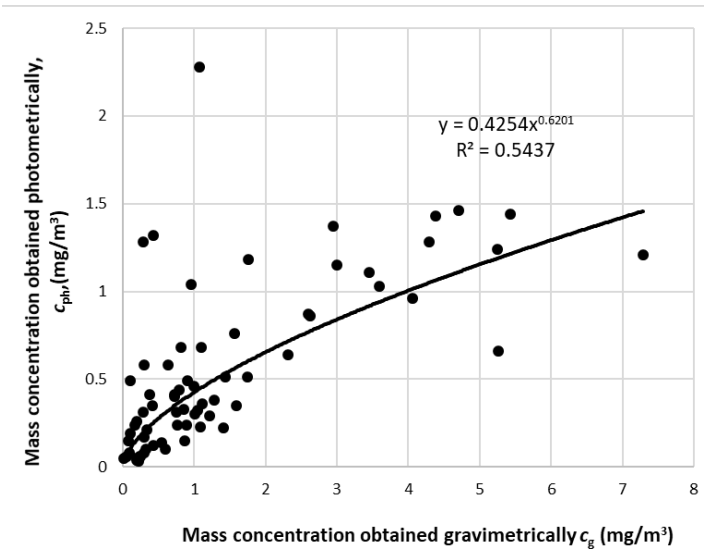

Fig. 2: Correlation of mass concentrations obtained by gravimetric method and photometric method.

The use of photometry is reliable only with a predefined correction factor for a particular case of work working place due to the weakness of the regression model with a low coefficient

of determination (R^2 = 0.54). Strong linear relationships (R^2 = 0.95 ÷ 0.99) were observed between mass concentrations of some other aerosol (diesel exhaust fume, welding fume, Arizona road dust ARD, and salt aerosol) measured photometrically and gravimetrically (Halterman et al. 2018). Aerosol type strongly influence sensor response, indicating the need for on-site calibration to convert sensor output to mass concentration. Once calibrated, however, the mass concentration estimated with low-cost sensors was highly correlated with that of reference instruments (Sousan et al. 2016).

In laboratory conditions at high concentrations (30-50 $mg \cdot m^{-3}$) the same model of optical device (Split2) also underestimates the gravimetrically obtained concentration of inhalable pine dust by an average of 32% (Thorpe 2007). An improvement in the measurement of Split2 compared to the reference IOM collector was obtained by redesigning the filter holder by SKC to improve the internal seals inside the sampler after it was determined that the previous design allowed dust around the backup filter (Thorpe and Walsh 2007).

Pearson correlation test of all measured values obtained by two measuring methods has shown medium strong correlation (k = 0.7). In two cases only, circular saw/raw oak wood dust and four side planer/dry oak wood dust, were found a very strong positive correlation between the mass concentration values measured by two methods (k = 0.8 and k = 0.9, resp.). This contributes to the high reliability of the test results in these cases, in which the efficiency of photometry is among the lowest and correction factor amounts 3.18 and 3.1, respectively.

Statistical results from Tab. 2 have shown that the correction factors for two types of wood species do not differ significantly for timber band saw, circular saw and four side planer. At the same working places, the gravimetrically obtained mass concentration of beech and oak wood dust significantly do not differ for the timber band saw, only (Tab. 3). There is the most significant difference (p = 0) of mass concentration measured gravimetrically near circular saw when processing raw and dry hardwood, in spite of the correction factor for the same cases with no significant difference.

Tab. 2: Comparison of correction factors for oak- and beech- wood dust.

Wood processing machine	**Wood dust**	**Number of samples**	**Homogeneity of variances test**		**t-test**
			F	**p**	**p**
Timber band saw	Raw oak wood	10	1.357	p > 0.05	**0.61**
	Raw beech wood	13			
Circular saw	Raw oak wood	11	2.666		**0.14**
	Dry beech wood	11			
Four side planer	Dry oak wood	13	1.073		**0.94**
	Dry beech wood	10			

F- test of variance; p-significant level.

Tab. 3: Comparison of gravimetrically determined mass concentrations near wood processing machines with respect to the type of wood dust.

Wood processing machine	**Wood dust**	**Number of samples**	**Homogeneity of variances test**		**t-test**	**u-test**
			F	**p**	**p**	**p**
Timber band saw	Raw oak wood	10	4.633	p < 0.05	-	**0.55**
	Raw beech wood	13				

Circular saw	Raw oak wood	11	24.91		-	**0.001**
	Dry beech wood	11				
Four side planer	Dry oak wood	13	2.144	p > 0.05	**0.044**	-
	Dry beech wood	10				

F- test of variance; p-significant level.

Statistical testing showed a significant difference between the correction factors for a timber band saw and a four side planer (Tab. 4). The mass concentration measured by the gravimetric method near woodworking machines differs significantly between a timber band saw and a four side planer and between a circular saw and a four side planer (Tab. 5).

Tab. 4: Comparison of correction factors for wood processing machines.

Wood processing machine	**Number of samples**	**Homogeneity of variances test**		**t-test**	**u-test**
		F	**p**	**p**	**p**
Timber band saw – Circular saw	23/22	2.430	p < 0.05	-	**0.09**
Timber band saw - Four side planer	23/23	2.403		-	**0.02**
Circular saw - Four side planer	22/23	1.011	p > 0.05	**0.54**	-

F- test of variance; p-significant level.

Tab. 5: Comparison of gravimetrically determined mass concentrations of wood dust measured next to woodworking machines.

Wood processing machine	**Number of samples**	**Homogeneity of variances test**		**t-test**	**u-test**
		F	**p**	**p**	**p**
Timber band saw – Circular saw	23/22	1.101	p > 0.05	**0.28**	-
Timber band saw - Four side planer	23/23	12.907	p < 0.05	-	**0.03**
Circular saw - Four side planer	22/23	11.729		-	**0.002**

F- test of variance; p-significant level.

According to the mean values of the correction factor from the diagram in Fig. 3, for photometric measurements of hardwood dust mass concentration, the use of value 2 as a correction factor for a timber band saw and value 3 as a correction factor for a circular saw can be suggested. Therefore, the correction factor 3.4 can be used for the photometric determination of the dust mass concentration of hardwoods next to the four side planer.

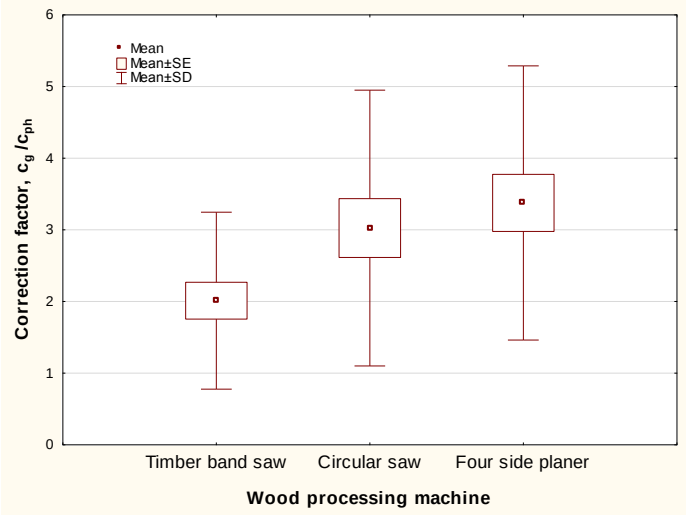

Fig. 3: Distribution diagram of mean values and data dissipation of correction factor for wood processing machines (SD-standard deviation, SE- standard error of mean).

In previous studies of the correction factor by type of wood, the lowest values are 1.0 for raw fir wood, and the highest 3.74 for dry oak wood dust (Čavlović et al. 2009). It is possible that, in addition to the mass concentration, the efficiency of photometry is influenced by other factors, the moisture content in the wood and the content of fine particles in the inhalable dust. In general, the efficiency of the photometric method decreased with increasing aerodynamic particle diameter (Koch et al. 1999, Koch et al. 2002, Tatum et al. 2002, Rando et al. 2005a,b). Authors Palmqvist and Gustafsson (1999) found that dust emissions from woodworking machine operation increase by reducing the average chip thickness and by reducing the moisture content of the wood material. The average thickness of the chips produced from a circular saw is smaller than the average thickness of the chips from a band saw (Kos et al. 2004). The particle size distribution in chipped beech wood material shows that the proportion of the smallest particles (less than 0.09 mm) formed on a four-sided planer is twice less than the proportion of the smallest particles formed on a circular saw and nine times less than the proportion of the smallest particles formed on a band saw (Beljo Lučić et al. 2005). In this regard, a model for estimation of percentage fraction of fine dust mass as a function of chip thickness was found (Rautio et al. 2007).

CONCLUSIONS

Determining the correction factor for using a photometric method to determine the mass concentration of wood dust is very complex due to many influencing factors on the efficiency of the optical device. This study showed that the efficiency of measuring the mass concentration of wood dust by photometry depends not only on the type of wood, but also on the type of processing. The research resulted in the obtained correction factors and suggested for application in determining the mass concentration of inhalable dust near timber band saw (c_g/c_{ph} = 2), circular saw (c_g/c_{ph} = 3) and four side planer (c_g/c_{ph} = 3.4). This indicates that photometry regularly underestimates the mass concentration measured gravimetrically.

In this case, in determining of dry and wet hardwood dust mass concentration, the strength of the optical device correction factor estimation model is small (R^2=0.54). In practice, the correction factor for an optical device should be defined on a case-by-case basis, taking into account the wood species and moisture content of the wood, the type of mechanical wood treatment and the quality of the exhaust devices.

The photometric method of continuous determination of mass concentration can be a useful method for detecting incidental levels of mass concentrations of wood dust, because wood processing workers in the Republic of Croatia should be additionally protected from exposure to hardwood dust, due to the participation of beech and oak in processing up to 65%.

REFERENCES

1. Baltrenas, P., Kvasaukas. M., 2005: Experimental investigation of particle concentration using mass and optical methods. Journal of Environmental Engineering and Landscape Management 13(2): 57-64.
2. Beljo Lučić, R., Kos, A., Antonović, A., Vujasinović, E., Šimičić, I., 2005: Properties of chipped wood generated during mechanical wood processing. Drvna Industrija 56(1): 11-19.
3. Campopiano, A., Basili, F., Angelosanto, F., Cannizzaro, A., Olori, A., Ramires, D., Iannò, A., Angelici, L., 2016: Field comparison of two inhalable samplers used in Italy to measure the wood dust exposure. International Journal of Occupational and Environmental Health 22(2): 159-166.
4. Čavlović, A., Beljo Lučić, R., Bešlić, I., Jug, M., Ištvanić, J., 2009: Correction factor for real-time determination of wood dust mass concentration by photometric method. Drvna Industrija 60(1): 33-42.
5. Dado, M., Mikusova, L., Hnilica, R., Očkajova, A., 2017: Calibration of photometer-based direct-reading aerosol monitors. MM Science Journal 10(5): 2069-2072.
6. Douwes, J., Cheung, K., Prezant, B., Sharp, M., Corbin, M., McLean, D., Mannetje, A., Schlunssen, V., Sigsgaard, T., Kromhout, H., LaMontagne, A.D., Pearce, N., McGlothlin, J.D., 2017: Wood dust in joineries and furniture manufacturing: An exposure determinant and intervention study. Annals of Work Exposures and Health 61(4): 416–428.
7. Halterman, A., Sousan, S., Peters, T.M., 2018: Comparison of respirable mass concentrations measured by a personal dust Monitor and a personal DataRAM to gravimetric measurements. Annals of Work Exposures and Health 62(1): 62–71.
8. Holm, S.E., Festa, J.L., 2019: A review of wood dust longitudinal health studies: Implications for an occupational limit value. Dose-Response: An International Journal 17(1): 1-5.
9. Kauppinen, T., Vincent, R., Liukkonen, T., Grzebyk, M., Kauppinen, A., Welling, I., Arezes, P., Blacks, N., Bochmann, F., Campelo, F., Costa, M., Elsigan, G., Goerens, R., Kikemenis, A., Kromhout, H., Miguel, S., Mirabelli, D., McEneany, R., Pesch, B., Platon, N., Schlunssen, V., Schulze, J., Sonntag, R., Verougstraete, V., De Vincente, M.A., Vuk, J., Zimmermann, M., Husgafvel-Pursiainen, K., Savolainen, K., 2006: Occupational exposure

to inhalable wood dust in the member states of the European Union. Annals of Occupational Hygiene 50(6): 549-561.

10. Klein, R.G., Schmezer, P., Amelung, F., Schroeder, H.G., Woeste, W., Wolf, J., 2001: Cancerogenicity assays of wood dust and wood additives in rats exposed by long-term inhalation. International Archives of Occupational and Environmental Health 74: 109-118.
11. Koch, W., Dunkhorst, W., Lödding H., 1999: Design and performance of a new personal aerosol monitor. Aerosol Science and Technology 31: 231-246.
12. Koch, W., Dunkhorst, W., Lödding, H., Thomassen, Y., Skaugset, N.P., Nikanov, A., Vincent, J., 2002: Evaluation of RespiCon® as a personal inhalable sampler in industrial environments. Journal for Environmental Monitoring 4: 657 – 662.
13. Kos, A., Beljo Lučić, R., Horvat, D., Šega, K., Bešlić, I., 2002: Influential factors on indoor air dustiness in woodworking companies. Drvna Industrija 53(3): 131 – 140.
14. Kos, A., Beljo Lučić, R., Šega, K., Rapp, A., 2004: Influence of woodworking machine cutting parameters on the surrounding air dustiness. Holz als Roh- und Werkstoff 62(3): 169 – 176.
15. Lanki, T., Alm, S., Ruuskanen, J., Janssen, N.A.H., Jantunen, M., Pekkanen, J., 2002: Photometrically measured continuous personal $PM_{2.5}$ exposure: Levels and correlation to a gravimetric method. Journal of Exposure Analysis and Environmental Epidemiology 12: 172-178.
16. Llorente, L.J., Pérez-Escuredo, J., Alvarez-Marcos, C., Suárez, C., Hermsen, M., 2009: Genetic and clinical aspects of wood dust related intestinal-type sinonasal adenocarcinoma: a review. European Archives of Oto-Rhino-Laryngology 266(1):1-7.
17. O'Shaughnessy, P.T., Slagley, J.M., 2002: Photometer response determination based on aerosol physical characteristics. American Industrial Hygiene Association Journal 63(5): 578-585.
18. Palmqvist, J., Gustafsson, S.I., 1999: Emission of dust in planing and milling of wood. Holz als Roh- und Werkstoff 57: 164 – 170.
19. Rando, R., Poovey, H., Mokadam, D, Brisolara, J., Glindmeyer, H., 2005: Field performance of the RespiConTM for size-selective sampling of industrial wood processing dust. Journal of Occupational and Environmental Hygiene 2(4): 219 – 226.
20. Rando, R.J., Gibson, R.A., Kwon, C.W., Poovey, H.G., Glindmeyer, H.W., 2005: On-filter determination of collected wood dust by diffuse infrared Fourier-transform spectroscopy (DRIFTS). Journal of Environmental Monitoring 7(7): 675 – 680.
21. Rautio, S., Hynynen, P., Welling, I., Hemmilä, P., Usenius, A., Närhi, P., 2007: Modelling of airborne dust emission in CNC MDF milling. Holz al Roh und Werkstof 65(5): 335-341.
22. Rosén, G., Andersson, I.M., Walsh, P.T., Clark, R.D.R., Saamanen, A., Heinonen, K., Riipinen, H., Paakkonen, R., 2005: A review of video exposure monitoring as an occupational hygiene tool. Annals of Occupational Hygiene 49(3): 201–217.
23. Sousan, S., Koehler, K., Thomas, G., Park, J.H., Hillman, M., Halterman, A., Peters, T.M., 2016: Inter-comparison of low-cost sensors for measuring the mass concentration of occupational aerosols a Department of Occupational. Aerosol science and technology 50(5): 462–473.

24. Spee, T., Van de Rijdt-Van Hoof, E., Van Hoof, W., Noy, D., Kromhout, H., 2006: Exposure to wood dust among carpenters in the construction industry in The Netherlands. Annals of Occupational Hygiene 51(3): 241-248.
25. Tatum, V., Ray, A.E., Rovell-Rixx, D., 2002: Performance of the RespiCon personal aerosol sampler in forest products industry workplaces. American Industrial Hygiene Association Journal 63(3): 311-316.
26. Thomas, A., Gerbhart, J., 1994: Correlation between gravimetry and light-scatering photometry for atmospheric aerosols. Atmospheric Environment 28(5): 935-938.
27. Thorpe, A., 2007: Assessment of personal direct-reading dust monitors for the measurement of airborne inhalable dust. Annals of Occupational Hygiene 51(1): 97–112.
28. Thorpe, A., Walsh, P.T., 2007: Comparison of portable, real-time dust monitors sampling actively, with size-selective adaptors, and passively. Annals of Occupational Hygiene 51(8): 679–691.
29. Thorpe, A., Walsh, P.T., 2013: Direct-reading inhalable dust monitzoring. An assessment of current measurement methods. Annals of Occupational Hygiene 57(7): 824-841.

ANKA OZANA ČAVLOVIĆ*
UNIVERSITY OF ZAGREB
FACULTY OF FORESTRY
P.O. Box 422
10002 ZAGREB
CROATIA
*Corresponding author: acavlovic@unizg.sumfak.hr

IVAN BEŠLIĆ
INSTITUTE FOR MEDICAL RESEARCH AND OCCUPATIONAL HEALTH
P.O. Box 291
10001 ZAGREB
CROATIA

WOOD RESEARCH doi.org/10.37763/wr.1336-4561/66.4.689699
e-ISSN 2729-8906
66(4): 2021 689-699 pp.

THE BRIQUETTES PROPERTIES FROM SEED SUNFLOWER HUSK AND WOOD LARCH SHAVINGS

VERONICA DRĂGUȘANU (JAPALELA), AUREL LUNGULEASA, COSMIN SPÎRCHEZ
TRANSILVANIA UNIVERSITY OF BRAȘOV
ROMANIA

(RECEIVED AUGUST 2020)

ABSTRACT

The paper aims to use the residue of sunflower seed hulls to obtain organic briquettes and to improve their properties by using larch shavings obtained in the process of solid wood planning. The physical-mechanical properties of briquettes made on a hydraulic machine, calorific value, ash content and volatile content were evaluated. The obtain results highlighted the briquettes obtained from larch waste, but also the acceptable characteristics of the briquettes obtained from sunflower seed husks. The main conclusions of this study is that briquettes obtained from unprocessed sunflower seed husks are acceptable in terms of physical-mechanical and calorific characteristics, even if they do not reach the level of briquettes obtained from larch shavings.

KEYWORDS: Breaking strength, briquette, density, larch shavings, sunflower seed husk.

INTRODUCTION

Nowadays, energy resources are constantly decreasing and solid fuels such as wood briquettes are becoming increasingly sought after on the energy market. Lignocellulosic briquettes have a clean combustion in thermal power plants, and the price is much lower than of coals. Vegetable briquettes are all the more sought after as they are obtained from residues obtained from food processing. The sunflower (*Helianthus annuus*) is an annual plant of the Asteraceae family, originating from America. It is one of the most cultivated plants for its oil-rich seeds, from which sunflower oil is extracted. The residues obtained from the manufacture of sunflower oil are enormous is quantity, of the order of dozens of wagons per year, and their higher use is made in the field of lignocellulosic composites, pellets and briquettes and even by direct combustion. It is much better to use briquettes than to use the lignocellulosic residues directly, in order to capitalize the advantages given by the briquetting/pelletizing process, meaning the concentration of a large amount of energy in

a small volume of briquettes. Also, the existence of a kit for automatic feeding of briquettes/pellets with an independence of 12-24 hours makes it possible to automate the loading of the thermal power plant and facilities this activity.

Rosa et al. (2019) analyzed the chemical composition of sunflower seed hulls, obtaining at moisture content of 6.7%, as protein (nitrogen x 5.3) 18.2%, ash content of 3.8% and raw fiber of 11.3%. Oil factories have a current capacity of 400 t/24 hours which results about 100 tons of peeled seeds, meaning a ratio of 1:4. Worldwide in 2007 there were 31 million tons of sunflower seed production. Popescu et al. (2013) analyzed the use of residues from the manufacture of sunflower oil to obtain bioethanol. This biomass is also presented as a renewable and sustainable and very little capitalized. Zygarlicke and Folkedahl (2003) made a chemical analysis (proximate and ultimate analysis) of sunflower seed hulls with wood chips and fossil coal. In terms of a proximate analysis, the following were found: the moisture content was 11.4% for sunflower hulls, 5.2% for wood chips and 20% for coal, volatile matter was 72.21% foe sunflower hulls, 78.54% for wood chips and 37.71% for coal, fixed carbon of 13.53% sunflower hulls, 15.71% for wood chips and 37.25% for coal, and the ash content was 2.85% for sunflower hulls, 0.55% for wood chips and 5.14% for coal. In terms of an ultimate analysis, the following were identified: the hydrogen content was 7% for sunflower seed hulls, 46.46% for wood chips and 53.37% for fossil coal, the oxygen content was 41.89% was for sunflower seed hulls, 46.34% for wood chips and 34.72% for fossil coal from Brazil, and the calorific value was 18035.8 $kJ \cdot kg^{-1}$ for sunflower seed hulls, 18059.05 $kJ \cdot kg^{-1}$ for wood chips and 21689.93 $kJ \cdot kg^{-1}$ for fossil coals from Brazil. Spîrchez et al. (2018) analyzed the manufacturing flow of sunflower oil and found that there were two types of manufacturing residues, namely food from which halvah and fatty acids can be obtained, and another in the form of sunflower seed hulls that can be used in the composites and briquettes/pellets industry. Plíštil et al. (2005) obtained briquettes from several straws and crops using a hydraulic briquetting machine. The method of breaking the briquettes by compression was used to quantify the strength, as a ratio between the maximum breaking force and their diameter. By using pressures of maximum 20 MPa of the briquetting press, the densities below 850 $kg \cdot m^{-3}$ and breaking strength below 70 $N \cdot mm^{-1}$ were obtained. Brožek et al. (2012) evaluated the quality of lignocellulosic briquettes obtained from various wood and vegetable residues having as criteria the dimensions, moisture content, density, breaking strength, ash content, mechanical durability and calorific value.

Determining the strength of briquettes is a complicated problem because it isn't possible to quantify exactly what its breaking surface is. In general, there were several models in choosing the breaking surface is. In general, there were several models in choosing the breaking surface, respectively of linearity considering the diameter of the briquette (Plíštil et al. 2005), by quantifying the average surface remaining after flat pressing, by the flat surface left after pressing in the cage (Lunguleasa 2010) and by the central flat surface of the briquette determined by the diameter and length of the briquette (Spîrchez et al. 2018, Spîrchez et al. 2019), as seen in Fig. 1.

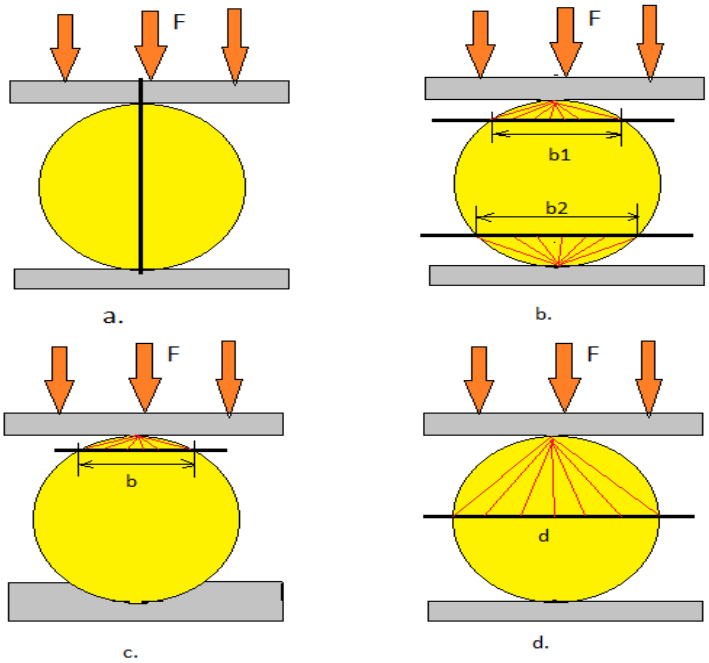

Fig. 1: Ways of quantifying the briquette breaking plane: a- linear; b-with two pressing surfaces; c-with a flat surface by arrangement in the cage; d-through the central of the briquette.

The conclusions on the bibliographic study can be quantified in terms of the briquettes themselves but also of the briquetting presses. Briquettes can be obtained from all categories of lignocellulosic residues with better or less good characteristics. The briquettes obtained from vegetable residue are less qualitative than those obtained from wood residue. Difficulties are also encountered in briquetting with hydraulic presses in which briquettes with a lower density and lower strength are obtained than when using industrial presses with helical conveyor or crank gear mechanism.

The paper aims to make good quality briquettes from sunflower seed hulls and larch shavings, made on a hydraulic briquetting machine Gold Mark type (Brașov, Romania), in order to compare their quality.

MATERIAL AND METHODS

The raw material used in the paper consisted of two parts: from the sunflower hulls obtained from an oil factory, taking over the residues of the hulls obtained from this technology and that obtained from the planning of larch wood. The larch (*Larix decidua*) shavings was also processed by crushing in a mill with laboratory hammers, working with its natural and unchanged state, but also with it in a shredded state to determine the content of calcined ash. The husk of the sunflower seeds was also crushed, in order to use them to obtain briquettes, but also to determine the ash content. For the raw material, the bulk density and their granulometry were determined. The bulk density was determined using constant volume conical recipients (to determine the volume) and a Kern type analytical scale (Germany) to determine the mass. Considering the volume of the cone trunk, the bulk density calculation formula was as follows:

$$\rho_b = \frac{3 \cdot m}{\pi \cdot h \cdot \left(R^2 + r^2 + Rr\right)} \cdot 10^6 \ [\text{kg} \cdot \text{m}^{-3}] \quad (1)$$

where: m - mass of the sample from the taper recipient, (g); h - height of the taper recipient, (mm); R - radius of the taper recipient, (mm); r-small radius of the taper recipient, (mm).

From each type of residues, lignocellulosic briquettes were made on a pneumatic briquetting machine Gold Star type (Brașov, Romania), provided with two pistons and a silo of about 1.5 m^3. The briquettes obtained were cleaned of fibres and were prepared to determine the physical-mechanical properties. In order to determine the density of the briquettes, their volume was considered as a straight circular cylinder, the calculation relation being the following:

$$\rho_b = \frac{3 \cdot m}{\pi \cdot d^2 \cdot l} \cdot 10^6 \ [\text{kg} \cdot \text{m}^{-3}] \quad (2)$$

where: ρ_b - density of briquettes, ($kg \cdot m^{-3}$); m - mass of briquettes, (g); d-diameter of the briquettes, (mm); l - length of briquettes, (mm).

The breaking strength by compression of the briquettes considered the stress distribution during the breaking as well as the shape of the briquette after breaking, using the model from Fig.1d, with the following relationship:

$$\sigma_c = \frac{F}{d \cdot l} \left[\frac{N}{mm^2}\right] \quad (3)$$

where: F - maximum breaking force, (N); d - diameter of the briquette, (mm); l - briquette length, (mm).

The calorific value of larch briquettes and sunflower hulls was determined experimentally with an XRY-1C type calorimeter bomb, produced by Shanghai Changji Geological Instrument Co. (China) on pieces of briquettes with a mass of 0.6-0.8 g. The testing included 3 distinct stages: preparations of the installation and the wood material, the actual test and taking over the results with their statistical interpretation. The results were expressed by the high and low calorific value, in $kJ \cdot kg^{-1}$. The installation software used the following calculation relationship to determine the higher calorific value of the analyzed lignocellulosic material:

$$HCV = \frac{K \cdot (T_f - T_i)}{m} - Q_{wc} [kJ/kg] \quad (4)$$

where: HCV - high calorific value, ($kJ \cdot kg^{-1}$); K - calorimetric coefficient, (kJ/ºC); T_f - final temperature of the calorimetric installation, (ºC); T_i - initial temperature of the calorimetric installation, (ºC); m - mass of the test piece, (kg); Q_{wc} - the amount of additional heat due to the burning of nickel wire and cotton wire, ($kJ \cdot kg^{-1}$).

The ash content obtained on the base of ASTM E1755-01: 2003 was determined on shredded material sorted with a 0.4 x 0.4 mm sieve, overtaking the fraction that passed through this sieve. The idea of using such a small material is given by the duration of calcination of the lignocellulosic material. The material that is subjected to this test is dry, because the moisture content greatly influences the final result. Because the test is performed by means of a crucible, the final relation of obtaining the ash content was:

$$A_c = \frac{(m_{ac} - m_c)}{(m_{sc} - m_c)} \cdot 100\ [\%] \quad (5)$$

where: A_c - ash content, (%); m_{ac} - ash mass with crucible, m_c-mass of crucible, (g); m_{sc} - mass of oven dry sample with crucible, (g).

As the weighed values were very low, it was necessary to use an analytical balance with 3 decimal units. In order to protect the calcification oven (not to deposit soot on the interior walls) it was necessary to burn the crucible with lignocellulosic sample on a flame with butane gas, until it no longer smokes, which is why the black ash content was determined, with a similar relationship with Eq. 5.

The volatile content was determined based on the EN 15148 (2009) standard, using an electric oven with the possibility of reaching a temperature of 900 ± 10ºC and 1.5 h by a crucible with a silica lid, which doesn't allow the oxidation of the lignocellulosic material inside. The calculation relation didn't take into account the moisture content of the lignocellulosic material, because the material was dried at 105ºC, up to 0% moisture content.

$$V_c = \frac{m_v}{m_s - m_{cl}} \cdot 100\ [\%] \quad (6)$$

where: m_v - mass of substances lost during heat treatment, (g); m_s - mass of dry sample with crucible and lid, (g); m_{cl} - mass of empty crucible with lid, (g).

Statistically, the Minitab 18 program (Minitab LLC, State College, Pennsylvania, USA) was used, with the calculation of the survey average for a confidence interval of 95%. Also, where was necessary the Excel Microsoft was used, in addition with some common statistical parameters of trend and spread such as arithmetic mean and standard deviation that were also used.

RESULTS AND DISCUSSION

Regarding the characteristics of the larch shavings, its bulk density (determined with relation 1) was 118.5 $kg \cdot m^{-3}$. If we consider that at 10% moisture content, the density of solid larch wood is 600 $kg \cdot m^{-3}$ (Wood handbook 2020), it can be started that the shavings used has a degree of looseness of 4.56. The granulometry of the larch shavings, determined on

5 independent samples is presented in Fig. 2. A good distribution of values is observed, and the polynomial equation of 2nd degree best approximates the Gaussian distribution of values.

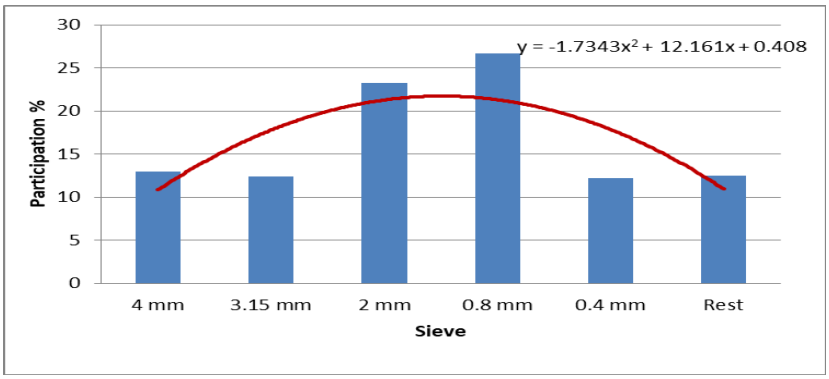

Fig. 2: Grading of larch shavings

The average dimensions of the 30 specimens made of larch shavings were: the diameter of 40.8 ± 0.1 mm and the length of 30.3 ± 5.3 mm. Regarding the diameter of the briquettes, in the conditions in which the diameter of the extrusion channel of 40 mm is known, the degree of expansion of the briquette diameter after pressing of only 2% can be determined, a very good value, which shows the very good compaction of the larch carving. The average density of these briquettes was 1024.8 ± 147.3 kg·m^{-3}, a very good value, above the requirements required by European standards in the field ÖNORM M7135 (2000), (Fig. 3).

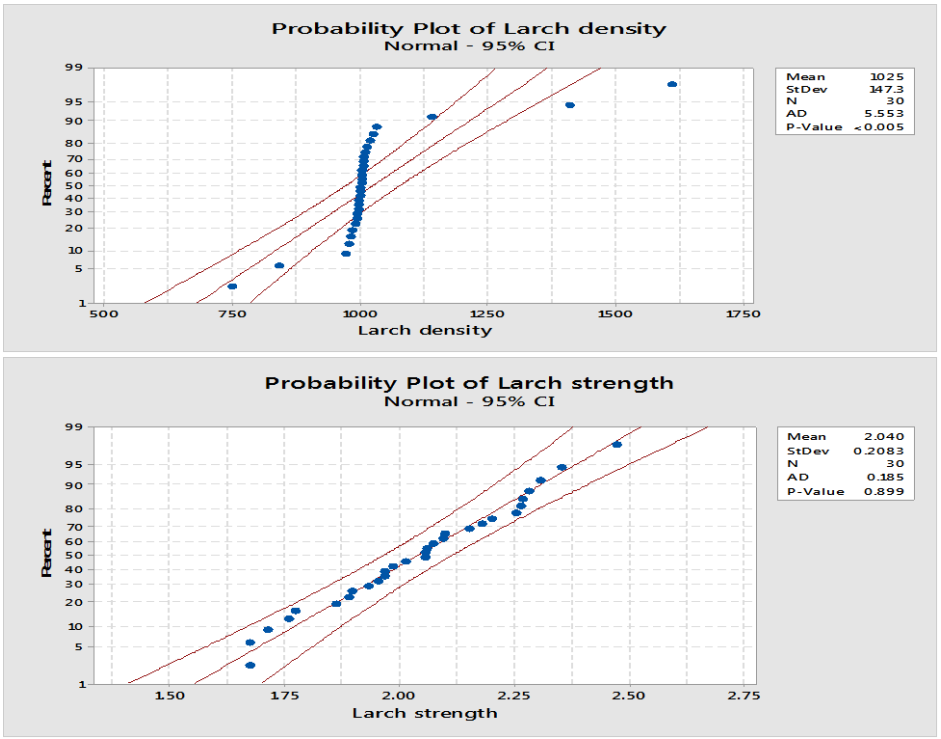

Fig. 3: Probability plot of density and strength of briquettes obtained from larch shavings.

The breaking strength of larch briquettes, calculated with relation to Eq. 3 was 2.04 ± 0.2 $N \cdot mm^{-2}$, also a very good value, comparable to that found by another research in the field (Spirchez et al 2019) . The calorific value of the larch briquettes was 19375 $kJ \cdot kg^{-1}$ (HCV) and 18906 $kJ \cdot kg^{-1}$ (LCV). The ash content of larch briquettes was 0.4% the current value of softwood species (WHW 2020, Krajnic 2015) and within the norms of the European standard ÖNORM M7135, 2000, which provides a value of less than 6% (Fig. 4).

Regarding the husk of the sunflower seeds, they had a bulk density, determined with the relation (1), of 207 ± 19 $kg \cdot m^{-3}$ in raw state and of 301 ± 26 $kg \cdot m^{-3}$ in ground state (the sort that passed through the sieve of 0.4 x 0.4 mm). The dimensions of the briquettes obtained with the Gold Mark press were the following: the average diameter 40.8 ± 0.5 mm and the length of 44 ± 5 mm. The degree of return of the briquettes after leaving the briquetting press was as in the case of briquettes made from larch shavings of 2%.

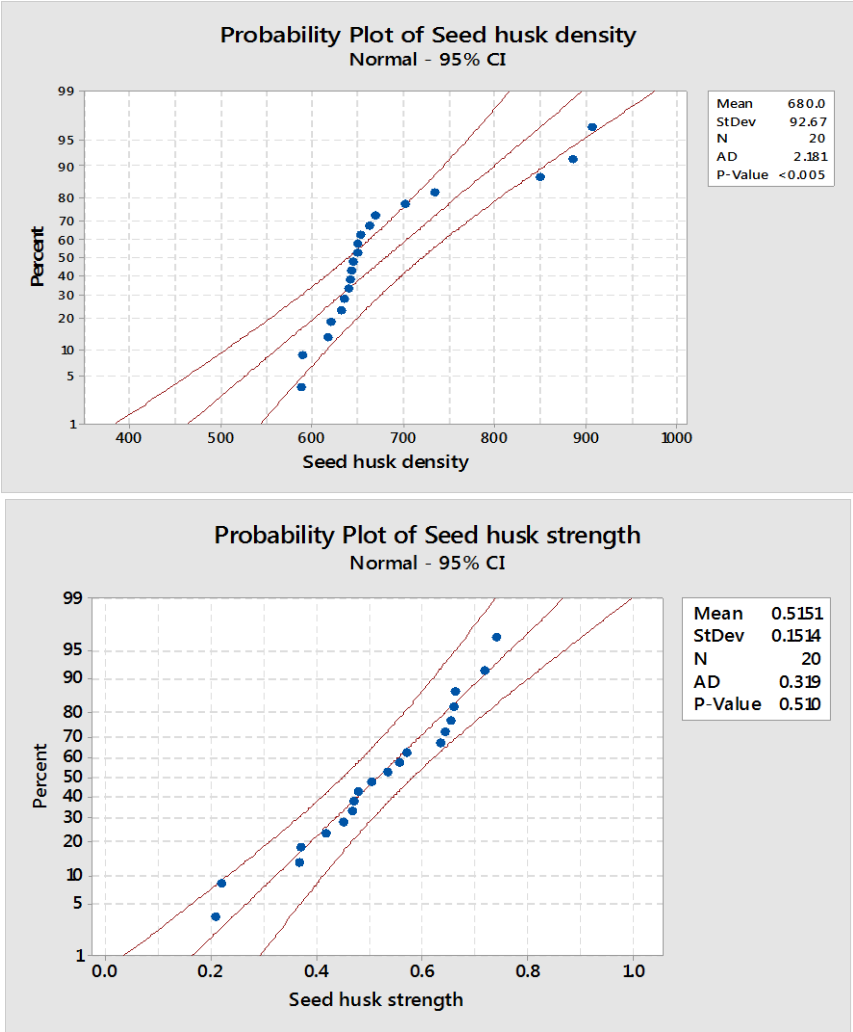

Fig. 4: Probability plot of seed husk density and strength.

The effective density of briquettes obtained directly from non-ground hulls was 680 ± 7.3 $kg \cdot m^{-3}$, and that of briquettes obtained from ground hulls was 854 ± 73.7 $kg \cdot m^{-3}$. The big difference between the two densities is given by the fact that the small chips fit better in

the briquette structure, thus decreasing the free spaces in the briquette. The breaking strength of the briquettes was 0.51 $N \cdot mm^{-2}$ for those obtained from large seed hulls and 0.09 $N \cdot mm^{-2}$ for those obtained from ground hulls. There is a big difference between the two resistances, which isn't proportional to the density, which leads to the finding that the resistance of the briquettes depends on the size of the lignocellulosic particles (with the increase of the particle size the resistance will increase). This finding is also specific to the composite materials industry, the OSB boards type with long chip having higher resistance to the classic wood chipboards. Therefore, it can be concluded that it isn't necessary to grind the sunflower seed hulls, but on the contrary if we leave them in their natural state, we will obtain briquettes with higher properties.

Because a large difference was observed in the strengths of the two types briquettes (from larch shavings and sunflower seed hulls), a mixture of chips was obtained experimentally in different percentages of seed hulls, respectively 25, 50 and 75%. The results were inconclusive, the resistance of the briquettes obtained experimentally not only didn't improve but decreased in all cases. For example, in the case of briquettes with 50% larch shavings and 50% sunflower seed hulls, the resistance of the briquettes was 0.21 $N \cdot mm^{-2}$, less than half that of the briquettes with 100% sunflower seed hulls. Therefore, it can be concluded that the mixture of sunflower seed hulls and larch carving is compatible and that other solutions must be found to improve seed hulls. Therefore, it can be concluded that the mixture of sunflower seed hulls and larch carving is incompatible and that other solutions must be found to improve the resistance of the briquettes in the sunflower seed husk.

In order to observe the influence of the briquetting press on the physical-mechanical properties of the briquettes obtained from the sunflower seed hulls, some briquettes made on an industrial screw press were taken, which had an average density of 921.8 ± 27.6 $kg \cdot m^{-3}$ and an average resistance of 0.46 ± 0.07 $N \cdot mm^{-2}$, as seen in Fig. 5.

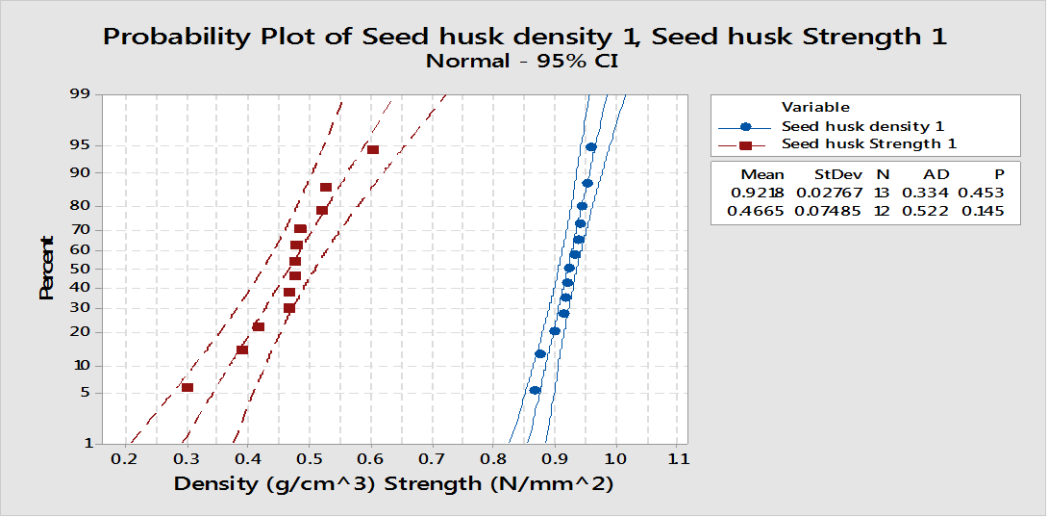

Fig. 5: Probability plot of seed husk density ($g \cdot cm^{-3}$) and strength ($N \cdot mm^{-2}$).

It is observed that although the density of briquettes increased greatly from 680 $kg \cdot m^{-3}$ on the hydraulic press to 921.8 $kg \cdot m^{-3}$ on the screw press (an increase of 35.4%), the strength of breaking by compression decreased from 0.51 $N \cdot mm^{-2}$ at 0.46 $N \cdot mm^{-2}$ (a decrease of 9.8%).

It can also be concluded that the breaking strength of briquettes obtained from sunflower seed hulls is much lower than that of briquettes obtained from larch carving, respectively about 4 times.

The high calorific value of the briquettes obtained from the sunflower seed hulls was of 19265 $kJ \cdot kg^{-1}$, while the lower calorific power as average value obtained was 18655 $kJ \cdot kg^{-1}$. There values were in concordance with those obtained from larch shavings or other wood residues (Verna et al. 2019). The ash content of sunflower seed hulls was 30.72% for black ash and 2.34% for calcined ash (Fig. 6). Ash content as calcined one wasn't too much as other vegetable residues (Brožek at al. 2012).

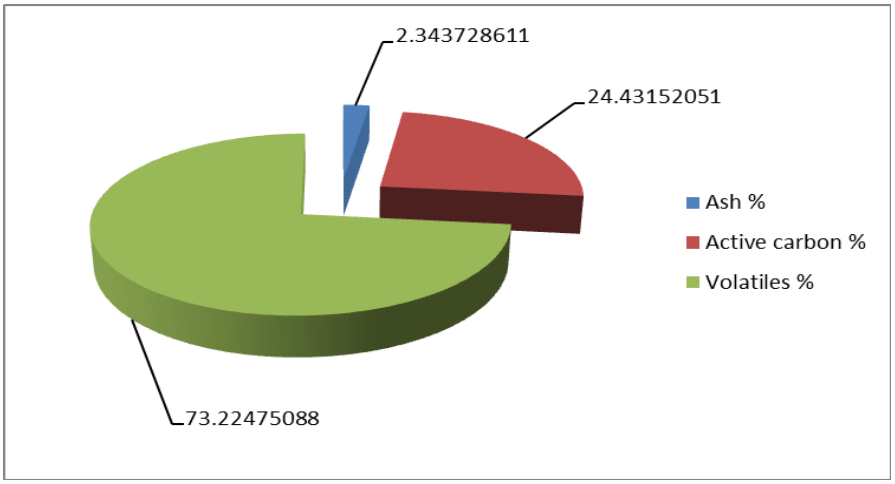

Fig. 6: The values of ash content, active carbon, and volatile for sunflower seed husk

A general conclusion of the paper can be that the larch shavings are very well compressible and briquettes with good mechanical properties from it are obtained, and the sunflower seed husk has weaker strength, even if the densities are acceptable. That is why it is recommended to use small bags to pack the briquettes, of maximum 8-10 kg, so that the briquettes don't crumble during transport on storage at the beneficiary.

CONCLUSIONS

The main conclusions obtained from the research carried out in this paper can be summarized as follows: *(1)* Both larch shavings and sunflower seed husk can be used in their natural state, without additional processing, to obtain briquettes with good physical and mechanical characteristics; *(2)* The briquettes obtained from larch shavings, had a density of 1024.8 $kg \cdot m^{-3}$ and a high calorific value of 19375 $kJ \cdot kg^{-1}$; *(3)* Even if they have lower mechanical strengths, the briquettes obtained from sunflower seed husk are calorically efficient with calorific value of 19265 $kJ \cdot kg^{-1}$, close to wood briquettes; *(4)* The ash content of 2.34% falls within the limits of briquettes obtained from plant resources and wood waste; *(5)* Through the experiments in this paper it can be started that the briquettes from the sunflower seed hulls become a viable alternative to the wood briquettes.

REFERENCES

1. ASTM E-1755-01, 2003: Standard method for the determination of ash in biomass.
2. Boutin, J.P., Gervasoni, G.,, Help, R., Seyboth, K., Lamers, P., Ratton, M., McCormick, K., Mundaca, L., Plepys, A., 2007: Alternative energy sources in transition countries. The case of bio-energy in Ukraine. Environmental Engineering and Management Journal 6(1): 3-11.
3. Bridgwater, A.,V., 2012: Review of fast pyrolysis of biomass and product upgrading. Biomass and Bioenergy 38: 68-94.
4. Brožek, M., Novakova, A., Kolarova, M., 2012: Quality evaluation of briquettes made from wood waste. Research in Agricultural Engineering 58: 30-35.
5. Demirbas, A., 2011: Resource facilities and biomass conversion processing for fuels and chemicals. Energy Conversion Management 42(11): 1357-1368.
6. DIN 51900-1, 2000: Determining the gross calorific value of solid and liquid fuels using the bomb calorimeter, and calculation of net calorific value-Part 1: General information,
7. EN 15148, 2009: Solid biofuels. Determination of the content of volatile matter.
8. Garcia, A.M., Barcia, B.M.J., Hernandez, J.A., 2008: Preparation of active carbon from a commercial holm-oak charcoal: Study of micro and meso-porosity. Journal Wood Science and Technology 37(5): 499-509.
9. Gavrilescu, D., 2008: Energy from biomass in pulp and paper. Environmental Engineering and Management Journal 7(5): 537-546.
10. Guler, C., Sahin, H.I., Yeniay, S., 2016: The potential for using corn stalks as a raw material for production particleboard with industrial wood chips. Wood Research 61(2): 299-307.
11. Jezerska, L., Zajonc, O., Vyletelek, J., Zegzulka, J., 2016: Mechanical material properties effect on pelletization. Wood Research 61(2): 307-321.
12. Kaliyan, N., Morey, R.V., 2009: Factors affecting strength and durability of densified biomass product. Biomass and Bioenergy 33(3): 359-379.
13. Krajnic, N., 2015: Wood fuels handbook. Food and agriculture organization of the united nations (FAO) Pristina.
14. Kuhlman, T., Diego, V., Koomen, E., 2013: Exploring the potential of reed as a bioenergy crop in the Netherlands. Biomass and Bioenergy 55: 41-52.
15. Lunguleasa, A., 2010: The compressive strength of wooden briquettes used as renewable fuels. Environmental and Engineering Management Journal 9(7): 977-981.
16. Lunguleasa, A., 2011: Compaction coefficient of wooden briquettes used as renewable fuels, Environmental and Engineering Management Journal 10(9): 1263-1268.
17. ÖNORM M7135, 2000: Pellets and briquettes-requirements and test conditions.
18. Okello, C., Pindozzi, S., Faugno, S., Boccia, L., 2013: Bioenergy potential of agricultural and forest rezidues in Uganda. Biomass and Bioenergy 56: 515-525.
19. Popescu, B., Șenilă, L., Vărăticeanu, C., Șimon, G., 2013: Cellulosic bioethanol from sunflower seed hulls-a renewable energy source. Studia Ubb Ambientium 1-2: 105-110.

20. Rosa, P.M., Antoniassi, R., Freitas, S.C., Bizzo, H.R., Zanotto, D.L., Oliveira, M.F., Castiglioni, V.B.R., 2009: Chemical composition of Brazilian sunflower varieties. Helia 32(50): 145-156.
21. Spîrchez, C., Lunguleasa, A., Croitoru, C., 2018: Ecological briquettes from sunflower seed husk. In: International Conference Renewable Energy and Environment Engineering (REEE 2018), Pp 1-8, Paris.
22. Spîrchez, C., Lunguleasa, A., Matei, M., 2019: Particularities of hollow-core briquettes obtained out of spruce and oak wooden waste. Maderas-Ciencia y tecnologia 20(1): 139-152.
23. Verna, V.K., Bram, S., De Rucky, J., 2009: Small scale biomass systems: Standards, quality, labeling and market driving factors. An outlook. Biomass and Bioenergy 33(10): 1393-1402.
24. WHM, 2020: Wood handbook wood as an engineering material. General technical report 113. Madison, WI:U.S. Department of Agriculture, Forest Service, Forest Products Laboratory, 463 pp.
25. Zygarlicke, C., Folkedahl, B., 2003: Effects of biomass blending on combustion ash. Project: Impacts of Cofiring Biomass with Fossil Fuels, DOE Cooperative Agreement No. DE-FC26-98FT40320.

VERONICA DRĂGUȘANU (JAPALELA), AUREL LUNGULEASA, COSMIN SPÎRCHEZ*
TRANSILVANIA UNIVERSITY OF BRAȘOV
DEPARTMENT OF WOOD PROCESSING AND DESIGN OF WOODEN PRODUCTS
29 EROILOR BLVD, 500036
BRAȘOV
ROMANIA
*Corresponding author: spirchez.cosmin@gmail.com